Aus dem Institut für Systemische Neurowissenschaften

der Heinrich-Heine-Universität Düsseldorf

Analyse der Auswirkungen von Alterung, Neurodegeneration und Depression auf die mittels Magnetresonanztomographie gemessene Hirnfunktion

Dissertation

zur Erlangung des Grades eines Dr. rer. med. von der

Medizinischen Fakultät der Heinrich-Heine-Universität Düsseldorf

vorgelegt von

Jan Kasper

(2024)

Als Inauguraldissertation gedruckt mit der Genehmigung der
Medizinischen Fakultät der Heinrich-Heine-Universität Düsseldorf
gez.:
Dekanin/Dekan:
Gutachter/innen:

Teile dieser Arbeit wurden veröffentlicht:

1) Kasper, J., Eickhoff, S. B., Caspers, S., Peter, J., Dogan, I., Wolf, R. C., Reetz, K., Dukart, J., Orth, M. (2023). Local synchronicity in dopamine-rich caudate nucleus influences Huntington's disease motor phenotype. *Brain*, Volume 146, Issue 8, Pages 3319–3330. https://doi.org/10.1093/brain/awad043

2) Kasper, J., Caspers, S., Lotter, L. D., Hoffstaedter, F., Eickhoff, S. B., Dukart, J. (2024). Resting-State Changes in Aging and Parkinson's Disease Are Shaped by Underlying Neurotransmission: A Normative Modeling Study. *Biological Psychiatry: Cognitive Neuroscience and Neuroimaging*. https://doi.org/10.1016/j.bpsc.2024.04.010

3) Wang, X., Hoffstaedter, F., Kasper, J., Eickhoff, S. B., Patil, K. R., Dukart, J. (2024). Lifetime Exposure to Depression and Neuroimaging Measures of Brain Structure and Function. *JAMA Netw Open.* 2024;7(2):e2356787. https://doi.org/10.1001/jamanetworkopen.2023.56787

Zusammenfassung

In den letzten Jahrzehnten hat die wissenschaftliche Gemeinschaft Fortschritte bei der Kartierung der funktionellen Organisation des menschlichen Gehirns erzielt. Funktionelle Veränderungen im typischen Alterungsprozess und in einigen neurodegenerativen Erkrankungen, sowie ihre pathologischen Krankheitspfade konnten identifiziert werden. Viele der zugrunde liegenden (Patho-)Mechanismen sind jedoch nach wie vor unklar, deren Kenntnis den Weg zu neuen diagnostischen Biomarkern und therapeutischen Zielen ebnen könnte. Multimodale Assoziationen, wie räumliche Korrelationen (Ko-lokalisationen) zwischen neurochemischen Eigenschaften und Veränderungen der Hirnfunktion oder -struktur, geben Aufschluss über biologische Entitäten, die vom Alterungsprozess oder damit verbundenen neurologischen Erkrankungen besonders betroffen sein könnten. Darüber hinaus könnten solche Assoziationen selbst als diagnostische oder prognostische Biomarker für Hirnerkrankungen dienen. Im Gegensatz zu neurologischen Erkrankungen sind die Auswirkungen psychiatrischer Erkrankungen wie Depressionen auf die funktionelle Organisation des Gehirns noch nicht abschließend geklärt, was teilweise auf die Heterogenität der Krankheitsbilder zurückzuführen ist. Mit Hilfe großer Datensätze könnte dieses Hindernis überwunden und Hirnveränderungen in einer Detailtiefe abgebildet werden, die in Studien mit geringerer Stichprobengröße nicht erreicht wurde. In den drei hier vorgestellten Studien wurden Daten aus der funktionellen Magnetresonanztomographie im Ruhezustand (*resting-state fMRI*) verwendet, um die lokalen Ausprägungen altersbedingter typischer und pathologischer Hirnveränderungen bei Menschen mit Morbus Huntington, Morbus Parkinson und mit Depressionserfahrungen zu untersuchen. In den ersten beiden Studien wurden die lokalen funktionellen Veränderungen im typischen Alterungsprozess und bei zwei neurodegenerativen Erkrankungen abgebildet. Die Assoziationen dieser Veränderungen mit anderen neuronalen und klinischen Daten lieferten Hinweise auf potentiell besonders vulnerable Zellen und Biomarker für die Schwere der Erkrankung. In der dritten Studie untersuchten wir den Effekt verschiedener Kriterien erlebter Depressionen auf die Hirnfunktion und -struktur und identifizierten die Kriterien, die am stärksten mit Gehirnveränderungen assoziiert waren. Die Ergebnisse deuten auf spezifische neurochemische Eigenschaften hin, die neuronale Veränderungen unter verschiedenen Bedingungen beeinflussen können, was zum Verständnis der untersuchten neurodegenerativen Erkrankungen und Alterungsprozesse beiträgt und die zukünftige Entwicklung neuer Pharmakotherapien unterstützen könnte. Die Depressionskriterien, die am stärksten mit funktionellen Veränderungen assoziiert waren, könnten auf einen anhaltenden Effekt der Depression oder ihrer Behandlung auf die Hirnfunktion hinweisen und sollten bei der Planung künftiger Studien zu Depressionen berücksichtigt werden.

Summary

In recent decades, the scientific community has made progress in mapping the functional organization of the human brain. Functional alterations in the typical aging process and in several neurodegenerative diseases, as well as their pathological pathways, have been identified. However, many underlying (patho-)mechanisms remain unclear, the knowledge of which could pave the way for new diagnostic biomarkers and therapeutical targets. Multimodal associations, such as spatial correlations (co-localizations) between neurochemical properties and alterations in brain function or structure, provide insights into biological entities that may be particularly affected by the aging process or related neurological diseases. Additionally, such associations themselves could serve as diagnostic or prognostic biomarkers for brain diseases. In contrast to neurological diseases, the effects of psychiatric diseases such as depression on the functional organization of the brain have not yet been conclusively clarified, which is partly due to the heterogeneity of the clinical picture. With the help of large data sets, this obstacle could be overcome and changes in the brain could be mapped in a level of detail that has not yet been achieved in studies with smaller sample sizes. In the three studies presented here, data from resting-state functional magnetic resonance imaging (resting-state fMRI) were used to investigate the regional characteristics of age-related typical and pathological brain alterations in people with Huntington's disease, Parkinson's disease, and experience of depression. In the first two studies, the local functional alterations in the typical aging process and in two neurodegenerative diseases were mapped. Associations of these alterations with other neuronal and clinical data provided indications of potential particularly vulnerable cells and biomarkers of disease severity. In the third study, we examined how various criteria of experienced depression affect brain function and structure and identified the criteria most strongly associated with brain alterations. The results suggested specific neurochemical properties that may influence neuronal alterations in different conditions, aiding our understanding of the studied neurodegenerative diseases and aging processes, and potentially supporting the future development of new pharmacotherapies. Depression criteria that were identified as most strongly associated with functional changes may indicate a persistent effect of depression or its treatment on brain function and should be considered when planning future studies on depression.

Abkürzungsverzeichnis

BOLD: Blood Oxygenation Level Dependent

CAG: Cytosin-Adenin-Guanin

CRISPR/Cas: Clustered Regularly Interspaced Short Palindromic Repeats / CRISPR-associated

D_1 und D_2: Dopaminrezeptor 1 und 2

DSM: Diagnostic and Statistical Manual of Mental Disorders

DSM-5 TR: Die fünfte Version des DSM in überarbeiteter Verfassung (engl: Text revision)

fMRT: Funktionelle Magnetresonanztomographie (engl.: functional magnet resonance imaging; fMRI)

GABA und $GABA_A$: Gamma-Aminobuttersäure (engl.: gamma-Aminobutyric acid) und $GABA_A$-Rezeptor

HD: Morbus Huntington (engl.: Huntington's disease)

HTT: Huntingtin

ICD: International Statistical Classification of Diseases and Related Health Problems

MDD: Major Depressive Disorder

mHTT: Mutiertes Huntingtin

MSN: Mittelgroße dornentragende Projektionsneurone (engl.: medium spiny neurons)

ND: Neurodegenerative Erkrankungen (engl.: neurodegenerative disease)

NT: Neurotransmitter

PD: Morbus Parkinson (engl.: Parkinson's disease)

PET: Positronen-Emissions-Tomographie

Rs-fMRI: Funktionelle MRT im Ruhezustand (engl.: resting-state fMRI)

SPECT: Einzelphotonen-Emissionscomputertomographie (engl.: single photon emission computed tomography)

WHO: Weltgesundheitsorganisation (engl.: World Health Organization)

ZNS: Zentrales Nervensystem

Inhaltsverzeichnis

1 Einleitung

Erkrankungen des Gehirns, ob psychiatrisch oder neurologisch, können mit substantiell verringerter Lebensqualität und -dauer einhergehen (1–6). Neurodegenerative Erkrankungen (engl.: *neurodegenerative diseases*, ND) sind chronisch-progrediente neurologische Erkrankungen, deren Auftrittswahrscheinlichkeiten signifikant mit dem Alter korrelieren (7). Hinsichtlich des demographischen Wandels hin zu einer älteren Gesellschaft ist zu erwarten, dass die Ausgaben für die Patientenversorgung steigen und das Risiko einer Versorgungsnotlage für Patienten mit ND zunimmt (8). Die weltweiten Inzidenzen von Morbus Alzheimer und Morbus Parkinson (engl.: *Parkinson's disease*, PD), der häufigsten Formen von ND, betragen 32 Millionen (im Jahr 2020 bei über 65-Jährigen (9)) und 9,4 Millionen (bei über 60-jährigen (10)). Innerhalb von 10 Jahren (2007 – 2017) stieg global die Sterblichkeitsrate durch Morbus Alzheimer (und anderen Demenzformen) um 46,2 % und durch PD um 38,8 % (11).

Die Pathomechanismen von ND sind nicht ausreichend verstanden, weshalb bis dato keine kurativen Therapien existieren und ärztliche Behandlungen auf Symptomminimierung abzielen (12). Da der weiträumige neuronale Zelltod der Symptomemergenz vorausgeht (13), sind Therapieeffekte limitiert. Frühzeitige Diagnosen besitzen jedoch das Potential, adäquate Therapien zu ermöglichen, die die Symptomatik reduzieren und normale Funktionalität erhalten und somit die Lebensqualität langfristig sicherstellen. Notwendig hierfür ist allerdings ein fundierteres Verständnis der, der Krankheit zu Grunde liegenden, neurologischen Mechanismen, um therapeutische Angriffspunkte und diagnostische Biomarker zu identifizieren.

Neurodegenerative Erkrankungen zeichnen sich primär durch progressiven Verlust (Atrophie) von Hirnsubstanz aus und unterscheiden sich in ihren neuronalen Ursprungsgebieten (14), Pfaden der Degeneration (15) und folglich auch in der symptomatischen Ausprägung. Neuere Untersuchungen unterstützen die Hypothese, dass die Pathophysiologie der Neurodegeneration mit einer Veränderung der strukturellen (16) und funktionellen (17, 18) neuronalen Vernetzung assoziiert ist. Hirnfunktionsveränderungen sind jedoch nicht nur mit Erkrankungen assoziiert, sondern finden sich auch im typischen Alterungsprozess, d. h. bei Personen ohne diagnostizierte Erkrankungen, die funktionell oder strukturell das Gehirn betreffen (19). So erscheint eine genaue Abgrenzung zwischen typischen Altersprozessen und Neurodegeneration, sowohl für das Verständnis von Pathomechanismen, als auch für die Identifikation diagnostischer Biomarkern, von hoher Notwendigkeit. Eine Abgrenzung könnte durch die Untersuchung von biologischen Charakteristika, die mit den funktionellen Veränderungen des Gehirns assoziierten sind, ermöglicht werden. Die Topographie von typischen und pathologischen Hirnfunktionsänderungen in einigen ND ist zwar

bekannt, der Zusammenhang mit zugrundeliegenden biologischen Entitäten jedoch nur unzureichend verstanden.

Eine Möglichkeit, die neurobiologischen Mechanismen von Hirnfunktionsveränderungen zu untersuchen, wäre, Zelleigenschaften und neuronale Aktivität direkt zu messen. Einzelzellableitungen neuronaler Aktivität oder histologische Untersuchungen zur Bestimmung von Zelleigenschaften sind jedoch invasiv und deshalb unter ethischen Gesichtspunkten beim Menschen problematisch und nur in wenigen Ausnahmefällen (wie bei Patienten, denen therapiebedingt bereits Elektroden implantiert wurden) hinnehmbar (20). Eine weitere Möglichkeit, die Brücke zwischen Hirnfunktionsänderungen und Zelleigenschaften zu schlagen, bieten multimodale Korrelationsanalysen von Daten, die mittels bildgebender Verfahren wie der funktionellen Magnetresonanztomographie (fMRT, engl.: *fMRI*), Positron-Emissions-Tomographie (PET) oder Einzelphotonen-Emissionscomputertomographie (SPECT) gewonnen wurden. Mithilfe von PET und SPECT können neurochemische Eigenschaften des zentralen Nervensystems (ZNS) abgebildet und die primär in Zellen ausgeprägten Neurotransmittersysteme identifiziert werden.

Durch die Bemühungen der wissenschaftlichen Gemeinschaft im Bereich „Open Science“ stehen heute umfassende hirnbildgebende und verhaltensbezogene Datensätze zur Verfügung, wie etwa die der UK-Biobank (21) oder der deutschen Biobank NAKO (22). Ihr immenser Stichprobenumfang ermöglicht eine systematische Analyse von Alters- und Krankheitseffekten über eine große Altersspanne hinweg. Zusätzlich zu funktionellen und strukturellen Daten des Gehirns hat sich die Bandbreite an verfügbaren Modalitäten erweitert, insbesondere um Hirnkarten der räumlichen Verteilung verschiedener Neurotransmittersysteme in Gesunden (23, 24). Die Kombination von funktionellen Karten und der normalen Verfügbarkeit verschiedener Neurotransmittersysteme im menschlichen Gehirn ermöglicht es, Einblicke in die mögliche Rolle von Neurotransmittersystemen bei funktionellen Änderungen zu erhalten (23, 24). Solche multimodalen Assoziationen liefern Erklärungsansätze für die Wirksamkeit bisheriger Pharmazeutika und könnten richtungsweisend für die Entwicklung neuer Pharmakotherapien sein. Des Weiteren können große Kohorten von erkrankten Personen in genügend große Teilmengen für statistische Untersuchungen spezifischer Krankheitsausprägungen aufgeteilt werden. Im Vergleich zu Fall-Kontroll-Studien erleichtern diese großen Datensätze die Erforschung von Zusammenhängen zwischen Hirnfunktionsveränderungen und einzelnen Symptomen. Herausstechende Krankheitsausprägungen könnten dabei in Zusammenhang mit konkreten Hirnfunktionsveränderungen gebracht werden. In den ersten beiden hier dargestellten Studien nutzten wir den Ansatz der multimodalen Assoziationen, um den Zusammenhang zwischen Hirnveränderungen und zu Grunde liegender Neurochemie in den beiden neurodegenerativen Erkrankungen Morbus Huntington (Studie 1) und Morbus Parkinson (Studie 2) und im gesunden Alterungsprozess (Studie 2) zu analysieren. Hier nutzten wir die Verteilungskarten verschiedener Neurotransmittersysteme, die in unabhängigen PET- und SPECT-Studien erhoben

wurden, sowie MRT-Daten aus verschiedenen Zentren aus Deutschland (Morbus Huntington) und der UK-Biobank (Morbus Parkinson und die Kohorte, die zur Analyse von typischen Alterungsprozessen verwendet wurde).

Eine weitere Klasse von Gehirnerkrankungen stellen psychiatrische Störungen dar. Neben neurologischen Erkrankungen können auch diese mit strukturellen (25) und funktionellen (26, 27) Hirnveränderungen einhergehen. Im Unterschied zu ND beschreiben psychiatrische Erkrankungen Störungen von Verhalten und Emotionen, deren Ursache nicht zwangsläufig auf neuronaler Ebene gefunden werden kann (bzw. bislang gefunden werden konnte). Ähnlich zu neurodegenerativen Erkrankungen sind die Ursachen komplex und können sowohl zwischen verschiedenen Störungen als auch zwischen Individuen variieren. Neben Demenz ist die depressive Störung die weltweit häufigste psychiatrische Erkrankung und war bereits 2008 drittgrößte Mitwirkende zur weltweiten Krankheitslast, mit steigender Tendenz (28). Obwohl Assoziationen mit Hirnfunktionsveränderungen gefunden wurden, ist die Studienlage nach wie vor inkonsistent (27), was unter anderem auf die Schwierigkeit einer einheitlichen Definition von Depression bzw. Depressionserfahrungen zurückgeführt wird (29). Welche Symptome individueller Depressionserfahrungen im Lebensverlauf mit messbaren Hirnfunktionsveränderungen einhergehen, blieb hinsichtlich geringer Kohortengrößen früherer Studien ein ungelöstes Problem. Dieses Problem versuchen wir in der dritten Studie mithilfe von Daten aus der UK-Biobank zu überwinden.

Das dem Promotionsvorhaben übergeordnete Ziel besteht darin, die Ursachen für Gehirnveränderungen durch neurodegenerative und psychiatrische Erkrankungen und durch den typischen Alterungsprozess zu identifizieren. Um einen Beitrag zum Erreichen dieses Zieles zu leisten, wurden lokale Veränderungen des Gehirns aus, im Ruhezustand gemessenen, fMRT-Daten abgeleitet und ihre Assoziationen zu neurochemischen oder verhaltensbezogenen Daten analysiert. Die folgenden Abschnitte erläutern die Hintergründe, Bedeutungen und Zusammenhänge der in den Studien verwendeten Methodik und stellen dar, weshalb diese Ansätze zur Erlangung der Studienziele verwendet wurden. Die sich daraus abgeleiteten Fragestellungen, die in den einzelnen Studien adressiert wurden, bilden den Abschluss dieses Kapitels.

1.1 Hirnfunktionsmessung mittels funktioneller MRT im Ruhezustand

Die Entwicklung bildgebender Verfahren im 20. Jahrhundert stellt einen Meilenstein für die Erforschung der neuronalen Informationsverarbeitung des menschlichen ZNS dar. Strukturelle und jüngst auch funktionelle neuronale Eigenschaften können heute in kleinen, distinkten Raumbereichen des gesamten Gehirns *in vivo* untersucht werden. Die fMRT ist eine nicht-invasive Methode, bei der das Konzentrationsverhältnis von sauerstoffreichem zu sauerstoffarmem Blut in kleinen, dreidimensionalen Hirnbereichen (Voxeln), berechnet wird. Dabei bedient man sich der

Tatsache, dass sauerstoffarmes Blut andere magnetische Eigenschaften besitzt als sauerstoffreiches Blut. Nimmt die neuronale Feuerrate innerhalb eines Voxels zu, erhöht sich der regionale Verbrauch von Glukose und Sauerstoff. Die Konzentrationsveränderung wird kompensiert durch bedarfsgelenkte und rapide Erhöhung des Blutflusses innerhalb dieser Region (sog. neurovaskuläre Kopplung). Diese lokale Oxygenierung führt zu einer Veränderung des Verhältnisses von desoxygenierten zu oxygenierten Erythrozyten, welches durch Anlegen eines externen, starken Magnetfelds sowie Störimpulse kontrastiert werden kann. Dieses Verhältnis, auch BOLD-Signal (*blood oxygenation level-dependent signal*) genannt, ist das in der fMRT gemessene Signal pro Voxel. Um nun Aussagen über die Funktionsweise des Gehirns zu treffen, kann man Probanden im MRT gewisse Aufgaben vollführen lassen, oder sie bitten, mehrere Minuten bewegungslos abzuwarten. Während im ersten Fall neuronale Korrelate konkreter motorischer oder kognitiver Funktionen im Vordergrund stehen, möchte man im zweiten Fall, der sog. Ruhezustands-fMRT (engl.: *rs-fMRI*), die funktionelle Organisation des gesamten Gehirns oder einzelner Hirnregionen untersuchen. Innerhalb der letzten Jahrzehnte wurden verschiedene miteinander funktionell gekoppelte Regionen (Ruhezustandsnetzwerke) identifiziert, d. h. Verbünde multipler, anatomisch nicht notwendigerweise benachbarter Regionen, deren BOLD-Signale in Abwesenheit einer konkreten Aufgabe korrelieren (30–32). Neben dieser sog. funktionellen Konnektivität etablierte sich in jüngerer Zeit ein weiterer Ansatz, in dem die Hirnfunktion über lokale (wie voxelweise) Eigenschaften des BOLD-Signals quantifiziert wird (33–35). Dafür zeigten u. a. Yang et al. (2007), dass niedere Frequenzen im BOLD-Signal der oszillatorischen Aktivität von Neuronenkomplexen entsprechen könnten (36).

In den hier berichteten Studien wurde Hirnfunktion mittels dreier etablierter (37, 38) Metriken quantifiziert, die komplementäre Informationen über lokale neuronale Aktivität (39) und Synchronizität (34, 35) im Ruhezustand liefern können. Sowohl im typischen Alterungsprozess (19, 40–44) als auch in beiden neurodegenerativen Erkrankungen (23, 45–49) fanden frühere Untersuchungen Hinweise auf veränderte kortikale und sub-kortikale neuronale Aktivität und Synchronizität. Ein Konsens, ob eine Depression mit Veränderungen der Gehirnfunktion einhergeht, konnte jedoch nicht gefunden werden (auf potentielle Ursachen wird im Abschnitt „1.7 Depressive Störungen“ eingegangen) (29, 50, 51).

In den ersten beiden hier dargestellten Studien wurde zunächst die veränderte Hirnfunktion im typischen Alterungsprozess und in neurodegenerativen Erkrankungen charakterisiert. Anschließend untersuchten wir, ob diese Veränderungen mit neurochemischen Eigenschaften, konkret den Rezeptoren und Transportern verschiedener Neurotransmitter, assoziiert sind. Die Bedeutung der Neurotransmission zur Hirnfunktion soll im nächsten Abschnitt erläutert werden.

1.2 Neuronale Signalübertragung und Neurotransmitter

Eine normale Hirnfunktion wird gewährleistet durch die balancierte Aktivität inhibitorischer und exzitatorischer Neurone, die in einer speziellen Netzwerkarchitektur (dem sog. Konnektom) zusammenwirken. Die Art der Signalübertragung (inhibitorisch oder exzitatorisch) wird dabei durch die in der Zelle primär vorhandenen Neurotransmitterrezeptoren festgelegt. Seit der Entdeckung des ersten Neurotransmitters durch Otto Loewi im Jahr 1921 (52) wurden bis heute über 200 weitere Neurotransmitter identifiziert (53), welche sich in ihrer Struktur, Funktion und räumlichen Verteilung im Gehirn unterscheiden. Diese Botenstoff-Diversität wird evolutionsbiologisch als Folge der behavioralen Adaption an veränderte äußere Einflüsse während der Artenentwicklung, sowie der notwendigen Verbesserung kognitiver Fähigkeiten und der damit einhergehenden komplexeren Hirnfunktionen diskutiert (54).

Neurotransmitter lassen sich hinsichtlich ihrer Stoffklassen primär in Aminosäuren und Amine unterteilen. Weitere Klassen umfassen lösliche Gase, Neuropeptide oder Endokannabinoide. Die Gamma-Aminobuttersäure (GABA) und das Anion der Glutamatsäure (Glutamat) sind die am häufigsten im ZNS vertretenen inhibitorischen und exzitatorischen Neurotransmitter und sind essentiell für eine normale Hirnentwicklung (55, 56), Gedächtnisleistung (56, 57) und Kognition (56, 58). Unterschiedliche Amine des ZNS spielen unterschiedliche Rollen für das Verhalten, die Kognition und das Gedächtnis, aber auch für die Motorfunktion und Stimmung (59–72). Einige der verschiedenen Funktionen von Neurotransmitterklassen wurden einzelnen Rezeptorsubtypen zugeordnet (73–76). Ist die Menge an verfügbarem Neurotransmitter oder die normale Funktion der Neurone einer gewissen Neurotransmitterklasse gestört, führe dies zu einer Imbalance in der Kette von inhibitorischer und exzitatorischer Signalübertragung und letztlich einer gestörten neuronalen Feuerrate, die auch das BOLD-Signal verändern sollte. Histologische Untersuchungen von post-mortem Hirngewebe, sowie *in vivo* Untersuchungen mit bildgebenden oder spektroskopischen Verfahren an gesunden und erkrankten Probanden brachten Erkenntnisse über die normalen Verteilungen und pathologische Veränderungen in der Verfügbarkeit von Neurotransmittersystemen innerhalb des ZNS. Insbesondere Rezeptoren von GABA und Glutamat, als auch von Dopamin, Serotonin, Noradrenalin, Histamin und Acetylcholin zeigten veränderte Verfügbarkeiten in einer Reihe von neurodegenerativen und psychiatrischen Erkrankungen (53).

Frühere Studien fanden Hinweise auf veränderte Verfügbarkeiten verschiedener Neurotransmittersysteme, insbesondere von Monoaminen, sowohl im normalen Alterungsprozess (77–91) als auch in den beiden hier untersuchten neurodegenerativen Erkrankungen (92–104). Solche Hinweise auf reduzierte Verfügbarkeit gewisser Systeme weisen darauf hin, dass diese Systeme zwar betroffen sein können, jedoch nicht, ob eine besonders Vulnerabilität für die funktionellen Veränderungen in den Zellen dieser Neurotransmittersysteme vorliegt. Hinweise auf eine solche Vulnerabilität, die bisher aufgrund der methodologischen Schwierigkeiten, beide

Modalitäten zeitgleich zu messen, unklar blieb, sollten in den ersten beiden Studien mithilfe räumlicher Korrelationsanalysen gefunden werden.

1.3 Räumliche Korrelationsanalysen

Wie zuvor beschrieben zeigen eine Reihe von ND eine veränderte Verfügbarkeit verschiedener Neurotransmittersysteme. Die Vulnerabilität solcher Zellen für den neurodegenerativen Prozess wurde somit zwar identifiziert, jedoch blieb unklar, ob ebenjene Systeme auch vulnerabel für die (der Degeneration vorangehenden) funktionellen Veränderungen sind. Im Falle einer besonderen Vulnerabilität für die durch die Erkrankung induzierten funktionellen Veränderungen sollten Regionen, deren Zellen die meisten Rezeptoren oder Transporter dieses Systems beinhalten, auch die stärksten gemessenen Veränderungen aufweisen und somit eine Korrelation zwischen Verfügbarkeit und Funktionsveränderung vorliegen (23). Hinsichtlich der pathologischen Krankheitspfade in ND könnte sich der Krankheitsverlauf auch in der räumlichen Korrelationsstärke zeigen: Steigt die Zahl der an funktionellen Veränderungen betroffenen Regionen und ist die Stärke der Veränderung abhängig von der Neurotransmitterverfügbarkeit, sollte auch die räumliche Korrelationsstärke mit dem Krankheitsprozess zunehmen. In den ersten beiden hier dargestellten Studien nutzten wir diesen Ansatz der räumlichen Korrelationsanalyse, um Hinweise auf die Vulnerabilität verschiedener Neurotransmittersysteme bei Morbus Huntington, Morbus Parkinson und dem typischen Alterungsprozess zu finden und darin Biomarker für die Krankheitsschwere zu identifizieren. Zur Evaluation der Vulnerabilität spezifischer Neurotransmittersysteme in Morbus Parkinson wurden ihre individuellen Korrelationskoeffizienten mit einem normativen Modell verglichen, das auf Basis der Korrelationen der Kontrollkohorte erstellt wurde.

1.4 Typisches Altern und normative Modellierung

Mit dem Begriff „Altern“ soll hier die stetige Entwicklung eines einzelnen Organismus (hier im Besonderen dessen Gehirns) ab dem mittleren Erwachsenenalter (40 - 60 Jahre) bis zum hohen Alter (> 80 Jahre) oder Tod bezeichnet werden. Mit Ausnahme einiger Nesseltierarten, deren Ontogenese umkehren kann (105), ist Altern unausweichlich und im Menschen ein Hauptrisikofaktor für motorische und kognitive Einschränkungen, sowie neurodegenerative Erkrankungen (7, 106). So ließe sich annehmen, dass eine (latente) funktionelle oder strukturelle Veränderung und potentiell eine nicht-diagnostizierte Erkrankung des Gehirns vorliegt, je älter ein Proband ist. Neun Kennzeichen des biologischen Alterungsprozesses wurden von López-Otín und Kollegen herausgearbeitet, darunter genetischen Veränderungen, der Verlust der Proteostasis und die (mutmaßlich daraus folgende) veränderte interzelluläre Kommunikation (107). Der Verlust der Proteostasis führt zur Aggregation fehlgefalteter Proteine, die potentiell als Ursache für

Zellfunktionsveränderungen und Zelltod angesehen werden (15). Schreitet dieser Prozess fort, mündet er in Proteinopathien wie einigen neurodegenerativen Erkrankungen, bei denen sich fehlgefaltete und schädliche Proteine im Krankheitsverlauf entlang gewisser krankheitsabhängiger Pfade im Gehirn verteilen (15). Veränderte interzelluläre Kommunikation im Alterungsprozess kann durch Neuroinflammation (107) verursacht werden, z. B. als Konsequenz von Gewebeschäden oder eines geschwächten Immunsystems und äußert sich unter anderem durch eine im Alter verringerte synaptische Transmission zwischen Neuronen (108). Hinsichtlich dieser typischen Charakteristika des Alterns soll hier anstelle von „gesundem" von „typischem" in Abgrenzung zum „atypischen" (in Sinne einer Normabweichung) Altern des Gehirns gesprochen werden.

Um nun Alterungseffekte von Krankheitseffekten auf eine gewisse Metrik unterscheiden zu können, bietet sich bei großem Stichprobenumfang die normative Modellierung an, welche in den letzten Jahren durch methodische Weiterentwicklung (109, 110) und die Verbreitung großer Datenmengen (111) in den Neurowissenschaften an Bedeutung gewann (112). Im klinischen Alltag findet normative Modellierung bereits in Somatogrammen Verwendung, um einzuschätzen, ob ein Körpermaß zu einem gewissen Alter im Normbereich liegt (113). Um dem Begriff „normativ" gerecht zu werden, so dass die Modelle die Eigenschaften der zu Grunde liegende Population möglichst genau approximieren, sollte die Datenbasis aus einer großen, heterogenen Stichprobe bestehen und die Daten auf möglichst gleicher Art erhoben werden, um Effekte der Akquisitionspraxis und Stichprobenverzerrung zu minimieren.

Im Allgemeinen soll bei der normativen Modellierung ein möglichst authentisches Referenzmodel erstellt werden, welches die „normale" bzw. „typische" Beziehung zwischen verschiedenen Variablen innerhalb einer Population beschreibt und insbesondere auch die Varianz innerhalb der Variablen berücksichtigt. Normative Modelle im klinischen Kontext modellieren beispielsweise die typische Abhängigkeit einer gewissen Metrik (wie der Hirnfunktion) von klinisch relevanten Variablen (wie dem chronologischen Alter). Nicht-lineare, heteroskedastische Modelle können die Heterogenität der Variablenausprägung in der untersuchten Stichprobe altersaufgelöst abbilden, wobei die Generalisierbarkeit und Präzision dieser Modelle durch die Repräsentativität und Größe der zu Grunde liegenden Stichprobe abhängt (111). Mithilfe dieser Modelle können die Abweichungen einzelner Individuen von der Norm quantifiziert werden. Dieser Ansatz wurde in der zweiten Studie verwendet. Hier wurden mithilfe bildgebender Daten der UK Biobank normative Modelle des Alterseffekts auf die Korrelationsstärke zwischen Hirnfunktionsmetriken und der Verfügbarkeit diverser Neurotransmittersysteme erstellt und analysiert. Diese Alterseffekte, d. h. Veränderungen in der Korrelationsstärke, dienten als Hinweise für eine besondere Vulnerabilität von Zellen mit bestimmen Neurotransmitterprofilen auf altersbedingte funktionelle Veränderungen. Anschließend nutzten wir die erstellten normativen Modelle, um atypische Korrelationsstärken in

Probanden mit diagnostizierter Parkinsonerkrankung zu quantifizieren und Hinweise auf vulnerable Systeme in dieser Erkrankung zu erlangen.

1.5 Morbus Parkinson

Wie bereits erwähnt ist PD die weltweit zweithäufigste neurodegenerative Erkrankung und stark assoziiert mit dem Alter. Ihre Diagnose stützt sich auf sog. kardinale motorische Symptome bestehend aus Akinese/Bradykinese in Verbindung mit muskulärem Rigor, Ruhetremor und posturaler Instabilität (114). Unterstützt wird die Diagnose durch positives Ansprechen auf Levodopa (ein Dopamin-Vorgänger-Protein, welches im Gehirn zu Dopamin umgewandelt wird), sowie einen unilateralen Beginn und langsame klinische Progression der motorischen Symptomatik (im Gegensatz zu atypischen Parkinson-Syndromen). Zu den primären neuronalen Merkmalen von PD gehören die intraneuronale Aggregation von fehlgefalteten α-Synuclein in Lewy-Körperchen und Lewy-Neuriten (115) sowie der fortschreitende Verlust dopaminerger Neuronen in der Substantia Nigra (pars compacta). Diese Degeneration setzt bereits vor Emergenz der ersten Symptome ein – zum Zeitpunkt der Manifestation sind bereits über 50 % der Neurone abgestorben (116–119). Deshalb stehen die kardinalen Parkinson-Symptome nicht für eine frühzeitige Diagnose zur Verfügung. Obwohl einige genetische Polymorphismen mit PD assoziiert sind, wird die häufigste Ursache Umweltfaktoren zugeschrieben (120). Laut der Braak-Hypothese (121) verbreiten sich α-Synuclein-Aggregationen bzw. Lewy-Körperchen im Krankheitsverlauf von den initialen Gebieten (Bulbus olfactorius, Nervus vagus, Medulla oblongata) über den Hirnstamm, das basale Vorderhirn und letztlich über den gesamten Kortex (15) und involvieren auch nicht-dopaminerge Pfade (122). Auch andere neurochemische (darunter GABAerge, cholinerge, serotonerge und cannabinoide) Systeme sind von der Degeneration betroffen (123). Warum die Erkrankung jedoch ebenjenen Pfad einschlägt und welche Eigenschaften besonders vulnerable Zellen besitzen, ist nicht abschließend geklärt (122, 124). Mit Hilfe dieses Wissens könnten jedoch neue, vielversprechende Ansatzpunkte für Therapien oder Diagnostik identifiziert werden. Wissenschaftliche Institutionen unternehmen immense Bemühungen, krankheitsmodifizierende Therapien zu entwickeln und Biomarker zur Früherkennung zu identifizieren (125), getrieben durch neueste Erkenntnisse in Ätiologie, Pathogenese und Pathophysiologie (12). Dieser Fortschritt zeigt sich auch in dem weiten Spektrum der Angriffsziele und Methodik solcher Therapien, von (unter vielen anderen (12)) der Verhinderung der Proteinfehlfaltung (126, 127) über die Stärkung neuroprotektiver Eigenschaften (128, 129), bis hin zur Entwicklung neuer Pharmakotherapien (125), die eher weniger beachtete Neurotransmittersysteme anvisieren. Gleichzeitig animieren die neueren Erkenntnisse in der Grundlagenforschung zur Suche nach diagnostischen Biomarkern für (insbesondere frühes) PD. Biomarker werden heute auf verschiedensten Ebenen gesucht, darunter auf biochemischer,

behavioraler (wie digitale Biomarker (130)), oder hirnstruktureller und -funktioneller Ebene auf Grundlage von Bildgebungsdaten (12, 131, 132).

1.6 Morbus Huntington

Morbus Huntington (HD) ist die häufigste autosomal dominant vererbbare neurodegenerative Bewegungserkrankung (133). Ihre Prävalenz ist ortsabhängig: In europäischen Ländern sind zwischen 100 bis 130 pro Millionen, in Ostasien dagegen nur 1 bis 7 pro Millionen Menschen betroffen (134). Anders als bei PD ist die Ursache für die Emergenz von HD bekannt: Eine erhöhte Wiederholung des Basentripletts bestehend aus Cytosin-Adenin-Guanin (CAG) im Huntingtin-Gen führt zur Formation eines mutierten Huntingtin-Proteins (mHTT) (135). Das Alter der Manifestation hängt dabei mit der Anzahl der CAG-Wiederholungen im Huntingtin-Gen zusammen und führt zu einer groben Klassifizierung von HD in *Adult-Onset* (Manifestation zwischen dem 35. und 55. Lebensjahr (136)) und *Juvenile-Onset* (Manifestation vor dem 21. Lebensjahr, bei ca. 4-10 % aller Patienten mit HD (137)) (138). Während Personen mit juveniler Huntington-Krankheit primär von abnormalen willkürlichen Bewegungen betroffen sind, zeigen Patienten, bei denen sich HD erst im Erwachsenenalter manifestiert, eine Triade bestehend aus motorischen, kognitiven, und psychiatrischen Symptomen (138, 139). Die Überlebenszeit nach klinischer Manifestation hängt stark von der Anzahl der CAG-Wiederholungen und somit dem Alter bei Symptombeginn ab und beträgt im Median ca. 20 Jahre (140). Neben individuellen Unterschieden ist die CAG-Wiederholungslänge auch gewebeabhängig (141) und variiert deshalb zwischen einzelnen Hirnregionen. Besonders stark von einer erhöhten CAG-Wiederholung betroffen sind mittelgroße dornentragende Projektionsneurone (engl.: *medium spiny neurons*, MSN) des Striatums, weshalb diese auch die größte Anzahl an mHTT aufweisen und bereits einige Jahre vor klinischer Manifestation atrophieren (142). Paradoxerweise ist jedoch nicht bloß die mutierte Form, sondern auch das physiologische Huntingtin (HTT) für einen selektiven Verlust kortikostriataler Neurone in HD verantwortlich (143). Trotz klarer Evidenz für die kausale Ursache des Zellabbaus sind die Ursachen für die pathologischen Pfade und die Eigenschaften vulnerabler Zellen in HD unbekannt. Wie PD ist HD heute nicht heilbar und therapeutische Strategien zielen auf Minimierung der psychiatrischen und motorischen Symptomatik oder Verlangsamung des Krankheitsfortschritts. Auch hier sind, dank des Erkenntnisgewinns zu molekularen Pathomechanismen, sowie der Entwicklung neuerer Methoden (insbesondere auf genetischer Ebene) verschiedene therapeutische Angriffspunkte im Fokus aktueller Forschung (144). Ansätze auf pharmakologischer Basis zielen auf die Modulation verschiedener Neurotransmittersysteme (gegen motorische und psychiatrische Symptomatik (145)) oder auf eine verlangsamte Aggregation bzw. Verringerung von mHTT (146, 147). Weitere Ansätze umfassen Stammzelltherapien, wie beispielsweise zum Ersatz degenerierter MSN (148), Gentherapie oder Geneditierung (CRISPR/Cas) zur Verringerung der Produktion von

mHTT (144, 149, 150). Anders als in PD kann mit molekulargenetischer Diagnostik das Huntingtin-Gen auf eine erhöhte CAG-Wiederholung zu diagnostischen Zwecken untersucht werden. Sowohl in HD, das im Erwachsenenalter auftritt (151), als auch in juvenilem HD (152) korreliert die Anzahl an CAG-Wiederholungen sowohl mit dem Alter der motorischen Manifestation, als auch dem Sterbealter (153). Sind familiäre Fälle von HD jedoch nicht bekannt oder gegeben, bedarf es anderer diagnostischer Möglichkeiten, um HD zu identifizieren und von anderen Erkrankungen abzugrenzen. In der ersten hier dargestellten Studie wurde nach Hinweisen für vulnerable Neurotransmittersysteme in HD gesucht und analysiert, ob die Assoziationsstärken zwischen funktionellen Hirnveränderungen und der Verfügbarkeit von Neurotransmittersystemen Rückschlüsse auf das Krankheitsstadium erlauben und somit potentiell prognostische Biomarker darstellen.

1.7 Depressive Störungen

Psychische Störungen bezeichnen eine Gruppe von Krankheiten, deren Betroffene Störungen von Kognition, Emotion, oder Verhalten erfahren. Anders als bei neurodegenerativen Erkrankungen sind psychische Störungen nicht zwangsläufig durch strukturelle Hirnveränderungen charakterisiert oder diese sind noch nicht identifiziert. Depressive Störungen sind die weltweit zweihäufigste Form psychischer Erkrankungen, deren absolute Anzahl an Betroffenen von 1990 bis 2019 von ca. 170 auf 280 Millionen anstieg. Geschätzt 3,8 % der Weltbevölkerung erfahren Depression in ihrem Leben (154). Depressionen können sowohl isoliert, als auch als Komorbidität von neurodegenerativen Erkrankungen auftreten (155–157). Je nach Klassifikationssystem werden verschiedene Arten von depressiven Erfahrungen oder Störungen definiert, die sich in ihrer Intensität, Dauer, sowie ihrem Kontext (z. B. bei biopolaren Störungen) unterscheiden. Zu den häufigsten Klassifikationssystemen gehören das von der American Psychiatric Association veröffentlichte *Diagnostic and Statistical Manual of Mental Disorders* (DSM) und das von der Weltgesundheitsorganisation (WHO) veröffentlichte internationale Klassifikationssystem für Krankheiten (ICD). Nach Annäherungsbemühungen (158) gleichen sich die aufgelisteten depressiven Symptome beider Systeme weitestgehend, dennoch bleibt das Krankheitsbild der Depression uneinheitlich und ihre Ausprägung heterogen. Ein heute in der Forschung häufig verwendeter Krankheitsbegriff ist die schwere depressive Störung (engl.: *major depressive disorder*, MDD), welche erstmals 1980 in der 3. Edition des DSM definiert wurde. Die Heterogenität des Krankheitsbildes wird bei Betrachtung des diagnostischen Verfahrens deutlich: Für die Diagnose einer MDD nach der heute aktuellen Version (DSM-5 TR) müssen Patienten aus einem Kanon von neun Symptomen fünf über einen Zeitraum von mindestens zwei Wochen aufweisen. Darunter muss zwingend eine depressive Verstimmung, über die meiste Zeit des Tages, oder ein substantiell verringertes Interesse für fast alle täglichen Aktivitäten vorliegen. In der heute aktuellen 11. Version des ICD werden Depressive Störungen primär in eine „einzelepisodische depressive Störung“ (ICD-11: 6A70) oder eine

„wiederkehrende depressive Störung“ (ICD-11: 6A71) unterteilt (159). Analog zur DSM muss für mindestens zwei Wochen tägliche eine gedrückte Stimmung oder Anhedonie in Kombination mit weiteren unterstützenden Symptomen vorliegen. Nach heutiger Ansicht existiert eine Fülle von sich gegenseitig beeinflussenden biologischen (wie z. B. genetische Disposition), psychologischen (wie Ruminationsneigung), und sozialen (wie Deprivation) Faktoren, die zur Entstehung einer Depressionserfahrung beitragen können (159). Verschiedene Studien an Patienten mit Depressionen lieferten jedoch unter Verwendung bildgebender Verfahren Inkonsistenzen in den funktionellen und strukturellen Veränderungen, deren Ursache auch in der Heterogenität der Depressionssymptomatik und folglich der untersuchten Kohorten vermutet wird (29). In der dritten Studie wird das Ziel verfolgt, in einer genügend großen Kohorte von Probanden mit Depressionserfahrungen der UK Biobank diejenigen Depressionskriterien zu identifizieren, die mit funktionellen und strukturellen Veränderungen assoziiert sind.

1.8 Ziele dieser Arbeit

Diese Arbeit dient dem Zweck, Hinweise für die, dem Alterungsprozess und bestimmten neurodegenerativen Krankheitsprozessen zu Grunde liegenden, (Patho-)Mechanismen des menschlichen Gehirns zu erhalten. Dafür untersuchten wir funktionelle Veränderungen und ihre Assoziation mit neurochemischen Eigenschaften im typischen Alterungsprozess, bei Morbus Huntington und bei Morbus Parkinson. Unter Einbeziehung klinischer Charakteristika wurde zudem das Potential der untersuchten Maße als diagnostische und prognostische Biomarker für neurodegenerativen Erkrankungen untersucht. Darüber hinaus wurden die im Rahmen dieser Studien gewonnenen Hirnfunktionsdaten verwendet, um die inkonsistente Studienlage zu funktioneller Veränderung in depressiven Störungen zu verbessern. Die folgenden Studien wurden im Rahmen meiner Doktorarbeit publiziert und bilden den Kern meines Dissertationsvorhabens.

Studie 1:

Die erste Studie verfolgte zwei Hauptziele. Zum einen sollte der Einfluss von Morbus Huntington auf die neuronale Aktivität und Synchronizität in kortikalen, subkortikalen und zerebellären Regionen untersucht werden. Hierbei wurde ein möglicher Zusammenhang zwischen der Krankheitsschwere und den lokalen funktionellen Veränderungen in, durch die HD-Pathologie besonders betroffenen, Hirnregionen analysiert. Dazu wurden in zwei unabhängigen Kohorten von Patienten mit HD (n = 84) und Kontrollprobanden (n = 88) (Observation & Replikation) Hirnkarten lokaler Hirnfunktionsveränderung aus den individuellen rs-fMRI-Daten abgeleitet. Zum anderen sollte die Rolle von zehn verschiedenen Rezeptoren oder Transportern (darunter vier serotonerge und

drei dopaminerge) auf die veränderte Hirnfunktion über alle Hirnregionen hinweg untersuchen werden, um Hinweise auf besonders vulnerable Zelltypen zu erhalten. Hierfür wurden räumliche Korrelationen (Ko-lokalisationen) der funktionellen Veränderung mit der Verfügbarkeit verschiedener Rezeptoren und Transporter untersucht und deren Zusammenhang mit klinischen Skalen der Krankheitsschwere analysiert.

Studie 2:

Ähnlich der ersten Studie lag das Ziel der zweiten Studie darin, die Effekte des typischen Alterungsprozesses und von Morbus Parkinson auf Metriken lokaler neuronaler Aktivität und Synchronizität zu analysieren sowie den Einfluss neurochemischer Eigenschaften auf die funktionelle Veränderung zu untersuchen. Zunächst sollten die aus vorherigen Studien bekannten Alterseffekte auf die Hirnfunktion reproduziert werden, um darauf aufbauend diejenigen Neurotransmittersysteme zu identifizieren, die am stärksten mit diesen Alterseffekten assoziiert sind und somit potentiell besonders vulnerabel für Alterungseffekte sind.

Für diese Ziele wurden rs-fMRI-Daten der UK-Biobank (160) verwendet, um individuelle Karten lokaler Hirnfunktion abzuleiten. Hinweise auf die Beteiligung verschiedener Neurotransmittersysteme an der Hirnfunktion auf individueller und Populationsebene (n = 25917) sollten über räumliche Korrelationen der funktionellen Karten mit 19 verschiedenen Neurotransmitterkarten identifiziert werden. Anschließend wurde die potentielle Vulnerabilität der untersuchten Rezeptoren und Transporter hinsichtlich der durch Parkinson bedingten funktionellen Veränderungen analysiert und prognostische Biomarker zu identifizieren versucht. Unter Berücksichtigung von Alters- und Geschlechtseffekten wurden normative Modelle der Korrelationsstärke in einer typischen Kohorte mithilfe neuester nicht-linearer Modellierungsmethoden erstellt. Die Korrelationsstärke in den Daten von Probanden mit Morbus Parkinson (n = 58) wurden mit denen der normativen Modelle verglichen. Signifikante Abweichungen von den normativen Modellen und deren Abhängigkeit von der Krankheitsdauer sollten Hinweise für eine besondere Vulnerabilität spezifischer Neurotransmittersysteme für Hirnfunktionsveränderungen bei Morbus Parkinson, sowie potentielle Biomarker für den Krankheitsverlauf liefern.

Studie 3:

Im Unterschied zu den ersten beiden Studien stand in der dritten Studie die Depression als psychiatrische Erkrankung des Gehirns im Fokus. Ziel dieser Studie war es, die Effekte verschiedener Depressionserfahrungen auf die Hirnfunktion und -struktur zu quantifizieren und

damit zur Klärung der inkonsistenten Studienlage zu Gehirnveränderungen bei Depressionen beizutragen. Darüber hinaus sollten jene Kriterien bestimmt werden, die am stärksten mit funktionellen und strukturellen Veränderungen des Gehirns assoziiert sind.

Hier wurden erneut die in der zweiten Studie entstandenen Karten individueller Hirnfunktion der UK Biobank, sowie zusätzlich erstellte Karten der Volumina von grauer Substanz verwendet. Anhand von sechs verschiedenen Kriterien von Depressionserfahrungen bildeten wir Gruppen von Probanden mit Depressionserfahrungen (n = 20484), die ein bis zu sechs dieser Kriterien erfüllten. Für jede dieser Gruppen wurden Veränderungen der Hirnfunktionsmaße und Volumina der grauen Substanz relativ zu einer gesunden Kontrollkohorte (n = 25462) auf Gruppenlevel evaluiert.

2 Studie 1: Local synchronicity in dopamine-rich caudate nucleus influences Huntington's disease motor phenotype

Jan Kasper[1,2], Simon B. Eickhoff[1,2], Svenja Caspers[3,4], Jessica Peter[5], Imis Dogan[6,7], Robert Christian Wolf[8], Kathrin Reetz[6,7], Juergen Dukart[1,2,†], Michael Orth[5,9†]

[†]These authors contributed equally to this work.

[1] Institute of Neuroscience and Medicine, Brain & Behaviour (INM-7), Research Centre Jülich, Jülich, Germany

[2] Institute of Systems Neuroscience, Medical Faculty & University Hospital Düsseldorf, Heinrich Heine University Düsseldorf, Düsseldorf, Germany

[3] Institute of Neuroscience and Medicine (INM-1), Research Centre Jülich, Jülich, Germany

[4] Institute of Anatomy I, Medical Faculty & University Hospital Düsseldorf, Heinrich Heine University Düsseldorf, Düsseldorf, Germany

[5] University Hospital of Old Age Psychiatry and Psychotherapy, Bern University, Switzerland

[6] Department of Neurology, RWTH Aachen University, Aachen, Germany

[7] JARA-BRAIN Institute Molecular Neuroscience and Neuroimaging, Research Centre Jülich GmbH and RWTH Aachen University, Jülich/Aachen, Germany

[8] Center for Psychosocial Medicine, Department of General Psychiatry, Heidelberg University, Germany

[9] Neurozentrum Siloah, Bern, Switzerland

Publiziert in: *Brain*, Volume 146, Issue 8, August 2023, Pages 3319–3330,

https://doi.org/10.1093/brain/awad043; (161)

Korrespondierender Autor:

Professor Michael Orth, MD, PhD

University Hospital of Old Age Psychiatry and Psychotherapy

Bolligenstr. 111

3000 Bern 60

Switzerland

Eigenanteil:

Konzeption des Forschungsansatzes, Studiendesign, Datenverarbeitung & Durchführung statistischer Analysen, Analyse und Interpretation der Daten, Erstellung und Überarbeitung des Manuskripts inklusive der Visualisierungen.

BRAIN
ORIGINAL ARTICLE

Local synchronicity in dopamine-rich caudate nucleus influences Huntington's disease motor phenotype

Jan Kasper,[1,2] Simon B. Eickhoff,[1,2] Svenja Caspers,[3,4] Jessica Peter,[5] Imis Dogan,[6,7,8] Robert Christian Wolf,[9] Kathrin Reetz,[6,7,8] Juergen Dukart[1,2,†] and Michael Orth[5,10,†]

[†]These authors contributed equally to this work.

Structural grey and white matter changes precede the manifestation of clinical signs of Huntington's disease by many years. Conversion to clinically manifest disease therefore likely reflects not merely atrophy but a more widespread breakdown of brain function. Here, we investigated the structure–function relationship close to and after clinical onset, in important regional brain hubs, particularly caudate nucleus and putamen, which are central to maintaining normal motor behaviour. In two independent cohorts of patients with premanifest Huntington's disease close to onset and very early manifest Huntington's disease (total $n = 84$; $n = 88$ matched controls), we used structural and resting state functional MRI.

We show that measures of functional activity and local synchronicity within cortical and subcortical regions remain normal in the premanifest Huntington's disease phase despite clear evidence of brain atrophy. In manifest Huntington's disease, homeostasis of synchronicity was disrupted in subcortical hub regions such as caudate nucleus and putamen, but also in cortical hub regions, for instance the parietal lobe. Cross-modal spatial correlations of functional MRI data with receptor/neurotransmitter distribution maps showed that Huntington's disease-specific alterations co-localize with dopamine receptors D1 and D2, as well as dopamine and serotonin transporters. Caudate nucleus synchronicity significantly improved models predicting the severity of the motor phenotype or predicting the classification into premanifest Huntington's disease or motor manifest Huntington's disease.

Our data suggest that the functional integrity of the dopamine receptor-rich caudate nucleus is key to maintaining network function. The loss of caudate nucleus functional integrity affects network function to a degree that causes a clinical phenotype. These insights into what happens in Huntington's disease could serve as a model for what might be a more general relationship between brain structure and function in neurodegenerative diseases in which other brain regions are vulnerable.

1 Institute of Neuroscience and Medicine, Brain & Behaviour (INM-7), Research Centre Jülich, 52428 Jülich, Germany
2 Institute of Systems Neuroscience, Medical Faculty & University Hospital Düsseldorf, Heinrich Heine University Düsseldorf, 40225 Düsseldorf, Germany
3 Institute of Neuroscience and Medicine (INM-1), Research Centre Jülich, 52428 Jülich, Germany
4 Institute of Anatomy I, Medical Faculty & University Hospital Düsseldorf, Heinrich Heine University Düsseldorf, 40225 Düsseldorf, Germany
5 University Hospital of Old Age Psychiatry and Psychotherapy, University of Bern, 3000 Bern 60, Switzerland
6 Department of Neurology, RWTH Aachen University, 52056 Aachen, Germany
7 JARA-BRAIN Institute Molecular Neuroscience and Neuroimaging, Research Centre Jülich GmbH, 52425 Jülich Germany
8 RWTH Aachen University, 52056 Aachen, Germany

Received August 21, 2022. Revised January 08, 2023. Accepted February 03, 2023. Advance access publication February 16, 2023

9 Center for Psychosocial Medicine, Department of General Psychiatry, Heidelberg University, 69047 Heidelberg, Germany
10 Neurozentrum Siloah, 3073 Gümligen, Switzerland

Correspondence to: Professor Michael Orth, MD, PhD
University Hospital of Old Age Psychiatry and Psychotherapy
Bolligenstr. 111, 3000 Bern 60, Switzerland
E-mail: Michael.Orth@siloah.ch

Keywords: local synchronicity; fALFF; dopamine receptors; caudate nucleus; total motor score

Introduction

In Huntington's disease, a movement disorder with cognitive decline and behavioural abnormalities, the most vulnerable regions to the pathological events caused by the *HTT* CAG repeat expansion mutation include the striatum, i.e. the caudate nucleus and putamen. Striatal atrophy can be observed a long time before clinical manifestations of Huntington's disease without causing an overt clinical phenotype.[1-3] Clinical manifestations of Huntington's disease therefore likely reflect the breakdown of network brain function, so normal behaviour can no longer be maintained. Task-based functional MRI has demonstrated abnormal activation in premanifest Huntington's disease (e.g. Klöppel *et al.*[4] and Wolf *et al.*[5]). In addition, resting state functional MRI (rs-fMRI), i.e. fMRI in the absence of a task, has revealed many changes of functional connectivity 'between' regions in various networks (for reviews see Gregory and Scahill[6] and Pini *et al.*[7]). In sensorimotor networks, functional connectivity at rest is reduced before, and increased after, motor signs of disease emerge.[8-11] The ongoing degenerative process eventually disrupts the ability of a given network to assume the different functional states needed to maintain, for instance, normal motor performance, so that the first subtle motor signs of Huntington's disease emerge.[12] Hyperconnectivity in motor-manifest Huntington's disease may then reflect a compensatory effort to maximize network activity of the remaining neuronal populations within the connected regions. This may come at the expense of flexibility of these connections when complex motor tasks require dynamic network activity. For example, the sensorimotor network needs to assume different activity states necessary to initiate, maintain or terminate a movement. This could explain the association of increased functional connectivity at rest with poorer motor performance.[10,11]

The degenerative process in Huntington's diseases particularly affects connectivity between key, or hub, regions for network function such as the caudate nucleus, thalamus and prefrontal regions.[13,14] It remains less well understood how these important regions themselves function in Huntington's disease and how their local function relates to their endowment with specific neurotransmitter systems. Conceivably, overall network function depends on intact white matter connections between the above regions and functional integrity of the regions themselves.[15] As long as overall network function is maintained carriers of the Huntington's disease-causing *HTT* mutation remain in the premanifest phase. In contrast, in the very early clinically manifest stages of Huntington's disease, the disease process will have affected the connections between regions, function within important hub regions, such as caudate nucleus and putamen, or a mixture of both, ultimately resulting in network dysfunction and the emergence of clinical signs of Huntington's disease. Caudate nucleus and putamen (striatum) play an important role in movement, cognition and emotion regulation as a hub region within the dopaminergic system[16,17]; the striatum contains dopamine receptors and transporters that are consequently lost in Huntington's disease.[18-20] Pharmacological interventions targeting the dopaminergic system such as dopamine receptor antagonists or inhibitors of presynaptic vesicular uptake of dopamine can influence the motor phenotype in Huntington's disease.[21] Medication, such as L-dopa or dopamine antagonists, modulates functional connectivity of striatal regions.[22] Therefore, striatal function and its role in causing abnormal movements in Huntington's disease may be closely linked to the dopamine neurotransmitter and transporter system.

Here, we investigated regional brain functional and structural alterations in Huntington's disease and their relationship to neurotransmitter systems with high expression in important regional brain hubs in Huntington's disease, in particular caudate nucleus and putamen, both of which are central to maintain normal motor behaviour. We hypothesized that in premanifest Huntington's disease, function in regional hubs, in particular caudate nucleus and putamen, remains normal despite substantial atrophy. In contrast, in early manifest Huntington's disease, we expected to see changes in local brain function in association with the presence of clinical symptoms, in particular in the motor domain. Given the clinical evidence of improvements of the degree of motor dysfunction with medication that targets the dopamine transmitter system we further expected to observe local brain dysfunction, in particular in those regions that express dopamine receptors.

Materials and methods

Participants

We included two cohorts (the first cohort was recruited at Ulm university, the second at Aachen university) of mainly right-handed participants (five left-handers) with a molecular genetic diagnosis of a CAG repeat expansion (≥39) in the Huntingtin gene. For each cohort separately, we recruited a healthy volunteer group (controls) matched for age and sex with the respective Huntington's disease group (Table 1). Premanifest Huntington's disease participants had a diagnostic confidence level score of ≤2 on the motor part of the Unified Huntington's Disease Rating Scale (UHDRS[23]); manifest Huntington's disease had a diagnostic confidence level score of 4, reflecting the presence of unequivocal motor signs of Huntington's disease. The first cohort (32 manifest, 23 premanifest, 49 controls) served to generate data for all initial exploratory analyses with the key hypotheses and findings pre-registered at https://osf.io/q2nyr. Data from the second cohort (29 manifest and 39 controls) were used for subsequent independent replication of any effects observed in the first cohort according to the pre-registered analysis plan (https://osf.io/q2nyr).

Table 1 Demographic, clinical and *HTT* CAG repeat characteristics of all groups

–	Cohort 1			Cohort 2		
	ManHD	HC	PreHD	HC	ManHD	HC
n	32	30	23	19	29	39
Age, years	47.9 (8.6)	46.6 (9.6)	40.6 (8.6)	44.2 (9)	52.2 (9.9)	50.3 (13.6)
Sex (M/F)	22/10	18/12	9/14	10/9	17/12	18/21
UHDRS TMS	20.1 (12.6) *	0.6 (0.9)	3.9 (3.2) *	1 (1.2)	34.1 (18)	–
UHDRS TFC	11.5 (1.6) *	13 (0)	13 (0)	13 (0)	8.6 (3.2)	–
UHDRS FA	22.9 (2.4) *	25 (0)	25 (0)	25 (0)	19.8 (5.4)	–
CAG repeats	43.3 (1.9)	–	41.8 (1.8)	–	43.7 (3.7)	–
Disease burden	364 (65.5)	–	252.4 (73.4)	–	394.5 (89.7)	–
Handedness (L/both/R)	0/0/32	0/0/30	0/0/23	0/0/19	4/0/25	1/1/37

The first cohort comprised patients with manifest Huntington's disease (ManHD), their age-matched healthy controls (HC), and pre-manifest Huntington's disease (preHD) and their age-matched controls; the second cohort consisted of patients with manifest Huntington's disease and their healthy control group. If available, the mean and standard deviation of the UHDRS subscores, total motor score (TMS), function assessment (FA) and total functional capacity (TFC), the *HTT* CAG repeats and the disease burden score are given. Significant differences regarding age, sex and clinical scores between premanifest Huntington's disease or manifest Huntington's disease and the respective control group are highlighted with asterisks (*$P < 0.001$). Statistical key figures are listed in Supplementary Table 1. F = female; L = left; M = male; R = right.

All participants underwent a thorough neuropsychiatric examination. Participants were clinically characterized using the UHDRS motor scale to derive a total motor score. The UHDRS functional assessment (FA) scale and total functional capacity scale (TFC) were used to measure functional impairment.[23]

Participants with a history of another neurological disorder, a history of head trauma or learning disabilities were excluded from the study. The burden of Huntington's disease pathology was calculated using a formula based on age and CAG repeat length (CAGn-35.5 × age).[24] Participants with a neurological or a psychiatric disorder (other than Huntington's disease) according to the *Diagnostic and Statistical Manual of Mental Disorders*, Fourth Edition (DSM-IV-TR) criteria, substance abuse or dependence were excluded. Participants' consent was obtained according to the Declaration of Helsinki, and the study was approved by the local ethics committees (Ulm University and Aachen University, Germany). Participants gave written informed consent following a complete description of the study's aims and procedures.

MRI data

For structural imaging, in the first cohort 3D magnetization-prepared rapid gradient-echo (MPRAGE) data were acquired using a 3 T Magnetom ALLEGRA (Siemens) head MRI system [echo time (TE) = 3.67 ms; repetition time (TR) = 2200 ms; inversion time (TI) = 1200 ms; slice plane = axial; slice thickness = 1.1 mm]. In the second cohort, a 3 T PRISMA (Siemens) head MRI system was used (TE = 2.98 ms; TR = 2300 ms; TI = 900 ms; slice plane = axial; slice thickness = 1 mm).

T_2^*-weighted (resting-state) images were obtained using echo-planar imaging in an axial orientation (Cohort 1: TR = 2000ms, TE = 30 ms, flip angle 80°, 33 slices, slice thickness 3 mm; Cohort 2: TR = 2210 ms, TE = 30 ms, flip angle 90°, 30 slices, slice thickness 3.1 mm). Participants were explicitly instructed to relax without falling asleep, to keep their eyes closed, not to think about anything special and move as little as possible. None of the patients reported that they had fallen asleep during the rs-fMRI scan.

Preprocessing of imaging data

All resting state fMRI and structural imaging data were preprocessed using Statistical Parametric Mapping software SPM12[25] and the CONN toolbox[26] implemented in MATLAB (v2020b). Functional images were corrected for head motion and distortions (realign and unwarp) followed by co-registration of functional data to structural images. Functional images were normalized into Montreal Neurological Institute (MNI) space using structural information, resampled to a resolution of 3 mm^3 isotropic and spatially smoothed with a 6 mm full width at half maximum (FWHM) Gaussian kernel. The first four frames of the functional images were discarded in order to obtain magnetic equilibrium. Mean white matter and CSF signals as well as 24 parameters of motion[27] were regressed out using the CONN toolbox. Motion parameters were used to identify data to be excluded due to excessive head movement (frame-wise displacement > 3 mm and rotation > 2°).

Resting-state functional MRI

To investigate regional neuronal activity at rest we computed the voxel-wise fractional amplitude of low-frequency fluctuations (fALFF). fALFF expresses the contribution of low-frequency fluctuations within a specific frequency band relative to the whole detectable frequency range.[28] Mathematically, fALFF is the square root of the ratio of summed, squared bandpass filtered (0.008–0.09 Hz) blood oxygenation level–dependent (BOLD) signal to summed, squared, full spectrum BOLD signal over the whole resting-state time course.[28] In addition, as another measure of local activity, we also examined local synchronization as measured by local correlation (LCOR). LCOR is defined as the summed correlation coefficients of BOLD signal in the voxel of interest with other voxels in its proximity, with distances weighted by a Gaussian kernel (25 mm FWHM).[29]

Voxel-wise group comparisons

For each pair-wise comparison, we first regressed out voxel-wise effects of age and sex from the fALFF and LCOR maps using voxel-wise regression coefficients calculated from all study data. Because manifest Huntington's disease participants were older than pre-manifest participants, differences in fALFF and LCOR patterns could result from a mixture of age- and disease-related effects. Therefore, to account for age-related effects, we used voxel-wise regression coefficients calculated from the control data only.[30] This step-wise procedure ensured comparability with the spatial

Table 2 Statistical key data of significant co-localizations between functional alteration and neurotransmitter systems

Cohort	Co-localization		Before atrophy correction			After atrophy correction		
			Fisher's z (r)	Cohen's d	P-value	Fisher's z (r)	Cohen's d	P-value
1	LCOR	D1	−0.21	−1.03	<0.01	−0.17	−0.88	<0.01
		D2	−0.17	−0.8	<0.01	−0.16	−0.76	<0.01
		DAT	−0.18	−1.09	<0.01	−0.15	−0.92	<0.01
		SERT	−0.17	−1.01	<0.01	−0.15	−0.91	<0.01
2	LCOR	D1	−0.17	−0.89	$<0.01_d$	−0.14	−0.7	$<0.01_d$
		D2	−0.13	−0.66	$<0.01_d$	−0.11	−0.52	0.01_d
		DAT	−0.17	−0.74	$<0.01_d$	−0.15	−0.63	$<0.01_d$
		SERT	−0.19	−0.84	$<0.01_d$	−0.15	−0.66	$<0.01_d$
2	fALFF	5-HT1b	−0.25	−1.03	<0.01	−0.16	−0.7	<0.01
		μ	−0.17	−0.84	<0.01	n.s.	n.s.	n.s.

Listed key data are: mean Fisher's z-transformed correlation coefficient across all subjects, effect size Cohen's *d* and P-value. P-values of directed hypothesis testing are labelled with subscript d. DAT = dopamine transporter; n.s. = not significant; SERT = serotonin transporter; μ = μ-opioid receptor.

correlation analyses, which uses this step-wise procedure to account for the effects of confounds. To adjust for the potential impact of local atrophy on fALFF and LCOR alterations, we repeated all analyses after additionally regressing out the voxel-wise grey matter volumes (spatially smoothed with a 6 mm FWHM Gaussian kernel) from all data for each pair-wise comparison.[31]

Voxel-wise analyses of variance for group comparisons were conducted in SPM12. For all comparisons, a voxel-wise threshold of $P < 0.001$ was applied combined with an exact permutation-based (1000 permutations) cluster defining threshold ($P < 0.05$).[32] In addition, to test whether regressing out age removed additional variance associated with Huntington's disease we repeated the voxel-wise group comparisons of Huntington's disease and healthy controls without controlling for age.

Spatial correlations between rs-fMRI data and neurotransmitter receptor distributions

We examined whether Huntington's disease related alterations in fALFF and LCOR were spatially linked to the presence of specific neurotransmitter systems. To this end, we first calculated individual alterations in fALFF and LCOR in each region (the mean of all voxels making up that region) using the Neuromorphometrics atlas (119 regions as provided by SPM12 after excluding white matter and CSF) in each control or Huntington's disease participant. For each participant, we calculated regional z-scores of fALFF or LCOR relative to the mean of the respective control group [(value of Huntington's disease participant) – (mean of controls)/(standard deviation of controls)] in each region so that the z-score reflects how much each Huntington's disease participant differs from normal. Next, for each Huntington's disease participant we computed a Spearman correlation between these 119 z-scores and the distribution of specific receptor/neurotransmitter maps as derived using positron emission and single photon emission computer tomography in independent healthy cohorts. Maps were available for serotonergic (5-HT1a, 5-HT1b, 5-HT2a), dopaminergic (D1, D2), dopamine uptake transporter (DAT) and serotonin transporters (SERT), as well as for dopamine synthesis capacity measured using fluorodopa PET (FDOPA) integrated into the JuSpace toolbox.[33] To approximate a normal distribution, the correlation coefficients were Fisher's z-transformed. An exact orthogonal permutation-based ($n = 10\,000$) P-value was computed to test whether the Fisher's z-transformed correlation coefficients were significantly different from a null distribution.[34] A detailed description of the workflow within the JuSpace toolbox is provided by Dukart *et al.*[33] After identifying which neurotransmitter systems were associated with functional alterations, we computed ANOVAs to test for the effects of drugs on the respective correlation coefficients. For each participant, we included binary fixed factors indicating whether the drugs taken were known to have a main mechanism of action on the respective neurotransmitter systems. To investigate the effect of atlas choice on our findings, we repeated the spatial correlation analyses using the Schaefer cortical parcellation atlas with 100 regions (17 networks)[35] in combination with the subcortical and cerebellar regions (21 regions) from the Neuromorphometrics atlas.

Relationship of structural and functional imaging data with clinical phenotypes

Next, we tested whether the significant co-localizations of fALFF or LCOR with a receptor/transporter identified above related to clinical phenotypes. For this purpose, we computed Spearman correlations of three UHDRS subscores (total motor score, functional assessment, and total functional capacity) with the Fisher z-transformed correlation coefficients that provided a measure of co-localization of fALFF and LCOR alterations with respective neurotransmitter systems. To compare the results in both manifest Huntington's disease groups, we assessed statistical differences regarding the UHDRS subscore, CAG repeats and disease burden. All analyses were corrected for multiple comparisons using the Benjamini–Hochberg procedure.

We then used linear regression analysis (forward selection; probability of F for entry: $P \leq 0.05$) to predict total motor scores in all Huntington's disease participants, premanifest and clinically manifest, with caudate and putamen volumes (mean of left and right, corrected for total intracranial volume), caudate and putamen LCOR, sex, anti-dopaminergic or serotonergic medication (as dichotomous variable) and disease burden as independent variables. In a step-wise linear regression, independent variables are included one at a time in successive order of incremental predictive value (i.e. the predictor explaining most of the variance is entered first). Next, we predicted the clinical classification of premanifest or clinically manifest Huntington's disease. We used the classification by the clinicians; as this is often a judgement call rather than based on data, we also used a classification based on a total motor score of 10 (an arbitrary cut-off) or 14, which based on large data sets distinguished with very high confidence healthy individuals

from Huntington's disease patients with motor manifestations.[36] For this, we computed binary logistic regression analyses with the same variables as for the above linear regression analysis. We did not include medication because only two premanifest Huntington's disease participants were on medication.

Data availability

The data underlying this article will be shared on reasonable request to the corresponding author.

Results

Participants

Patients with manifest Huntington's disease in the first cohort were in the early stages of disease according to their UHDRS total functional capacity score (mean 11.5 SD ± 1.6, so mainly stage 1). In the first cohort, more manifest Huntington's disease participants were male ($\chi^2 = 4.77$; $P = 0.03$) and they were older [$t(53) = 3.13$; $P = 0.003$] than premanifest Huntington's disease. Participants with manifest Huntington's disease in the second cohort had significantly higher UHDRS total motor scores [$t(57) = -3.49$; $P < 0.001$] and significantly lower functional assessment [$t(55) = 2.89$; $P = 0.006$] and total functional capacity scores [$t(56) = 4.44$; $P < 0.001$] than the first cohort, whereas CAG repeats, age, sex and disease burden were similar. Manifest patients in the second cohort were still in the early UHDRS total functional capacity stages of Huntington's disease (mean 8.6, SD ± 3.2, so mainly stage 2). In the first cohort, 12 patients with manifest Huntington's disease took either dopamine receptor antagonists (tiapride $n = 5$; quetiapine $n = 2$; sulpiride, aripiprazole, risperidone each $n = 1$) or tetrabenazine ($n = 2$) and 8 patients were on one or more antidepressants (mirtazapine $n = 5$; citalopram $n = 2$; venlafaxine $n = 1$; sertraline $n = 3$; duloxetine $n = 1$; agomelatine $n = 3$). Fifteen patients were on no medication. In the second cohort, 18 patients were on one or more dopamine receptor antagonists (tiapride $n = 9$; quetiapine $n = 4$; olanzapine, aripiprazole, risperidone each $n = 1$) or tetrabenazine ($n = 4$) and 19 patients took one or more antidepressants (mirtazapine $n = 9$; citalopram $n = 1$; venlafaxine $n = 3$; sertraline $n = 3$; duloxetine $n = 2$; fluoxetine $n = 1$; amitriptyline $n = 1$). Three patients were on no medication. All participants were on stable medication for at least 6 months before the study.

Demographic and clinical details for both cohorts as well as respective group comparisons are provided in Table 1. Key statistical data from the group comparisons are provided in Supplementary Table 1.

Reduced fALFF and increased local synchronization in important hub regions in manifest Huntington's disease

Using voxel-wise analyses, we first explored whether manifest and premanifest Huntington's disease participants differed from controls in the spontaneous resting-state activity (fALFF) or their local synchronization (LCOR). Premanifest participants were similar to their age- and sex-matched controls in voxel-wise fALFF and LCOR. In contrast, fALFF was reduced in early manifest Huntington's disease in the first cohort relative to controls across many cortical areas, basal ganglia, the limbic system and the cerebellum (Fig. 1A). This included the important hub regions bilateral putamen, caudate nucleus, hippocampus, right inferior and superior parietal cortex and left superior frontal regions. In the more progressed early manifest second cohort further hub regions in addition to those in Cohort 1 showed reduced fALFF such as bilateral thalamus, precuneus and insula (Fig. 1C). Manifest Huntington's disease participants also had less fALFF than premanifest participants in bilateral inferior and left superior parietal lobe (Supplementary Fig. 1). The reduced local activity in these regions was accompanied by increased local synchronization (higher LCOR) in early manifest Huntington's disease participants in the cortex (including limbic regions), the thalamus and the cerebellum (Fig. 1A). This pattern was qualitatively similar yet anatomically much more widespread in the clinically more advanced second Huntington's disease cohort (Fig. 1C). Statistical key figures for clusters with significant group differences are provided in Supplementary Table 2. The results were largely similar but less pronounced when not controlling for the effects of age (Supplementary Fig. 2).

Functional brain alterations may be caused by the underlying atrophy of caudate nucleus [right: $t(97) = 6.16$, $P < 0.001$; left: $t(97) = 4.97$, $P = 0.073$] and putamen [right: $t(97) = 5.2$, $P = 0.003$; left: $t(97) = 5.07$, $P = 0.049$] already present in the premanifest Huntington's disease group. To investigate the extent to which atrophy contributed to Huntington's disease functional alterations, we regressed out voxel-wise grey matter volumes from all data. In general, this resulted in reduced cluster sizes in the *t*-contrasts (for statistics, see Supplementary Table 3). No cluster of cortical and subcortical fALFF reductions survived atrophy correction in the first cohort. In the second cohort, the striatal and thalamic fALFF reduction did not survive atrophy correction, whereas clusters comprising frontal, parietal, temporal, occipital and (para-)cingulate areas (cf. Fig. 1D, red) did suggest that in more progressed early manifest Huntington's disease the functional consequences are more pronounced than would be explained by atrophy. Local synchronicity remained significantly increased after atrophy correction in clusters covering frontal, temporal including limbic and cerebellar areas in both cohorts (cf. Fig. 1B and D, blue) including the important subcortical and cortical hub regions bilateral superior parietal cortex (only Cohort 2), hippocampus and superior frontal cortex, left thalamus (only Cohort 1), bilateral precuneus (only Cohort 2) and the cerebellum.

Huntington's disease fMRI alterations relate to dopamine and serotonin system distribution

Next, we examined whether the functional alterations observed in Huntington's disease co-localized with the expression of neurotransmitter systems. To this end, we expressed each Huntington's disease patient's fALFF, or LCOR, as a difference to the mean of controls, normalized by the standard deviation (z-score), and correlated this with the spatial distribution of specific neurotransmitter systems derived from independent cohorts of healthy individuals (Table 2; all statistics are listed in Supplementary Table 4). In premanifest Huntington's disease, no co-localization was found between fALFF or LCOR alteration and the total expression in the brain of any of the evaluated neurotransmitter receptors or transporters. In the manifest Huntington's disease group of the first cohort, there was no significant co-localization with any of the neurotransmitter receptors or transports in regions with altered fALFF, suggesting that the degree of functional change was not related to any of them (Fig. 2A). In addition, a significant association was observed in the second more advanced early manifest Huntington's disease cohort between fALFF alterations and the distribution of the serotonergic 5-HT-1B

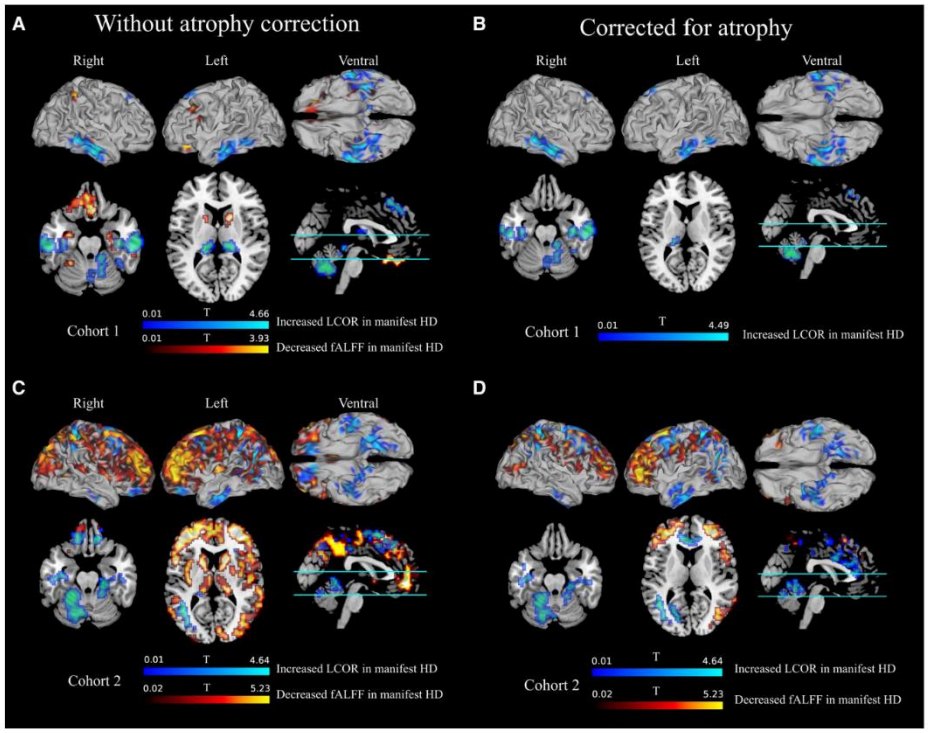

Figure 1 Voxel-wise fALFF and LCOR contrasts of patients with Huntington's disease relative to their respective healthy controls. In a number of clusters where fALFF was significantly reduced in manifest Huntington's disease of the first (**A** and **B**) or second (**C** and **D**) cohort, and LCOR significantly higher in manifest Huntington's disease. *Left panels*: the atrophy-uncorrected contrasts; *right panels*: the atrophy-corrected contrasts. Anatomical regions covered by clusters and the MNI coordinates of the voxel with the peak t-value are listed in Supplementary Tables 2 and 3.

receptor and opioid μ receptor (Fig. 2B). Co-localizations with 5-HT-1B remained significant after correction for atrophy (Supplementary Fig. 3B).

With respect to LCOR, there was a significant negative correlation of LCOR alterations in manifest Huntington's disease with the distribution of the dopaminergic D1 and D2 receptors as well as of the dopamine and serotonin transporters (Table 2 and Fig. 2C). We next examined the dependence of LCOR alteration on the respective receptor/transporter availability for each atlas region (Fig. 3). In both cohorts, LCOR was higher than normal in regions expressing low levels of D1, D2, DAT and SERT signal while regions with the highest signal of D1, D2 and DAT showed increased (caudate), decreased (pallidum and putamen) or no clear assignment (nucleus accumbens) in local synchronization. Regions rich in SERT showed increased (thalamus, amygdala), decreased (basal forebrain, putamen, pallidum) or no clear assignment (nucleus accumbens) in local synchronization in both cohorts (see corresponding rank-rank-plots of the Spearman correlations in Supplementary Fig. 4).

These associations were also significant when comparing manifest and premanifest Huntington's disease after adjustment for age (Supplementary Fig. 5A). All of the associations of LCOR alterations with specific neurotransmitter receptors and transporters observed in the first Huntington's disease cohort were also replicated in comparisons of manifest Huntington's disease of the second cohort with their respective healthy controls (Fig. 2D) and were similar when correcting for atrophy (Supplementary Fig. 3E and F). When using the Schaefer cortical parcellation atlas in combination with the Neuromorphometrics atlas, we find largely similar associations in both cohorts between functional alterations and the respective neurotransmitter systems with and without atrophy correction (fALFF: Supplementary Figs 6A and B and 7A and B; LCOR: Supplementary Figs 6E and F and 7E and F; Supplementary Table 5).

Because we found co-localizations of functional changes with receptors and transporters of the dopaminergic and serotonergic systems, we examined whether anti-dopaminergic (dopamine receptor antagonists or tetrabenazine) or serotonergic medication influenced the observed spatial correlation coefficients. Of 32 patients with manifest Huntington's disease in the first cohort, 12 subjects were taking dopaminergic and 8 serotonergic medications. Of 29 patients with manifest Huntington's disease in the second

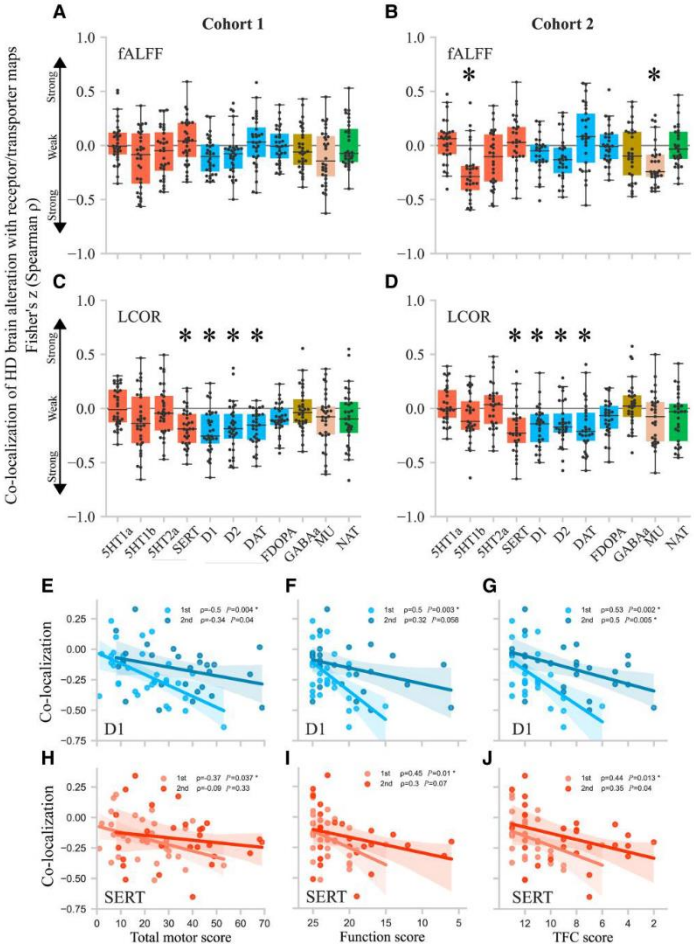

Figure 2 Co-localizations of Huntington's disease brain activity and synchronicity alteration (z-score) with receptor/transporter distribution. The figure plots the correlation (Fisher's z-transformed correlation coefficients) with neurotransmitter maps of the difference of each Huntington's disease patient's fALFF (**A**, Cohort 1; **B**, Cohort 2) or LCOR (**C**, Cohort 1; **D**, Cohort 2) to the mean of controls (z-score). The more the distributions of the correlation coefficients differ from zero, the stronger the correlation of brain activity/synchronicity alteration with the total neurotransmitter signal in the respective cohort of patients with Huntington's disease. The distribution of Fisher's z-transformed correlation coefficients was significantly different from null (*$P < 0.05$) in Cohort 2 for fALFF for 5HT1b ($P < 0.001$) and the μ-opioid receptor (MU, $P = 0.003$) and LCOR in both cohorts for the serotonin transporter (SERT, $P = 0.001$, Cohort 1; $P < 0.001$, Cohort 2); D1 ($P < 0.001$; both cohorts), D2 ($P = 0.003$, Cohort 1; $P = 0.006$, Cohort 2) and dopamine uptake transporter (DAT, $P < 0.001$, Cohort 1; $P = 0.003$, Cohort 2). Because coefficients were negative this indicates a loss of function (fALFF or LCOR) that was spatially correlated to whole-brain expression of the respective neurotransmitter system. Horizontal lines within box plots represent medians, whiskers limit the 1.5-fold of the interquartile range and crosses highlight outliers. Red corresponds to the serotonin system (5HT1a, 5HT1b, 5HT2a, SERT), blue to the dopamine system [D1, D2, fluoro-dopa (FDOPA), DAT], brown to GABAa receptors, beige to the opioid system and green to the noradrenaline transporter (NAT). **E**–**J** show the link between strength of co-localization of LCOR alteration and D1 (**E**–**G**) or SERT (**H**–**J**) expression and motor symptom severity, or functional impairment, derived from the subscores of the Unified Huntington's Disease Rating Scale total motor score (**E** and **H**), functional assessment score (**F** and **I**) and total functional capacity score (**G** and **J**). Brighter and darker blue (D1) or red (SERT) dots correspond to the Fisher z-transformed correlation coefficients and rating scale scores in manifest Huntington's disease of the first or the second cohort. *P*-values are false discovery rate-corrected and ρ the corresponding Spearman correlation coefficients. Lines and coloured backgrounds represent linear fits and the first confidence interval. n.s. = not significant; 1st = Cohort 1; 2nd = Cohort 2.

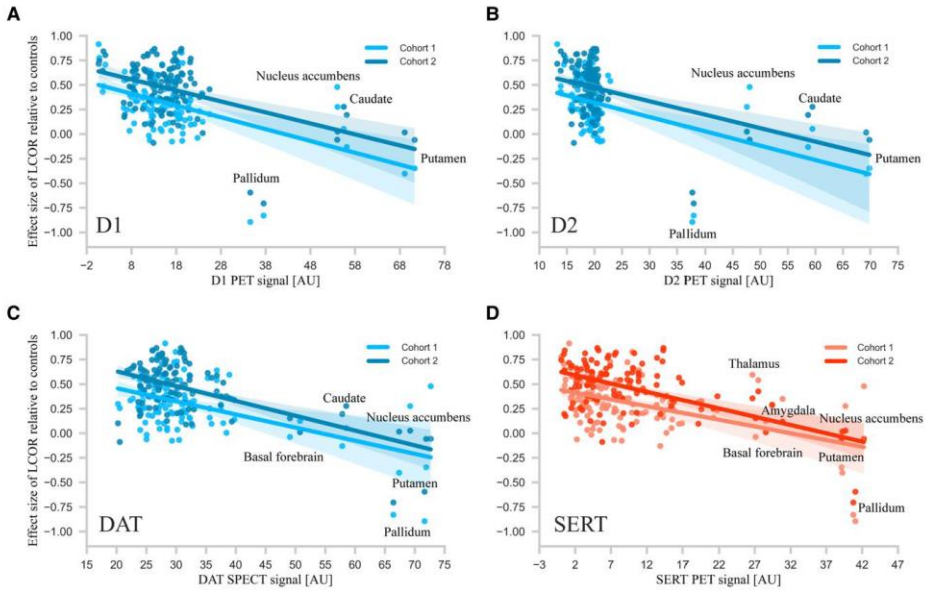

Figure 3 Regional differences in altered synchronicity (LCOR) and their relation to the expression of D1, D2, and transporters of dopamine and serotonin. The figure plots for each region the dependence of effect size (Cohen's *d*) of LCOR alterations after atrophy correction in manifest Huntington's disease with D1 (**A**, blue), D2 (**B**, blue) receptor, dopamine transporter (DAT; **C**, blue) or serotonin transporter (SERT; **D**, red) availability. The correlations between the amount of receptor/transporter expression and LCOR alterations indicate that LCOR is reduced in subcortical regions expressing the most neurotransmitter/receptor and increased in cortical areas with the least expression. Lines represent linear fits and the first confidence interval.

cohort, 18 were taking dopaminergic and 19 serotonergic medications. Except for a weak significant effect of dopaminergic medication on the co-localization of LCOR with DAT in the first cohort [$P = 0.033$; $F(1,28) = 5.04$], dopaminergic or serotonergic medication had no significant effect on the remaining spatial correlation coefficients. Detailed statistics for the respective cohorts can be found in the Supplementary Table 6.

Reduced local synchronization in D1, or SERT, rich regions is associated with symptom severity

We next evaluated whether the strength of the above co-localizations with specific receptors and transporters was also associated with motor or functional impairment observed in the respective manifest Huntington's disease populations. In the first cohort, the strength of co-localization between LCOR alteration (manifest versus controls) and D1, or SERT, signalling was significantly correlated with UHDRS total motor score (D1: $P = 0.004$, $\rho = -0.5$; SERT: $P = 0.037$, $\rho = -0.37$) and functional impairment measured with the UHDRS functional assessment (D1: $P = 0.003$, $\rho = 0.5$; SERT $P = 0.01$, $\rho = 0.45$) and total functional capacity scales (D1: $P = 0.002$, $\rho = 0.53$; SERT: $P = 0.013$, $\rho = 0.44$), suggesting that reduced local synchronization in D1, or SERT, rich regions is associated with motor signs of Huntington's disease increase and patients are more affected in their activities of daily living (Fig. 2E–G). The same correlation was found for the LCOR alteration when comparing manifest with premanifest Huntington's disease (Supplementary Fig. 5B). The correlation between LCOR-D1 co-localization and UHDRS total motor score (not significant after correction for multiple comparisons, $P = 0.04$, $\rho = -0.34$) and total functional capacity score ($P = 0.005$, $\rho = 0.5$) was replicated in the second manifest Huntington's disease cohort (Fig. 2H–J and Supplementary Table 7). Following atrophy correction, correlations between clinical scores and the strength of co-localization of D1 with LCOR remained significant in the first (motor: $P = 0.007$, $\rho = -0.47$; function: $P = 0.017$, $\rho = 0.42$; total functional capacity: $P = 0.016$, $\rho = 0.42$) but not in the second cohort (Supplementary Fig. 8A–F and manifest versus premanifest; Supplementary Fig. 8G–L).

Caudate volume and caudate LCOR predict Huntington's disease motor phenotype

Using a multiple linear regression, we were able to significantly predict total motor score [$R^2 = 0.64$, $F(3,78) = 45.86$, $P < 0.001$]. Volume of the caudate ($\beta = -9.68$, $P < 0.001$; explained variance 51%), LCOR of the caudate ($\beta = 81.17$, $P < 0.001$; explained variance 9%) and disease burden ($\beta = 0.05$, $P = 0.004$; explained variance 4%) all explained a significant part of the variance in the total motor score. Anti-dopaminergic medication did not contribute significantly to the model.

Using a logistic regression, we were also able to significantly predict clinical classification into presymptomatic and manifest

Huntington's disease [$\chi^2(2) = 53.42$, $P < 0.001$]. The model explained 67% of the variance in clinical classification and correctly classified 85.5% of cases. Significant predictors in the classification model were volume of the caudate ($\beta = -2.72$, $P = 0.001$) and disease burden ($\beta = 0.02$, $P = 0.013$). When using clinical classification based on a UHDRS total motor score of 10, we were also able to predict the clinical classification [$\chi^2(3) = 66.40$, $P < 0.001$]. The model explained 75% of variance and correctly classified 92.7% of cases. Significant predictors in that classification model were volume of the caudate ($\beta = -2.76$, $P = 0.001$), LCOR of the caudate ($\beta = 17.35$, $P = 0.027$) and disease burden ($\beta = 0.02$, $P = 0.012$).

Discussion

Inheriting the *HTT* mutation likely promotes events in vulnerable brain regions, such as the striatum, that ultimately result in the loss of neurons, in particular medium spiny striatal neurons.[37] From being structurally normal a long time before unequivocal motor manifestations of Huntington's disease occur, the brains of Huntington's disease gene carriers develop degenerative changes with no or only very minor motor or cognitive differences to healthy controls.[1,38,39] This is accompanied by subtle functional and effective connectivity changes between regions in networks governing motor behaviour or cognition[40-42] until the neurodegenerative changes impact brain function to a degree that causes unequivocal clinical signs of Huntington's disease. It is likely that this event reflects the point in time when brain function can no longer be sufficiently maintained to support normal motor and cognitive functions. In contrast to long-range functional connections, we find that functional activity within cortical and subcortical regions remains normal in the premanifest Huntington's disease phase despite clear evidence of brain atrophy. As long as in a given network the individual grey matter network hubs can maintain their local functionality, the overall functional network capability may suffice to enable normal behaviour without any clinical signs of disease or compromise in the activities of daily living. Our data of reduced regional functional activity in very early manifest Huntington's disease suggest that, subsequently, signs of Huntington's disease emerge when function declines within the important hub regions caudate nucleus, putamen, bilateral superior parietal cortex, hippocampus and bilateral superior frontal regions. As patients advance, the functional abnormalities become more widespread to include further hub regions such as thalamus, precuneus and insula.

As substantial atrophy is not associated with regional functional loss in premanifest Huntington's disease the relationship between structural and functional changes is therefore not linear within the period leading up to the eventual conversion to manifest disease. Structural loss exceeds functional loss, suggesting that networks subserving essential motor behaviours have some functional reserve to compensate for structural loss.[43] When this reserve is exhausted the amount of functional change seems proportional to the degree of atrophy in a narrow time window very early in the motor manifest stage. Even with only slightly more advanced disease, as in the second cohort, the degree of functional change exceeded what would have been predicted if the degree of atrophy related linearly to function. This indicates that the degenerative changes underlying brain atrophy may have to reach a certain threshold to affect function in important network hub regions and cause conversion to clinically manifest disease; following conversion, any further loss of brain tissue can have more pronounced, disproportionate, functional consequences. A model for compensation posits that increased long-range functional network connectivity maintains the level of behaviour despite structural loss.[43] Here, we show that a loss of overall activity in important hub regions may affect how these hubs synchronize their remaining activity. The synchronized cooperative efforts of the hubs within a network, in turn, ensure that network performance can maintain normal behaviour. This was the case in premanifest Huntington's disease where, in addition to normal local activity, a measure of regional synchronicity, LCOR, remained normal, similar to what has been reported for regional homogeneity, a related measure.[44] As clinical signs of network dysfunction emerged in early manifest Huntington's disease, regional synchronicity differed from normal. In contrast to the consistent reduction of fALFF as an indicator for local overall activity, local synchronicity (LCOR) was higher in some regions and lower in others. Independent of structural loss, synchronicity was higher than normal in caudate nucleus, temporal lobe, superior frontal gyrus, supplementary motor area, the limbic system, thalamus and cerebellum while synchronicity was reduced in the putamen.

Local functional activity and synchronicity may depend on the type(s) of neurotransmitters and receptors that contribute to function in a given region. We therefore next related the patterns of several neurotransmitter systems derived from SPECT/PET maps in healthy people to the spatial patterns of structural and functional alterations in Huntington's disease. The synchronicity was reduced mainly in subcortical regions such as the putamen, which are rich in D1, D2, dopamine transporters and serotonin transporters. However, the dopamine receptor-rich caudate nucleus showed markedly increased synchronicity similar to other important regions that were not associated with these neurotransmitter systems. With the exception of the caudate nucleus the dopamine receptor-rich regions most vulnerable to Huntington's disease pathogenesis[19,45] therefore seem to lose their ability to synchronize their local activity. This, in turn, may prompt cortical network partners to over-synchronize, perhaps in an effort to compensate for the consequences the loss of synchronicity in the basal ganglia has for overall network function or simply because they lack the basal ganglia input they normally receive. The Huntington's disease–associated degenerative brain changes affecting important network hub regions thus likely compromise their functional ability and, eventually, after passing a threshold, disrupt the functional homeostasis of networks in which these subcortical and cortical regions play an important role. Indeed, connectivity analyses have suggested that connections between rich club hubs were those most vulnerable.[13,14] Impaired network function then results in the manifestation of clinical signs of Huntington's disease. Our data support the assumption that rich club hub function itself determines their influence on network function relevant for behaviour, showing that increasing dysfunction of dopamine receptor-rich basal ganglia was associated with a higher total motor score and more pronounced impairments in activities of daily living. The caudate nucleus, the region first affected pathologically,[46,47] may play a particularly prominent role given that motor behaviour was worse as synchronicity and atrophy increased in this region. Importantly, caudate nucleus synchronicity significantly improved the models predicting total motor score (in addition to caudate volume and disease burden) or predicting the classification into premanifest or motor manifest Huntington's disease. This emphasizes the particularly relevant contribution of this hub region to the Huntington's disease motor phenotype. The functional connections of the human striatum with many different cortical areas

follow a topographical organization so that specific areas in the striatum form functional units with their cortical partners.[16] In line with this notion, depending on the striatum's respective functional connections with the cortex, i.e. limbic, sensory-motor or executive, dopamine release was observed in the corresponding striatal subdivisions.[17] In Huntington's disease, the degenerative process does not affect the whole striatum indiscriminately.[48] Therefore, the functional consequences within cortico-basal ganglia circuitry likely depend on which striatal subdivisions are most affected. Thus, functional change within the striatum may also not be homogeneous, as shown by our LCOR data that differed in caudate nucleus and putamen. This could, in turn, contribute to different clinical symptoms in Huntington's disease including, but not limited to, abnormal motor behaviour.[12] As the disease advances, functional brain changes may occur in other important brain regions in association with other neurotransmitter systems, as suggested by the significant association between fALFF alterations and the distribution of the serotonergic 5-HT-1B and opioid μ receptors that was only observed in the second, more advanced Huntington's disease cohort.

Fractional amplitude of low-frequency fluctuations and LCOR both estimate local activity. However, there are several conceptual differences. fALFF is based on the amplitude of the local BOLD signal, so it may be more susceptible to non-neuronal processes affecting oxygen delivery (such as heart rate, blood pressure, respiration). Restriction to low frequencies removes some, but not all, of these confounding effects. In contrast, LCOR is presumably more robust to such non-neuronal influences and reflects local connectivity/synchronisation. We cannot distinguish synchronized inhibition from synchronized excitation in a given region. Both lead to an increase in LCOR. Neurotransmitter systems, like dopamine or serotonin, may modulate the quality of local neuronal activity, inhibitory or excitatory, rather than overall BOLD amplitude. This may explain why we observed an association with neurotransmitter systems and LCOR rather than fALFF.

We infer on the evolution of the structure–function relationships and their repercussions for behaviour from cross-sectional data. In addition, our receptor/neurotransmitter distribution data derive from the association with the anatomical distribution of neurotransmitter systems in normal brains, with no direct evidence in Huntington's disease. We therefore interpret our data cautiously. However, the inclusion of two different Huntington's disease cohorts, each with their own matched control group, is a strength of the cross-sectional approach we have taken. A further limitation is that some participants were medicated with drugs targeting the receptors we were examining, e.g. dopamine receptors. Medication may therefore have influenced the function of the regions they target.[22] However, apart from a correlation of anti-dopaminergic medication and DAT data in the first cohort statistical modelling of the influence of anti-dopamine medication or selective serotonin reuptake inhibitors did not change the relationships we report, including for predictions of the motor phenotype. Medication may have had an effect on the motor phenotype and brain function. However, given that medication, in particular anti-dopaminergic medication, had no effect on the prediction model, it must have influenced both function and the motor phenotype in the direction predicted by our regression models. Therefore, we do not think that medication has had a major influence on our data and the conclusions we draw.

Taken together, we show an association between local dysfunction in important network hubs and the emergence of clinical signs of Huntington's disease that is not dependent on the amount of structural loss similar to what has been described in Huntington's disease mouse models.[49] These network hubs belong to the rich club of highly interconnected cortical and subcortical areas so called because of the amount of connections they have to other hubs, suggesting they play a particularly important role in network function.[50] This indicates that the functional integrity of these rich club hub regions is crucial for maintaining functional network homeostasis across all networks in which they are involved, and possibly also between networks.[51] The caudate nucleus emerged as functionally particularly relevant. In the caudate nucleus and the putamen medium-spiny GABAergic projection neurons that receive dopaminergic input are the most abundant type of neuron[18,52]; cholinergic or GABAergic inter-neurons help regulate their activity.[53] Once functional homeostasis can no longer be maintained in the striatum, networks subserving for instance motor behaviour start to fail and motor signs of disease emerge. It remains unclear whether this alone suffices to impact network function and cause a clinical phenotype. Alternatively, network dysfunction may not be caused solely when the hubs themselves are functionally compromised but also involves abnormal connectivity between these rich club network partners.[13,14] Given the extensive white matter changes that can already be observed in very early manifest Huntington's disease,[54] structural properties of network connections are compromised by Huntington's disease pathogenesis. This can impair synchronization of information transfer in relation to the integrity of white matter connections between these partners. We have previously shown that close to the predicted onset of manifest Huntington's disease the timing accuracy of synchronization and desynchronization following transcranial magnetic stimulation input to the motor cortex was affected compared with healthy controls in association with worse performance on a task that requires the repeated initiation, execution and termination of movement.[55] The earliest changes in local synchronicity may be observed in hubs, such as the dopamine receptor-rich caudate nucleus, that are particularly vulnerable to Huntington's disease pathogenesis. Importantly, assessing local synchronicity in the caudate nucleus, in addition to structural measures such as volume, improved predictions of the UHDRS total motor score, a measure of the severity of the Huntington's disease motor phenotype. This points to the importance of distinguishing between the structural and functional impact of expressing mutant huntingtin in the caudate nucleus. This may be different in other disorders in which other networks and their hub regions, and neurotransmitter systems, seem most vulnerable, such as in Parkinson's disease or Alzheimer's disease.[56] Insight into what happens in Huntington's disease could serve as a model for what might be a more general rule in neurodegenerative diseases.

Acknowledgements

We thank all participants for taking part in this research.

Funding

J.D. has received funding from the European Union's Horizon 2020 research and innovation program under grant agreement No. 826421, 'TheVirtualBrain-Cloud'. S.C. and S.B.E. have received funding from the European Union's Horizon 2020 research and innovation program under grant agreement No. 945539 (Human Brain Project SGA3). No funding was received towards this work.

Competing interests

The authors report no competing interests.

Supplementary material

Supplementary material is available at *Brain* online.

References

1. Paulsen JS, Long JD, Ross CA, *et al*. Prediction of manifest Huntington's disease with clinical and imaging measures: A prospective observational study. *Lancet Neurol*. 2014;13:1193-1201.
2. Tabrizi SJ, Langbehn DR, Leavitt BR, *et al*. Biological and clinical manifestations of Huntington's disease in the longitudinal TRACK-HD study: Cross-sectional analysis of baseline data. *Lancet Neurol*. 2009;8:791-801.
3. Wolf RC, Thomann PA, Thomann AK, *et al*. Brain structure in preclinical Huntington's disease: A multi-method approach. *Neurodegener Dis*. 2013;12:13-22.
4. Klöppel S, Gregory S, Scheller E, *et al*. Compensation in preclinical Huntington's disease: Evidence from the track-on HD study. *EBioMedicine*. 2015;2:1420-1429.
5. Wolf RC, Sambataro F, Vasic N, *et al*. Longitudinal functional magnetic resonance imaging of cognition in preclinical Huntington's disease. *Exp Neurol*. 2011;231:214-222.
6. Gregory S, Scahill RI. Functional magnetic resonance imaging in Huntington's disease. *Int Rev Neurobiol*. 2018;142:381-408.
7. Pini L, Jacquemot C, Cagnin A, *et al*. Aberrant brain network connectivity in presymptomatic and manifest Huntington's disease: A systematic review. *Hum Brain Mapp*. 2020;41:256-269.
8. Poudel GR, Egan GF, Churchyard A, Chua P, Stout JC, Georgiou-Karistianis N. Abnormal synchrony of resting state networks in premanifest and symptomatic Huntington disease: The IMAGE-HD study. *J Psychiatry Neurosci*. 2014;39:87-96.
9. Unschuld PG, Joel SE, Liu X, *et al*. Impaired cortico-striatal functional connectivity in prodromal Huntington's disease. *Neurosci Lett*. 2012;514:204-209.
10. Werner CJ, Dogan I, Saß C, *et al*. Altered resting-state connectivity in Huntington's disease: Resting-state connectivity in HD. *Hum Brain Mapp*. 2014;35:2582-2593.
11. Wolf RC, Sambataro F, Vasic N, *et al*. Abnormal resting-state connectivity of motor and cognitive networks in early manifest Huntington's disease. *Psychol Med*. 2014;44:3341-3356.
12. Nair A, Razi A, Gregory S, Rutledge RB, Rees G, Tabrizi SJ. Imbalanced basal ganglia connectivity is associated with motor deficits and apathy in Huntington's disease. *Brain*. 2022;145:991-1000.
13. Harrington DL, Rubinov M, Durgerian S, *et al*. Network topology and functional connectivity disturbances precede the onset of Huntington's disease. *Brain*. 2015;138(Pt 8):2332-2346.
14. McColgan P, Seunarine KK, Razi A, *et al*. Selective vulnerability of rich club brain regions is an organizational principle of structural connectivity loss in Huntington's disease. *Brain*. 2015;138(Pt 11):3327-3344.
15. McColgan P, Gregory S, Razi A, *et al*. White matter predicts functional connectivity in premanifest Huntington's disease. *Ann Clin Transl Neurol*. 2017;4:106-118.
16. Marquand AF, Haak KV, Beckmann CF. Functional corticostriatal connection topographies predict goal-directed behaviour in humans. *Nat Hum Behav*. 2017;1:0146.
17. Tziortzi AC, Haber SN, Searle GE, *et al*. Connectivity-based functional analysis of dopamine release in the Striatum using diffusion-weighted MRI and positron emission tomography. *Cerebral Cortex*. 2014;24:1165-1177.
18. Augood SJ, Faull RL, Emson PC. Dopamine D1 and D2 receptor gene expression in the striatum in Huntington's disease. *Ann Neurol*. 1997;42:215-221.
19. Ginovart N. PET Study of the pre- and post-synaptic dopaminergic markers for the neurodegenerative process in Huntington's disease. *Brain*. 1997;120:503-514.
20. Vonsattel JPG. Huntington disease models and human neuropathology: Similarities and differences. *Acta Neuropathol*. 2008;115:55-69.
21. Burgunder JM, Guttman M, Perlman S, Goodman N, van Kammen DP, Goodman L. An international survey-based algorithm for the pharmacologic treatment of chorea in Huntington's disease. *PLoS Curr*. 2011;3:RRN1260.
22. Grimm O, Kopfer V, Küpper-Tetzel L, *et al*. Amisulpride and L-DOPA modulate subcortical brain nuclei connectivity in resting-state pharmacologic magnetic resonance imaging. *Hum Brain Mapp*. 2020;41:1806-1818.
23. Huntington Study Group. Unified Huntington's Disease Rating Scale: Reliability and consistency. *Mov Disord*. 1996;11:136-142.
24. Penney JB, Vonsattel JP, Macdonald ME, Gusella JF, Myers RH. CAG repeat number governs the development rate of pathology in Huntington's disease. *Ann Neurol*. 1997;41:689-692.
25. Friston KJ, Holmes AP, Worsley KJ, Poline JP, Frith CD, Frackowiak RSJ. Statistical parametric maps in functional imaging: A general linear approach. *Hum Brain Mapp*. 1994;2:189-210.
26. Whitfield-Gabrieli S, Nieto-Castanon A. CONN: A functional connectivity toolbox for correlated and anticorrelated brain networks. *Brain Connect*. 2012;2:125-141.
27. Friston KJ, Williams S, Howard R, Frackowiak RSJ, Turner R. Movement-related effects in fMRI time-series: Movement artifacts in fMRI. *Magn Reson Med*. 1996;35:346-355.
28. Zou QH, Zhu CZ, Yang Y, *et al*. An improved approach to detection of amplitude of low-frequency fluctuation (ALFF) for resting-state fMRI: Fractional ALFF. *J Neurosci Methods*. 2008;172:137-141.
29. Deshpande G, LaConte S, Peltier S, Hu X. Integrated local correlation: A new measure of local coherence in fMRI data. *Hum Brain Mapp*. 2009;30:13-23.
30. Dukart J, Schroeter ML, Mueller K. The Alzheimer's disease neuroimaging initiative. Age correction in dementia—Matching to a healthy brain. *PLoS One*. 2011;6:e22193.
31. Dukart J, Bertolino A. When structure affects function—The need for partial volume effect correction in functional and resting state magnetic resonance imaging studies. *PLoS ONE*. 2014;9:e114227.
32. Eklund A, Nichols TE, Knutsson H. Cluster failure: Why fMRI inferences for spatial extent have inflated false-positive rates. *Proc Natl Acad Sci USA*. 2016;113:7900-7905.
33. Dukart J, Holiga S, Rullmann M, *et al*. Juspace: A tool for spatial correlation analyses of magnetic resonance imaging data with nuclear imaging derived neurotransmitter maps. *Hum Brain Mapp*. 2021;42:555-566.
34. Aickin M. Invalid permutation tests. *Int J Math Math Sci*. 2010;2010:1-10.
35. Schaefer A, Kong R, Gordon EM, *et al*. Local–global parcellation of the human cerebral cortex from intrinsic functional connectivity MRI. *Cerebral Cortex*. 2018;28:3095-3114.
36. Braisch U, Hay B, Muche R, *et al*. Identification of extreme motor phenotypes in Huntington's disease. *Am J Med Genet B Neuropsychiatr Genet*. 2017;174:283-294.
37. Hong EP, MacDonald ME, Wheeler VC, *et al*. Huntington's disease pathogenesis: Two sequential components. *J Huntingtons Dis*. 2021;10:35-51.

38. Gorges M, Müller HP, Mayer IMS, *et al.* Intact sensory-motor network structure and function in far from onset premanifest Huntington's disease. *Sci Rep*. 2017;7:43841.
39. Scahill RI, Zeun P, Osborne-Crowley K, *et al.* Biological and clinical characteristics of gene carriers far from predicted onset in the Huntington's disease young adult study (HD-YAS): A cross-sectional analysis. *Lancet Neurol*. 2020;19:502-512.
40. Wolf RC, Sambataro F, Vasic N, *et al.* Longitudinal task-negative network analyses in preclinical Huntington's disease. *Eur Arch Psychiatry Clin Neurosci*. 2014;264:493-505.
41. Wolf RC, Grön G, Sambataro F, *et al.* Brain activation and functional connectivity in premanifest Huntington's disease during states of intrinsic and phasic alertness. *Hum Brain Mapp*. 2012;33:2161-2173.
42. Wolf RC, Sambataro F, Vasic N, *et al.* Default-mode network changes in preclinical Huntington's disease. *Exp Neurol*. 2012; 237:191-198.
43. Gregory S, Long JD, Klöppel S, *et al.* Testing a longitudinal compensation model in premanifest Huntington's disease. *Brain*. 2018;141:2156-2166.
44. Sarappa C, Salvatore E, Filla A, *et al.* Functional MRI signal fluctuations highlight altered resting brain activity in Huntington's disease. *Brain Imaging Behav*. 2017;11:1459-1469.
45. Pavese N, Politis M, Tai YF, *et al.* Cortical dopamine dysfunction in symptomatic and premanifest Huntington's disease gene carriers. *Neurobiol Dis*. 2010;37:356-361.
46. Rüb U, Seidel K, Heinsen H, Vonsattel JP, den Dunnen WF, Korf HW. Huntington's disease (HD): The neuropathology of a multisystem neurodegenerative disorder of the human brain. *Brain Pathology*. 2016;26:726-740.
47. Wijeratne PA, Young AL, Oxtoby NP, *et al.* An image-based model of brain volume biomarker changes in Huntington's disease. *Ann Clin Transl Neurol*. 2018;5:570-582.
48. Bohnen NI, Koeppe RA, Meyer P, *et al.* Decreased striatal monoaminergic terminals in Huntington disease. *Neurology*. 2000;54:1753-1759.
49. Chang WT, Puspitasari F, Garcia-Miralles M, *et al.* Connectomic imaging reveals Huntington-related pathological and pharmaceutical effects in a mouse model. *NMR Biomed*. 2018; 31:e4007.
50. van den Heuvel MP, Sporns O. Rich-club organization of the human connectome. *J Neurosci*. 2011;31:15775-15786.
51. de Pasquale F, Spadone S, Betti V, Corbetta M, Della Penna S. Temporal modes of hub synchronization at rest. *NeuroImage*. 2021;235:118005.
52. Surmeier DJ, Reiner A, Levine MS, Ariano MA. Are neostriatal dopamine receptors co-localized? *Trends Neurosci*. 1993;16:299-305.
53. Tepper JM, Koós T, Wilson CJ. GABAergic microcircuits in the neostriatum. *Trends Neurosci*. 2004;27:662-669.
54. Tabrizi SJ, Scahill RI, Owen G, *et al.* Predictors of phenotypic progression and disease onset in premanifest and early-stage Huntington's disease in the TRACK-HD study: Analysis of 36-month observational data. *Lancet Neurol*. 2013;12:637-649.
55. Casula EP, Mayer IMS, Desikan M, Tabrizi SJ, Rothwell JC, Orth M. Motor cortex synchronization influences the rhythm of motor performance in premanifest Huntington's disease. *Mov Disord*. 2018;33:440-448.
56. Seeley WW, Crawford RK, Zhou J, Miller BL, Greicius MD. Neurodegenerative diseases target large-scale human brain networks. *Neuron*. 2009;62:42-52.

Supplementary Tables and Figures

Supplementary Table 1: Statistical key data of group comparisons regarding age, sex, and clinical scores.

	Cohort 1: Manifest Huntington's disease vs controls	Cohort 1: Premanifest Huntington's disease vs controls	Cohort 2: Manifest Huntington's disease vs controls
Age	n.s.	n.s.	n.s.
Sex	n.s.	n.s.	n.s.
UHDRS Motor	$t(60)=8.44$, $p<.001$	$t(40)=3.7$, $p<.001$	-
UHDRS TFC	$t(60)=-5.16$, $p<.001$	n.s.	-
UHDRS FA	$t(60)=-4.89$, $p<.001$	n.s.	-

Supplementary Table 2: Anatomical regions covered by clusters of significant group differences in fALFF and LCOR – before atrophy correction.

Anatomical region	Cluster size	Cluster p-values (corrected)	Peak T-values	Peak MNI-Coordinates
COHORT 1: less fALFF in manifest Huntington's disease compared with controls				
Right: Caudate nucleus, putamen, ventral striatum, pallidum, olfactory cortex	179	<.001	5.68	**15 15 6**
Left: Caudate nucleus, putamen, ventral striatum, pallidum	65	0.002	5.60	-12 21 -3
Right: Temporal gyri (middle, inferior)	46	0.013	4.98	54 -21 -15
Left: Orbital gyri (medial, anterior, posterior), superior frontal gyrus (medial orbital) **Bilateral**: Gyrus rectus	127	<.001	4.72	-21 33 -18
Right: Parietal gyri (inferior, superior), postcentral gyrus	58	0.004	4.58	39 -45 51
Left: Cerebellum (4, 5, 6, Crus 1), fusiform gyrus	41	0.024	4.57	-36 -45 -27
Left: Fusiform gyrus, hippocampus, inferior temporal gyrus, parahippocampal gyrus	40	0.024	4.52	-30 -9 -27
Right: Parahippocampal gyrus, fusiform gyrus, hippocampus, inferior temporal gyrus	45	0.014	4.36	36 -21 -24
Left: Frontal gyri (middle, inferior: triangular and opercular part)	44	0.016	4.17	-45 24 33
COHORT 1: less fALFF in manifest Huntington's disease compared with preHD				
Right: Inferior parietal gyrus	39	0.027	4.74	**39 -57 48**
Left: Parietal gyri (inferior, superior)	40	0.024	3.93	-36 -51 45
COHORT 2: less fALFF in manifest Huntington's disease compared with controls				
Bilateral: Caudate nucleus, putamen, ventral striatum, pallidum **Right:** Olfactory cortex	561	<.001	8.50	**-9 9 -3**

Left: Thalamus (pulvinar medial, mediodorsal medial magnocellular, ventral lateral, ventral posterolateral, lateral posterior, pulvinar lateral, mediodorsal lateral parvocellular, anteroventral nucleus, pulvinar anterior), gyrus rectus **Bilateral:** Frontal gyri (middle, superior, inferior (triangular, orbital, and opercular part), superior medial, medial orbital), precentral gyrus, postcentral gyrus, parietal gyri (inferior, superior), supplementary motor area, occipital gyri (middle, superior), precuneus, temporal gyri (middle, superior, inferior), insular, middle cingulate and paracingulate gyrus, anterior cingulate gyrus (pregenual, supracallosal, subgenual), cuneus, rolandic operculum, calcarine fissure and surrounding cortex, paracentral lobule, orbital gyri (anterior, posterior, medial, lateral) **Left:** Inferior temporal gyrus, gyrus rectus **Right**: Heschl gyrus	9506	<.001	8.12	33 45 15
Left: Insula, rolandic operculum, inferior frontal gyrus (opercular part)	80	0.001	5.68	-36 -9 6
Right: Thalamus (pulvinar medial, pulvinar lateral, ventral posterolateral, ventral lateral, mediodorsal lateral parvocellular, lateral posterior, pulvinar anterior, intralaminar, anteroventral nucleus), hippocampus	47	0.021	5.61	21 -27 12
COHORT 1: higher LCOR in manifest Huntington's disease than in controls				
Right: Temporal gyri (inferior, middle), fusiform gyrus, parahippocampal gyrus, hippocampus, thalamus (pulvinar medial, pulvinar lateral, ventral posterolateral, pulvinar anterior, pulvinar inferior, medial geniculate, ventral lateral, lateral posterior), cerebellum (4 & 5)	637	<.001	6.47	**48 -36 -15**
Right: Cerebellum (3, 4, 5, 6, 8, 9, Crus 1, Crus 2), fusiform gyrus **Left**: Cerebellum (3, 6, 7b, 8, 9, Crus 1, Crus 2) **Medial**: Vermis (III-X)	495	<.001	5.44	6 -57 -33
Left: Temporal gyri (inferior, middle), hippocampus, thalamus (pulvinar medial, pulvinar inferior, lateral posterior, pulvinar anterior, pulvinar lateral, ventral posterolateral, medial geniculate, lateral geniculate) fusiform gyrus, parahippocampal gyrus	496	<.001	5.33	-15 -27 0
Bilateral: Superior frontal gyrus (medial, dorsolateral), Supplementary motor area	163	0.003	4.20	-6 27 54
COHORT 2: higher LCOR in manifest HD than in controls				
Left: Parietal gyri (inferior, superior), precuneus, occipital gyri (middle, superior, inferior), postcentral gyrus, temporal gyri (middle, inferior, superior), middle cingulate and paracingulate gyri, cuneus, precentral gyrus, paracentral lobule, posterior cingulate gyrus	1439	<.001	6.07	**-36 -63 24**
Right: Postcentral gyrus, precuneus, parietal gyri (inferior, superior), middle cingulate and paracingulate gyri, paracentral lobule, superior occipital gyrus, precentral gyrus, cuneus, supplementary motor area	774	<.001	5.88	27 -39 45
Left: Precentral gyrus, frontal gyri (superior, middle, inferior (opercular part)), supplementary motor area, paracentral lobule	263	<.001	5.30	-24 -12 48
Bilateral: Supplementary motor area, superior frontal gyrus, medial superior frontal gyrus, middle cingulate and paracingulate gyri **Right:** Frontal gyri (middle, inferior (opercular part)), precentral gyrus	678	<.001	5.22	24 -6 45

Right: Cerebellum (3-5), parahippocampal gyrus, fusiform gyrus	84	0.036	5.03	21 -27 -24
Left: Temporal gyri (inferior, middle), fusiform gyrus, hippocampus	177	0.001	4.94	-45 -18 -24
Left: Cerebellum (6, crus 1), fusiform gyrus, hippocampus, parahippocampal gyrus, precuneus, calcarine fissure and surrounding cortex, thalamus (pulvinar medial), inferior temporal gyrus **Bilateral:** Cerebellum (3,4,5), lingual gyrus, vermis (III-VI)	748	<.001	4.92	-18 -54 -18
Right: Fusiform gyrus, inferior temporal gyrus, parahippocampal gyrus, hippocampus	110	0.013	4.75	45 -15 -27
Left: Orbital gyrus (medial, anterior, posterior), gyrus rectus, frontal gyri (inferior pars orbitalis, middle, superior, medial orbital)	102	0.017	4.57	-12 36 -27
Right: Orbital gyrus (medial, anterior), gyrus rectus, frontal gyri (inferior pars orbitalis, middle), insula	112	0.012	4.53	15 33 -27

Cluster labeling was performed with Automated-Anatomical-Labeling (AAL3) (Rolls et al., 2020), an expansion for SPM12. Highlighted MNI-coordinates indicate the regions with the highest T-value within a cluster. Abbreviation: MNI: montreal neurological institute (brain atlas).

Supplementary Table 3: Anatomical regions covered by clusters of significant group differences in fALFF and LCOR – after atrophy correction.

Anatomical region	Cluster size	Cluster p-values (corrected)	Peak T-values	Peak MNI-Coordinates
COHORT 2: less fALFF in manifest HD than in controls				
Right: Frontal gyri (inferior (orbital, opercular and triangular), middle, superior (dorsolateral and medial)), supplementary motor area	711	<.001	8.13	**33 45 15**
Left: Postcentral gyrus, superior parietal gyrus precentral gyrus, precuneus, supramarginal gyrus, inferior frontal gyrus (opercular part)	578	<.001	5.91	-27 -63 60
Right: Parietal gyri (superior, inferior) postcentral gyrus, precuneus, occipital gyri (middle & superior), cuneus, rolandic operculum, middle cingulate and paracingulate gyri **Left**: Precuneus	530	<.001	5.90	57 -18 27
Left: Frontal gyri (superior, middle, inferior (triangular, orbital, opercular), precentral gyrus, orbitofrontal cortex (posterior) **Bilateral**: Superior frontal gyrus (medial), supplementary motor area **Right**: Middle cingulate gyrus	1410	<.001	5.90	-48 45 3
Left: Temporal gyri (middle and inferior)	43	0.027	4.96	-51 -57 -6
Right: Pre- and postcentral gyrus	63	0.004	4.83	60 0 30

Right: Temporal gyri (middle and superior), middle occipital gyrus, angular gyrus	128	<.001	4.49	42 -66 -12
Right: Inferior frontal gyrus (opercular & triangular part), rolandic operculum	64	0.004	4.37	48 21 12
COHORT 1: higher LCOR in manifest HD than in controls				
Right: Temporal gyri (middle and inferior), fusiform gyrus, parahippocampal gyrus, hippocampus, cerebellum (4, 5, 6)	452	<.001	6.21	**51 -36 -15**
Bilateral: Cerebellum (3, 6, 8, 9, crus 1, crus 2) **Medial**: Vermis (III-X), **Right:** Cerebellum (4,5), **Left**: Cerebellum (7b) Vermis (3 – 10)	464	<.001	5.44	**6 -57 -33**
Left: Temporal gyri (middle and inferior), fusiform gyrus, hippocampus, parahippocampal gyrus, thalamus (pulvinar lateral, pulvinar medial, pulvinar anterior, pulvinar inferior; ventral posterolateral, medial geniculate, lateral geniculate)	351	<.001	5.15	-36 -30 -15
Bilateral: Superior frontal gyrus, supplementary motor area	93	0.025	4.31	-9 24 57
COHORT 2: higher LCOR in manifest HD than in controls				
Right: gyrus, precuneus, middle cingulate and paracingulate gyri, parietal gyri (superior, inferior), paracentral lobule, precentral gyrus, cuneus, supplementary motor area, superior occipital gyrus	678	<.001	6.75	**24 -36 51**
Left: Parietal gyri (inferior, superior), precuneus, occipital gyri (middle, superior, inferior), postcentral gyrus, temporal gyri (middle, inferior, superior), middle cingulate and paracingulate gyri, calcarine fissure, precentral gyrus, cuneus, paracentral lobule, posterior cingulate gyrus, supplementary motor area	1295	<.001	6.11	-36 -33 36
Left: Precentral gyrus, frontal gyri (superior, middle, inferior (opercular)), supplementary motor area, paracentral lobule	346	<.001	5.79	-24 -12 48
Right: Frontal gyri (middle, inferior (opercular)), precentral gyrus **Bilateral**: supplementary motor area, middle cingulate and paracingulate gyri, superior frontal gyrus (medial, superior) **Left**: Anterior cingulate cortex, supracallosal	734	<.001	5.24	21 -3 48
Left: Temporal gyri (inferior, middle, superior), fusiform gyrus	228	<.001	4.94	-45 -21 -33
Bilateral: Cerebellum (3,4,5), lingual gyrus, fusiform gyrus, parahippocampal gyrus **Left**: Cerebellum (6, 10, crus 1), hippocampus, precuneus, calcarine fissure **Medial**: Vermis (III-VII)	644	<.001	4.64	-24 -45 -27
Bilateral: Anterior cingulate cortex (supracallosal and pregenual), medial superior frontal gyrus **Right**: Middle cingulate and paracingulate gyri	213	<.001	4.57	-12 30 21
Right: Fusiform gyrus, inferior temporal gyrus, parahippocampal gyrus, hippocampus	163	0.001	4.48	48 -21 -30

Cluster labeling was performed with Automated-Anatomical-Labeling (AAL3) (Rolls et al., 2020), an expansion for SPM12. Highlighted MNI-coordinates indicate the regions with the highest T-value within a cluster. Abbreviation: MNI: montreal neurological institute (brain atlas).

Supplementary Table 4: Statistical key figures of the co-localization fALFF and LCOR alteration with receptor and transporter maps.

Before atrophy correction

	Cohort 1: Manifest vs controls						Cohort 1: Premanifest vs controls					
	fALFF			LCOR			fALFF			LCOR		
PET/ SPECT	**p**	**z(r)**	**d**	**p**	**z(r)**	**d**	**p**	**z(r)**	**d**	**p**	**z(r)**	**d**
5-HT1$_a$	0.57	0.03	0.15	0.74	0.01	0.08	0.75	0.02	0.11	0.55	-0.04	-0.16
5-HT1$_b$	0.04	-0.12	-0.47	0.07	-0.12	-0.42	0.21	0.08	0.39	0.57	0.04	0.14
5-HT2$_a$	0.23	-0.07	-0.29	0.68	-0.02	-0.1	0.93	0.01	0.02	0.61	-0.03	-0.15
D_1	0.05	-0.1	-0.59	**<0.01**	**-0.21**	**-1,03**	0.80	0.01	0.10	0.69	-0.03	-0.12
D_2	0.18	-0.07	-0.35	**<0.01**	**-0.17**	**-0.8**	0.35	0.06	0.28	0.91	0.01	0.03
DAT	0.61	0.03	0.14	**<0.01**	**-0.18**	**-1,09**	0.82	-0.02	-0.06	0.62	-0.03	-0.18
FDOPA	1	0	0	0.02	-0.1	-0.69	0.56	0.03	0.17	0.78	0.01	0.08
GABA$_a$	0.53	-0.03	-0.16	0.8	-0.01	-0.06	0.79	-0.02	-0.08	0.28	-0.07	-0.34
MU	0.15	-0.1	-0.41	0.16	-0.1	-0.4	0.45	0.06	0.25	0.29	0.09	0.35
NAT	0.9	0.01	0.03	0.16	-0.09	-0.33	0.69	0.03	0.11	0.62	-0.03	-0.14
SERT	0.55	0.04	0.17	**<0.01**	**-0.17**	**-1,01**	0.81	0.02	0.07	0.88	-0.01	-0.05
	Cohort 1: Manifest vs premanifest						**Cohort 2: Manifest vs controls**					
5-HT1$_a$	0.78	0.01	0.07	0.49	0.03	0.22	0.57	0.03	0.15	0.35	0.04	0.21
5-HT1$_b$	0.02	-0.14	-0.61	0.07	-0.12	-0.44	**<0.01**	**-0.25**	**-1.03**	0.06	-0.08	-0.35
5-HT2$_a$	0.28	-0.07	-0.32	0.96	0	-0.01	0.03	-0.12	-0.48	0.79	0.01	0.06
D_1	0.08	-0.08	-0.47	**<0.01**	**-0.16**	**-0.83**	0.09	-0.08	-0.46	**<0.01$_d$**	**-0.17**	**-0.89**
D_2	0.1	-0.09	-0.45	**0.01**	**-0.14**	**-0.64**	0.03	-0.11	-0.58	**<0.01$_d$**	**-0.13**	**-0.66**
DAT	0.56	0.04	0.18	**<0.01**	**-0.13**	**-0.69**	0.30	0.08	0.29	**<0.01$_d$**	**-0.17**	**-0.74**
FDOPA	0.75	-0.02	-0.09	**<0.01**	**-0.14**	**-0.93**	0.93	0	0.03	**0.02**	**-0.09**	**-0.55**
GABA$_a$	0.66	-0.03	-0.13	0.6	0.03	0.16	0.21	-0.07	-0.29	0.46	0.04	0.17
MU	0.09	-0.12	-0.47	0.08	-0.12	-0.50	**<0.01**	**-0.17**	**-0.84**	0.14	-0.09	-0.38
NAT	0.8	-0.02	-0.07	0.39	-0.06	-0.23	0.93	0	-0.02	0.13	-0.08	-0.35
SERT	0.65	0.03	0.14	**<.01**	**-0.14**	**-0.77**	0.67	0.03	0.13	**<.01$_d$**	**-0.19**	**-0.84**

After atrophy correction

	Cohort 1: Manifest vs controls						Cohort 1: Premanifest vs controls					
5-HT1$_a$	0.64	0.02	0.12	0.47	0.03	0.17	0.81	0.01	0.09	0.50	-0.04	-0.19
5-HT1$_b$	0.22	-0.08	-0.29	0.10	-0.11	-0.38	0.17	0.08	0.43	0.55	0.04	0.15
5-HT2$_a$	0.48	-0.04	-0.18	0.89	-0.01	-0.04	0.96	0.00	-0.02	0.53	-0.04	-0.19
D_1	0.80	-0.01	-0.08	**<0.01**	**-0.17**	**-0.88**	0.60	0.02	0.20	0.66	-0.03	-0.13
D_2	0.58	0.03	0.17	**<0.01**	**-0.16**	**-0.76**	0.26	0.07	0.36	0.92	0.01	0.03
DAT	0.12	0.10	0.41	**<0.01**	**-0.15**	**-0.92**	0.90	-0.01	-0.03	0.59	-0.03	-0.20
FDOPA	0.44	0.04	0.21	0.03	-0.09	-0.65	0.44	0.04	0.23	0.74	0.02	0.10
GABA$_a$	0.82	-0.01	-0.06	0.93	0.00	0.02	0.68	-0.02	-0.12	0.27	-0.07	-0.36
MU	0.60	-0.04	-0.14	0.17	-0.10	-0.39	0.33	0.08	0.32	0.32	0.09	0.32

NAT	0.31	0.05	0.26	0.37	-0.05	-0.21	0.65	0.03	0.13	0.66	-0.03	-0.13
SERT	0.13	0.09	0.43	**<0.01**	**-0.15**	**-0.91**	0.70	0.03	0.11	0.84	-0.01	-0.07
	Cohort 1: Manifest vs premanifest						**Cohort 2: Manifest vs controls**					
5-HT1$_a$	0.96	0.00	0.01	0.21	0.06	0.36	0.96	0.00	-0.01	0.24	0.05	0.26
5-HT1$_b$	0.10	-0.10	-0.41	0.10	-0.11	-0.41	**<0.01**	**-0.16**	**-0.70**	0.44	-0.04	-0.17
5-HT2$_a$	0.63	-0.03	-0.13	0.80	0.02	0.07	0.12	-0.09	-0.35	0.50	0.04	0.16
D_1	0.64	-0.02	-0.13	**0.01**	**-0.13**	**-0.69**	0.65	0.02	0.13	**<0.01**$_d$	**-0.14**	**-0.70**
D_2	0.49	-0.04	-0.19	0.02	-0.13	-0.59	0.74	0.02	0.10	**0.01**$_d$	**-0.11**	**-0.52**
DAT	0.50	0.05	0.20	**0.01**	**-0.10**	**-0.56**	0.06	0.16	0.51	**<0.01**$_d$	**-0.15**	**-0.63**
FDOPA	0.86	-0.01	-0.05	**0.00**	**-0.13**	**-0.92**	0.15	0.07	0.39	0.08	-0.07	-0.43
GABA$_a$	0.92	0.01	0.03	0.44	0.05	0.24	0.48	-0.04	-0.18	0.31	0.05	0.24
MU	0.30	-0.08	-0.29	0.09	-0.13	-0.50	0.05	-0.11	-0.53	0.25	-0.07	-0.28
NAT	1.00	0.00	0.00	0.67	-0.03	-0.12	0.45	0.04	0.22	0.46	-0.04	-0.16
SERT	0.61	0.03	0.15	**0.01**	**-0.12**	**-0.67**	0.11	0.12	0.46	**<0.01**$_d$	**-0.15**	**-0.66**

FDR-corrected significant co-localizations are characterized by bold values. P-values of directed hypothesis testing are labeled with subscript d. Listed key figures are: p-value, mean Fisher's z transformed correlation coefficient across all subjects, and the effect size Cohen's d. Abbreviations: DAT: dopamine transporter, FDOPA: fluorodopa, MU: μ-opioid receptor, NAT: noradrenaline transporter, SERT: serotonin transporter. SPECT: single photon emission computed tomography.

Supplementary Table 5: Statistical key figures of the co-localization fALFF and LCOR alteration with receptor and transporter maps using the combined Schäfer and Neuromorphometrics atlas.

Before atrophy correction

	Cohort 1: Manifest vs controls						Cohort 1: Premanifest vs controls					
	fALFF			LCOR			fALFF			LCOR		
PET/ SPECT	p	z(r)	d	p	z(r)	d	p	z(r)	d	p	z(r)	d
5-HT1$_a$	0.65	-0.02	-0.12	0.45	0.03	0.18	0.89	0	0.05	0.51	-0.04	-0.18
5-HT1$_b$	0.98	-0.09	-0.40	0.03	-0.11	-0.52	0.53	0.04	0.19	0.98	0	0
5-HT2$_a$	0.30	-0.05	-0.29	0.75	-0.01	-0.08	0.65	-0.03	-0.13	0.23	-0.07	-0.34
D_1	0.07	-0.08	-0.51	**<.01**	**-0.15**	**-0.90**	0.74	0.02	0.12	0.82	-0.01	-0.07
D_2	0.25	-0.05	-0.32	**<.01**	**-0.17**	**-1.17**	0.67	0.02	0.13	0.71	-0.02	-0.11
DAT	0.79	0.01	0.07	**<.01**	**-0.14**	**-0.95**	0.75	-0.02	-0.09	0.79	-0.02	-0.11
FDOPA	0.60	-0.02	-0.15	0.03	-0.08	-0.73	0.67	0.02	0.12	0.77	0.01	0.09
GABA$_a$	0.96	0	-0.01	0.80	0.01	0.07	0.50	-0.04	-0.20	0.15	-0.10	-0.45
MU	0.15	-0.11	-0.39	0.35	-0.07	-0.29	0.46	0.07	0.23	0.22	0.12	0.44
NAT	0.97	0	0	**<.01**	**-0.12**	**-0.64**	0.63	-0.03	-0.16	0.15	-0.07	-0.43
SERT	0.95	0	0.02	**<.01**	**-0.15**	**-0.92**	0.83	-0.02	-0.07	0.57	-0.03	-0.20
	Cohort 1: Manifest vs premanifest						Cohort 2: Manifest vs controls					
5-HT1$_a$	0.54	-0,03	-0,15	0,3	0,05	0,3	0,13	-0,07	-0,35	0,19	0,05	0,33
5-HT1$_b$	0,05	-0,12	-0,51	0,17	-0,08	-0,35	**<0.01**	**-0,26**	**-1,15**	0,27	-0,06	-0,25
5-HT2$_a$	0,47	-0,04	-0,23	0,53	0,03	0,18	0,02	-0,12	-0,54	0,58	0,03	0,14
D_1	0,10	-0,07	-0,45	**<0.01**	**-0,14**	**-0,8**	0,15	-0,07	-0,41	**<0.01**$_d$	**-0,15**	**-0,75**

D_2	0,23	-0,05	-0,35	**<0.01**	**-0,13**	**-0,78**	0,03	-0,1	-0,61	**<0.01$_d$**	**-0,1**	**-0,56**
DAT	0,72	0,02	0,11	**<0.01**	**-0,12**	**-0,71**	0,34	0,07	0,26	**<0.01$_d$**	**-0,16**	**-0,73**
FDOPA	0,72	-0,01	-0,10	**<0.01**	**-0,11**	**-0,89**	0,74	0,02	0,09	**0,02**	**-0,11**	**-0,64**
$GABA_a$	0,87	0,01	0,06	0,21	0,08	0,4	0,39	-0,05	-0,23	0,26	0,06	0,26
MU	0,09	-0,13	-0,47	0,13	-0,12	-0,45	**<0.01**	**-0,21**	**-0,94**	0,17	-0,1	-0,36
NAT	0,75	0,01	0,09	0,28	-0,05	-0,29	0,57	0,03	0,19	0,03	-0,1	-0,55
SERT	0,82	0,01	0,06	0,02	-0,1	-0,61	0,88	0,01	0,04	**<0.01$_d$**	**-0,18**	**-0,85**

After atrophy correction

	Cohort 1: Manifest vs controls						Cohort 1: Premanifest vs controls					
5-HT1_a	0,36	-0,05	-0,24	0,31	0,05	0,25	0,96	0	-0,02	0,47	-0,04	-0,21
5-HT1_b	0,16	-0,08	-0,33	0,03	-0,11	-0,52	0,50	0,04	0,21	0,93	0	0,02
5-HT2_a	0,25	-0,06	-0,33	0,87	-0,01	-0,04	0,50	-0,04	-0,2	0,19	-0,08	-0,39
D_1	0,72	-0,02	-0,11	**<0.01**	**-0,13**	**-0,81**	0,61	0,02	0,19	0,75	-0,02	-0,10
D_2	0,55	0,03	0,16	**<0.01**	**-0,17**	**-1,15**	0,48	0,03	0,24	0,7	-0,02	-0,12
DAT	0,26	0,06	0,31	**<0.01**	**-0,12**	**-0,81**	0,84	-0,01	-0,06	0,74	-0,02	-0,14
FDOPA	0,73	0,01	0,10	0,06	-0,07	-0,63	0,56	0,03	0,17	0,71	0,02	0,12
$GABA_a$	0,68	-0,02	-0,12	0,72	0,02	0,10	0,34	-0,06	-0,27	0,13	-0,11	-0,48
MU	0,45	-0,06	-0,20	0,32	-0,08	-0,3	0,39	0,08	0,27	0,25	0,11	0,40
NAT	0,56	0,02	0,17	0,05	-0,08	-0,49	0,63	-0,03	-0,17	0,16	-0,07	-0,44
SERT	0,35	0,05	0,27	**<0.01**	**-0,13**	**-0,84**	0,92	-0,01	-0,03	0,49	-0,04	-0,25
	Cohort 1: Manifest vs premanifest						Cohort 2: Manifest vs controls					
5-HT1_a	0,47	-0,03	-0,16	0,13	0,08	0,45	**0,02**	**-0,11**	**-0,53**	0,15	0,06	0,36
5-HT1_b	0,12	-0,10	-0,42	0,15	-0,08	-0,37	**<0.01**	**-0,21**	**-0,9**	0,47	-0,04	-0,16
5-HT2_a	0,78	-0,02	-0,08	0,36	0,05	0,27	**0,01**	**-0,13**	**-0,58**	0,52	0,03	0,15
D_1	0,55	-0,03	-0,17	**0,01**	**-0,11**	**-0,67**	0,93	0	0,03	**<0.01$_d$**	**-0,12**	**-0,62**
D_2	0,80	-0,01	-0,07	**<0,01**	**-0,12**	**-0,71**	0,79	-0,01	-0,08	**0,01$_d$**	**-0,10**	**-0,52**
DAT	0,64	0,03	0,14	**0.01**	**-0,10**	**-0,61**	0,08	0,13	0,48	**<0,01$_d$**	**-0,14**	**-0,61**
FDOPA	0,85	-0,01	-0,05	**<0,01**	**-0,10**	**-0,83**	0,18	0,07	0,35	0,03d	-0,08	-0,49
$GABA_a$	0,71	0,02	0,12	0,14	0,09	0,47	0,30	-0,06	-0,27	0,28	0,06	0,24
MU	0,18	-0,10	-0,38	0,11	-0,13	-0,46	**0,01**	**-0,16**	**-0,68**	0,37	-0,06	-0,22
NAT	0,58	0,02	0,15	0,68	-0,02	-0,11	0,35	0,05	0,31	0,15	-0,06	-0,33
SERT	0,70	0,02	0,11	0,05	-0,09	-0,51	0,18	0,09	0,37	**<0.01$_d$**	**-0,15**	**-0,69**

FDR-corrected significant co-localizations are characterized by bold values. P-values of directed hypothesis testing are labeled with subscript d. Listed key figures are: p-value, mean Fisher's z transformed correlation coefficient across all subjects, and the effect size Cohen's d. Abbreviations: DAT: dopamine transporter, FDOPA: fluorodopa, MU: μ-opioid receptor, NAT: noradrenaline transporter, SERT: serotonin transporter. SPECT: single photon emission computed tomography.

Supplementary Table 6: Statistical key figures of the ANOVA of medication effects on the co-localizations with LCOR alteration.

		First cohort: Manifest vs controls					Second cohort: Manifest vs controls				
Receptor/ Transporter	**Effect of**	**Sum of squares**	**df**	**Mean Square**	**F**	**p**	**Sum of squares**	**df**	**Mean Square**	**F**	**p**
D1	Dopamine	0.00512	1	0.00512	0.119	0.733	0.00961	1	0.00961	0.244	0.626
	Serotonin	0.01445	1	0.01445	0.336	0.567	0.01427	1	0.01427	0.362	0.553
	Interaction	0.02555	1	0.02555	0.593	0.338	0.01247	1	0.01247	0.316	0.579
	Residuals	1.20574	28	0.04306			0.98579	25	0.03943		
D2	Dopamine	6.26e-4	1	6.26e-4	0.0119	0.914	0.00586	1	0.00586	0.140	0.712
	Serotonin	0.02078	1	0.02079	0.3947	0.525	0.03586	1	0.03586	0.855	0.364
	Interaction	0.002	1	0.002	0.0381	0.847	0.00964	1	0.00964	0.230	0.636
	Residuals	1.47395	28	0.05264			1.04835	25	0.04193		
DAT	Dopamine	**0.1097**	**1**	**0.1097**	**5.04**	**0.033**	0.0108	1	0.0108	0.203	0.656
	Serotonin	0.027	1	0.027	1.239	0.275	0.0979	1	0.0979	1.836	0.187
	Interaction	0.0105	1	0.0105	0.482	0.493	0.0139	1	0.0139	0.261	0.614
	Residuals	0.6092	28	0.0218			1.3332	25	0.0533		
SERT	Dopamine	0.03172	1	0.03172	1.0757	0.309	0.00540	1	0.00540	0.11278	0.740
	Serotonin	0.03017	1	0.03017	1.023	0.32	0.16047	1	0.16047	3.35447	0.079
	Interaction	0.00126	1	0.00126	0.0427	0.838	4.21e-4	1	4.21e-4	0.00881	0.926
	Residuals	0.82571	28	0.02949			1.19594	25	0.04784		

Significant effect is highlighted in bold numbers. Abbreviations: df: degrees of freedom, SERT: serotonin transporter. F: F-value, p: p-value.

Supplementary Table 7: Correlation of co-localization between LCOR alterations and receptor/transporter with symptom severity.

			Before atrophy correction						After atrophy correction					
			Motor		**Function**		**TFC**		**Motor**		**Function**		**TFC**	
			p	**ρ**	**p**	**ρ**	**p**	**ρ**	**p**	**ρ**	**p**	**ρ**	**p**	**ρ**
Cohort 1	Manifest vs controls	D1	**0.004**	**-0.50**	**0.003**	**0.50**	**0.002**	**0.53**	**0.007**	**-0.47**	**0.017**	**0.42**	**0.016**	**0.42**
		D2	0.269	-0.20	0.082	0.31	0.111	0.29	0.384	-0.16	0.149	0.26	0.225	0.22
		DAT	0.211	-0.23	0.106	0.29	0.097	0.30	0.374	-0.16	0.313	0.18	0.360	0.17
		SERT	**0.037**	**-0.37**	**0.010**	**0.45**	**0.013**	**0.44**	0.102	-0.29	0.065	0.33	0.073	0.32
	Manifest vs premanifest	D1	**0.002**	**-0.53**	**0.002**	**0.52**	**0.001**	**0.56**	**0.021**	**-0.41**	**0.035**	**0.37**	**0.026**	**0.39**
		D2	0.296	-0.19	0.114	0.28	0.135	0.27	0.393	-0.16	0.152	0.26	0.199	0.23
		DAT	0.199	-0.23	0.122	0.28	0.096	0.30	0.391	-0.16	0.336	0.18	0.328	0.18
		SERT	0.051	-0.35	**0.017**	**0.42**	**0.021**	**0.42**	0.130	-0.27	0.079	0.31	0.085	0.32
Cohort 2	Manifest vs controls	D1	0.04_d	-0.34	0.058_d	0.32	$\mathbf{0.005}_d$	**0.5**	0.116_d	-0.24	0.146_d	0.22	0.022_d	0.40
		SERT	0.33_d	-0.09	0.07_d	0.3	0.04_d	0.35	0.391_d	-0.06	0.091_d	0.28	0.047_d	0.34

Significant correlations are highlighted in bold numbers. P-values of directed hypothesis testing are labeled with subscript d. ρ is the Spearman correlation coefficient of the respective correlation analysis. **Abbreviations: DAT: dopamine transporter, SERT: serotonin transporter.**

Figure legends:

Supplementary Figure 1: **Voxel-wise contrasts of patients with manifest Huntington's disease relative to premanifest Huntington's disease gene carriers**. Red and yellow areas show cluster of significant lower fALFF in manifest HD. Anatomical regions covered by the clusters and the MNI coordinates of the voxel with the peak T-value are listed in Supplementary Table 2.

Supplementary Figure 2: Voxel-wise contrasts of patients with Huntington's disease relative to their respective healthy controls without considering age as a covariate. Red and yellow areas show cluster of significant lower fALFF and blue areas show clusters of significant higher LCOR manifest HD.

Supplementary Figure 3: Co-localizations of fALFF and LCOR alteration with neurotransmitter systems after atrophy correction in all pair-wise analyses. Co-localization of fALFF/LCOR alteration with neurotransmitter systems regaring manifest vs controls in cohort 1(**A/E**) and cohort 2 (**B/F**), premanifest vs controls (**C/G**), and manifest vs premanifest Huntington's disease (**D/H**). FDR-corrected significant co-localizations are highlighted by asterisks.

Supplementary Figure 4: Dependence of the ranked LCOR alterations on the ranked receptor/transporter availability. Each scatter plot shows for each region (dot) the rank of the effect size (Cohen's d) of LCOR alteration prior atrophy correction in Huntington's disease (cohort 1 in brighter, cohort 2 in darker blue or red (dopaminergic or serotonergic system)) against the rank of receptor/transporter availability. Lines and colored background represent linear fits and the first confidence interval.

Supplementary Figure 5: Cohort 1: manifest vs premanifest Huntington's disease: Co-localizations of LCOR alteration with neurotransmitter systems (**A:** PET/SPECT maps, **B-G**: Correlation between LCOR-D1 (**B, C, D**) and LCOR-SERT (**E, F, G**) co-localization and clinical symptoms. All results in this figure were obtained prior atrophy correction.

Supplementary Figure 6: Co-localizations of fALFF and LCOR alteration with neurotransmitter systems using the combined Schäfer and Neuromorphometrics atlas before atrophy correction in all pair-wise analyses. Co-localization of fALFF/LCOR alteration with neurotransmitter systems regaring manifest vs controls in cohort 1(**A/E**) and cohort 2 (**B/F**), premanifest vs controls (**C/G**), and manifest vs premanifest Huntington's disease (**D/H**). FDR-corrected significant co-localizations are highlighted by asterisks. Receptors and transporters

belonging to the serotonergic or dopaminergic system are colored in shades of red and blue respectively.

Supplementary Figure 7: Co-localizations of fALFF and LCOR alteration with neurotransmitter systems using the combined Schäfer and Neuromorphometrics atlas after atrophy correction in all pair-wise analyses. Co-localization of fALFF/LCOR alteration with neurotransmitter systems regaring manifest vs controls in cohort 1(**A/E**) and cohort 2 (**B/F**), premanifest vs controls (**C/G**), and manifest vs premanifest Huntington's disease (**D/H**). FDR-corrected significant co-localizations are highlighted by asterisks. Receptors and transporters belonging to the serotonergic or dopaminergic system are colored in shades of red and blue respectively.

Supplementary Figure 8: The effect of atrophy on the link between LCOR-D1 and LCOR-SERT co-localization to clinical scores. Manifest vs controls (**A**, cohort 1 in brighter, cohort 2 in darker color) and manifest vs premanifest Huntington's disease (**B**).

Supplementary Figure 9: Dependence of fALFF alteration on receptor/transporter availability prior atrophy correction. Each scatter plot shows for each region (dot) the effect size (Cohen's d) of fALFF alteration in Huntington's disease (cohort 1 in brighter, cohort 2 in darker color) against the 5-HT1b receptor availability. Lines and colored background represent linear fits and the first confidence interval.

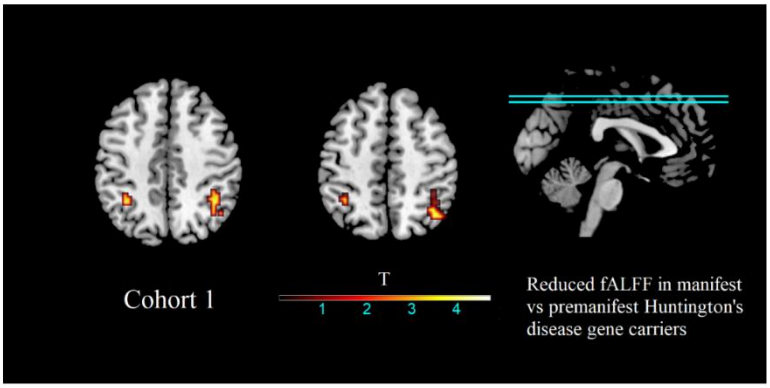

[Supplementary Figure 1]

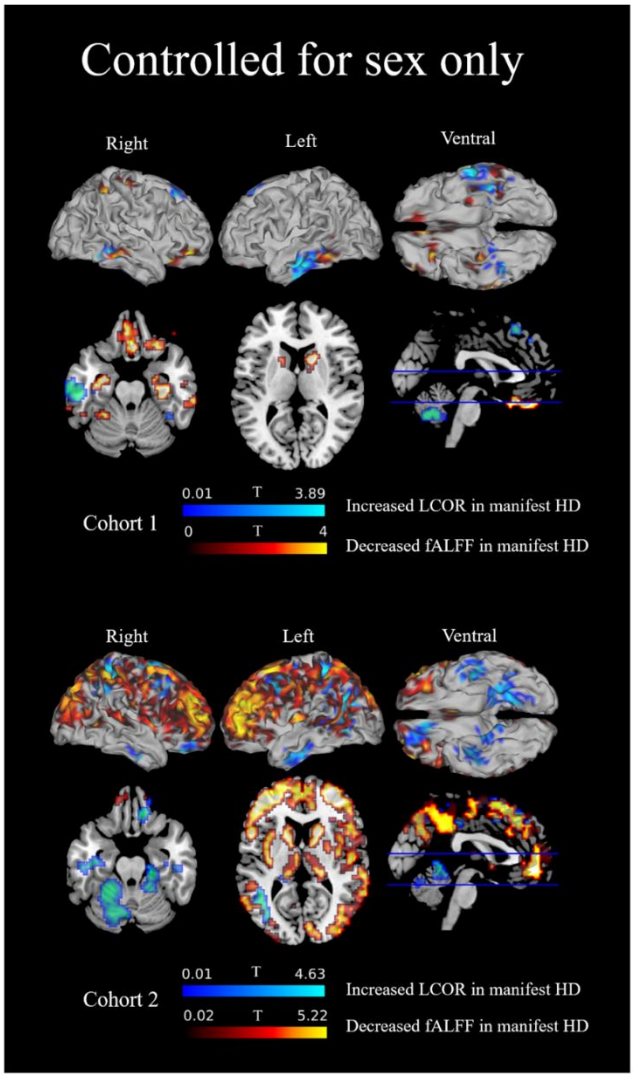

[Supplementary Figure 2]

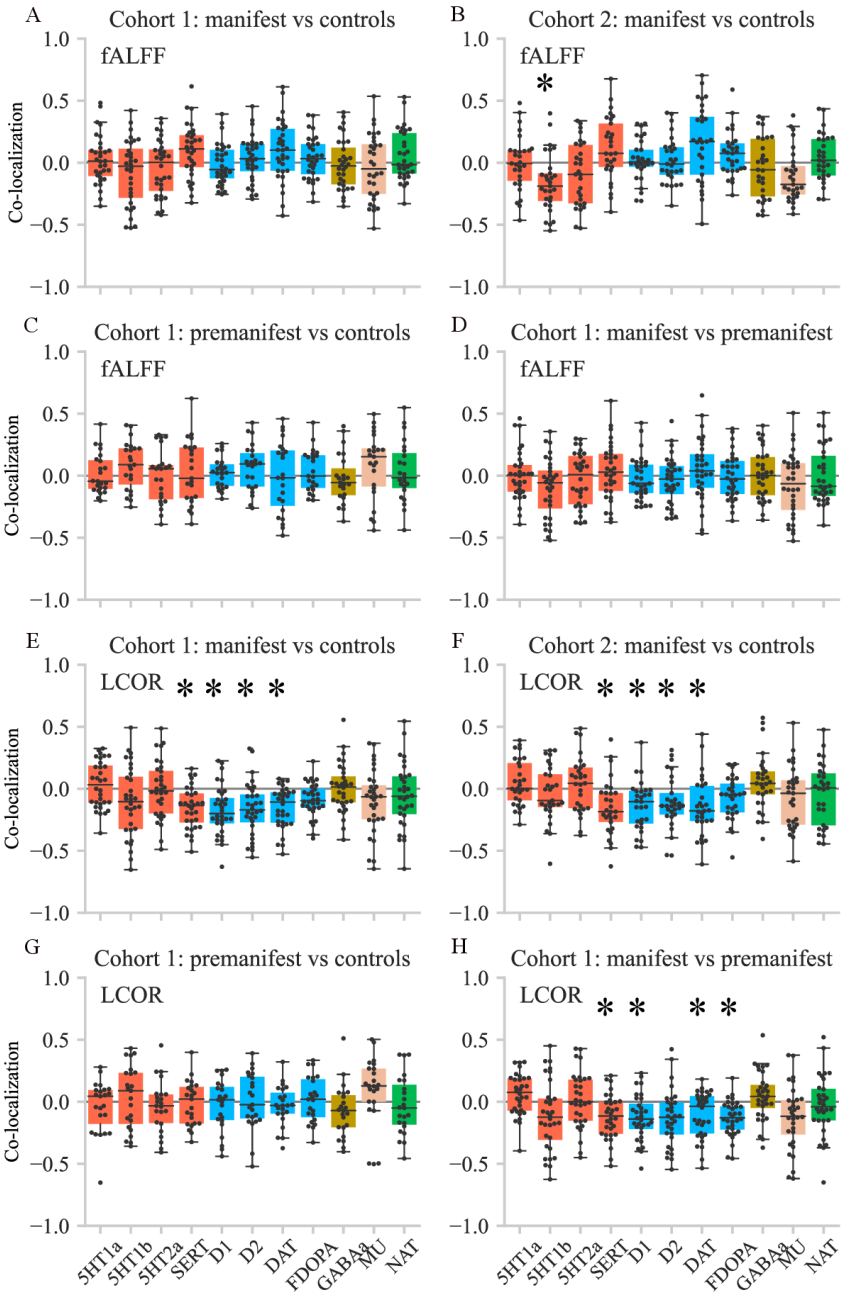

[Supplementary Figure 3]

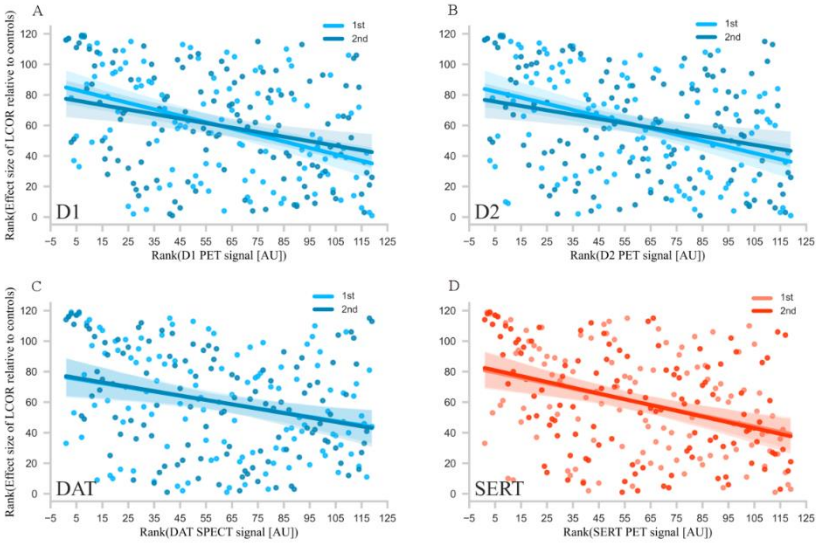

[Supplementary Figure 4]

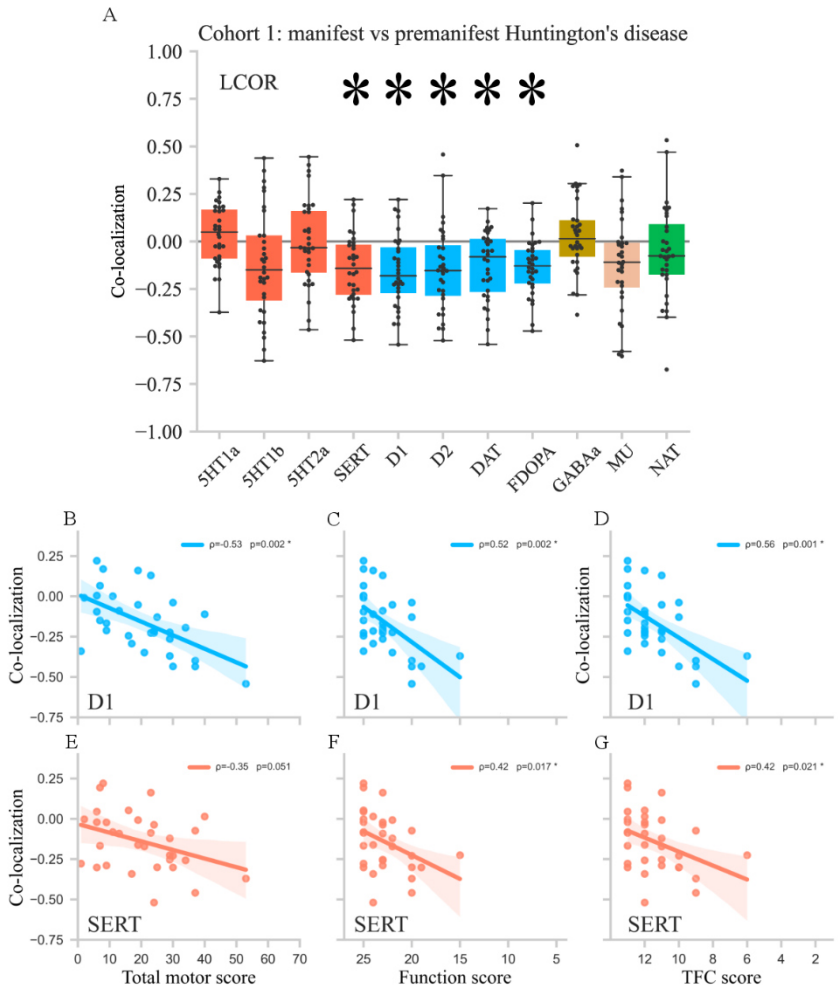

[Supplementary Figure 5]

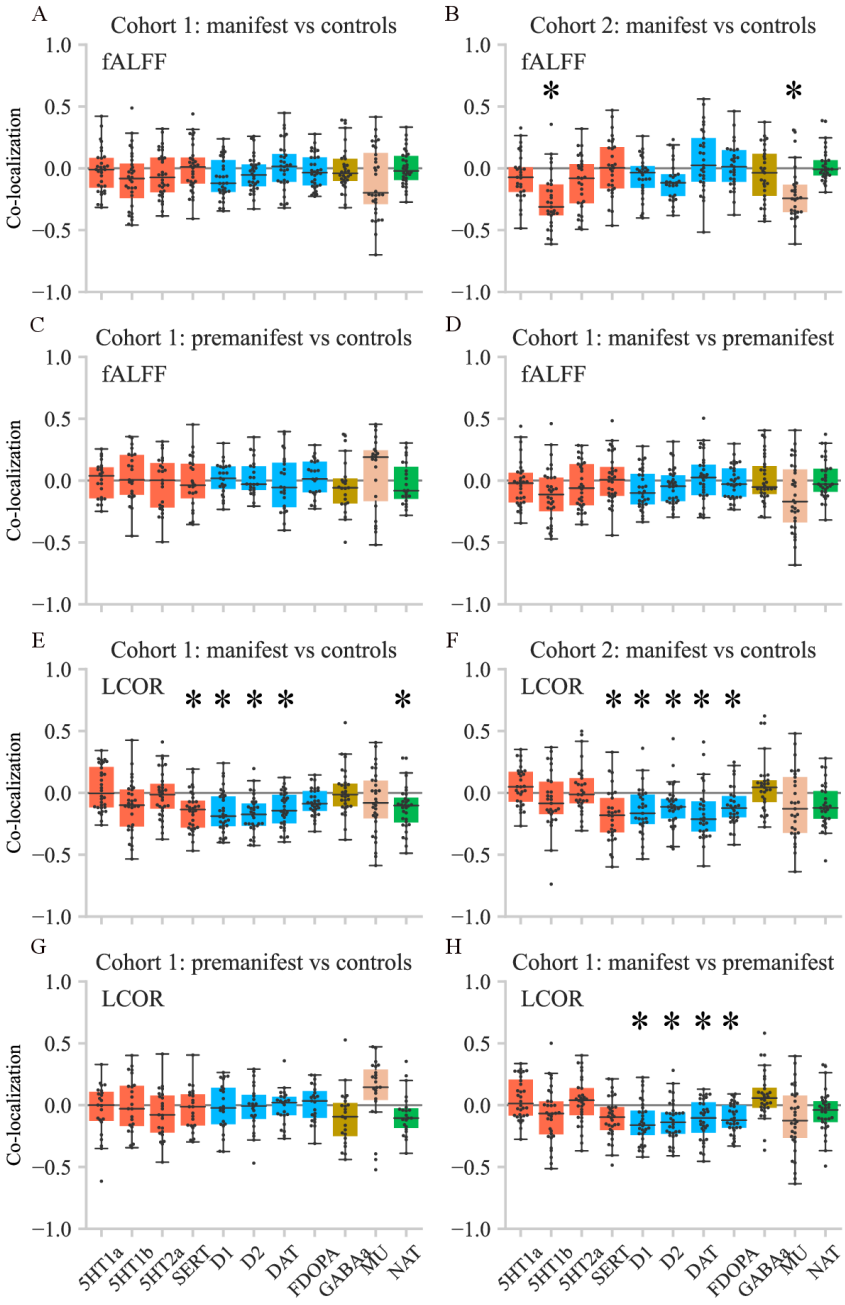

[Supplementary Figure 6]

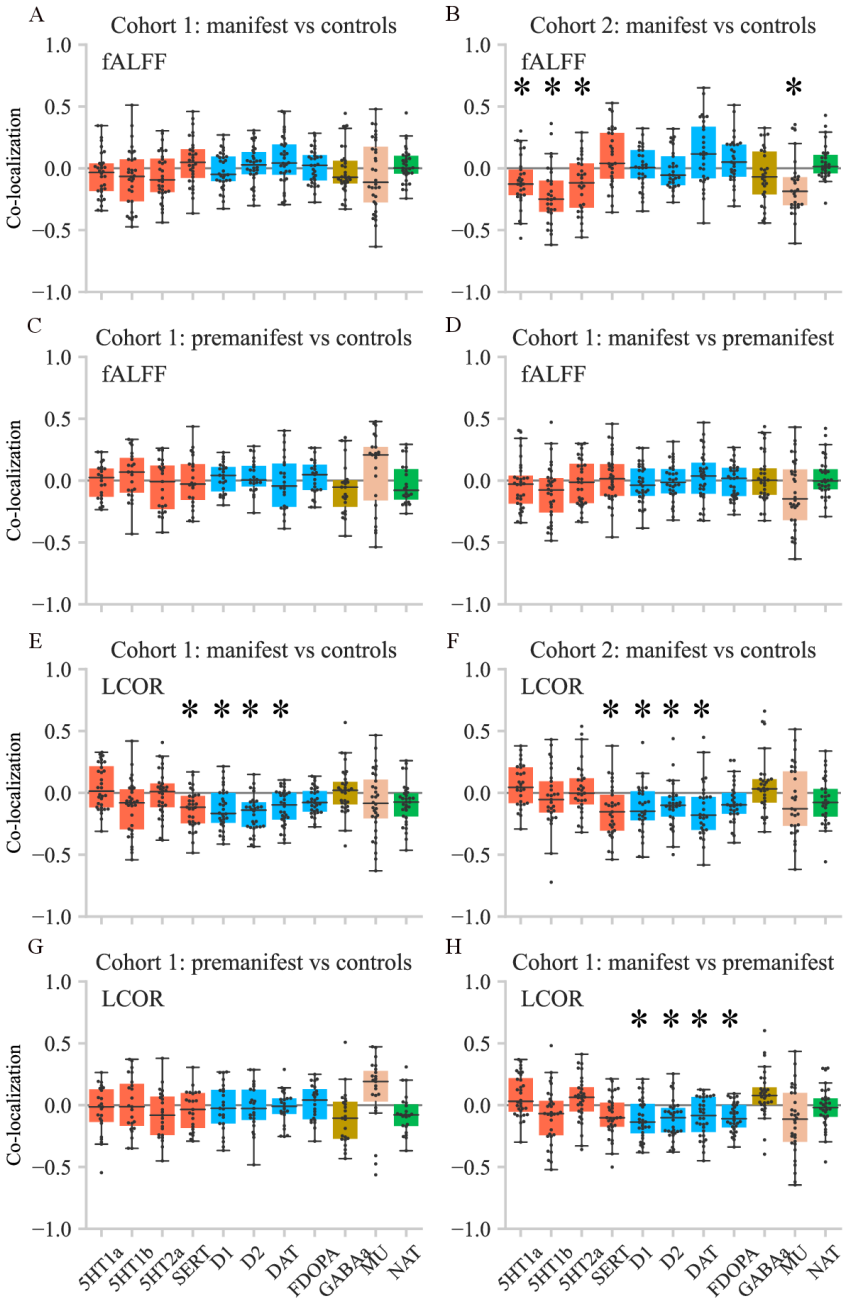

[Supplementary Figure 7]

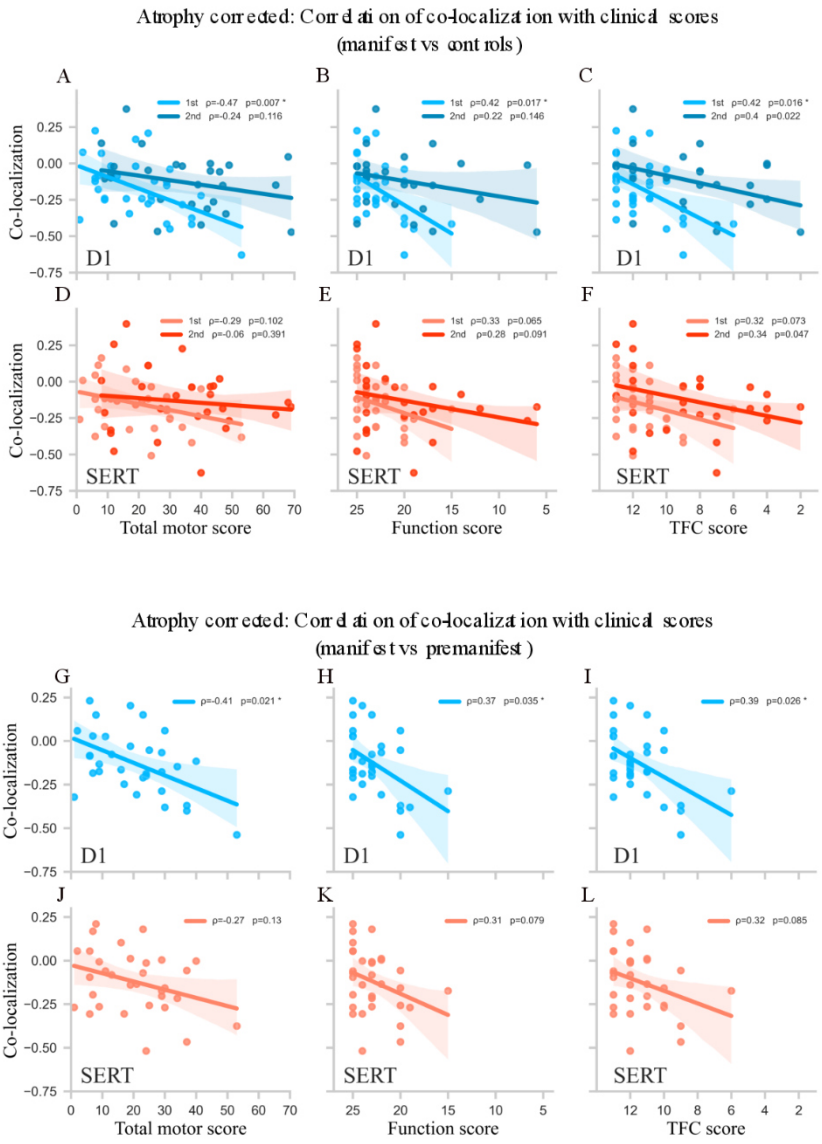

[Supplementary Figure 8]

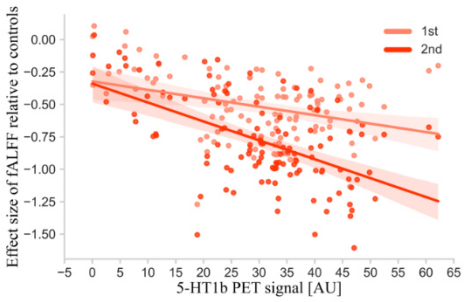

[Supplementary Figure 9]

References

Rolls, E.T., Huang, C.-C., Lin, C.-P., Feng, J., Joliot, M., 2020. Automated anatomical labelling atlas 3. NeuroImage 206, 116189. https://doi.org/10.1016/j.neuroimage.2019.116189

3 Studie 2: Resting-State Changes in Aging and Parkinson's Disease Are Shaped by Underlying Neurotransmission: A Normative Modeling Study

Jan Kasper[1,2], Svenja Caspers[3,4], Leon D. Lotter[1,2,5], Felix Hoffstaedter[1,2], Simon B. Eickhoff[1,2], Juergen Dukart[1,2]

[1]Institute of Systems Neuroscience, Medical Faculty and University Hospital Düsseldorf, Heinrich Heine University Düsseldorf, Düsseldorf, Germany

[2]Institute of Neuroscience and Medicine (INM-7), Research Centre Jülich, Jülich, Germany

[3]Institute for Anatomy I, Medical Faculty and University Hospital Düsseldorf, Heinrich Heine University Düsseldorf, Düsseldorf, Germany

[4]Institute of Neuroscience and Medicine (INM-1), Research Centre Jülich, Jülich, Germany

[5]Max Planck School of Cognition, Stephanstrasse 1A, 04103 Leipzig, Germany

Publiziert in: *Biological Psychiatry: Cognitive Neuroscience and Neuroimaging,* April 26, 2024, https://doi.org/10.1016/j.bpsc.2024.04.010; (162)

Korrespondierender Autor:

Juergen Dukart, PhD
Institute of Systems Neuroscience, Medical Faculty, Heinrich Heine University Düsseldorf
Institute of Neuroscience and Medicine - INM-7: Brain and Behaviour, Research Center Jülich
Wilhelm-Johnen-Straße,
52425 Jülich, Germany
E-Mail: j.dukart@fz-juelich.de

Eigenanteil:

Konzeption des Forschungsansatzes, Studiendesign, Datenverarbeitung & Durchführung statistischer Analysen, Analyse und Interpretation der Daten, Erstellung und Überarbeitung des Manuskripts inklusive der Visualisierungen.

Archival Report

Biological Psychiatry: CNNI

Resting-State Changes in Aging and Parkinson's Disease Are Shaped by Underlying Neurotransmission: A Normative Modeling Study

Jan Kasper, Svenja Caspers, Leon D. Lotter, Felix Hoffstaedter, Simon B. Eickhoff, and Juergen Dukart

ABSTRACT

BACKGROUND: Human healthy and pathological aging is linked to a steady decline in brain resting-state activity and connectivity measures. The neurophysiological mechanisms that underlie these changes remain poorly understood.

METHODS: Making use of recent developments in normative modeling and availability of in vivo maps for various neurochemical systems, we tested in the UK Biobank cohort (n = 25,917) whether and how age- and Parkinson's disease–related resting-state changes in commonly applied local and global activity and connectivity measures colocalize with underlying neurotransmitter systems.

RESULTS: We found that the distributions of several major neurotransmitter systems including serotonergic, dopaminergic, noradrenergic, and glutamatergic neurotransmission correlated with age-related changes across functional activity and connectivity measures. Colocalization patterns in Parkinson's disease deviated from normative aging trajectories for these, as well as for cholinergic and GABAergic (gamma-aminobutyric acidergic) neurotransmission. The deviation from normal colocalization of brain function and $GABA_A$ correlated with disease duration.

CONCLUSIONS: These findings provide new insights into molecular mechanisms underlying age- and Parkinson's-related brain functional changes by extending the existing evidence elucidating the vulnerability of specific neurochemical attributes to normal aging and Parkinson's disease. The results particularly indicate that alongside dopamine and serotonin, increased vulnerability of glutamatergic, cholinergic, and GABAergic systems may also contribute to Parkinson's disease–related functional alterations. Combining normative modeling and neurotransmitter mapping may aid future research and drug development through deeper understanding of neurophysiological mechanisms that underlie specific clinical conditions.

https://doi.org/10.1016/j.bpsc.2024.04.010

Understanding neurophysiological mechanisms that underlie healthy and pathological brain aging is essential for successful prevention, detection, and intervention strategies against age-related diseases and cognitive decline. Despite ample evidence for age-related decline in various brain functional measures, understanding of the neurophysiological mechanisms that underlie these changes is limited. Because the interplay among different neurotransmitter systems contributes substantially to the blood oxygen level–dependent (BOLD) signal, changes in these systems likely contribute to age-related functional alterations as observed using resting-state functional magnetic resonance imaging (rs-fMRI).

Most commonly applied rs-fMRI measures estimate either local activity or synchronicity by assessing temporal changes in regional BOLD amplitude or BOLD signal correlation across regions. Previous rs-fMRI studies have reported aging-related reductions in local brain activity primarily in medial and frontal regions (1–4). These alterations are complemented by reduced local synchronicity in cortical, subcortical, and cerebellar motor structures (5) and increased local synchronicity mainly in hippocampal and thalamic regions (4,6). Positron emission tomography (PET) studies of aging have found reduced serotonergic (7–11), dopaminergic (12–15), glutamatergic (16–18), cholinergic (19), and norepinephrinergic (20) neurotransmission and increased availability of $GABA_A$ (gamma-aminobutyric acid A) (21) and μ opioid (22) receptors. While both modalities point to complex functional reorganization during aging, the relationship between the respective rs-fMRI and PET findings remains poorly understood.

Studying associations between PET-derived regional receptor or transporter availability and rs-fMRI–derived functional signal has been shown to be a promising way to estimate their impact on the observed brain phenotypes (23,24). However, age-related changes in these associations have not been systematically addressed. These changes may reflect altered availability or functional decline of cell populations with corresponding neurochemical properties. Following this logic, disease-related changes in such

ISSN: 2451-9022

associations would support the notion of respective neurotransmitter systems being particularly affected by the respective neuropathology (25).

Understanding of typical age-related colocalization changes of brain function and neurotransmitter systems can inform the study of pathological deviations from such as is observed in Parkinson's disease (PD), for example (25). Normative models, as recently applied to MRI data (26–28), may prove suitable for characterizing such spatial colocalizations. Such models allow individual participants or patients to be compared with the typical trajectories derived from large representative populations by incorporating nonconstant percentiles of variation and variation within the cohort of interest (29).

Previous studies have provided evidence for increased vulnerability of specific neurotransmitter systems in PD including dopaminergic (30–35), serotonergic (36–38), glutamatergic (39,40), GABAergic (34), histaminergic (41), cholinergic (42–44), and norepinephrinergic (45,46) neurotransmission. In our previous work, functional alterations in PD were related to the availability of D_2 and serotonin 1B ($5\text{-}HT_{1B}$) receptors, supporting the notion of specific vulnerability of these neurotransmitter systems (25). However, whether and how far these PD-related alterations deviate from typical age-related colocalization changes remain to be shown.

To address these questions, we adopted a normative modeling approach to testing for aging effects on colocalizations between brain functional measures and underlying neurotransmission in the UK Biobank cohort. We tested for colocalization of PET-derived distributions for major neurotransmitter systems with commonly deployed rs-fMRI–derived activity and connectivity measures during aging and in PD.

METHODS AND MATERIALS

Cohorts

We included 25,917 adult participants from the UK Biobank not diagnosed with psychiatric, cognitive, or neurological disorders (Table S1) with known effects on brain structure and function as a control cohort. We also identified a group of 58 participants from the UK Biobank who were diagnosed with idiopathic PD (ICD-10, G20) before their imaging session. An overview of both groups is provided in Table 1.

Processing of Resting-State Functional Imaging Data

We used rs-fMRI data from the UK Biobank, initially processed according to their documentation (47). We normalized (Montreal Neurological Institute space), smoothed, and bandpass-filtered these images to enhance the signal-to-noise ratio of neuronal activity in the BOLD signal. Control measures were implemented to mitigate confounding effects of motion, white matter, and cerebrospinal fluid. Data quality was further improved by discarding images exhibiting distortions and artifacts, including those attributed to within-scanner motion. Details on preprocessing procedures, metrics calculation, and key figures for data analysis are provided in the Supplemental Methods.

Three complementary voxelwise maps of brain function, including measures of neuronal activity and synchronicity, were derived from individual, preprocessed rs-fMRI data. Fractional amplitude of low-frequency fluctuations (fALFF) (48) was computed as the power ratio of neuronal activity–related oscillations to the total detectable frequency range in the BOLD signal. Local correlation (LCOR) (49) and global correlation (GCOR) (50) characterized BOLD similarity, reflecting the voxel's correlation either with its local vicinity or with all other voxels, respectively.

Aging Effects and Sex Differences in fALFF, LCOR, and GCOR

Both voxelwise aging effects and sex differences were estimated by general linear modeling of (t statistic) contrast maps using a familywise error–corrected voxelwise threshold of $p < .05$ combined with a cluster-defining threshold of $k > 20$ including sex or age and total intracranial volume as covariates, respectively. Maps of annual changes in fALFF, LCOR, and GCOR were generated from voxelwise beta weights.

Spatial Colocalization of Brain Function and Neurotransmitter Systems and Effects of Aging in the Healthy Control Participant Group

We analyzed to what extent unthresholded group-level aging effects (maps of annual change) on fALFF, LCOR, and GCOR colocalized with specific neurotransmitter systems. Spearman correlation coefficients were derived using the default Neuromorphometrics atlas (119 regions), estimating the similarity of

Table 1. Demographic Characteristics of the Study Sample

	HC				
	Combined	Females	Males	Manifest PD	HC Matched to PD
Sample Size	25,917	14,000	11,917	58	17,400
Age, Years	64.03 ± 7.5	63.5 ± 7.4	64.7 ± 7.6	68.6 ± 6.5	67.6 ± 6.0
Age statistics	–	$t_{25915} = -12.48$, $p < .0001$, Cohen's $d = -0.16$		$t_{57.32} = 1.15$, $p = .26$	
Sex, Male	11,917 (46%)	–		32 (55.2%)	8988 (51.7%)
Sex statistics	–	–		$\chi^2_1 = 0.29$, $p = .59$	
TIV, L	1.548 ± 0.152	1.467 ± 0.116	1.643 ± 0.133	–	–
TIV statistics	–	$t_{25915} = -113.0$, $p < .0001$, Cohen's $d = -1.42$		–	–

Values are presented as n, mean ± SD, or n (%). Normative modeling of colocalizations between brain function and neurotransmitter systems was based on the data of HCs. Regional differences in brain measures in patients with PD were calculated with respect to an age- and sex-matched subcohort of HCs.

HC, healthy control participant; PD, Parkinson's disease; TIV, total intracranial volume.

aging effects in fALFF, LCOR, and GCOR with 19 distinct neurotransmitter maps as included in the JuSpace toolbox (25). To approximate a normal distribution, correlation coefficients were Fisher's *z*-transformed. As shown in our previous study (51), the choice of atlas (with a comparable number of parcels) has a negligible effect on the observed colocalization patterns. This atlas was used because it provides a neuroanatomically plausible delineation of cortical and subcortical structures.

Included PET maps were derived from independent healthy volunteer populations and covered serotonergic receptors [5-HT_{1A} (52), 5-HT_{1B} (53), 5-HT_{2A} (52), 5-HT_4 (52), 5-HT_6 (11)], dopaminergic receptors [D_1 (54), D_2 (55)], histamine H_3 receptor (56), dopamine uptake (24), serotonin (SERT) (52), norepinephrine (20), vesicular acetylcholine (VAChT) (57) transporters, cholinergic receptors [M1 (58), $\alpha4\beta2$ (59)], glutamate receptors [mGluR5 (60), NMDA (61)], and cannabinoid CB_1 (62), opioid μ (57), and the $GABA_A$ (24) receptor. Source publications and sample characteristics of each PET map are provided in Table S2. Ninety-five percent confidence intervals of Spearman correlation coefficients were estimated using the Bonett-Wright (63) procedure.

We recomputed correlations with all PET maps using single-participant measures of fALFF, LCOR, and GCOR for greater insight into how group-level aging effects are also reflected in the magnitude and spread across individual data. Before testing for aging effects across individual colocalizations, we examined whether Fisher's *z*-transformed Spearman correlation coefficients of the healthy population differed significantly from a null distribution (1-sample *t* test, alpha = 0.05). Aging effects on colocalization strengths were then estimated using linear regression analyses considering sex as a confound.

Higher Variation in Colocalization Between Brain Function and Neurotransmitter Systems With Aging

Distinct aging trajectories from healthy aging to the effects of diseases and impairments are known to manifest in altered brain function. Depending on the underlying neurophysiological processes, functional changes are likely to be architecturally aligned with the spatial patterns of affected neurotransmitter systems. Correspondingly, one would expect to observe increased variance in colocalizations in older than in younger participants. To test this hypothesis, we examined the heteroscedasticity to identify neurotransmitter systems affected by such age-related brain functional changes in 2 steps.

Using the White test, we first identified all pairs of brain function measures and PET maps whose correlation coefficients exhibited nonconstant variance across age. In a post hoc analysis, we tested for each colocalization pair with nonconstant variance (false discovery rate (FDR)–corrected p [p_{FDR}] $< .05$) whether the variance for individuals in the upper third age-range was higher than that for individuals in the lower third age range using the Goldfeld-Quandt-test (1-sided, i.e., increasing variance). We regressed out sex effects prior to the comparisons.

Normative Modeling of Brain Function: Neurotransmitter Colocalization and Deviations in PD

To model aging effects on the observed colocalization patterns, we generated normative models based on the Fisher's transformed correlation coefficients derived from the healthy participants using the PCNtoolkit (64) (cf. Supplemental Methods for more details on model construction and Figure 1 for a methodological overview).

For participants with PD, deviations (*z* scores) from these normative aging models were derived per neurotransmitter map. For each model, we examined whether the PD deviation scores were significantly different from a null distribution (*t* test, alpha = 0.05) and whether they were correlated with disease duration and cognitive scores (details are provided in Tables S23–S29). We also wanted to know which brain regions contributed most to significant deviations ($p_{FDR} < .05$) and whether functional differences from a normal subpopulation explain these regional contributions. To this end, we repeated the colocalization analysis in the data of the PD group using a leave-one-region-out approach (65) to obtain maps of regional contribution ($\Delta\rho^2$) to the deviation. Furthermore, we calculated regional functional differences (Cohen's *d*) in fALFF, LCOR, and GCOR in PD compared with an age- and sex-matched healthy subgroup (n = 17,400).

All analyses were corrected for multiple comparisons using either the Benjamini-Hochberg procedure or, in case of inflated p values due to large sample sizes, the Bonferroni-Holm correction. Additionally, to minimize the influence of underlying atrophy on colocalization changes, we repeated all analyses after regressing out individual voxelwise gray matter volumes from all functional maps.

RESULTS

Demographic Characteristics

From a total pool of 30,035 participants from the UK Biobank for whom all necessary data were available, our analysis was based on data of 25,917 participants for whom no diseases with known effect on brain function were reported.

The analysis was repeated on 25,914 participants after accounting for age-related atrophy, excluding 3 participants with structural data. Seventy-five participants in the total pool had reported a diagnosis of PD; 58 of them were classified as "manifest" because their first report of PD was dated before their imaging session. To compare regional measures of brain function in patients with PD with those of the healthy control participants (HCs), we defined an age- and sex-matched subcohort consisting of 17,400 participants (mean ± SD age in years: PD = 68.6 ± 6.5, HC = 67.6 ± 6.0, $p > .26$; PD 55.17% male and HC 51.7% male, $\chi^2_1 = 0.29$, $p = .59$). An overview of the groups is provided in Table 1.

Group-Level Aging Effects in Resting-State Measures and Their Colocalization to Underlying Neurotransmission

All 3 functional measures decreased with aging in most cortical, subcortical, and cerebellar regions. Each measure showed a widespread but distinct spatial pattern of age-related alterations with few regional increases (Figure 2A; Tables S3 and S4).

Next, we aimed to understand whether the topography of age-related changes was correlated with distributions of specific neurotransmitter systems. For this, we derived voxelwise

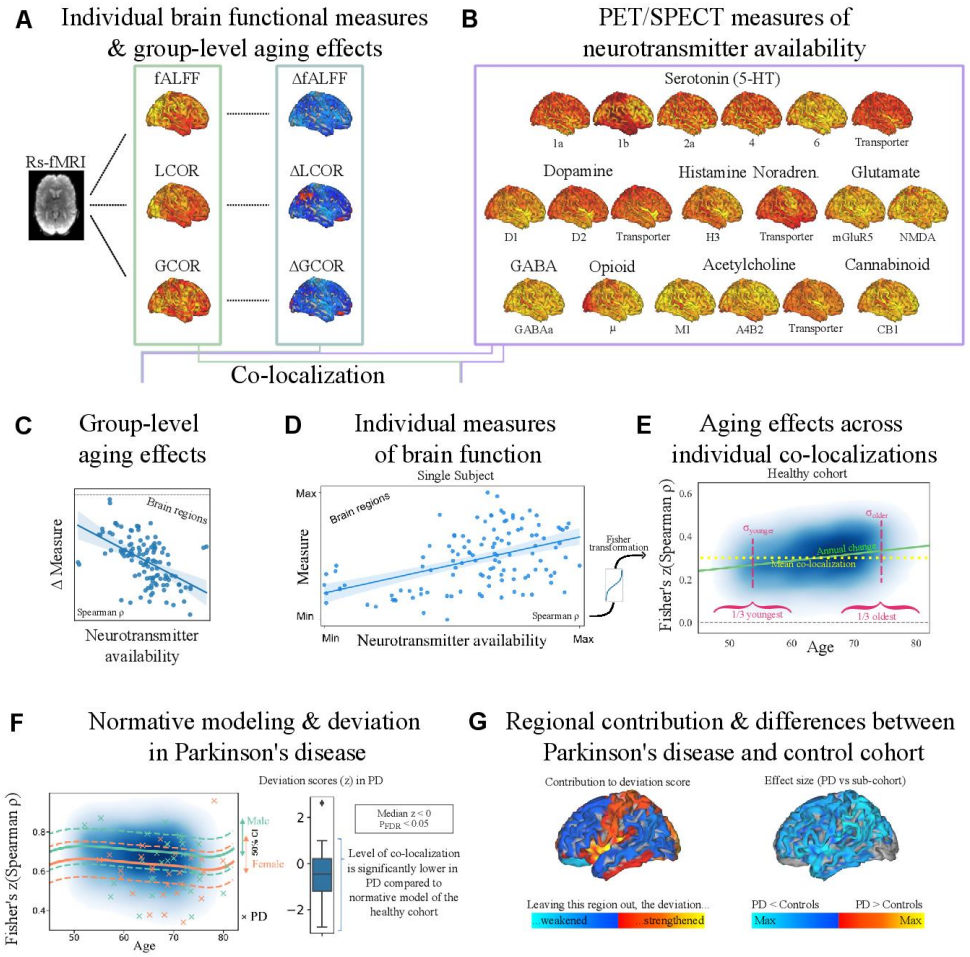

Figure 1. Methodological overview. We derived voxelwise maps of fALFF, LCOR, and GCOR from individual rs-fMRI data **(A)**. First, these data were used to explore group-level voxelwise aging changes in fALFF, LCOR, and GCOR in the healthy cohort ($n_{\text{healthy control}}$ = 25,917) (right column). **(B)** Second, we used PET maps of 19 neurotransmitter systems to calculate the spatial correlation (colocalization) with the **(C)** group-level aging effects and **(D)** individual fALFF, LCOR, and GCOR. **(E)** We Fisher's *z*-transformed the Spearman correlation coefficients ρ to ensure a normal distribution and examined the effects of age on the colocalization data of the healthy cohort. The blue cloud illustrates colocalization strengths (kernel density estimation of all transformed Spearman correlation coefficients) of the healthy cohort. For each pair of measure and neurotransmitter map, we analyzed mean colocalizations (yellow), linear aging effects (green), and differences in variances across participants in the youngest (44–60 years) and oldest (68–82 years) third of the sample (n_{Both} = 8639; red). Vertical dashed red lines were added for illustration purposes only and do not correspond to the actual variance of the respective subpopulation. **(F)** Next, we normatively modeled the colocalization strengths depending on age and sex (left) to calculate the deviation in participants with manifest PD (n_{PD} = 58; crosses). Here, we show the predicted means (solid lines) and 25% and 75% percentile (dashed lines) derived from the normative model for both men (blue) and women (orange). We analyzed whether the deviation (*z*) scores of participants with PD were significantly different from a null distribution (box plot). In this example, the distribution was significantly below a null distribution, indicating that patients with PD exhibited lower Spearman correlation coefficients than the norm. **(G)** Lastly, we quantified the mean regional contribution to the observed deviation score across participants with PD (left), as well as the functional differences in patients with PD compared to an age- and sex-matched subcohort of healthy control participants ($n_{\text{healthy control matched}}$ = 17,900) (right). The functional differences were quantified by calculating the regional effect sizes (Cohen's *d*). fALFF, fractional amplitude of low-frequency fluctuations; GABA, gamma-aminobutyric acid; GCOR, global correlation; LCOR, local correlation; PD, Parkinson's disease; PET, positron emission tomography; p_{FDR}, false discovery rate–corrected *p*; rs-fMRI, resting-state functional magnetic resonance imaging; SPECT, single photon emission computed tomography.

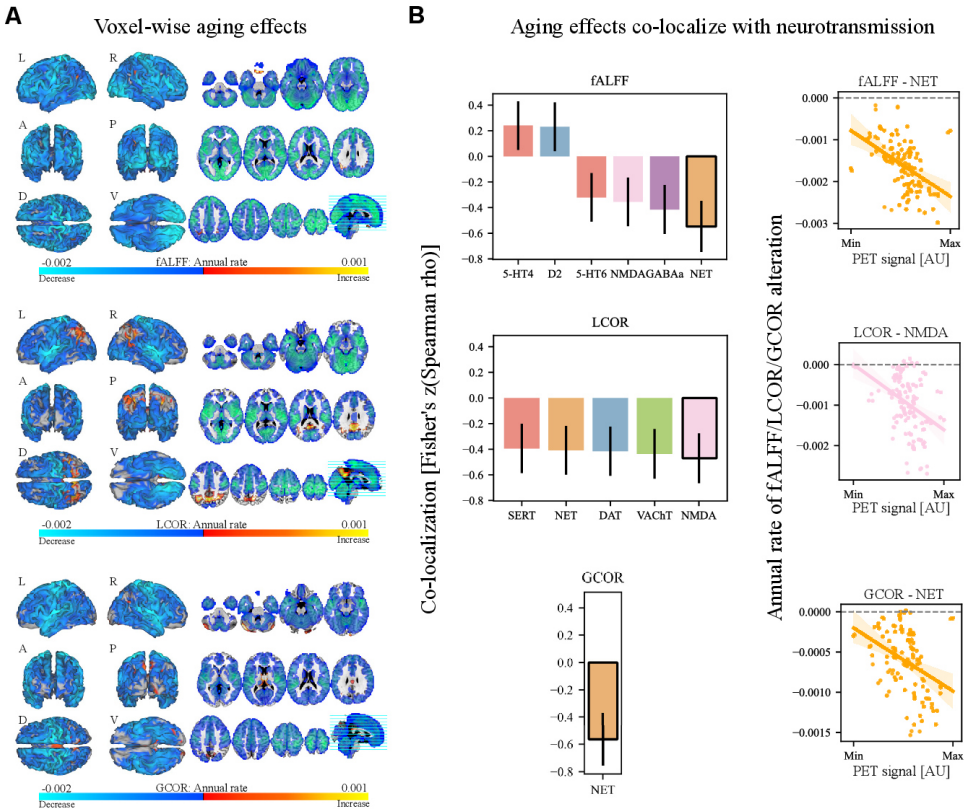

Figure 2. Group-level voxelwise aging effects for each functional measure and associations with neurotransmitter systems. **(A)** Colors in the voxelwise plots of thresholded group-level aging effects indicate annual decrease (blue) or increase (red) in fALFF (top), LCOR (middle), and GCOR (bottom). **(B)** Left column: significant ($p_{FDR} < .05$) linear correlations between annual rate in brain functional measure and neurotransmission. Vertical black lines indicate the uncertainty of Fisher's *z*-transformed Spearman correlation coefficient estimated according to Bonett and Wright (63). Right column: Exemplary scatterplots show how the annual change in fALFF, LCOR, or GCOR spatially correlate with the PET signal of specific neurotransmitter systems. Colors group receptors and transporters of the same neurotransmitter system, i.e., serotonin (red), dopamine (blue), acetylcholine (green), glutamate (pink), and GABA (purple), cannabinoid (mint), opioid (yellow), NET (orange), and histamine (turquoise). A, anterior; AU, arbitrary units; D, dorsal; DAT, dopamine transporter; fALFF, fractional amplitude of low-frequency fluctuations; GABA, gamma-aminobutyric acid; GCOR, global correlation; L, left; LCOR, local correlation; NET, norepinephrine transporter; P, posterior; PET, positron emission tomography; p_{FDR}, false discovery rate–corrected *p*; R, right; SERT, serotonin transporter; V, ventral; VAChT, vesicular acetylcholine transporter.

maps of age-related annual changes in all 3 measures and examined their spatial colocalization with the neurotransmitter systems. Annual changes in fALFF and LCOR were significantly correlated ($p_{FDR} < .05$) with serotonergic, dopaminergic, norepinephrinergic (also GCOR), and glutamate neurotransmission (Figure 2B; Figures S1 and S2; Tables S5 and S6). fALFF and LCOR changes correlated with GABAergic cholinergic neurotransmission, respectively. Except for the correlation between fALFF changes and NMDA, all findings remained significant after correcting for age-related atrophy. Scatterplots of the strongest correlations are shown in Figure 2B. Results for voxelwise sex differences are summarized in Figures S3–S5 and Tables S7–S10.

Individual Colocalization of Resting-State Measures and Neurotransmitter Systems Covaries With Age

The extent to which a specific neurotransmitter system contributed to the measured brain function was evaluated by its correlation strength. First, we computed individual

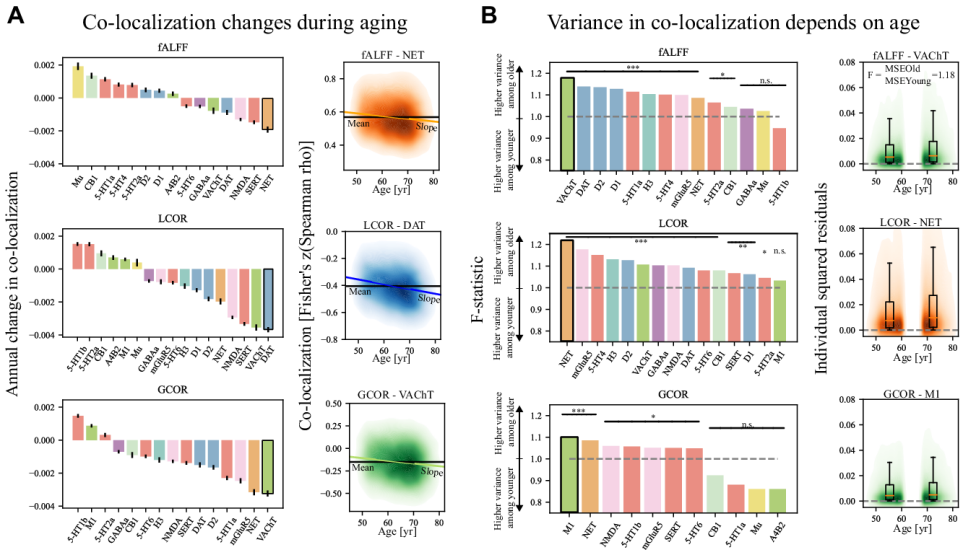

Figure 3. Single-participant colocalizations between brain functional measure and neurotransmitter systems depended on age. **(A)** Left column: overview of all significant linear aging effects ($p_{Bonferroni\text{-}Holm} < .05$) in the colocalization strengths (Fisher's *z*-transformed Spearman correlation coefficients) between each pair of brain functional measure (fALFF, LCOR, GCOR) and neurotransmitter system. Error bars correspond to the standard error of parameter (slope) estimation. Right column: Exemplary plots show how colocalization strengths between brain functional measures (fALFF, top; LCOR, middle; GCOR, bottom) and specific neurotransmitter systems depend on age. The black horizontal line indicates the population mean colocalization (see Figure S6 for an overview of all colocalization means). The colored clouds show the kernel density estimation of Fisher's *z*-transformed Spearman correlation coefficients of the healthy cohort. The slope of the colored line (linear fits) corresponds to the bar plots in the left column. **(B)** Left column: Each plot shows the effect size (*F* statistic) of MSE differences between younger and older adults. We show bar plots regarding neurotransmitter systems whose colocalization with the respective brain functional measure was previously shown to be significantly nonconstant (White test, $p_{FDR} < .05$). All pairs of brain function and PET map whose colocalization variance was significantly ($p_{FDR} < .05$) different in the older and the younger subpopulations are highlighted by asterisks (*$p_{FDR} < .05$, **$p_{FDR} < .01$, ***$p_{FDR} < .001$). *F* statistics (MSE of older adults divided by MSE of younger adults) above 1 correspond to a larger variance in the older subpopulation. Right column: Exemplary plots visualize the individual squared errors of the colocalizations between younger and older adults. Box plots show both distributions. Note that per definition, the squared errors are positive. Due to the kernel density estimation of all squared errors, the colored clouds exceed the null level. Colors group receptors and transporters of the same neurotransmitter system according to the same scheme as described in Figure 2. 5-HT, serotonin; DAT, dopamine transporter; fALFF, fractional amplitude of low-frequency fluctuation; GABA, gamma-aminobutyric acid; GCOR, global correlation; LCOR, local correlation; mGluR, metabotropic glutamate receptor; MSE, mean squared error; NET, norepinephrine transporter; n.s., not significant; PET, positron emission tomography; *p*FDR, false discovery rate–corrected *p*; SERT, serotonin transporter; VAChT, vesicular acetylcholine transporter.

colocalization strengths between each participant's resting-state measure and each neurotransmitter map. Due to the large cohort size, even very small effects in all functional measures were significantly associated with the 19 PET maps (all $ps_{Bonferroni\text{-}Holm} < .001$, median absolute Spearman correlation coefficient ranged from 0.03 to 0.68), with different neurotransmitter systems explaining between 0.1% and 46% of the variance in the respective resting-state measures (Figure S6 and Tables S11–S13, left columns). The direction of the correlations was highly similar across the 3 measures. Positive correlations were found for the norepinephrinergic, muscarinic, glutamatergic, and GABAergic systems and serotonergic receptors 5-HT_{1B}, 5-HT_{2A}, and 5-HT_6. Negative correlations were found for the dopaminergic, histaminergic, and opioid neurotransmitter systems, serotonin receptors 5-HT_{1A} and 5-HT_4, and SERT and VAChT. All associations remained significant after controlling for age-related atrophy (Tables S14–S16). If age-related changes in brain functions are predominantly influenced by specific neurotransmitter systems, correlation coefficients should systematically (that is, in simplest approximation, linearly) increase or decrease during aging. Thus, we evaluated whether and to what extent aging effects and their colocalizations with neurotransmitter systems observed at the cohort level were also reflected in the individual colocalization strength. Most of the observed correlations were significantly associated, with age explaining up to 3%, 4%, and 1% of the colocalization strength between fALFF (with NMDA and SERT), LCOR (with SERT), and GCOR (with VAChT) and the respective neurotransmitter systems, respectively (Figure 3A; Tables S11–S13, middle columns). Correction for atrophy lowered the correlation strengths for most associations, but the findings remained largely significant (Tables S14–S16, middle columns).

Variance in Colocalization Changes During Aging

Because aging might not only have affected average colocalization strengths but might also have led to increased variance (i.e., due to undetected neurodegenerative processes in a subpopulation), we tested for such changes using a 2-step procedure. Using the White test, we identified significant nonconstant variance in colocalization strength. For fALFF and LCOR, nonconstant variance was observed for all neurotransmitter classes, except for LCOR and the opioid system. For GCOR, significant nonconstant variance in colocalization was found for serotoninergic, norepinephrinergic, cannabinoid, opioid, glutamatergic, and cholinergic neurotransmission (Table S17, left columns). These effects remained significant after controlling for atrophy except for GCOR and 5-HT_{1B}, 5-HT_6, and SERT (Table S18, left columns). Because the previous analysis only detected differences in variance across age but not their direction, we proceeded to perform the Goldfeld-Quandt test. Here, we compared the colocalization variance between the youngest (44–60 years) and oldest (68–82 years) third (n_{Both} = 8639) of the study population for the previously identified significant nonconstant variances (Figure 3B).

For fALFF and LCOR, higher variability in colocalization was found in the older subpopulation for serotonergic, dopaminergic, noradrenergic, histaminergic, cannabinoid, glutamatergic, and cholinergic neurotransmission. In addition, for LCOR, we found significantly higher variance in the older population in colocalization with the GABA system. For GCOR, higher variability in colocalization was found regarding the serotonergic, noradrenergic, glutamatergic, and cholinergic system. The number of neurotransmitter colocalization pairs, as identified using the White test, that showed a higher variance in the older subpopulation was 11 of 14 for fALFF, 14 of 15 for LCOR, and 7 of 11 for GCOR (Figure 3B; Table S17, right columns). The effects remained largely similar after controlling for atrophy (Table S18, right columns).

Deviations From Normal Colocalization in Manifest PD

Having established this reference for colocalization of normal age-related changes with different neurotransmitter systems, next we aimed to test whether and how functional changes caused by progressive neurodegeneration deviated from the nonpathological colocalization patterns. For this, we adopted a normative modeling approach using the healthy aging population as a reference (models are visualized in Figures S7 and S8). A UK Biobank subgroup of patients with PD served as an example for the clinical relevance of our findings. For fALFF, patients with PD had a lower colocalization strength with serotonergic, GABAergic, muscarinic, and glutamatergic neurotransmission (Figure 4D). For LCOR and GCOR, patients with PD showed lower colocalizations with serotonergic, dopaminergic, GABAergic, histaminergic, norepinephrinergic, glutamatergic, and cholinergic neurotransmitter systems (Figure 4E, F; Table S19). The deviation in colocalization strength regarding LCOR and $GABA_A$ (Figure 4A, B) was negatively correlated with disease duration, with higher deviations being indicative of longer disease duration (Pearson's $r = -0.38$, $p_{FDR} = .027$) (Figure 4C; Tables S21 and S22). No significant correlations were found between PD-related deviations in colocalization strengths and the cognitive score (cf. Tables S23–S29). After atrophy correction, all deviations remained significant except for the LCOR-5-HT_{1B} and LCOR-VAChT associations (Table S20).

Lastly, we aimed to understand which regions contributed most to the observed colocalization alterations in PD. For fALFF, the main contributing regions to colocalization changes in PD were the basal ganglia, insula, and occipital regions. For LCOR and GCOR, the main contributing regions were the basal ganglia, subcallosal areas, thalamus (LCOR only), and basal forebrain, as well as the pre- and postcentral insula and occipital regions (Figures S9–S11). The effects remained largely similar after controlling for atrophy (Figures S12–S14). Regional contribution to the deviations found regarding the glutamatergic system were significantly correlated with regional alteration in PD in both synchronicity measures ($p_{FDR} < .05$) (Figures S15 and S16; Tables S29 and S30; Figure 4G, H: effect sizes in regions with FDR-significant differences in LCOR and GCOR in PD vs. matched HC; Tables S31 and S32: regional comparison of fALFF, LCOR, and GCOR in patients with PD vs. matched HCs; Figures S17–S19: regional effect sizes in fALFF, LCOR, and GCOR in patients with PD vs. matched HCs).

DISCUSSION

In the current study, we tested how age-related changes in commonly applied resting activity and connectivity measures colocalize with underlying neurotransmission. Consistent with previous studies of aging effects on brain function, we found widespread age-related decreases but also several increases in the 3 evaluated measures (2,3,66). These age-related changes showed a robust colocalization pattern with various major neurotransmitter systems, including monoamines, glutamate, choline, and GABA, at the group- and single-participant level. Variance in the colocalization patterns of these systems increased with age. Patients with PD showed significant deviations from typical age-related colocalization patterns in neurotransmitter systems related to the disease. The deviation in colocalization strength regarding the GABAergic system was correlated with disease duration.

Consistent with most studies that have reported aging effects in the brain, we found widespread age-related decreases in all 3 evaluated functional measures (1–5). The extent of the decreases is substantially higher in our study, covering basically all of the brain, with few exceptions as discussed below. Considering the large cohort size, the increased statistical power compared with previous studies with at most a few hundred participants is the most likely explanation for the observed discrepancy. In parallel, we observed spatially distinct age-related increases across the 3 evaluated measures covering parietal, precuneal, thalamic, gyrus rectus, and cerebellar regions. Recent theories of neurocognitive aging including dedifferentiation (67) and scaffolding (68) may provide potential explanations for these patterns of brain functional alteration. Neuronal compensation and inefficiency may be associated with increased or decreased cognitive functioning, respectively (69,70). With respect to directionality, our findings are consistent with several previous studies suggesting presumably compensation-related increases in

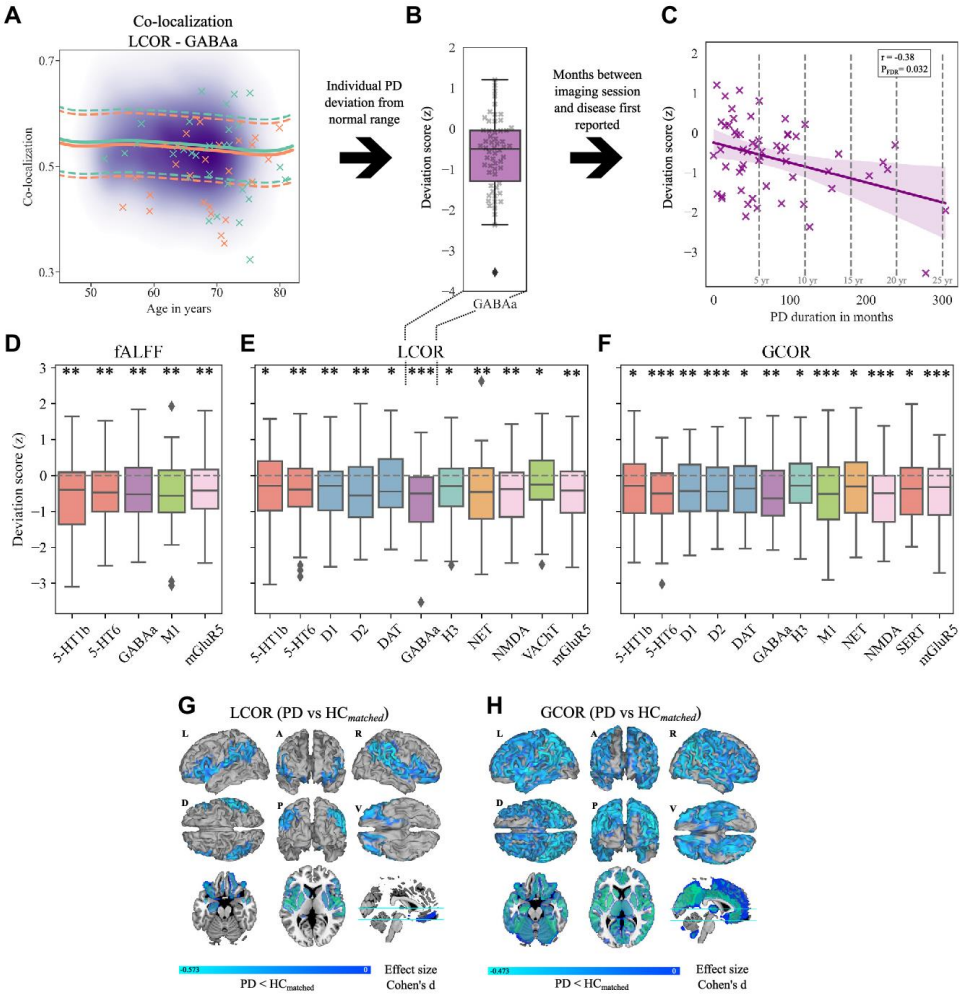

Figure 4. Participants with PD deviated from normative models of colocalization between brain function and neurotransmitter systems. **(A)** The purple cloud shows the kernel density plot of Fisher's *z*-transformed Spearman correlation coefficients of the healthy cohort regarding the spatial correlation of LCOR and $GABA_A$. Solid and dashed lines show the predicted mean and predicted 25% or 75% percentile of men (turquoise) and women (orange) derived from the normative models. Crosses indicate the colocalization levels of patients with PD. **(B)** Box plot showing the significant deviation from the norm (null) in patients with PD. **(C)** Deviation scores in the PD group were significantly correlated with disease duration. **(D–F)** Box plots showing the deviation scores that were significantly different from the norm (null) regarding **(D)** fALFF, **(E)** LCOR, and **(F)** GCOR. *, **, and *** indicate Bonferroni-Holm–corrected significant deviations of the distributions from a null distribution with exact $p < .05$, $p < .01$, and $p < .001$. Colors in box plots group receptors and transporters of the same neurotransmitter system according to the same scheme as described in Figure 2. **(G, H)** Significant ($p_{FDR} < .05$) regional differences (effect sizes, Cohen's *d*) between the PD group and the matched subgroup of HCs in **(G)** LCOR and **(H)** GCOR. Lower values in the PD group are indicated by blue areas. Effect sizes of all regions are provided in Figures S17–S19. 5-HT, serotonin; DAT, dopamine transporter; fALFF, fractional amplitude of low-frequency fluctuations; FDR, false discovery rate; $GABA_A$, gamma-aminobutyric acid A; GCOR, global correlation; HC, healthy control participant; L, left; LCOR, local correlation; mGluR, metabotropic glutamate receptor; NET, norepinephrine transporter; P, posterior; PD, Parkinson's disease; p_{FDR}, false discovery rate–corrected *p*; R, right; SERT, serotonin transporter; V, ventral; VAChT, vesicular acetylcholine transporter.

different connectivity metrics in the aging population (66,71). However, such locally restricted increases and the observed global decreases may also be attributed to a loss of functional differentiation leading to unorganized additional activation or suppression across different regions or to reduced neural efficiency leading to an inability to suppress specific activation patterns (69).

Supporting the previously reported complex reorganization of the excitation/inhibition balance during aging (72), we found that the group-level aging effects on brain function were associated with glutamatergic and GABAergic neurotransmission. The additional colocalization of the aging effects with monoaminergic and cholinergic systems may support the idea that the underlying changes are related to learning, memory, and other higher cognitive functions affected by aging (7,15,71,73). In contrast, age-related global connectivity primarily increased in thalamic and cerebellar regions, and the topography of these changes only aligns with norepinephrinergic neurotransmission. Both regions and in particular the thalamus show a high expression of norepinephrine receptors (74,75). While the modulatory role of norepinephrine in the cerebellum has been repeatedly associated with motor learning (76,77), its contribution to aging is controversial, with its activity being associated with prevention but also acceleration of the production and accumulation of amyloid-β and tau across the brain (78). On a functional level, these findings may be related to the functional decline of the norepinephrinergic system, which is considered to be a key factor in maintaining arousal and cognitive adaptation and control (79,80).

When testing for colocalization of functional measures with neurotransmission at the single-participant level, we found that age-related alterations in all 3 measures colocalized primarily with monoaminergic neurotransmission. Increases in variance observed for a variety of evaluated neurotransmitter systems complemented these findings. Considering the reportedly high prevalence of neuropathology in a cognitively normal older population (81,82), the individual colocalization changes—together with increased variance—may reflect such still undetected neurodegenerative processes. To test the sensitivity of the colocalization patterns to such neurodegenerative processes, we further adopted a normative modeling approach. A major advantage of normative models is their ability to represent population heterogeneity in the phenotype under investigation by means of normalized deviation scores (64). We applied this approach in patients with a diagnosis of PD, which was previously linked to monoaminergic neurotransmission as well as more recently to an imbalance between GABA and glutamate (83–85). In patients with PD, colocalization patterns significantly deviated from age- and sex-adjusted normative models across various neurotransmitter systems and all 3 functional metrics. Deviations in local activity colocalization were found primarily with respect to serotonergic, GABA, and glutamatergic neurotransmission, while deviations in colocalization of both connectivity measures were also present with respect to dopamine neurotransmission. We found that only the deviation in colocalization strength of local connectivity with $GABA_A$ receptors predicted disease duration, thereby supporting the suggested relevance of GABA pathology for clinical progression (83). The observed age-related increases in variance regarding GABAergic colocalization with brain function supports the notion of its contribution to potential pathophysiological changes in parts of the aging population. This interpretation is also supported by its association with disease duration in patients with PD in our study. Consistent with that, GABAergic system changes have recently been reported in PD and were associated with visual hallucinations and axial symptoms (such as postural instability, rigidity, and bradykinesia) (86–88). The observed distinct colocalization patterns of various neurotransmitter systems with functional changes in aging and PD point to distinct pathophysiological processes affecting the respective processes. Such insights, if confirmed by other modalities, may help with identification of novel drug targets as well as development of successful monitoring strategies for the respective pathophysiological changes.

The studied cohort was recruited as a representative sample of healthy UK residents. Because the metrics target local brain function, participants with diseases primarily affecting brain structure or function were excluded. Given the prevalence of mild depressive symptoms in the UK population of 11% (89) and the fact that 12.32% of our analyzed participants from the UK Biobank have a reference to ICD-10: F32, their exclusion would have biased the cohort. PD appearance and progression is highly heterogeneous. Because no scores for PD severity [i.e., Unified Parkinson's Disease Rating Scale (90) or Hoehn & Yahr stages (91)] and only a limited number of cognitive scores were available, we could only roughly approximate PD severity based on disease duration. Because PD medication is known to affect measures of brain function, it might have contributed to some of the effects observed in the PD cohort in the current study. However, the effects of PD medication on spatial colocalization have previously been shown to be rather negligible compared with the effects of PD (25). Additional healthy control biases in the UK Biobank (92) include a high average socioeconomic status and low alcohol and tobacco consumption. Although socioeconomic status may be associated with cognitive reserve through strengthened cognitive abilities during childhood (93,94), we estimate that deviations from the overall population results are small with respect to these primary biases. Further sampling of a more diverse population is needed to address the potential impact of such biases. Clinical scores of disease severity should be used to strengthen evidence for the observed association with GABAergic neurotransmission. Using PET maps from differently aged healthy populations might have introduced a further bias into our findings because proteomics such as receptor and transporter distributions may change during aging (79,95).

Conclusions

Here, we provided a detailed overview on aging effects on macroscopic brain functioning as observed using common rs-fMRI-derived measures of local activity and local and global connectivity. We linked these age-related changes to the distribution of various neurotransmitter systems, demonstrating a decline in colocalization strength together with increased variance during aging. By adopting a normative modeling approach to the example of PD, we further demonstrated the feasibility of using colocalization strength as a sensitive

measure of neurodegeneration, thus providing potentially valuable insight into the underlying neuropathological processes.

ACKNOWLEDGMENTS AND DISCLOSURES

This work was supported by the European Union's Horizon 2020 research and innovation program (Grant No. 826421 [to JD]); TheVirtualBrain-Cloud; the European Union's Horizon 2020 research and innovation program (Grant No. 945539 [to SC and SBE]) (Human Brain Project SGA3); and the Federal Ministry of Education and Research and the Max Planck Society, Germany (to LDL).

We are grateful for the immense work of the whole UK Biobank team, as well as all the volunteers who contributed to this dataset of inestimable value. This research has been conducted using the UK Biobank Resource under Application Number 41655.

The authors report no biomedical financial interests or potential conflicts of interest.

ARTICLE INFORMATION

From the Institute of Systems Neuroscience, Medical Faculty and University Hospital Düsseldorf, Heinrich-Heine-Universität Düsseldorf, Düsseldorf, Germany (JK, LDL, FH, SBE, JD); Institute of Neuroscience and Medicine (INM-7), Research Centre Jülich, Jülich, Germany (JK, LDL, FH, SBE, JD); Institute for Anatomy I, Medical Faculty and University Hospital Düsseldorf, Heinrich-Heine-Universität Düsseldorf, Düsseldorf, Germany (SC); Institute of Neuroscience and Medicine (INM-1), Research Centre Jülich, Jülich, Germany (SC); and Max Planck School of Cognition, Leipzig, Germany (LDL).

Address correspondence to Juergen Dukart, Ph.D., at j.dukart@fz-juelich.de.

Received Jan 14, 2024; revised Mar 15, 2024; accepted Apr 16, 2024.

Supplementary material cited in this article is available online at https://doi.org/10.1016/j.bpsc.2024.04.010.

REFERENCES

1. Biswal BB, Mennes M, Zuo X-N, Gohel S, Kelly C, Smith SM, *et al.* (2010): Toward discovery science of human brain function. Proc Natl Acad Sci USA 107:4734–4739.
2. Hu S, Chao HH-A, Zhang S, Ide JS, Li C-SR (2014): Changes in cerebral morphometry and amplitude of low-frequency fluctuations of BOLD signals during healthy aging: Correlation with inhibitory control. Brain Struct Funct 219:983–994.
3. Vieira BH, Rondinoni C, Garrido Salmon CE (2020): Evidence of regional associations between age-related inter-individual differences in resting-state functional connectivity and cortical thinning revealed through a multi-level analysis. Neuroimage 211:116662.
4. Montalà-Flaquer M, Cañete-Massé C, Vaqué-Alcázar L, Bartrés-Faz D, Peró-Cebollero M, Guàrdia-Olmos J (2022): Spontaneous brain activity in healthy aging: An overview through fluctuations and regional homogeneity. Front Aging Neurosci 14:1002811.
5. Wu T, Zang Y, Wang L, Long X, Li K, Chan P (2007): Normal aging decreases regional homogeneity of the motor areas in the resting state. Neurosci Lett 423:189–193.
6. Harrison TM, Maass A, Adams JN, Du R, Baker SL, Jagust WJ (2019): Tau deposition is associated with functional isolation of the hippocampus in aging. Nat Commun 10:4900.
7. Karrer TM, McLaughlin CL, Guaglianone CP, Samanez-Larkin GR (2019): Reduced serotonin receptors and transporters in normal aging adults: A meta-analysis of PET and SPECT imaging studies. Neurobiol Aging 80:1–10.
8. Sheline YI, Mintun MA, Moerlein SM, Snyder AZ (2002): Greater loss of 5-HT_{2A} receptors in midlife than in late life. Am J Psychiatry 159:430–435.
9. Nord M, Cselenyi Z, Forsberg A, Rosenqvist G, Tiger M, Lundberg J, *et al.* (2014): Distinct regional age effects on [^{11}C]AZ10419369 binding to 5-HT1B receptors in the human brain. Neuroimage 103:303–308.
10. Madsen K, Haahr MT, Marner L, Keller SH, Baaré WF, Svarer C, *et al.* (2011): Age and sex effects on 5-HT_4 receptors in the human brain: A [^{11}C]SB207145 PET study. J Cereb Blood Flow Metab 31:1475–1481.
11. Radhakrishnan R, Nabulsi N, Gaiser E, Gallezot J-D, Henry S, Planeta B, *et al.* (2018): Age-related change in 5-HT_6 receptor availability in healthy male volunteers measured with ^{11}C-GSK215083 PET. J Nucl Med 59:1445–1450.
12. Antonini A, Leenders KL, Reist H, Thomann R, Beer HF, Locher J (1993): Effect of age on D2 dopamine receptors in normal human brain measured by positron emission tomography and 11C-Raclopride. Arch Neurol 50:474–480.
13. Seaman KL, Smith CT, Juarez EJ, Dang LC, Castrellon JJ, Burgess LL, *et al.* (2019): Differential regional decline in dopamine receptor availability across adulthood: Linear and nonlinear effects of age. Hum Brain Mapp 40:3125–3138.
14. Wang Y, Chan GLY, Holden JE, Dobko T, Mak E, Schulzer M, *et al.* (1998): Age-dependent decline of dopamine D1 receptors in human brain: A PET study. Synapse 30:56–61.
15. Karrer TM, Josef AK, Mata R, Morris ED, Samanez-Larkin GR (2017): Reduced dopamine receptors and transporters but not synthesis capacity in normal aging adults: A meta-analysis. Neurobiol Aging 57:36–46.
16. Magnusson KR (2010): Selective vulnerabilities of N-methyl-D-aspartate (NMDA) receptors during brain aging. FrontiAgNeurosci 2:11.
17. Perry EK, Piggott MA, Court JA, Johnson M, Perry RH (1993): Transmitters in the developing and senescent human brain. Ann N Y Acad Sci 695:69–72.
18. Piggott MA, Perry EK, Perry RH, Court JA (1992): [^{3}H]MK-801 binding to the NMDA receptor complex, and its modulation in human frontal cortex during development and aging. Brain Res 588:277–286.
19. Zubieta JK, Koeppe RA, Frey KA, Kilbourn MR, Mangner TJ, Foster NL, Kuhl DE (2001): Assessment of muscarinic receptor concentrations in aging and Alzheimer disease with [11C]NMPB and PET. Synapse 39:275–287.
20. Ding Y-S, Singhal T, Planeta-Wilson B, Gallezot J-D, Nabulsi N, Labaree D, *et al.* (2010): PET imaging of the effects of age and cocaine on the norepinephrine transporter in the human brain using (S,S)-[^{11}C]O-methylreboxetine and HRRT. Synapse 64:30–38.
21. Cuypers K, Hehl M, Van Aalst J, Chalavi S, Mikkelsen M, Van Laere K, *et al.* (2021): Age-related GABAergic differences in the primary sensorimotor cortex: A multimodal approach combining PET, MRS and TMS. Neuroimage 226:117536.
22. Zubieta JK, Dannals RF, Frost JJ (1999): Gender and age influences on human brain mu-opioid receptor binding measured by PET. Am J Psychiatry 156:842–848.
23. Hansen JY, Shafiei G, Markello RD, Smart K, Cox SML, Nørgaard M, *et al.* (2022): Mapping neurotransmitter systems to the structural and functional organization of the human neocortex. Nat Neurosci 25:1569–1581.
24. Dukart J, Holiga Š, Chatham C, Hawkins P, Forsyth A, McMillan R, *et al.* (2018): Cerebral blood flow predicts differential neurotransmitter activity. Sci Rep 8:4074.
25. Dukart J, Holiga S, Rullmann M, Lanzenberger R, Hawkins PCT, Mehta MA, *et al.* (2021): JuSpace: A tool for spatial correlation analyses of magnetic resonance imaging data with nuclear imaging derived neurotransmitter maps. Hum Brain Mapp 42:555–566.
26. Marquand AF, Haak KV, Beckmann CF (2017): Functional corticostriatal connection topographies predict goal directed behaviour in humans. Nat Hum Behav 1:0146.
27. Wolfers T, Beckmann CF, Hoogman M, Buitelaar JK, Franke B, Marquand AF (2020): Individual differences *v.* the average patient: Mapping the heterogeneity in ADHD using normative models. Psychol Med 50:314–323.
28. Fraza CJ, Dinga R, Beckmann CF, Marquand AF (2021): Warped Bayesian linear regression for normative modelling of big data. Neuroimage 245:118715.
29. Ziegler G, Ridgway GR, Dahnke R, Gaser C, Alzheimer's Disease Neuroimaging Initiative (2014): Individualized Gaussian process-based

prediction and detection of local and global gray matter abnormalities in elderly subjects. Neuroimage 97:333–348.
30. Kaasinen V, Vahlberg T, Stoessl AJ, Strafella AP, Antonini A (2021): Dopamine receptors in Parkinson's disease: A meta-analysis of imaging studies. Mov Disord 36:1781–1791.
31. Kaasinen V, Någren K, Hietala J, Oikonen V, Vilkman H, Farde L, *et al.* (2000): Extrastriatal dopamine D2 and D3 receptors in early and advanced Parkinson's disease. Neurology 54:1482–1487.
32. Seeman P, Niznik HB (1990): Dopamine receptors and transporters in Parkinson's disease and schizophrenia. FASEB J 4:2737–2744.
33. Politis M, Piccini P, Pavese N, Koh S-B, Brooks DJ (2008): Evidence of dopamine dysfunction in the hypothalamus of patients with Parkinson's disease: An in vivo ^{11}C-raclopride PET study. Exp Neurol 214:112–116.
34. Takashima H, Terada T, Bunai T, Matsudaira T, Obi T, Ouchi Y (2022): In vivo illustration of altered dopaminergic and GABAergic systems in early Parkinson's disease. Front Neurol 13:880407.
35. Yao N-T, Zheng Q, Xu Z-Q, Yin J-H, Lu L-G, Zuo Q, *et al.* (2020): Positron emission computed tomography/single photon emission computed tomography in Parkinson disease. Chin Med J (Engl) 133:1448–1455.
36. Huot P, Fox SH, Brotchie JM (2011): The serotonergic system in Parkinson's disease. Prog Neurobiol 95:163–212.
37. Melse M, Tan SKH, Temel Y, van Kroonenburgh MJPG, Leentjens AFG (2014): Changes in 5-HT_{2A} Receptor Expression in Untreated, de novo Patients with Parkinson's disease. J Parkinsons Dis 4:283–287.
38. Varrone A, Svenningsson P, Forsberg A, Varnäs K, Tiger M, Nakao R, *et al.* (2014): Positron emission tomography imaging of 5-hydroxytryptamine$_{1B}$ receptors in Parkinson's disease. Neurobiol Aging 35:867–875.
39. Kang Y, Henchcliffe C, Verma A, Vallabhajosula S, He B, Kothari PJ, *et al.* (2019): 18F-FPEB PET/CT shows mGluR5 upregulation in Parkinson's disease. J Neuroimaging 29:97–103.
40. Zhang Z, Zhang S, Fu P, Zhang Z, Lin K, Ko JK-S, Yung KK-L (2019): Roles of glutamate receptors in Parkinson's disease. Int J Mol Sci 20:4391.
41. Sharma A, Muresanu DF, Patnaik R, Menon PK, Tian ZR, Sahib S, *et al.* (2021): Histamine H3 and H4 receptors modulate Parkinson's disease induced brain pathology. Neuroprotective effects of nanowired BF-2649 and clobenpropit with anti-histamine-antibody therapy. Prog Brain Res 266:1–73.
42. Meyer PM, Tiepolt S, Barthel H, Hesse S, Sabri O (2014): Radioligand imaging of α4β2* nicotinic acetylcholine receptors in Alzheimer's disease and Parkinson's disease. Q J Nucl Med Mol Imaging 58:376–386.
43. Asahina M, Suhara T, Shinotoh H, Inoue O, Suzuki K, Hattori T (1998): Brain muscarinic receptors in progressive supranuclear palsy and Parkinson's disease: A positron emission tomographic study. J Neurol Neurosurg Psychiatry 65:155–163.
44. van der Zee S, Kanel P, Gerritsen MJJ, Boertien JM, Slomp AC, Müller MLTM, *et al.* (2022): Altered cholinergic innervation in de novo Parkinson's disease with and without cognitive impairment. Mov Disord 37:713–723.
45. Nahimi A, Kinnerup MB, Sommerauer M, Gjedde A, Borghammer P (2018): Molecular imaging of the noradrenergic system in idiopathic Parkinson's disease. Int Rev Neurobiol 141:251–274.
46. Brumberg J, Tran-Gia J, Lapa C, Isaias IU, Samnick S (2019): PET imaging of noradrenaline transporters in Parkinson's disease: Focus on scan time. Ann Nucl Med 33:69–77.
47. Smith SM, Alfaro-Almagro F, Miller KL (2020): UK Biobank Brain Imaging Documentation. (version 1.8). Available at: https://biobank.ctsu.ox.ac.uk/crystal/crystal/docs/brain_mri.pdf. Accessed February 13, 2023.
48. Zou Q-H, Zhu C-Z, Yang Y, Zuo X-N, Long X-Y, Cao Q-J, *et al.* (2008): An improved approach to detection of amplitude of low-frequency fluctuation (ALFF) for resting-state fMRI: Fractional ALFF. J Neurosci Methods 172:137–141.
49. Deshpande G, LaConte S, Peltier S, Hu X (2009): Integrated local correlation: A new measure of local coherence in fMRI data. Hum Brain Mapp 30:13–23.
50. Saad ZS, Reynolds RC, Jo HJ, Gotts SJ, Chen G, Martin A, Cox RW (2013): Correcting brain-wide correlation differences in resting-state FMRI. Brain Connect 3:339–352.
51. Kasper J, Eickhoff SB, Caspers S, Peter J, Dogan I, Wolf RC, *et al.* (2023): Local synchronicity in dopamine-rich caudate nucleus influences Huntington's disease motor phenotype. Brain 146:3319–3330.
52. Beliveau V, Ganz M, Feng L, Ozenne B, Højgaard L, Fisher PM, *et al.* (2017): A high-resolution *in vivo* atlas of the human Brain's serotonin system. J Neurosci 37:120–128.
53. Gallezot J-D, Nabulsi N, Neumeister A, Planeta-Wilson B, Williams WA, Singhal T, *et al.* (2010): Kinetic modeling of the serotonin 5-HT $_{1B}$ receptor radioligand [^{11}C]P943 in humans. J Cereb Blood Flow Metab 30:196–210.
54. Kaller S, Rullmann M, Patt M, Becker G-A, Luthardt J, Girbardt J, *et al.* (2017): Test–retest measurements of dopamine D_1-type receptors using simultaneous PET/MRI imaging. Eur J Nucl Med Mol Imaging 44:1025–1032.
55. Sandiego CM, Gallezot J-D, Lim K, Ropchan J, Lin SF, Gao H, *et al.* (2015): Reference region modeling approaches for amphetamine challenge studies with [^{11}C]FLB 457 and PET. J Cereb Blood Flow Metab 35:623–629.
56. Gallezot J-D, Planeta B, Nabulsi N, Palumbo D, Li X, Liu J, *et al.* (2017): Determination of receptor occupancy in the presence of mass dose: [^{11}C]GSK189254 PET imaging of histamine H3 receptor occupancy by PF-03654746. J Cereb Blood Flow Metab 37:1095–1107.
57. Aghourian M, Legault-Denis C, Soucy JP, Rosa-Neto P, Gauthier S, Kostikov A, *et al.* (2017): Quantification of brain cholinergic denervation in Alzheimer's disease using PET imaging with [^{18}F]-FEOBV. Mol Psychiatry 22:1531–1538.
58. Naganawa M, Nabulsi N, Henry S, Matuskey D, Lin S-F, Slieker L, *et al.* (2021): First-in-human assessment of ^{11}C-LSN3172176, an M1 muscarinic acetylcholine receptor PET radiotracer. J Nucl Med 62:553–560.
59. Hillmer AT, Esterlis I, Gallezot JD, Bois F, Zheng MQ, Nabulsi N, *et al.* (2016): Imaging of cerebral $\alpha_4\beta_2$* nicotinic acetylcholine receptors with (−)-[^{18}F]Flubatine PET: Implementation of bolus plus constant infusion and sensitivity to acetylcholine in human brain. Neuroimage 141:71–80.
60. Smart K, Cox SML, Scala SG, Tippler M, Jaworska N, Boivin M, *et al.* (2019): Sex differences in [^{11}C]ABP688 binding: A positron emission tomography study of mGlu5 receptors. Eur J Nucl Med Mol Imaging 46:1179–1183.
61. Galovic M, Al-Diwani A, Vivekananda U, Torrealdea F, Erlandsson K, Fryer TD, *et al.* (2021): In vivo NMDA receptor function in people with NMDA receptor antibody encephalitis. medRxiv. https://doi.org/10.1101/2021.12.04.21267226.
62. Normandin MD, Zheng M-Q, Lin K-S, Mason NS, Lin S-F, Ropchan J, *et al.* (2015): Imaging the cannabinoid CB1 receptor in humans with [^{11}C]OMAR: Assessment of kinetic analysis methods, test-retest reproducibility, and gender differences. J Cereb Blood Flow Metab 35:1313–1322.
63. Bonett DG, Wright TA (2000): Sample size requirements for estimating Pearson, Kendall and spearman correlations. Psychometrika 65:23–28.
64. Rutherford S, Kia SM, Wolfers T, Fraza C, Zabihi M, Dinga R, *et al.* (2022): The normative modeling framework for computational psychiatry. Nat Protoc 17:1711–1734.
65. Lotter LD, Saberi A, Hansen JY, Misic B, Paquola C, Barker GJ, *et al.* (2023): Human cortex development is shaped by molecular and cellular brain systems. bioRxiv. https://doi.org/10.1101/2023.05.05.539537.
66. Vij SG, Nomi JS, Dajani DR, Uddin LQ (2018): Evolution of spatial and temporal features of functional brain networks across the lifespan. Neuroimage 173:498–508.
67. Koen JD, Rugg MD (2019): Neural dedifferentiation in the aging brain. Trends Cogn Sci 23:547–559.
68. Reuter-Lorenz PA, Park DC (2014): How does it STAC up? Revisiting the scaffolding theory of aging and cognition. Neuropsychol Rev 24:355–370.

69. McDonough IM, Nolin SA, Visscher KM (2022): 25 years of neurocognitive aging theories: What have we learned? Front Aging Neurosci 14:1002096.
70. Bunzeck N, Steiger TK, Krämer UM, Luedtke K, Marshall L, Obleser J, Tune S (2024): Trajectories and contributing factors of neural compensation in healthy and pathological aging. Neurosci Biobehav Rev 156:105489.
71. Behfar Q, Behfar SK, Von Reutern B, Richter N, Dronse J, Fassbender R, *et al.* (2020): Graph theory analysis reveals resting-state compensatory mechanisms in healthy aging and prodromal Alzheimer's disease. Front Aging Neurosci 12:576627.
72. Petitet P, Spitz G, Emir UE, Johansen-Berg H, O'Shea J (2021): Age-related decline in cortical inhibitory tone strengthens motor memory. Neuroimage 245:118681.
73. Bernier M, Croteau E, Castellano C-A, Cunnane SC, Whittingstall K (2017): Spatial distribution of resting-state BOLD regional homogeneity as a predictor of brain glucose uptake: A study in healthy aging. Neuroimage 150:14–22.
74. Oke AF, Carver LA, Gouvion CM, Adams RN (1997): Three-dimensional mapping of norepinephrine and serotonin in human thalamus. Brain Res 763:69–78.
75. Zitnik G, Chandler DJ, Waterhouse BD (2016): Norepinephrine and synaptic transmission in the cerebellum. In: Gruol DL, Koibuchi N, Manto M, Molinari M, Schmahmann JD, Shen Y, editors. Essentials of Cerebellum and Cerebellar Disorders. Cham, Germany: Springer International Publishing, 237–241.
76. Cartford MC, Gould T, Bickford PC (2004): A central role for norepinephrine in the modulation of cerebellar learning tasks. Behav Cogn Neurosci Rev 3:131–138.
77. Bickford P (1995): Aging and motor learning: A possible role for norepinephrine in cerebellar plasticity. Rev Neurosci 6:35–46.
78. Mather M (2021): Noradrenaline in the aging brain: Promoting cognitive reserve or accelerating Alzheimer's disease? Semin Cell Dev Biol 116:108–124.
79. Lee J, Kim H-J (2022): Normal aging induces changes in the brain and neurodegeneration progress: Review of the structural, biochemical, metabolic, cellular, and molecular changes. Front Aging Neurosci 14: 931536.
80. Guedj C, Monfardini E, Reynaud AJ, Farnè A, Meunier M, Hadj-Bouziane F (2017): Boosting norepinephrine transmission triggers flexible reconfiguration of brain networks at rest. Cereb Cortex 27:4691–4700.
81. Chételat G, La Joie R, Villain N, Perrotin A, De La Sayette V, Eustache F, Vandenberghe R (2013): Amyloid imaging in cognitively normal individuals, at-risk populations and preclinical Alzheimer's disease. Neuroimage Clin 2:356–365.
82. Markesbery WR, Jicha GA, Liu H, Schmitt FA (2009): Lewy body pathology in normal elderly subjects. J Neuropathol Exp Neurol 68: 816–822.
83. Błaszczyk JW (2016): Parkinson's disease and neurodegeneration: GABA-collapse hypothesis. Front Neurosci 10:269.
84. Kaur R, Mehan S, Singh S (2019): Understanding multifactorial architecture of Parkinson's disease: Pathophysiology to management. Neurol Sci 40:13–23.
85. Wang J, Wang F, Mai D, Qu S (2020): Molecular mechanisms of glutamate toxicity in Parkinson's disease. Front Neurosci 14:585584.
86. Firbank MJ, Parikh J, Murphy N, Killen A, Allan CL, Collerton D, *et al.* (2018): Reduced occipital GABA in Parkinson disease with visual hallucinations. Neurology 91:e675–e685.
87. Van Nuland AJM, Den Ouden HEM, Zach H, Dirkx MFM, Van Asten JJA, Scheenen TWJ, *et al.* (2020): GABAergic changes in the thalamocortical circuit in Parkinson's disease. Hum Brain Mapp 41:1017–1029.
88. O'Gorman Tuura RL, Baumann CR, Baumann-Vogel H (2018): Beyond dopamine: GABA, glutamate, and the axial symptoms of Parkinson disease. Front Neurol 9:806.
89. Arias de la Torre J, Vilagut G, Ronaldson A, Dregan A, Ricci-Cabello I, Hatch SL, *et al.* (2021): Prevalence and age patterns of depression in the United Kingdom. A population-based study. J Affect Disord 279:164–172.
90. Movement Disorder Society Task Force on Rating Scales for Parkinson's Disease (2003): The Unified Parkinson's Disease Rating Scale (UPDRS): Status and recommendations. Mov Disord 18:738–750.
91. Goetz CG, Poewe W, Rascol O, Sampaio C, Stebbins GT, Counsell C, *et al.* (2004): Movement Disorder Society Task Force report on the Hoehn and Yahr staging scale: Status and recommendations. Mov Disord 19:1020–1028.
92. Fry A, Littlejohns TJ, Sudlow C, Doherty N, Adamska L, Sprosen T, *et al.* (2017): Comparison of sociodemographic and health-related characteristics of UK Biobank participants with those of the general population. Am J Epidemiol 186:1026–1034.
93. Cermakova P, Formanek T, Kagstrom A, Winkler P (2018): Socioeconomic position in childhood and cognitive aging in Europe. Neurology 91:e1602–e1610.
94. Tari B, Künzi M, Pflanz CP, Raymont V, Bauermeister S (2023): Education is power: Preserving cognition in the UK Biobank. Front Public Health 11:1244306.
95. Nikhra V (2017): The aging brain: Recent research and concepts. GGS 1:1.

SUPPLEMENTARY INFORMATION

Resting State Changes In Aging and Parkinson's Disease Are Shaped by Underlying Neurotransmission – A Normative Modeling Study

Kasper *et al.*

Supplementary Methods

Preprocessing of resting-state functional imaging data

Initial preprocessing performed by the UK Biobank team consisted of primary T1 quality control, gradient distortion correction, motion correction, grand-mean intensity normalization, high-pass temporal filtering, echo planar imaging unwarping, gradient distortion correction unwarping, and the removal of structural artefacts via ICA+FIX. The resulting images were labeled "filtered_func_data_clean.nii" Further processing was conducted with SPM12[1], the FMIRB Software Library (FSL v5.0[2]), and the CONN toolbox[3] implemented in MATLAB (v2020b). Functional images were transformed into MNI space using a general reference template provided by FSL and a subject specific warping image. After resampling ($3mm^3$ isotropic) and smoothing (Gaussian kernel with 4 mm FWHM) with SPM, we applied a bandpass filter (0.008 – 0.09 Hz) to the BOLD signal, discarded the first five frames to ensure signal equilibrium, and regressed out 24 parameters of motion[4], as well as the mean signal from white matter and cerebrospinal fluid using CONN. Distorted images and artifacts were identified by low correlations ($r < 0.9$) between individual and a reference, preprocessed mean rs-fMRI image of 200 subjects. Visual inspection confirmed that failed spatial normalization or insufficient brain coverage in individual images were responsible for low correlation coefficients. We additionally excluded data from subjects with excessive in-scanner motion (maximum frame-wise rotation > 2° and movement > 3 mm).

Measures of local brain activity and synchronicity

We derived three complementary measures of local brain activity and synchronicity using the CONN toolbox. fALFF[5] is defined as the power ratio of low-frequency (0.008 – 0.09 Hz) oscillations to the total detectable frequency range in the BOLD signal. Local correlation (LCOR[6]) is the normalized sum of correlation coefficients of the BOLD signal in the voxel of interest with other voxels in its vicinity, with distances weighted by a Gaussian kernel (25 mm FWHM). Global correlation (GCOR[7]) is calculated in the same way as LCOR, but without distance-dependent weighting of the individual correlation coefficients. Thus, GCOR represents a measure of the global synchronicity of a voxel, whereas LCOR represents a measure of local coherence. Unlike fALFF, LCOR and GCOR do not depend on the amplitude of the BOLD signal, but rather on the similarity of the BOLD time series of all considered voxels. These three metrics provide a complementary characterization of the BOLD signal providing information about local neural activity as well as local and global functional connectivity.

Functional alterations in Parkinson's Disease and regional contribution to deviations from normative models

An estimation of disease duration was computed by the difference between the date of first occurrence of ICD-10 G20, (Data-Field 131022) and the date of imaging (Data-Field 53, Instance 2). For the significant ($P_{FDR} < 0.05$) deviations, we tested which regions contributed strongest to the observed deviations by repeating the spatial correlation analyses in the data of PD utilizing a leaving-one-region-out approach. As a measure of regional contribution to the deviation we calculated differences in squared correlation coefficients ($\Delta\rho^2$) between the reduced ($n_{Regions} = 118$: ρ_{LOO}^2) and the full ($n_{Regions} = 119$: ρ_{Total}^2) set of regions. We set $\Delta\rho^2$ positive if omitting this

specific region resulted in a more normal correlation coefficient (closer to the mean of the normative model), and negative if omitting led to stronger deviation from the normative model. We further evaluated whether these regional contributions to the observed co-localization strengths were spatially related to regional alterations in fALFF, LCOR, or GCOR by computing Pearson correlations between maps of $\Delta\rho^2$ and the regional effect size (Cohen's d) in fALFF, LCOR, GCOR for differences between PD and an age- and sex-matched subgroup of HC (n = 17 400). In order to evaluate the extent of significant functional alterations in PD, regions with significant differences in fALFF, LCOR, and GCOR in PD compared with the matched controls were identified using the Mann-Whitney-U test.

Preparation of individual structural data & correction of atrophy

To control for aging-related atrophy, we generated normalized and smoothed grey matter volumes. For this purpose, we warped individual T1-weighted images (*T1_brain_pve_1.nii.gz*) with individual warping coefficients (*T1_to_MNI_warp_coef.nii.gz*) (both provided by the UK Biobank) and normalized the warped images to MNI space using a template provided by FSL. We then changed the dimensions of the structural images to fit the functional data (using SPM: ImCalc) and smoothed them with a Gaussian kernel (4 mm FWHM). Next, the linear effects of grey matter signals from all fALFF, LCOR, and GCOR maps were regressed voxel-wise.

Normative modeling of brain function - neurotransmitter co-localization

The normative modeling was performed using the PCNtoolkit[8]. We modeled the co-localization level (i.e., the Spearman correlation coefficient) derived from spatial correlation analyses between neurotransmitter systems (n = 19) and individual brain functional measures (fALFF, LCOR, and GCOR) of all healthy controls. To account for non-linear trajectories and non-Gaussian variance of the normal co-localization levels, we used Bayesian linear regression (5 knot basis splines and sinh-arcsinh warping) with age and sex as covariates. For the illustration of the normative models (Figure 1F, 4A, Supplementary Figures 7 and 8), we predicted the normal co-localization levels and uncertainty for two artificial dummy subjects (male and female) in the age range of the sample [44.58 – 81.98] years and a sampling frequency of 0.2 years. Further details on the toolbox and guidance for conducting research can be found on the official website of PCNtoolkit provided by Marquand et al.[9].

Supplementary Tables

Supplementary Table 1: List of exclusion criteria for the control group.

	Subgroup	ICD-10
Mental and Behavioural disorders (F-labeled)	Physiological conditions	F01 - F03
	Psychoactive substance use	F10 – F19
	Schizophrenia, schizotypal, delusional, and schizoaffective disorder	F20 - F22, F25
	Mood affective disorders	F31, F33
	Intellectual disabilities	F70 – F72
Diseases of the central nervous system (G-labeled)	Inflammatory diseases	G04 – G07
	Systematic atrophies	G10 - G13, G14
	Extrapyramidal and movement disorders	G20 – G25
	Other degenerative diseases	G30-G32
	Demyelinating diseases	G35-G37
	Episodic and paroxysmal disorders	G40, G41, G45
Neoplasms (C-labeled)	Malignant neoplasm of the brain	C71

Supplementary Table 2: Characteristics of neurotransmitter PET maps used.

Atlas	Tracer	Sample size	% Male	Age (μ +- σ)	Source DOI
5-HT1a	[11C]CUMI-101	8	37.50	28.4 +- 8.8	10.1523/JNEUROSCI.2830-16.2016
5-HT1b	[11C]P943	65	75.38	33.7 +- 9.7	10.1038/jcbfm.2009.195
5-HT2a	[11C]CIMBI-36	29	51.72	22.6 +- 2.7	10.1523/JNEUROSCI.2830-16.2016
5-HT4	[11C]SB207145	59	69.49	25.9 +- 5.3	10.1523/JNEUROSCI.2830-16.2016
5-HT6	[11C]GSK215083	30	100	36.6 +- 9	10.2967/jnumed.117.206516
SERT	[11C]DASB	100	29	25.1 +- 5.8	10.1523/JNEUROSCI.2830-16.2016
D1	[11C]SCH23390	13	46	33 +- 13	10.1007/s00259-017-3645-0
D2	[11C]FLB457	55	47.27	32.5 +- 9.7	10.1038/jcbfm.2014.237
DAT	[123I]FP-CIT	174	62.64	61 +- 11	10.1038/s41598-018-22444-0
H3	[11C]GSK189254	8	87.5	31.7 +- 9	10.1177/0271678X16650697
NET	[11C]MRB	77	64.94	33.4 +- 9.2	10.1002/syn.20696
M1	[11C]LSN3172176	24	54.17	40.50 +- 11.7	10.2967/jnumed.120.246967
A4B2	[18F]FLUBATINE	30	66.67	33.5 +- 10.7	10.1016/j.neuroimage.2016.07.026
VAChT	[18F]FEOBV	18	27.78	66.8 +- 6.8	10.1038/mp.2017.183
mGluR5	[11C]ABP688	73	34.25	19.9 +- 3.04	10.1007/s00259-018-4252-4
NMDA	[18F]GE-179	29	72	41 +- 13	10.1101/2021.12.04.21267226
CB1	[11C]OMAR	77	63.64	30 +- 8.9	10.1038/jcbfm.2015.46
Opioid mu	[11C]CARFENTANIL	204	64.71	32.3 +- 10.8	10.1038/mp.2017.183
GABAa	[11C]FLUMAZENIL	6	100	43+-4	10.1038/s41598-018-22444-0

Supplementary Table 3: Regions covered by cluster of significant aging effects in fALFF, LCOR, and GCOR – *before atrophy correction*.

Anatomical region	Cluster size	Cluster p-values (corrected)	Peak T-values	Peak MNI-Coordinates
fALFF: Decreasing with age				
Bilateral: Superior frontal gyrus (dorsolateral), Middle temporal gyrus, Middle frontal gyrus, Postcentral gyrus, Middle occipital gyrus, Inferior temporal gyrus, Precuneus, Precentral gyrus, Superior temporal gyrus, Fusiform gyrus, Superior frontal gyrus (medial), Cerebellum (Crus 1), Inferior frontal gyrus (pars triangularis), Calcarine fissure and surrounding cortex, Inferior parietal gyrus, Lingual gyrus, Supplementary motor area, Cerebellum (8), Middle cingulate & paracingulate gyri, Insula, Cerebellum (6), Supramarginal gyrus, Superior parietal gyrus, Cerebellum (Crus 2), Cuneus, Angular gyrus, Rolandic operculum, Parahippocampal gyrus, Superior occipital gyrus, Inferior frontal gyrus (pars opercularis), Cerebellum (4,5), Superior temporal gyrus (pole), Putamen, Paracentral lobule, Hippocampus, Inferior occipital gyrus, Superior frontal gyrus (medial orbital), Cerebellum (9), Middle temporal gyrus (pole), Caudate nucleus, Anterior cingulate cortex (supracallosal), Gyrus rectus, Inferior frontal gyrus (pars orbitalis), Medial orbital gyrus, Anterior cingulate cortex (pregenual), Posterior orbital gyrus, Anterior orbital gyrus, Cerebellum (7b), Vermis (4,5), Olfactory cortex, Vermis (6), Amygdala, Posterior cingulate gyrus, Vermis (8), Heschl's gyrus, Lateral orbital gyrus, Thalamus (pulvinar medial), Vermis (9), Anterior cingulate cortex (subgenual), Ventral striatum, Vermis (7), Cerebellum (3), Vermis (3), Thalamus (mediodorsal medial magnocellular), Pallidum, Thalamus (ventral posterolateral), Thalamus (mediodorsal lateral parvocellular), Thalamus (ventral lateral), Vermis (1,2), Thalamus (pulvinar inferior), Thalamus (pulvinar anterior), Vermis (10), Thalamus (pulvinar lateral), Thalamus (lateral posterior), Thalamus (anteroventral nucleus), Thalamus (lateral geniculate), Thalamus (intralaminar), Substantia nigra pars compacta, Raphe nucleus, Thalamus (medial geniculate), Red nucleus, Cerebellum (10) **Left:** Ventral tegmental area, Thalamus (ventral anterior)	48649	<0.001	49.3	**45 0 -3**
fALFF: Increasing with age				
Left: Angular gyrus, Middle occipital gyrus, Inferior parietal gyrus, Middle temporal gyrus	118	<0.001	20.83	**-36 -54 24**
Right: Supramarginal gyrus, Angular gyrus	33	<0.001	11.39	**30 -45 36**
LCOR: Decreasing with age				
Bilateral: Middle temporal gyrus, Superior frontal gyrus (dorsolateral), Postcentral gyrus, Precentral gyrus, Superior temporal gyrus, Fusiform gyrus, Middle frontal gyrus, Calcarine fissure and surrounding cortex, Lingual gyrus, Supplementary motor area, Inferior frontal gyrus (pars triangularis), Inferior temporal gyrus, Superior frontal gyrus (medial), Cerebellum (8), Insula, Cerebellum (6), Cerebellum (Crus 1), Middle occipital gyrus, Rolandic operculum, Cuneus, Middle cingulate & paracingulate gyri, Parahippocampal gyrus, Supramarginal gyrus, Inferior frontal gyrus (pars opercularis), Cerebellum (4,5), Cerebellum (Crus 2), Putamen, Superior temporal gyrus (pole), Paracentral lobule, Inferior parietal gyrus, Hippocampus, Inferior occipital gyrus, Precuneus, Cerebellum (9), Caudate nucleus, Superior occipital gyrus, Anterior cingulate cortex (supracallosal), Superior parietal gyrus,	38017	<0.001	44.64	**45 3 -6**

Inferior frontal gyrus (pars orbitalis), Anterior cingulate cortex (pregenual), Middle temporal gyrus (pole), Superior frontal gyrus (medial orbital), Posterior orbital gyrus, Cerebellum (7b), Vermis (4,5), Gyrus rectus, Vermis (6), Amygdala, Olfactory cortex, Vermis (8), Heschl's gyrus, Vermis (9), Thalamus (pulvinar medial), Anterior cingulate cortex (subgenual), Vermis (7), Cerebellum (3), Vermis (3), Medial orbital gyrus, Thalamus (mediodorsal medial magnocellular), Ventral striatum, Pallidum, Lateral orbital gyrus, Thalamus (ventral posterolateral), Thalamus (mediodorsal lateral parvocellular), Anterior orbital gyrus, Thalamus (ventral lateral), Vermis (1,2), Thalamus (pulvinar inferior), Thalamus (pulvinar anterior), Vermis (10), Thalamus (pulvinar lateral), Thalamus (lateral posterior), Thalamus (anteroventral nucleus), Thalamus (lateral geniculate), Thalamus (intralaminar), Substantia nigra pars compacta, Raphe nucleus, Thalamus (medial geniculate), Red nucleus, Cerebellum (10) **Left:** Angular gyrus, Ventral tegmental area, Thalamus (ventral anterior)				
LCOR: Increasing with age				
Bilateral: Precuneus, Angular gyrus, Inferior parietal gyrus, Posterior cingulate gyrus, Middle occipital gyrus, Middle cingulate & paracingulate gyri, Superior parietal gyrus, Cuneus, Supramarginal gyrus, Middle temporal gyrus, Superior occipital gyrus, Postcentral gyrus **Left**: Calcarine fissure and surrounding cortex	1796	<0.001	24.87	**-33 -57 33**
Left: Gyrus rectus	27	<0.001	8.25	**-6 21 -30**
GCOR: Decreasing with age				
Bilateral: Middle temporal gyrus, Superior frontal gyrus (dorsolateral), Postcentral gyrus, Middle frontal gyrus, Precentral gyrus, Superior temporal gyrus, Inferior temporal gyrus, Superior frontal gyrus (medial), Fusiform gyrus, Inferior frontal gyrus (pars triangularis), Supplementary motor area, Middle occipital gyrus, Inferior parietal gyrus, Cerebellum (8), Insula, Lingual gyrus, Precuneus, Supramarginal gyrus, Middle cingulate & paracingulate gyri, Superior parietal gyrus, Cerebellum (6), Calcarine fissure and surrounding cortex, Rolandic operculum, Inferior frontal gyrus (pars opercularis), Cerebellum (4,5), Parahippocampal gyrus, Superior temporal gyrus (pole), Cuneus, Paracentral lobule, Superior occipital gyrus, Hippocampus, Middle temporal gyrus (pole), Angular gyrus, Cerebellum (9), Superior frontal gyrus (medial orbital), Anterior cingulate cortex (supracallosal), Inferior occipital gyrus, Putamen, Inferior frontal gyrus (pars orbitalis), Cerebellum (Crus 1), Anterior cingulate cortex (pregenual), Cerebellum (Crus 2), Gyrus rectus, Vermis (4,5), Caudate nucleus, Posterior orbital gyrus, Cerebellum (7b), Vermis (6), Amygdala, Vermis (8), Heschl's gyrus, Anterior cingulate cortex (subgenual), Olfactory cortex, Lateral orbital gyrus, Vermis (9), Vermis (7), Vermis (3), Cerebellum (3), Posterior cingulate gyrus, Thalamus (pulvinar medial), Ventral striatum, Pallidum, Medial orbital gyrus, Thalamus (mediodorsal medial magnocellular), Thalamus (ventral posterolateral), Vermis (1,2), Thalamus (pulvinar inferior), Anterior orbital gyrus, Thalamus (pulvinar anterior), Vermis (10), Thalamus (lateral geniculate), Thalamus (pulvinar lateral), Thalamus (intralaminar), Raphe nucleus, Thalamus (medial geniculate), Thalamus (mediodorsal lateral parvocellular), Cerebellum (10) **Left**: Thalamus (lateral posterior)	38929	<0.001	33.04	**45 9 -9**
GCOR: Increasing with age				

Bilateral: Thalamus (mediodorsal medial magnocellular), Caudate nucleus, Thalamus (ventral lateral), Thalamus (pulvinar medial), Thalamus (mediodorsal lateral parvocellular), Thalamus (anteroventral nucleus), Thalamus (lateral posterior), Hippocampus, Thalamus (intralaminar) **Left**: Thalamus (ventral anterior) **Right**: Thalamus (pulvinar anterior), Thalamus (pulvinar lateral), Posterior cingulate gyrus	206	<0.001	22.15	**-3 -3 9**
Left: Angular gyrus, Middle occipital gyrus	45	<0.001	16.7	**-33 -57 33**
Left: Cerebellum (Crus 1), Cerebellum (Crus 2), Cerebellum (6)	350	<0.001	15.56	**-45 -72 -30**
Bilateral: Precuneus, Superior parietal gyrus **Right**: Angular gyrus, Superior occipital gyrus, Cuneus	217	<0.001	13.5	**18 -60 45**
Bilateral: Posterior cingulate gyrus **Right**: Middle cingulate & paracingulate gyri	70	<0.001	12.07	**0 -24 27**
Right: Cerebellum (Crus 1), Lingual gyrus, Cerebellum (6), Calcarine fissure and surrounding cortex	164	<0.001	10.23	**12 -99 -12**

Supplementary Table 4: Regions covered by cluster of significant aging effects in fALFF, LCOR, and GCOR – *after atrophy correction*.

Anatomical region	Cluster size	Cluster p-values (corrected)	Peak T-values	Peak MNI-Coordinates
fALFF: Decreasing with age				
Bilateral: Superior frontal gyrus (dorsolateral), Middle frontal gyrus, Middle temporal gyrus, Postcentral gyrus, Middle occipital gyrus, Precentral gyrus, Inferior temporal gyrus, Precuneus, Superior temporal gyrus, Superior frontal gyrus (medial), Fusiform gyrus, Cerebellum (Crus 1), Inferior parietal gyrus, Inferior frontal gyrus (pars triangularis), Calcarine fissure and surrounding cortex, Lingual gyrus, Supplementary motor area, Cerebellum (8), Middle cingulate & paracingulate gyri, Insula, Cerebellum (6), Supramarginal gyrus, Superior parietal gyrus, Cerebellum (Crus 2), Angular gyrus, Cuneus, Rolandic operculum, Parahippocampal gyrus, Inferior frontal gyrus (pars opercularis), Superior occipital gyrus, Cerebellum (4,5), Superior temporal gyrus (pole), Putamen, Paracentral lobule, Hippocampus, Inferior occipital gyrus, Superior frontal gyrus (medial orbital), Middle temporal gyrus (pole), Cerebellum (9), Caudate nucleus, Anterior cingulate cortex (supracallosal), Gyrus rectus, Inferior frontal gyrus (pars orbitalis), Medial orbital gyrus, Anterior cingulate cortex (pregenual), Posterior orbital gyrus, Anterior orbital gyrus, Cerebellum (7b), Vermis (4,5), Posterior cingulate gyrus, Olfactory cortex, Vermis (6), Amygdala, Vermis (8), Heschl's gyrus, Lateral orbital gyrus, Thalamus (pulvinar medial), Vermis (9), Anterior cingulate cortex (subgenual), Ventral striatum, Vermis (7), Cerebellum (3), Vermis (3), Thalamus (mediodorsal medial magnocellular), Pallidum, Thalamus (ventral posterolateral), Thalamus (mediodorsal lateral parvocellular), Thalamus (ventral lateral), Vermis (1,2), Thalamus (pulvinar inferior), Thalamus	49470	<0.001	42.83	**0 -36 24**

(pulvinar anterior), Vermis (10), Thalamus (pulvinar lateral), Thalamus (lateral posterior), Thalamus (anteroventral nucleus), Thalamus (lateral geniculate), Thalamus (intralaminar), Substantia nigra pars compacta, Raphe nucleus, Thalamus (medial geniculate), Red nucleus, Cerebellum (10). **Left**: Ventral tegmental area, Thalamus (ventral anterior)				
fALFF: Increasing with age				
Bilateral: Gyrus rectus	30	<0.001	7.87	**6 21 -30**
LCOR: Decreasing with age				
Bilateral: Middle temporal gyrus, Superior frontal gyrus (dorsolateral), Postcentral gyrus, Precentral gyrus, Superior temporal gyrus, Middle frontal gyrus, Fusiform gyrus, Calcarine fissure and surrounding cortex, Lingual gyrus, Supplementary motor area, Inferior frontal gyrus (pars triangularis), Inferior temporal gyrus, Superior frontal gyrus (medial), Cerebellum (8), Insula, Cerebellum (6), Middle occipital gyrus, Cerebellum (Crus 1), Rolandic operculum, Middle cingulate & paracingulate gyri, Cuneus, Inferior frontal gyrus (pars opercularis), Parahippocampal gyrus, Supramarginal gyrus, Cerebellum (4,5), Putamen, Superior temporal gyrus (pole), Cerebellum (Crus 2), Paracentral lobule, Hippocampus, Inferior parietal gyrus, Inferior occipital gyrus, Cerebellum (9), Caudate nucleus, Precuneus, Superior occipital gyrus, Anterior cingulate cortex (supracallosal), Inferior frontal gyrus (pars orbitalis), Superior parietal gyrus, Anterior cingulate cortex (pregenual), Middle temporal gyrus (pole), Superior frontal gyrus (medial orbital), Posterior orbital gyrus, Cerebellum (7b), Vermis (4,5), Vermis (6), Gyrus rectus, Amygdala, Olfactory cortex, Vermis (8), Heschl's gyrus, Vermis (9), Thalamus (pulvinar medial), Anterior cingulate cortex (subgenual), Vermis (7), Cerebellum (3), Ventral striatum, Vermis (3), Thalamus (mediodorsal medial magnocellular), Medial orbital gyrus, Pallidum, Lateral orbital gyrus, Thalamus (ventral posterolateral), Anterior orbital gyrus, Thalamus (mediodorsal lateral parvocellular), Thalamus (ventral lateral), Vermis (1,2), Thalamus (pulvinar inferior), Thalamus (pulvinar anterior), Vermis (10), Thalamus (pulvinar lateral), Thalamus (lateral posterior), Thalamus (anteroventral nucleus), Thalamus (lateral geniculate), Thalamus (intralaminar), Substantia nigra pars compacta, Raphe nucleus, Thalamus (medial geniculate), Red nucleus, Cerebellum (10) **Left**: Angular gyrus, Ventral tegmental area, Thalamus (ventral anterior)	38027	<0.001	34.38	**48 6 -9**
LCOR: Increasing with age				
Bilateral: Precuneus, Angular gyrus, Inferior parietal gyrus, Posterior cingulate gyrus, Middle occipital gyrus, Middle cingulate & paracingulate gyri, Superior parietal gyrus, Cuneus **Left**: Middle temporal gyrus, Calcarine fissure and surrounding cortex **Right**: Supramarginal gyrus, Superior occipital gyrus	1670	<0.001	16.87	**-33 -60 33**
Left: Gyrus rectus	30	<0.001	8.23	**-6 21 -30**
Right: Anterior orbital gyrus, Medial orbital gyrus	26	<0.001	7.7	**30 51 -18**
GCOR: Decreasing with age				

Bilateral: Middle temporal gyrus, Superior frontal gyrus (dorsolateral), Postcentral gyrus, Middle frontal gyrus, Precentral gyrus, Superior temporal gyrus, Inferior temporal gyrus, Superior frontal gyrus (medial), Inferior frontal gyrus (pars triangularis), Fusiform gyrus, Middle occipital gyrus, Supplementary motor area, Inferior parietal gyrus, Insula, Cerebellum (8), Lingual gyrus, Precuneus, Supramarginal gyrus, Middle cingulate & paracingulate gyri, Superior parietal gyrus, Calcarine fissure and surrounding cortex, Cerebellum (6), Rolandic operculum, Inferior frontal gyrus (pars opercularis), Cerebellum (4,5), Parahippocampal gyrus, Cuneus, Superior temporal gyrus (pole), Paracentral lobule, Superior occipital gyrus, Hippocampus, Middle temporal gyrus (pole), Angular gyrus, Cerebellum (9), Inferior occipital gyrus, Superior frontal gyrus (medial orbital), Anterior cingulate cortex (supracallosal), Inferior frontal gyrus (pars orbitalis), Putamen, Anterior cingulate cortex (pregenual), Cerebellum (Crus 2), Gyrus rectus, Cerebellum (Crus 1), Vermis (4,5), Posterior orbital gyrus, Caudate nucleus, Cerebellum (7b), Vermis (6), Amygdala, Vermis (8), Heschl's gyrus, Olfactory cortex, Anterior cingulate cortex (subgenual), Lateral orbital gyrus, Vermis (9), Vermis (3), Cerebellum (3), Vermis (7), Posterior cingulate gyrus, Thalamus (pulvinar medial), Medial orbital gyrus, Ventral striatum, Pallidum, Thalamus (mediodorsal medial magnocellular), Thalamus (ventral posterolateral), Vermis (1,2), Thalamus (pulvinar inferior), Anterior orbital gyrus, Thalamus (pulvinar anterior), Thalamus (lateral geniculate), Vermis (10), Thalamus (pulvinar lateral), Thalamus (intralaminar), Raphe nucleus, Thalamus (medial geniculate), Thalamus (mediodorsal lateral parvocellular) **Left**: Cerebellum (10), Thalamus (lateral posterior	39066	<0.001	28.32	**45 9 -12**
GCOR: Increasing with age				
Bilateral: Thalamus (mediodorsal medial magnocellular), Caudate nucleus, Thalamus (ventral lateral), Thalamus (pulvinar medial), Thalamus (mediodorsal lateral parvocellular), Thalamus (anteroventral nucleus), Thalamus (lateral posterior), Hippocampus, Thalamus (intralaminar) **Left**: Thalamus (ventral anterior) **Right**: Thalamus (pulvinar anterior), Posterior cingulate gyrus	206	<0.001	19.61	**3 -12 12**
Left: Cerebellum (Crus 1), Cerebellum (Crus 2), Cerebellum (6)	380	<0.001	15.75	**-45 -72 -30**
Bilateral: Precuneus **Left**: Superior parietal gyrus **Right**: Superior occipital gyrus, Cuneus	180	<0.001	12.52	**15 -63 42**
Bilateral: Posterior cingulate gyrus´ **Right**: Middle cingulate & paracingulate gyri	68	<0.001	12.14	**0 -24 27**
Right: Cerebellum (Crus 1), Cerebellum (6), Cerebellum (Crus 2), Lingual gyrus, Fusiform gyrus, Calcarine fissure and surrounding cortex	199	<0.001	11.78	**12 -99 -12**

Supplementary Table 5: Co-localization of **aging in brain functional measures** (unthresholded voxel-wise maps of annual change) and neurotransmitter systems – *before atrophy correction*.

	fALFF		LCOR		GCOR	
Neurotransmitter system	Rho	P_{FDR}	Rho	P_{FDR}	Rho	P_{FDR}
5-HT1a	0.1	0.6343	0.1	0.6216	0.1	0.1429
5-HT1b	-0.15	0.5644	-0.15	0.5798	-0.15	0.659
5-HT2a	-0.12	0.592	-0.12	0.5798	-0.12	0.9195
5-HT4	**0.24**	**0.0399**	0.24	0.5798	0.24	0.5239
5-HT6	**-0.31**	**0.0044**	-0.31	0.3043	-0.31	0.5239
A4B2	-0.05	0.7282	-0.05	0.9755	-0.05	0.9195
CB1	0.17	0.5644	0.17	0.5798	0.17	0.9195
D1	0.05	0.7282	0.05	0.8403	0.05	0.1178
D2	**0.23**	**0.0421**	0.23	0.5798	0.23	0.9739
DAT	0.02	0.8802	**0.02**	**0.0006**	0.02	0.7522
GABAa	**-0.39**	**0.0038**	-0.39	0.5798	-0.39	0.1985
H3	<0.01	0.9941	<0.01	0.6836	<0.01	0.9195
M1	-0.14	0.5644	-0.14	0.5798	-0.14	0.7522
Mu	0.31	0.2216	0.31	0.5798	0.31	0.8353
NET	**-0.5**	**0.0038**	**-0.5**	**0.0209**	**-0.5**	**0.0171**
NMDA	**-0.34**	**0.0421**	**-0.34**	**0.0033**	-0.34	0.9195
SERT	-0.09	0.5644	**-0.09**	**0.0006**	-0.09	0.9195
VAChT	-0.03	0.833	**-0.03**	**0.0006**	-0.03	0.1411
mGluR5	-0.3	0.1183	-0.3	0.6216	-0.3	0.1411

Bold numbers highlight significant correlations. Rho: Spearman correlation coefficient.

Supplementary Table 6: Co-localization of **aging in brain functional measures** (unthresholded voxel-wise maps of annual change) and neurotransmitter systems – *after atrophy correction*.

	fALFF		LCOR		GCOR	
Neurotransmitter system	Rho	P_{FDR}	Rho	P_{FDR}	Rho	P_{FDR}
5-HT1a	0.09	0.6088	0.09	0.6497	0.09	0.1254
5-HT1b	-0.17	0.4982	-0.17	0.5704	-0.17	0.6017
5-HT2a	-0.14	0.6017	-0.14	0.5704	-0.14	0.8934
5-HT4	**0.23**	**0.0407**	0.23	0.5704	0.23	0.6017
5-HT6	**-0.29**	**0.0095**	-0.29	0.3616	-0.29	0.6017
A4B2	-0.06	0.6088	-0.06	0.9926	-0.06	0.9099
CB1	0.15	0.6017	0.15	0.5704	0.15	0.8934
D1	0.07	0.6017	0.07	0.9573	0.07	0.0703
D2	**0.24**	**0.0337**	0.24	0.5704	0.24	0.9762

DAT	0.05	0.6387	**0.05**	**0.0006**	0.05	0.6017
GABAa	**-0.38**	**0.0038**	-0.38	0.5704	-0.38	0.2346
H3	<0.01	0.9796	<0.01	0.729	<0.01	0.8934
M1	-0.13	0.6017	-0.13	0.5704	-0.13	0.7047
Mu	0.29	0.2878	0.29	0.5704	0.29	0.8381
NET	**-0.48**	**0.0085**	**-0.48**	**0.0228**	**-0.48**	**0.0114**
NMDA	-0.31	0.0731	**-0.31**	**0.0057**	-0.31	0.8934
SERT	-0.08	0.6017	**-0.08**	**0.0006**	-0.08	0.8934
VAChT	-0.01	0.9232	**-0.01**	**0.0006**	-0.01	0.1254
mGluR5	-0.28	0.1664	-0.28	0.6497	-0.28	0.1254

Bold numbers highlight significant correlations. Rho: Spearman correlation coefficient.

Supplementary Table 7: Anatomical regions covered by sex-differences (T-contrasts) - *before atrophy correction*.

Anatomical region	**Cluster size**	**Cluster p-values (corrected)**	**Peak T-values**	**Peak MNI-Coordinates**
FALFF: Female < Male				
Bilateral: Postcentral gyrus, middle frontal gyrus, precentral gyrus, middle occipital gyrus, superior temporal gyrus (incl. pole), calcarine fissure and surrounding cortex, dorsolateral and medial superior frontal gyrus, lingual gyrus, middle temporal gyrus (incl. pole), inferior parietal gyrus, insula, supplementary motor area, fusiform gyrus, supramarginal gyrus, inferior frontal gyrus (pars triangularis & orbitalis), inferior temporal gyrus, superior parietal gyrus, rolandic operculum, cuneus, superior occipital gyrus, cerebellum (4,5,6,7b,8,9,10) crus1, crus2), vermis (4,5,6,8) middle cingulate gyrus, paracentral lobule, inferior occipital gyrus, putamen, precuneus, orbital gyrus (posterior, medial, anterior, lateral), parahippocampal gyrus, anterior cingulate cortex (subgenual, pregenual, supracallosal), hippocampus, Heschl gyrus, angular gyrus, amygdala, gyrus rectus, thalamus (pulvinar medial, mediodorsal medial magnocellular, ventral posterolateral, mediodorsal lateral parvocellular, pulvinar lateral, ventral lateral, pulvinar anterior, anteroventral nucleus, intralaminar, lateral geniculate, medial geniculate), caudate, pallidum, olfactory cortex, ventral striatum, raphe nucleus (dorsal), substantia nigra (pars compacta), red nucleus, **Left**: Thalamus (ventral anterior), Ventral tegmental area	29898	<0.001	29.31	**-57 -3 15**
Right: Cerebellum (7b, 8, crus1, crus2)	58	<0.001	19.43	**54 -54 -42**
Right: Caudate	47	<0.001	11.11	**18 -9 27**
FALFF: Female > Male				
Bilateral: Cerebellum 9, Vermis 9	182	<0.001	23.01	**0 -54 -51**

Bilateral: Frontal gyrus (medial pars orbitalis, superior dorsolateral & medial), gyrus rectus, anterior cingulate gyrus (subgenual), orbital gyrus (anterior & medial) **Right**: Anterior cingulate gyrus (pregenual)	497	<0.001	22.65	**-15 69 9**
Bilateral: Precuneus, cingulate gyrus (middle & posterior), calcarine fissure and surrounding cortex, vermis (4,5) **Left:** Cuneus **Right:** Lingual gyrus	974	<0.001	20.82	**6 -57 21**
Right: Temporal gyrus (inferior, middle, superior)	574	<0.001	19.08	**66 -15 -15**
Bilateral: Superior frontal gyrus (medial) **Left:** Frontal gyrus (superior, middle), supplementary motor area	369	<0.001	15.14	**-27 18 57**
Bilateral: Superior frontal gyrus (medial) **Left:** Frontal gyrus (superior, middle), supplementary motor area	390	<0.001	15.03	**30 18 57**
Bilateral: Vermis (7) **Right:** Cerebellum (6, 7b, 8, crus1, crus2)	421	<0.001	12.17	**27 -75 -33**
Left: Temporal gyrus (middle & inferior)	319	<0.001	11.98	**-69 -27 -9**
Left: Cerebellum (6,7b,8, crus1, crus2)	315	<0.001	11.63	**-36 -63 -39**
Left: Parietal gyrus (superior & inferior), occipital gyrus (middle), angular gyrus	104	<0.001	11.51	**-36 -72 39**
Right: Gyrus rectus, orbital gyrus (medial)	24	<0.001	10.29	**9 21 -24**
Right: Angular gyrus, occipital gyrus (middle)	51	<0.001	10.00	**45 -66 33**
Left: Frontal gyrus (superior, middle, inferior pars orbitalis)	37	<0.001	9.96	**-27 36 -9**
Left: Orbital gyrus (medial), gyrus rectus	20	<0.001	9.93	**-12 21 -24**
Left: Parahippocampal gyrus, fusiform gyrus, temporal gyrus (inferior)	34	<0.001	9.05	**-33 -39 -9**
Right: Parahippocampal gyrus, fusiform gyrus, hippocampus	28	<0.001	8.98	**33 -36 -12**
Right: Frontal gyrus (middle, inferior pars orbitalis), orbital gyrus (anterior)	25	<0.001	8.00	**33 39 -6**
LCOR: Female < Male				
Bilateral: Middle frontal gyrus, Postcentral gyrus, Middle occipital gyrus, Middle temporal gyrus, Precentral gyrus, Superior frontal gyrus (dorsolateral), Superior temporal gyrus, Inferior parietal gyrus, Inferior frontal gyrus (pars triangularis), Precuneus, Fusiform gyrus, Supplementary motor area, Calcarine fissure and surrounding cortex, Lingual gyrus, Insula, Supramarginal gyrus, Superior parietal gyrus, Cerebellum (Crus 1), Cerebellum (6), Middle cingulate & paracingulate gyri, Cerebellum (8), Superior frontal gyrus (medial), Cuneus, Angular gyrus, Cerebellum (Crus 2), Rolandic operculum, Inferior frontal gyrus (pars opercularis), Superior occipital gyrus, Cerebellum (4,5), Inferior temporal gyrus, Putamen, Superior temporal gyrus (pole), Paracentral lobule, Inferior occipital gyrus, Parahippocampal gyrus, Inferior frontal gyrus (pars orbitalis), Cerebellum (9), Middle temporal gyrus (pole), Cerebellum (7b), Anterior cingulate cortex (supracallosal), Anterior	37792	<0.001	30.05	**48 -15 15**

cingulate cortex (pregenual), Posterior orbital gyrus, Vermis (4,5), Hippocampus, Vermis (8), Heschl's gyrus, Vermis (6), Amygdala, Lateral orbital gyrus, Anterior orbital gyrus, Vermis (7), Cerebellum (3), Vermis (9), Pallidum, Thalamus (pulvinar medial), Medial orbital gyrus, Vermis (3), Thalamus (mediodorsal medial magnocellular), Thalamus (ventral posterolateral), Caudate nucleus, Thalamus (mediodorsal lateral parvocellular), Thalamus (pulvinar anterior), Thalamus (ventral lateral), Thalamus (intralaminar), Thalamus (pulvinar lateral), Thalamus (pulvinar inferior), Thalamus (medial geniculate), Thalamus (lateral geniculate), Olfactory cortex, Vermis (10), Vermis (1,2), Cerebellum (10) **Right:** Gyrus rectus, Superior frontal gyrus (medial orbital), Thalamus (lateral posterior), Thalamus (anteroventral nucleus), Posterior cingulate gyrus				
Bilateral: Substantia nigra pars compacta, Red nucleus **Left**: Ventral tegmental area		<0.001	9.79	**0 -18 -12**
LCOR: Female > Male				
Bilateral: Superior frontal gyrus (medial orbital), Superior frontal gyrus (dorsolateral), Gyrus rectus, Caudate nucleus, Superior frontal gyrus (medial), Medial orbital gyrus, Anterior cingulate cortex (subgenual), Anterior orbital gyrus, Middle frontal gyrus, Olfactory cortex, Thalamus (lateral posterior) **Left**: Anterior cingulate cortex (pregenual), Anterior cingulate cortex (supracallosal), Ventral striatum, Thalamus (pulvinar medial), Thalamus (ventral lateral), Thalamus (anteroventral nucleus)	1465	<0.001	34.53	**15 69 6**
Right: Middle temporal gyrus, Inferior temporal gyrus, Cerebellum (Crus 1), Cerebellum (6), Superior temporal gyrus, Fusiform gyrus, Cerebellum (Crus 2), Middle temporal gyrus (pole)	491	<0.001	22.7	69 -21 -18
Left: Hippocampus, Parahippocampal gyrus	51	<0.001	16.17	-33 -39 -3
Left: Inferior temporal gyrus, Middle temporal gyrus, Cerebellum (Crus 1), Cerebellum (7b), Cerebellum (6)	508	<0.001	15.84	-66 -27 -21
Right: Hippocampus, Parahippocampal gyrus	46	<0.001	14.41	33 -36 0
Bilateral: Cerebellum (9), Vermis (9)	47	<0.001	13.55	0 -48 -48
Right: Thalamus (mediodorsal medial magnocellular)	24	<0.001	13.14	0 -18 0
Bilateral: Precuneus, Posterior cingulate gyrus, Middle cingulate & paracingulate gyri, Calcarine fissure and surrounding cortex **Left**: Cuneus	269	<0.001	12.06	-9 -54 18
Right: Medial orbital gyrus, Olfactory cortex, Gyrus rectus, Posterior orbital gyrus	83	<0.001	11.58	9 15 -24
Left: Medial orbital gyrus, Olfactory cortex, Posterior orbital gyrus, Gyrus rectus, Parahippocampal gyrus	66	<0.001	10.09	-12 15 -24
GCOR: Female < Male				
Bilateral: Middle temporal gyrus, Middle frontal gyrus, Superior frontal gyrus (dorsolateral), Postcentral gyrus, Precuneus, Middle occipital gyrus, Precentral gyrus, Superior temporal gyrus, Inferior parietal gyrus, Superior frontal gyrus (medial), Inferior frontal gyrus (pars triangularis), Fusiform gyrus, Supplementary motor area, Calcarine fissure and surrounding cortex, Middle cingulate & paracingulate gyri, Lingual gyrus, Inferior temporal gyrus, Insula, Supramarginal gyrus, Cerebellum (8), Superior parietal gyrus, Angular gyrus, Cuneus, Cerebellum (6), Rolandic operculum, Inferior frontal gyrus (pars opercularis), Superior occipital gyrus, Cerebellum (4,5), Superior temporal gyrus (pole), Putamen, Parahippocampal gyrus, Paracentral lobule, Inferior occipital gyrus, Anterior cingulate cortex (supracallosal), Inferior frontal gyrus (pars orbitalis), Cerebellum (9), Superior frontal gyrus (medial orbital), Anterior cingulate cortex (pregenual), Hippocampus, Middle temporal gyrus (pole), Cerebellum (Crus 2), Anterior orbital gyrus, Posterior orbital gyrus, Vermis (4,5), Cerebellum (7b), Posterior cingulate gyrus, Caudate nucleus, Gyrus rectus, Medial orbital gyrus, Heschl's gyrus, Vermis (8), Vermis (6), Cerebellum (Crus 1), Amygdala, Lateral orbital gyrus, Thalamus (pulvinar medial), Vermis (9), Cerebellum (3), Ventral striatum, Anterior cingulate cortex (subgenual), Pallidum, Vermis (7), Vermis (3), Thalamus (mediodorsal medial magnocellular), Olfactory cortex, Thalamus (ventral posterolateral), Thalamus (mediodorsal lateral parvocellular), Thalamus (pulvinar inferior), Thalamus (pulvinar anterior), Thalamus (ventral lateral), Thalamus (pulvinar lateral), Thalamus (intralaminar), Thalamus (lateral geniculate), Substantia nigra pars compacta, Vermis (1,2), Thalamus (medial geniculate), Thalamus (lateral posterior), Thalamus (anteroventral nucleus), Vermis (10), Red nucleus, Raphe nucleus, Cerebellum (10)	43115	<0.001	26.55	**45 -15 9**

Left: Ventral tegmental area, Thalamus (ventral anterior)				
GCOR: Female > Male				
Right: Caudate nucleus	65	<0.001	18.82	**12 0 21**
Left: Hippocampus	42	<0.001	17.68	**-30 -39 3**
Left: Caudate nucleus, Thalamus (lateral posterior), Thalamus (pulvinar medial)	63	<0.001	16.76	**-12 -6 21**
Right: Superior frontal gyrus (medial), Superior frontal gyrus (dorsolateral), Superior frontal gyrus (medial orbital)	60	<0.001	15.08	**15 69 3**
Right: Hippocampus	33	<0.001	14.35	**33 -36 0**
Left: Superior frontal gyrus (dorsolateral), Superior frontal gyrus (medial), Superior frontal gyrus (medial orbital)	47	<0.001	13.77	**-12 69 6**
Left: Cerebellum (Crus 1), Cerebellum (Crus 2), Cerebellum (7b)	305	<0.001	12.84	**-51 -66 -30**
Right: Cerebellum (Crus 1), Cerebellum (Crus 2), Cerebellum (7b), Inferior temporal gyrus, Cerebellum (6)	194	<0.001	12.78	**54 -60 -33**
Bilateral: Cerebellum (9)	25	<0.001	10.74	**0 -51 -54**
Left: Medial orbital gyrus, Posterior orbital gyrus, Olfactory cortex, Parahippocampal gyrus, Gyrus rectus	29	<0.001	8.71	**-12 12 -24**
Right: Medial orbital gyrus, Olfactory cortex, Gyrus rectus	23	<0.001	8.02	**12 12 -24**

Supplementary Table 8: Anatomical regions covered by sex-differences (T-contrasts) - *after atrophy correction.*

Anatomical region	Cluster size	Cluster p-values (corrected)	Peak T-values	Peak MNI-Coordinates
FALFF: Female < Male				
Bilateral: Postcentral gyrus, Middle frontal gyrus, Precentral gyrus, Middle occipital gyrus, Superior temporal gyrus, Calcarine fissure and surrounding cortex, Superior frontal gyrus (dorsolateral), Lingual gyrus, Middle temporal gyrus, Inferior parietal gyrus, Insula, Fusiform gyrus, Supplementary motor area, Supramarginal gyrus, Inferior frontal gyrus (pars triangularis), Inferior temporal gyrus, Superior parietal gyrus, Rolandic operculum, Cuneus, Superior occipital gyrus, Cerebellum (6), Inferior frontal gyrus (pars opercularis), Middle cingulate & paracingulate gyri, Cerebellum (8), Paracentral lobule, Cerebellum (4,5), Inferior occipital gyrus, Superior temporal gyrus (pole), Putamen, Precuneus, Cerebellum (Crus 1), Superior frontal gyrus (medial), Middle temporal gyrus (pole), Inferior frontal gyrus (pars orbitalis), Parahippocampal gyrus, Posterior orbital gyrus, Vermis (4,5), Cerebellum (9), Cerebellum (Crus 2), Anterior orbital gyrus, Caudate nucleus, Hippocampus, Anterior cingulate cortex (supracallosal), Medial orbital gyrus, Anterior cingulate cortex (pregenual), Vermis (8), Heschl's gyrus, Angular gyrus, Amygdala, Vermis (6), Gyrus rectus, Cerebellum (7b), Lateral orbital gyrus, Thalamus (pulvinar medial), Thalamus (mediodorsal medial magnocellular), Cerebellum (3), Pallidum, Olfactory cortex, Vermis (9), Vermis (7), Ventral striatum, Vermis (3), Thalamus (ventral posterolateral), Thalamus (mediodorsal lateral	30583	<0.001	29.07	**48 -15 9**

parvocellular), Superior frontal gyrus (medial orbital), Thalamus (pulvinar inferior), Thalamus (ventral lateral), Thalamus (pulvinar anterior), Thalamus (anteroventral nucleus), Thalamus (pulvinar lateral), Thalamus (intralaminar), Vermis (10), Thalamus (lateral geniculate), Thalamus (lateral posterior), Substantia nigra pars compacta, Raphe nucleus, Anterior cingulate cortex (subgenual), Thalamus (medial geniculate), Red nucleus, Cerebellum (10) **Left**: Ventral tegmental area, Thalamus (ventral anterior)				
fALFF: Female > Male				
Bilateral: Superior frontal gyrus (medial orbital), Superior frontal gyrus (dorsolateral), Superior frontal gyrus (medial), Gyrus rectus, Anterior cingulate cortex (subgenual), Anterior orbital gyrus, Medial orbital gyrus **Left**: Anterior cingulate cortex (pregenual), Olfactory cortex	494	<0.001	22.53	**15 69 6**
Bilateral: Precuneus, Middle cingulate & paracingulate gyri, Posterior cingulate gyrus, Cuneus, Calcarine fissure and surrounding cortex, Vermis (4,5) **Right**: Lingual gyrus	934	<0.001	21.06	**6 -57 21**
Bilateral: Cerebellum (9)	147	<0.001	20.43	**-3 -54 -48**
Right: Middle temporal gyrus, Inferior temporal gyrus, Superior temporal gyrus	597	<0.001	20.27	**63 -15 -15**
Bilateral: Superior frontal gyrus (medial) **Right**: Superior frontal gyrus (dorsolateral), Middle frontal gyrus, Supplementary motor area	361	<0.001	14.73	**30 18 57**
Left: Superior frontal gyrus (dorsolateral), Middle frontal gyrus, Supplementary motor area, Superior frontal gyrus (medial)	356	<0.001	14.72	**-30 18 57**
Left: Middle temporal gyrus, Inferior temporal gyrus	384	<0.001	12.76	**-69 -27 -9**
Right: Cerebellum (Crus 1), Cerebellum (Crus 2), Cerebellum (7b), Cerebellum (6), Cerebellum (8)	286	<0.001	11.02	**30 -75 -33**
Right: Gyrus rectus, Medial orbital gyrus	23	<0.001	10.87	**12 21 -27**
Right: Angular gyrus, Middle occipital gyrus	49	<0.001	10.75	**45 -66 30**
Left: Inferior parietal gyrus, Angular gyrus, Middle occipital gyrus, Superior parietal gyrus	80	<0.001	10.49	**-36 -72 39**
Left: Cerebellum (Crus 2), Cerebellum (Crus 1), Cerebellum (7b), Cerebellum (8), Cerebellum (6)	178	<0.001	10.25	**-30 -75 -33**
Left: Inferior frontal gyrus (pars orbitalis), Middle frontal gyrus, Superior frontal gyrus (dorsolateral)	24	<0.001	7.68	**-27 39 -9**
LCOR: Female < Male				
Bilateral: Middle frontal gyrus, Postcentral gyrus, Middle occipital gyrus, Middle temporal gyrus, Precentral gyrus, Superior frontal gyrus (dorsolateral), Superior temporal gyrus, Inferior parietal gyrus, Inferior frontal gyrus (pars triangularis), Precuneus, Fusiform gyrus, Calcarine fissure and surrounding cortex, Supplementary motor area, Lingual gyrus, Insula, Supramarginal gyrus, Superior parietal gyrus, Cerebellum (Crus 1), Cerebellum (6), Middle cingulate & paracingulate gyri, Cerebellum (8), Superior frontal gyrus (medial), Cuneus,	38244	<0.001	32.67	**45 -15 12**

Cerebellum (Crus 2), Angular gyrus, Rolandic operculum, Inferior frontal gyrus (pars opercularis), Superior occipital gyrus, Cerebellum (4,5), Inferior temporal gyrus, Superior temporal gyrus (pole), Putamen, Paracentral lobule, Inferior occipital gyrus, Parahippocampal gyrus, Inferior frontal gyrus (pars orbitalis), Cerebellum (9), Middle temporal gyrus (pole), Anterior cingulate cortex (supracallosal), Cerebellum (7b), Anterior cingulate cortex (pregenual), Hippocampus, Posterior orbital gyrus, Vermis (4,5), Vermis (6), Vermis (8), Heschl's gyrus, Amygdala, Anterior orbital gyrus, Lateral orbital gyrus, Vermis (9), Vermis (7), Cerebellum (3), Pallidum, Thalamus (pulvinar medial), Medial orbital gyrus, Vermis (3), Thalamus (mediodorsal medial magnocellular), Thalamus (ventral posterolateral), Thalamus (mediodorsal lateral parvocellular), Caudate nucleus, Thalamus (pulvinar anterior), Thalamus (ventral lateral), Thalamus (pulvinar inferior), Thalamus (intralaminar), Vermis (10), Thalamus (pulvinar lateral), Thalamus (lateral geniculate), Thalamus (medial geniculate), Olfactory cortex, Vermis (1,2), Cerebellum (10) **Right**: Gyrus rectus, Superior frontal gyrus (medial orbital), Thalamus (lateral posterior), Thalamus (anteroventral nucleus), Posterior cingulate gyrus				
Bilateral: Substantia nigra pars compacta, Red nucleus **Left**: Ventral tegmental area	36	<0.001	9.74	**0 -18 -12**
LCOR: Female > Male				
Bilateral: Superior frontal gyrus (medial orbital), Superior frontal gyrus (dorsolateral), Gyrus rectus, Superior frontal gyrus (medial), Anterior cingulate cortex (subgenual), Medial orbital gyrus, Anterior orbital gyrus, Middle frontal gyrus, Olfactory cortex **Left**: Anterior cingulate cortex (pregenual)	1171	<0.001	34.43	**-15 69 6**
Right: Middle temporal gyrus, Inferior temporal gyrus, Cerebellum (Crus 1), Cerebellum (6), Superior temporal gyrus, Fusiform gyrus, Cerebellum (Crus 2), Middle temporal gyrus (pole)	487	<0.001	22.36	**69 -21 -18**
Bilateral: Caudate nucleus, Thalamus (lateral posterior) **Left:** Ventral striatum, Thalamus (pulvinar medial), Thalamus (ventral lateral), Thalamus (anteroventral nucleus)	270	<0.001	17	**-3 -6 15**
Left: Middle temporal gyrus, Inferior temporal gyrus, Cerebellum (Crus 1), Cerebellum (6), Cerebellum (7b)	489	<0.001	15.81	**-66 -24 -21**
Left: Hippocampus, Parahippocampal gyrus	46	<0.001	14.74	**-33 -36 -3**
Right: Hippocampus, Parahippocampal gyrus	37	<0.001	13.22	**33 -36 0**
Bilateral: Precuneus, Posterior cingulate gyrus, Middle cingulate & paracingulate gyri, Calcarine fissure and surrounding cortex **Left**: Cuneus	269	<0.001	12.87	**-9 -54 18**
Right: Medial orbital gyrus, Olfactory cortex, Gyrus rectus, Posterior orbital gyrus	80	<0.001	11.73	**9 15 -27**
Left: Medial orbital gyrus, Olfactory cortex, Posterior orbital gyrus, Gyrus rectus, Parahippocampal gyrus	69	<0.001	10.75	**-12 15 -24**

Bilateral: Cerebellum (9)	22	<0.001	10.71	**0 -48 -48**
GCOR: Female < Male				
Bilateral: Middle temporal gyrus, Middle frontal gyrus, Superior frontal gyrus (dorsolateral), Postcentral gyrus, Precuneus, Middle occipital gyrus, Precentral gyrus, Superior temporal gyrus, Inferior parietal gyrus, Superior frontal gyrus (medial), Inferior frontal gyrus (pars triangularis), Fusiform gyrus, Supplementary motor area, Calcarine fissure and surrounding cortex, Middle cingulate & paracingulate gyri, Lingual gyrus, Inferior temporal gyrus, Insula, Supramarginal gyrus, Cerebellum (8), Superior parietal gyrus, Angular gyrus, Cuneus, Cerebellum (6), Rolandic operculum, Inferior frontal gyrus (pars opercularis), Superior occipital gyrus, Cerebellum (4,5), Superior temporal gyrus (pole), Putamen, Parahippocampal gyrus, Paracentral lobule, Inferior occipital gyrus, Anterior cingulate cortex (supracallosal), Cerebellum (9), Inferior frontal gyrus (pars orbitalis), Superior frontal gyrus (medial orbital), Hippocampus, Anterior cingulate cortex (pregenual), Middle temporal gyrus (pole), Cerebellum (Crus 2), Anterior orbital gyrus, Posterior orbital gyrus, Vermis (4,5), Cerebellum (7b), Posterior cingulate gyrus, Caudate nucleus, Gyrus rectus, Medial orbital gyrus, Cerebellum (Crus 1), Vermis (6), Heschl's gyrus, Amygdala, Vermis (8), Lateral orbital gyrus, Thalamus (pulvinar medial), Vermis (9), Anterior cingulate cortex (subgenual), Cerebellum (3), Ventral striatum, Vermis (7), Pallidum, Vermis (3), Thalamus (mediodorsal medial magnocellular), Olfactory cortex, Thalamus (ventral posterolateral), Thalamus (mediodorsal lateral parvocellular), Thalamus (pulvinar inferior), Thalamus (pulvinar anterior), Thalamus (ventral lateral), Thalamus (pulvinar lateral), Vermis (10), Thalamus (intralaminar), Thalamus (lateral geniculate), Substantia nigra pars compacta, Vermis (1,2), Thalamus (medial geniculate), Thalamus (anteroventral nucleus), Red nucleus, Thalamus (lateral posterior), Raphe nucleus, Cerebellum (10) **Left**: Ventral tegmental area, Thalamus (ventral anterior)	43309	<0.001	28.94	**45 -15 9**
GCOR: Female > Male				
Right: Caudate nucleus	63	<0.001	17.97	**12 0 21**
Left: Hippocampus	41	<0.001	16.75	**-30 -39 3**
Left Caudate nucleus, Thalamus (lateral posterior), Thalamus (pulvinar medial)	60	<0.001	16.34	**-15 -12 24**
Right: Superior frontal gyrus (medial), Superior frontal gyrus (dorsolateral), Superior frontal gyrus (medial orbital)	60	<0.001	15.82	**15 69 3**
Left: Superior frontal gyrus (dorsolateral), Superior frontal gyrus (medial), Superior frontal gyrus (medial orbital)	46	<0.001	13.85	**-12 69 6**
Right: Hippocampus	32	<0.001	13.59	**30 -36 6**
Left: Cerebellum (Crus 1), Cerebellum (Crus 2), Cerebellum (7b)	295	<0.001	12.94	**-45 -42 -39**
Right: Cerebellum (Crus 1), Cerebellum (Crus 2), Cerebellum (7b), Inferior temporal gyrus, Cerebellum (6)	170	<0.001	12.55	**54 -63 -33**
Left: Medial orbital gyrus, Posterior orbital gyrus, Olfactory cortex, Gyrus rectus	29	<0.001	8.35	**-12 12 -24**
Right: Medial orbital gyrus, Olfactory cortex, Gyrus rectus	22	<0.001	8.07	**12 12 -24**

Supplementary Table 9: Co-localization of **sex differences in brain functional measures** (unthresholded voxel-wise T-maps) and neurotransmitter systems – *before atrophy correction*.

	fALFF		LCOR		GCOR	
Neurotransmitter system	Rho	P_{FDR}	Rho	P_{FDR}	Rho	P_{FDR}
5-HT1a	0.01	0.9855	0.01	0.8937	0.01	0.5794
5-HT1b	0.12	0.6393	0.12	0.4761	0.12	0.1514
5-HT2a	0.08	0.7707	0.08	0.8735	0.08	0.5682
5-HT4	-0.13	0.3764	-0.13	0.0574	-0.13	0.0809
5-HT6	0.21	0.084	**0.21**	**0.0019**	**0.21**	**0.0005**
A4B2	<0.01	0.9855	<0.01	0.2618	<0.01	0.2429
CB1	-0.12	0.7283	-0.12	0.9522	-0.12	0.7879
D1	-0.07	0.6826	-0.07	0.252	-0.07	0.9835
D2	0.01	0.9855	0.01	0.554	0.01	0.6187
DAT	0.11	0.4722	0.11	0.8735	0.11	0.6838
GABAa	0.25	0.0522	**0.25**	**0.0009**	**0.25**	**0.0005**
H3	-0.01	0.9855	-0.01	0.9522	-0.01	0.5682
M1	0.13	0.6254	0.13	0.5209	0.13	0.2896
Mu	-0.22	0.5527	-0.22	0.5209	-0.22	0.5794
NET	**0.57**	**0.0038**	**0.57**	**0.0009**	**0.57**	**0.0005**
NMDA	0.29	0.1086	0.29	0.252	0.29	0.113
SERT	0.21	0.084	0.21	0.9522	0.21	0.5794
VAChT	0.23	0.057	0.23	0.252	0.23	0.5794
mGluR5	0.25	0.2611	**0.25**	**0.0043**	**0.25**	**0.0005**

Bold numbers highlight significant correlations. Rho: Spearman correlation coefficient.

Supplementary Table 10: Co-localization of **sex differences in brain functional measures** (unthresholded voxel-wise T-maps) and neurotransmitter systems – *after atrophy correction*.

	fALFF		LCOR		GCOR	
Neurotransmitter system	Rho	P_{FDR}	Rho	P_{FDR}	Rho	P_{FDR}
5-HT1a	-0.01	0.9831	-0.01	0.9168	-0.01	0.5968
5-HT1b	0.1	0.6522	0.1	0.52	0.1	0.1485
5-HT2a	0.07	0.8329	0.07	0.9019	0.07	0.5706
5-HT4	-0.15	0.2344	-0.15	0.0483	-0.15	0.0711
5-HT6	0.2	0.1194	**0.2**	**0.0025**	**0.2**	**0.0005**
A4B2	<0.01	0.9831	<0.01	0.2677	<0.01	0.2705
CB1	-0.14	0.6522	-0.14	0.9168	-0.14	0.8053
D1	-0.08	0.6413	-0.08	0.2434	-0.08	0.9567
D2	-0.01	0.9831	-0.01	0.5261	-0.01	0.6028
DAT	0.11	0.5023	0.11	0.9019	0.11	0.7061
GABAa	0.25	0.0503	**0.25**	**0.0009**	**0.25**	**0.0005**
H3	-0.03	0.9164	-0.03	0.9168	-0.03	0.5706
M1	0.12	0.6413	0.12	0.5261	0.12	0.281
Mu	-0.23	0.5023	-0.23	0.5261	-0.23	0.5968
NET	**0.57**	**0.0019**	**0.57**	**0.0009**	**0.57**	**0.0005**
NMDA	0.28	0.1194	0.28	0.2434	0.28	0.1086
SERT	0.19	0.1194	0.19	0.9168	0.19	0.5968
VAChT	0.22	0.0849	0.22	0.2434	0.22	0.5968
mGluR5	0.25	0.2344	**0.25**	**0.0047**	**0.25**	**0.0005**

Bold numbers highlight significant correlations. Rho: Spearman correlation coefficient.

Supplementary Table 11: Co-localization strength of **fALFF** with neurotransmitter systems and the effects of age and sex – *before atrophy correction*.

	Co-localization strength*			Linear aging effects**			Sex differences**		
Neurotransmitter system	Median rho	IQR rho	Mean Fisher's z(rho)	Pearson r	Slope	P_{BH}	T	Cohen's d	P_{BH}
5-HT1a	-0.21	0.09	-0.2	0.11	0.0011	<0.001	11.26	0.14	<0.001
5-HT1b	0.43	0.07	0.46	-0.02	-0.0002	0.1079	-3.57	-0.04	0.0069
5-HT2a	0.4	0.09	0.42	0.08	0.0008	<0.001	8.18	0.1	<0.001
5-HT4	-0.29	0.09	-0.29	0.08	0.0008	<0.001	12.37	0.15	<0.001
5-HT6	0.27	0.08	0.27	-0.06	-0.0005	<0.001	-3.74	-0.05	0.0035
A4B2	0.1	0.1	0.11	0.02	0.0003	0.0027	5.91	0.07	<0.001
CB1	-0.14	0.14	-0.13	0.09	0.0013	<0.001	13.24	0.17	<0.001
D1	-0.42	0.08	-0.44	0.04	0.0004	<0.001	9.16	0.11	<0.001
D2	-0.47	0.09	-0.51	0.04	0.0005	<0.001	-0.81	-0.01	1
DAT	-0.68	0.06	-0.82	-0.07	-0.0009	<0.001	-9.61	-0.12	<0.001
GABAa	0.4	0.07	0.43	-0.06	-0.0005	<0.001	-7.43	-0.09	<0.001
H3	-0.28	0.11	-0.27	0.01	0.0002	0.3196	1.96	0.02	0.9435
M1	0.33	0.07	0.34	-0.02	-0.0001	0.2195	1.34	0.02	1
μ	-0.5	0.13	-0.53	0.11	0.0019	<0.001	13.58	0.17	<0.001
NET	0.51	0.12	0.57	-0.13	-0.0019	<0.001	-29.86	-0.37	<0.001
NMDA	-0.13	0.07	-0.13	-0.17	-0.0013	<0.001	-19.67	-0.25	<0.001
SERT	-0.5	0.07	-0.54	-0.17	-0.0015	<0.001	-25.48	-0.32	<0.001
VAChT	-0.56	0.11	-0.63	-0.05	-0.0008	<0.001	-14.58	-0.18	<0.001
mGluR5	0.3	0.1	0.32	<0.01	0.0001	1	-1.27	-0.02	1

* The distribution of all Fisher's z-transformed Spearman correlation coefficients (Rho) regarding a specific neurotransmitter system were all significantly (one-sample t-test, P_{BH}<0.0001) different from a null-distribution.

**Aging effects and sex differences based on linear regression and comparison (t-test, alpha=0.05), respectively, between men and women in individual Fisher's z-transformed Spearman correlation coefficients. Not significant aging effects and sex differences are highlighted in red. P_{BH}: Bonferroni-Holm corrected P-value

Supplementary Table 12: Co-localization strength of **LCOR** with neurotransmitter systems and the effects of age and sex – *before atrophy correction*.

	Co-localization strength*			Linear aging effects**			Sex differences**		
Neurotransmitter system	Median rho	IQR rho	Mean Fisher's z(rho)	Pearson r	Slope	P_{BH}	T	Cohen's d	P_{BH}
5-HT1a	-0.3	0.1	-0.31	-0.01	-0.0001	1	-1.57	-0.02	1
5-HT1b	0.32	0.11	0.33	0.12	0.0015	<0.001	5.78	0.07	<0.001
5-HT2a	0.2	0.11	0.2	0.13	0.0015	<0.001	9.1	0.11	<0.001
5-HT4	-0.4	0.1	-0.42	0.01	0.0001	1	5.99	0.07	<0.001
5-HT6	0.29	0.12	0.31	-0.06	-0.0008	<0.001	-3.68	-0.05	0.0045
A4B2	0.03	0.1	0.04	0.06	0.0007	<0.001	2.74	0.03	0.1164
CB1	-0.25	0.13	-0.25	0.07	0.0009	<0.001	7.17	0.09	<0.001
D1	-0.26	0.14	-0.25	-0.08	-0.0013	<0.001	0.83	0.01	1
D2	-0.43	0.13	-0.46	-0.11	-0.0018	<0.001	-6.78	-0.08	<0.001
DAT	-0.39	0.16	-0.41	-0.2	-0.0037	<0.001	-10.78	-0.14	<0.001
GABAa	0.49	0.09	0.54	-0.06	-0.0007	<0.001	-1.72	-0.02	1
H3	-0.21	0.16	-0.2	-0.06	-0.001	<0.001	-2.68	-0.03	0.1421
M1	0.22	0.11	0.23	0.05	0.0006	<0.001	7.7	0.1	<0.001
μ	-0.51	0.13	-0.54	0.02	0.0004	0.0071	7.9	0.1	<0.001
NET	0.59	0.13	0.67	-0.11	-0.002	<0.001	-23.75	-0.3	<0.001
NMDA	0.15	0.14	0.15	-0.2	-0.0029	<0.001	-12.5	-0.16	<0.001
SERT	-0.29	0.15	-0.3	-0.21	-0.0033	<0.001	-15.87	-0.2	<0.001
VAChT	-0.33	0.19	-0.34	-0.17	-0.0035	<0.001	-14.03	-0.18	<0.001
mGluR5	0.38	0.14	0.41	-0.04	-0.0008	<0.001	-3.3	-0.04	0.0183

* The distribution of all Fisher's z-transformed Spearman correlation coefficients (Rho) regarding a specific neurotransmitter system were all significantly (one-sample t-test, $P_{BH}<0.0001$) different from a null-distribution. IQR: Interquartile range of Spearman correlation coefficients.

**Aging effects and sex differences based on linear regression and comparison (t-test, alpha=0.05), respectively, between men and women in individual Fisher's z-transformed Spearman correlation coefficients. Not significant aging effects and sex differences are highlighted in red. P_{BH}: Bonferroni-Holm corrected P-value

Supplementary Table 13: Co-localization strength of **GCOR** with neurotransmitter systems and the effects of age and sex – *before atrophy correction*.

	Co-localization strength*			Linear aging effects**			Sex differences**		
Neurotransmitter system	Median rho	IQR rho	Mean Fisher's z(rho)	Pearson r	Slope	P_{BH}	T	Cohen's d	P_{BH}
5-HT1a	-0.24	0.21	-0.24	-0.1	-0.0023	<0.001	-9.21	-0.12	<0.001
5-HT1b	0.14	0.16	0.14	0.09	0.0015	<0.001	-11.82	-0.15	<0.001
5-HT2a	0.1	0.17	0.1	0.02	0.0003	0.0405	-1.57	-0.02	1
5-HT4	-0.28	0.16	-0.28	-0.01	-0.0002	1	1.87	0.02	1
5-HT6	0.19	0.19	0.19	-0.05	-0.001	<0.001	-15.69	-0.2	<0.001
A4B2	0.08	0.2	0.08	<0.01	-0.0001	1	-4.11	-0.05	0.0007
CB1	-0.26	0.22	-0.25	-0.04	-0.0009	<0.001	-9.82	-0.12	<0.001
D1	-0.2	0.22	-0.2	-0.01	-0.0002	1	-7.96	-0.1	<0.001
D2	-0.29	0.21	-0.29	-0.07	-0.0016	<0.001	-9.41	-0.12	<0.001
DAT	-0.23	0.22	-0.23	-0.07	-0.0015	<0.001	-8.61	-0.11	<0.001
GABAa	0.31	0.16	0.32	-0.04	-0.0007	<0.001	-14.42	-0.18	<0.001
H3	-0.17	0.28	-0.17	-0.04	-0.0012	<0.001	-10.8	-0.14	<0.001
M1	0.09	0.14	0.09	0.06	0.0009	<0.001	-7.28	-0.09	<0.001
μ	-0.36	0.25	-0.37	-0.01	-0.0003	1	-2.01	-0.03	0.8398
NET	0.5	0.23	0.53	-0.11	-0.0032	<0.001	-19.34	-0.24	<0.001
NMDA	0.16	0.19	0.16	-0.07	-0.0013	<0.001	-11.4	-0.14	<0.001
SERT	-0.17	0.18	-0.18	-0.08	-0.0014	<0.001	-8.72	-0.11	<0.001
VAChT	-0.15	0.28	-0.15	-0.12	-0.0032	<0.001	-11.21	-0.14	<0.001
mGluR5	0.27	0.27	0.28	-0.09	-0.0025	<0.001	-18.49	-0.23	<0.001

* The distribution of all Fisher's z-transformed Spearman correlation coefficients (Rho) regarding a specific neurotransmitter system were all significantly (one-sample t-test, P_{BH}<0.0001) different from a null-distribution. IQR: Interquartile range of Spearman correlation coefficients.

**Aging effects and sex differences based on linear regression and comparison (t-test, alpha=0.05), respectively, between men and women in individual Fisher's z-transformed Spearman correlation coefficients. Not significant aging effects and sex differences are highlighted in red. P_{BH}: Bonferroni-Holm corrected P-value

Supplementary Table 14: Co-localization strength of **fALFF** with neurotransmitter systems and the effects of age and sex – *after atrophy correction*.

	Co-localization strength*			Linear aging effects**			Sex differences**		
Neurotransmitter system	Median rho	IQR rho	Mean Fisher's z(rho)	Pearson r	Slope	P_{BH}	T	Cohen's d	P_{BH}
5-HT1a	-0.21	0.09	-0.2	0.1	0.001	<0.0001	11.86	0.15	<0.0001
5-HT1b	0.43	0.07	0.46	-0.02	-0.0002	0.0992	-3	-0.04	0.0512
5-HT2a	0.4	0.09	0.42	0.08	0.0007	<0.0001	8.91	0.11	<0.0001
5-HT4	-0.29	0.09	-0.29	0.07	0.0007	<0.0001	13.28	0.17	<0.0001
5-HT6	0.26	0.08	0.27	-0.04	-0.0003	<0.0001	-4.02	-0.05	0.0011
A4B2	0.1	0.1	0.11	0.02	0.0002	0.0699	6.24	0.08	<0.0001
CB1	-0.14	0.14	-0.13	0.08	0.0011	<0.0001	13.85	0.17	<0.0001
D1	-0.42	0.08	-0.44	0.06	0.0006	<0.0001	8.53	0.11	<0.0001
D2	-0.47	0.08	-0.51	0.05	0.0005	<0.0001	-0.49	-0.01	1
DAT	-0.68	0.06	-0.82	-0.04	-0.0005	<0.0001	-10.81	-0.14	<0.0001
GABAa	0.4	0.07	0.43	-0.03	-0.0003	<0.0001	-8.64	-0.11	<0.0001
H3	-0.28	0.11	-0.27	0.02	0.0002	0.0665	2.15	0.03	0.6061
MI	0.33	0.07	0.34	0	0	1	1.61	0.02	1
μ	-0.5	0.13	-0.53	0.09	0.0016	<0.0001	14.11	0.18	<0.0001
NET	0.51	0.12	0.57	-0.11	-0.0016	<0.0001	-30.12	-0.38	<0.0001
NMDA	-0.13	0.07	-0.13	-0.13	-0.001	<0.0001	-20.97	-0.26	<0.0001
SERT	-0.5	0.06	-0.54	-0.14	-0.0012	<0.0001	-26.31	-0.33	<0.0001
VAChT	-0.56	0.1	-0.63	-0.04	-0.0006	<0.0001	-14.69	-0.18	<0.0001
mGluR5	0.3	0.1	0.32	0.02	0.0002	0.0218	-1.76	-0.02	1

* The distribution of all Fisher's z-transformed Spearman correlation coefficients (Rho) regarding a specific neurotransmitter system were all significantly (one-sample t-test, P_{BH}<0.0001) different from a null-distribution. IQR: Interquartile range of Spearman correlation coefficients.

**Aging effects and sex differences based on linear regression and comparison (t-test, alpha=0.05), respectively, between men and women in individual Fisher's z-transformed Spearman correlation coefficients. Not significant aging effects and sex differences are highlighted in red. P_{BH}: Bonferroni-Holm corrected P-value

Supplementary Table 15: Co-localization strength of **LCOR** with neurotransmitter systems and the effects of age and sex – *after atrophy correction*.

	Co-localization strength*			Linear aging effects**			Sex differences**		
Neurotransmitter system	Median rho	IQR rho	Mean Fisher's z(rho)	Pearson r	Slope	P_{BH}	T	Cohen's d	P_{BH}
5-HT1a	-0.3	0.1	-0.31	0	-0.0001	1	-1.91	-0.02	1
5-HT1b	0.32	0.11	0.33	0.11	0.0013	<0.0001	6.45	0.08	<0.0001
5-HT2a	0.2	0.11	0.2	0.12	0.0014	<0.0001	9.47	0.12	<0.0001
5-HT4	-0.4	0.1	-0.42	0.01	0.0002	0.4093	6.14	0.08	<0.0001
5-HT6	0.29	0.12	0.31	-0.05	-0.0006	<0.0001	-3.92	-0.05	0.0017
A4B2	0.04	0.1	0.04	0.06	0.0006	<0.0001	3.15	0.04	0.0312
CB1	-0.25	0.13	-0.25	0.06	0.0009	<0.0001	7.21	0.09	<0.0001
D1	-0.26	0.14	-0.25	-0.07	-0.001	<0.0001	0.2	0	1
D2	-0.43	0.13	-0.46	-0.09	-0.0015	<0.0001	-7.34	-0.09	<0.0001
DAT	-0.39	0.16	-0.41	-0.17	-0.0032	<0.0001	-11.62	-0.15	<0.0001
GABAa	0.49	0.09	0.54	-0.04	-0.0005	<0.0001	-2.53	-0.03	0.2167
H3	-0.21	0.16	-0.2	-0.05	-0.0008	<0.0001	-2.91	-0.04	0.0689
M1	0.22	0.11	0.23	0.06	0.0007	<0.0001	7.82	0.1	<0.0001
μ	-0.51	0.13	-0.54	0.02	0.0003	0.041	7.89	0.1	<0.0001
NET	0.59	0.12	0.67	-0.1	-0.0017	<0.0001	-23.99	-0.3	<0.0001
NMDA	0.15	0.14	0.15	-0.18	-0.0026	<0.0001	-13.3	-0.17	<0.0001
SERT	-0.29	0.15	-0.3	-0.19	-0.003	<0.0001	-16.56	-0.21	<0.0001
VAChT	-0.33	0.19	-0.34	-0.15	-0.0032	<0.0001	-14.51	-0.18	<0.0001
mGluR5	0.38	0.14	0.41	-0.03	-0.0005	0.0001	-3.83	-0.05	0.0025

* The distribution of all Fisher's z-transformed Spearman correlation coefficients (Rho) regarding a specific neurotransmitter system were all significantly (one-sample t-test, P_{BH}<0.0001) different from a null-distribution. IQR: Interquartile range of Spearman correlation coefficients.

**Aging effects and sex differences based on linear regression and comparison (t-test, alpha=0.05), respectively, between men and women in individual Fisher's z-transformed Spearman correlation coefficients. Not significant aging effects and sex differences are highlighted in red. P_{BH}: Bonferroni-Holm corrected P-value

Supplementary Table 16: Co-localization strength of **GCOR** with neurotransmitter systems and the effects of age and sex – *after atrophy correction*.

	Co-localization strength*			Linear aging effects**			Sex differences**		
Neurotransmitter system	Median rho	IQR rho	Mean Fisher's z(rho)	Pearson r	Slope	P_{BH}	T	Cohen's d	P_{BH}
5-HT1a	-0.24	0.21	-0.24	-0.1	-0.0021	<0.0001	-9.63	-0.12	<0.0001
5-HT1b	0.14	0.16	0.14	0.08	0.0013	<0.0001	-11.41	-0.14	<0.0001
5-HT2a	0.1	0.17	0.1	0.02	0.0003	0.1381	-1.41	-0.02	1
5-HT4	-0.28	0.16	-0.28	-0.01	-0.0002	0.8886	2	0.03	0.8675
5-HT6	0.19	0.19	0.19	-0.04	-0.0007	<0.0001	-16.16	-0.2	<0.0001
A4B2	0.08	0.2	0.08	-0.01	-0.0001	1	-3.85	-0.05	0.0023
CB1	-0.26	0.22	-0.25	-0.04	-0.0009	<0.0001	-9.9	-0.12	<0.0001
D1	-0.2	0.22	-0.2	0	0.0001	1	-8.6	-0.11	<0.0001
D2	-0.29	0.21	-0.3	-0.06	-0.0014	<0.0001	-9.96	-0.12	<0.0001
DAT	-0.23	0.22	-0.23	-0.05	-0.0011	<0.0001	-9.43	-0.12	<0.0001
GABAa	0.31	0.16	0.32	-0.02	-0.0004	0.02	-15.39	-0.19	<0.0001
H3	-0.17	0.28	-0.17	-0.04	-0.001	<0.0001	-11.03	-0.14	<0.0001
M1	0.09	0.14	0.09	0.07	0.0009	<0.0001	-7.33	-0.09	<0.0001
μ	-0.37	0.25	-0.37	-0.01	-0.0004	0.5992	-2	-0.03	0.8633
NET	0.5	0.23	0.53	-0.1	-0.0028	<0.0001	-19.76	-0.25	<0.0001
NMDA	0.16	0.19	0.16	-0.05	-0.0008	<0.0001	-12.25	-0.15	<0.0001
SERT	-0.17	0.18	-0.18	-0.06	-0.0011	<0.0001	-9.47	-0.12	<0.0001
VAChT	-0.15	0.28	-0.15	-0.1	-0.0028	<0.0001	-11.69	-0.15	<0.0001
mGluR5	0.27	0.27	0.28	-0.08	-0.002	<0.0001	-19.23	-0.24	<0.0001

* The distribution of all Fisher's z-transformed Spearman correlation coefficients (Rho) regarding a specific neurotransmitter system were all significantly (one-sample t-test, P_{BH}<0.0001) different from a null-distribution. IQR: Interquartile range of Spearman correlation coefficients.

**Aging effects and sex differences based on linear regression and comparison (t-test, alpha=0.05), respectively, between men and women in individual Fisher's z-transformed Spearman correlation coefficients. Not significant aging effects and sex differences are highlighted in red. P_{BH}: Bonferroni-Holm corrected P-value

Supplementary Table 17: Statistical key figures of the White- and Goldfeld-Quandt-test for heteroskedasticity in the co-localizations (Fisher's z-transformed Spearman correlation coefficients) – *before atrophy correction*.

	White-test						Goldfeld-Quandt-test					
	fALFF		LCOR		GCOR		fALFF		LCOR		GCOR	
Neurotrans-mitter system	F	pFDR	F	pFDR	F	pFDR	F	pFDR	F	pFDR	F	pFDR
5-HT1a	**13.43**	**<0.0001**	2.78	0.07	**23.07**	**<0.0001**	**1.11**	**6.5E-07**	-	-	0.88	1
5-HT1b	**4.01**	**0.025**	2.79	0.07	**4.81**	**0.015**	0.95	0.99	-	-	**1.06**	**0.013**
5-HT2a	**4.66**	**0.015**	**7.46**	**0.0008**	0.49	0.68	**1.06**	**0.025**	**1.05**	**0.022**	-	-
5-HT4	**14.68**	**<0.0001**	**28.91**	**<0.0001**	1.16	0.40	**1.10**	**<0.0001**	**1.15**	**<0.0001**	-	-
5-HT6	1.03	0.40	**7.88**	**0.0006**	**4.76**	**0.015**	-	-	**1.08**	**0.0003**	**1.05**	**0.021**
A4B2	1.13	0.38	2.64	0.07	**22.04**	**<0.0001**	-	-	-	-	0.86	1
CB1	**4.63**	**0.015**	**7.9**	**0.0006**	**6.66**	**0.003**	**1.04**	**0.027**	**1.08**	**0.0003**	0.92	1
D1	**16.01**	**<0.0001**	**4.52**	**0.014**	1.79	0.24	**1.13**	**<0.0001**	**1.06**	**0.003**	-	-
D2	**19.55**	**<0.0001**	**16.12**	**<0.0001**	0.22	0.80	**1.14**	**<0.0001**	**1.13**	**<0.0001**	-	-
DAT	**14.98**	**<0.0001**	**13.47**	**<0.0001**	1.27	0.38	**1.14**	**<0.0001**	**1.09**	**<0.0001**	-	-
GABAa	**6.19**	**0.004**	**11.34**	**<0.0001**	1.95	0.22	1.04	0.06	**1.10**	**<0.0001**	-	-
H3	**13.53**	**<0.0001**	**16.36**	**<0.0001**	0.44	0.68	**1.10**	**<0.0001**	**1.13**	**<0.0001**	-	-
MI	0.45	0.67	**4.78**	**0.011**	**10.46**	**0.0001**	-	-	1.03	0.07	**1.10**	**<0.0001**
μ-opioid	**4.1**	**0.02**	3.13	0.052	**29.49**	**<0.0001**	1.03	0.13	-	-	0.86	1
NET	**13.24**	**<0.0001**	**50.27**	**<0.0001**	**9.07**	**0.0004**	**1.09**	**<0.0001**	**1.22**	**<0.0001**	**1.09**	**0.0004**
NMDA	2.42	0.11	**17.32**	**<0.0001**	**7.51**	**0.002**	-	-	**1.10**	**<0.0001**	**1.06**	**0.013**
SERT	0.13	0.88	**14.51**	**<0.0001**	**4.97**	**0.015**	-	-	**1.07**	**0.002**	**1.05**	**0.020**
VAChT	**37.62**	**<0.0001**	**18.68**	**<0.0001**	0.59	0.66	**1.18**	**<0.0001**	**1.11**	**<0.0001**	-	-
mGluR5	**10.91**	**<0.0001**	**25.01**	**<0.0001**	**7.29**	**0.002**	**1.10**	**<0.0001**	**1.18**	**<0.0001**	**1.05**	**0.020**

Bold numbers highlight significant results. F: F-statitstic.

Supplementary Table 18: Statistical key figures of the White- and Goldfeld-Quandt-test for heteroskedasticity in the co-localizations (Fisher's z-transformed Spearman correlation coefficients) – *after atrophy correction*.

	White-test						Goldfeld-Quandt-test					
	fALFF		LCOR		GCOR		fALFF		LCOR		GCOR	
Neurotrans-mitter system	F	pFDR	F	pFDR	F	pFDR	F	pFDR	F	pFDR	F	pFDR
5-HT1a	**11.59**	**<0.0001**	2.16	0.12	**26.28**	**<0.0001**	**1.11**	**<0.0001**	-	-	0.87	1
5-HT1b	**3.77**	**0.034**	3.12	0.053	3.6	0.058	0.95	0.99	-	-	-	-
5-HT2a	**4.9**	**0.013**	**6.59**	**0.002**	0.18	0.83	**1.07**	**0.001**	1.04	0.051	-	-
5-HT4	**12.72**	**<0.0001**	**23.09**	**<0.0001**	0.49	0.74	**1.09**	**<0.0001**	**1.14**	**<0.0001**	-	-
5-HT6	0.77	0.52	**6.29**	**0.003**	2.67	0.12	-	-	**1.07**	**0.001**	-	-
A4B2	1.05	0.42	1.61	0.20	**25.34**	**<0.0001**	-	-	-	-	0.85	1
CB1	**3.95**	**0.030**	**6.89**	**0.002**	**7.28**	**0.003**	**1.04**	**0.042**	**1.07**	**0.001**	0.92	1
D1	**13.64**	**<0.0001**	**3.31**	**0.046**	0.83	0.63	**1.12**	**<0.0001**	**1.05**	**0.012**	-	-
D2	**17.44**	**<0.0001**	**12.64**	**<0.0001**	0.78	0.63	**1.13**	**<0.0001**	**1.11**	**<0.0001**	-	-
DAT	**15.27**	**<0.0001**	**9.5**	**0.0002**	0.41	0.75	**1.14**	**<0.0001**	**1.07**	**0.001**	-	-
GABAa	**5.54**	**0.007**	**8.01**	**0.0006**	0.33	0.76	1.03	0.07	**1.08**	**0.0002**	-	-
H3	**11.57**	**<0.0001**	**14.99**	**<0.0001**	0.4	0.75	**1.09**	**<0.0001**	**1.12**	**<0.0001**	-	-
MI	0.34	0.75	**3.64**	**0.036**	**7.87**	**0.002**	-	-	1.02	0.13	**1.09**	**0.0003**
μ-opioid	**3.46**	**0.042**	3.04	0.054	**29.43**	**<0.0001**	1.02	0.18	-	-	0.86	1
NET	**10.95**	**<0.0001**	**37.38**	**<0.0001**	**5.24**	**0.017**	**1.08**	**0.0002**	**1.19**	**<0.0001**	**1.06**	**0.008**
NMDA	2.62	0.09	**12.42**	**<0.0001**	**4**	**0.044**	-	-	**1.08**	**0.0004**	1.04	0.13
SERT	0.06	0.94	**10.68**	**<0.0001**	2.92	0.10	-	-	**1.05**	**0.018**	-	-
VAChT	**35.68**	**<0.0001**	**15.35**	**<0.0001**	0.94	0.62	**1.18**	**<0.0001**	**1.09**	**<0.0001**	-	-
mGluR5	**11.86**	**<0.0001**	**22.69**	**<0.0001**	**4.03**	**0.044**	**1.11**	**<0.0001**	**1.17**	**<0.0001**	1.03	0.13

Bold numbers highlight significant results. F: F-statitstic.

Supplementary Table 19: Deviation scores of subjects with manifest PD compared to normative models – *before atrophy correction*.

	fALFF		LCOR		GCOR	
Neurotransmitter system	Median Z	P_{FDR}	Median Z	P_{FDR}	Median Z	P_{FDR}
5-HT1a	-0.13	0.4435	0.07	0.797	0.01	0.775
5-HT1b	**-0.4**	**0.0043**	**-0.29**	**0.0478**	**-0.29**	**0.0163**
5-HT2a	-0.26	0.1052	0	0.7309	-0.01	0.5572
5-HT4	-0.16	0.9167	-0.08	0.2989	-0.22	0.2844
5-HT6	**-0.47**	**0.0043**	**-0.39**	**0.0056**	**-0.51**	**0.0001**
A4B2	-0.07	0.9167	0.13	0.2677	-0.19	0.3655
CB1	-0.2	0.4435	-0.28	0.1216	-0.18	0.139
D1	-0.21	0.6035	**-0.29**	**0.0056**	**-0.43**	**0.0019**
D2	0.03	0.3857	**-0.56**	**0.0021**	**-0.45**	**0.0005**
DAT	-0.39	0.4435	**-0.45**	**0.0212**	**-0.37**	**0.0118**
GABAa	**-0.52**	**0.0089**	**-0.5**	**<0.0001**	**-0.64**	**0.0019**
H3	-0.25	0.0805	**-0.3**	**0.0245**	**-0.29**	**0.0306**
M1	**-0.56**	**0.0031**	-0.17	0.1156	**-0.52**	**0.0005**
Mu	-0.26	0.3275	-0.27	0.2523	0	0.5121
NET	-0.18	0.2474	**-0.46**	**0.0011**	**-0.31**	**0.0306**
NMDA	-0.09	0.9167	**-0.38**	**0.0021**	**-0.5**	**0.0005**
SERT	-0.25	0.9167	-0.41	0.0772	**-0.37**	**0.0337**
VAChT	-0.23	0.3319	**-0.26**	**0.0478**	-0.22	0.1279
mGluR5	**-0.43**	**0.0061**	**-0.43**	**0.0023**	**-0.33**	**0.0005**

Bold numbers highlight significant correlations. Median Z: Median deviation score of all subjects with manifest Parkinson's disease.

Supplementary Table 20: Deviation scores of subjects with manifest PD compared to normative models – *after atrophy correction*.

	fALFF		LCOR		GCOR	
Neurotransmitter system	Median Z	P_{FDR}	Median Z	P_{FDR}	Median Z	P_{FDR}
5-HT1a	-0.18	0.3879	0.05	0.8283	0.01	0.803
5-HT1b	**-0.38**	**0.0052**	-0.31	0.0512	**-0.38**	**0.0137**
5-HT2a	-0.21	0.101	-0.01	0.729	-0.01	0.5539
5-HT4	-0.2	0.9584	-0.11	0.299	-0.22	0.3222
5-HT6	**-0.45**	**0.0058**	**-0.41**	**0.0066**	**-0.43**	**0.0001**
A4B2	-0.09	0.9584	0.13	0.2565	-0.16	0.3484
CB1	-0.22	0.3805	-0.29	0.1182	-0.24	0.123
D1	-0.17	0.7212	**-0.38**	**0.0066**	**-0.49**	**0.002**
D2	0	0.3805	**-0.52**	**0.0023**	**-0.47**	**0.0007**
DAT	-0.31	0.4792	**-0.47**	**0.0244**	**-0.26**	**0.014**
GABAa	**-0.58**	**0.0128**	**-0.48**	**0.0001**	**-0.6**	**0.002**
H3	-0.29	0.0753	**-0.31**	**0.0256**	**-0.3**	**0.0347**
M1	**-0.59**	**0.0032**	-0.21	0.1203	**-0.59**	**0.0006**
Mu	-0.26	0.3115	-0.29	0.2242	0	0.4845
NET	-0.13	0.3805	**-0.48**	**0.0012**	**-0.29**	**0.0347**
NMDA	-0.09	0.962	**-0.35**	**0.0023**	**-0.46**	**0.0006**
SERT	-0.25	0.9584	-0.41	0.0813	**-0.35**	**0.043**
VAChT	-0.19	0.3805	-0.24	0.0512	-0.22	0.1384
mGluR5	**-0.42**	**0.0058**	**-0.39**	**0.0027**	**-0.3**	**0.0007**

Bold numbers highlight significant correlations. Median Z: Median deviation score of all subjects with manifest Parkinson's disease.

Supplementary Table 21: Correlation between deviation scores and reported disease duration in subjects with manifest PD – *before atrophy correction*.

	fALFF		LCOR		GCOR	
Neurotransmitter system	Pearson r	P_{FDR}	Pearson r	P_{FDR}	Pearson r	P_{FDR}
5-HT1a	-	-	-	-	-	-
5-HT1b	-0.16	0.3969	-0.2	0.6141	-0.13	0.9659
5-HT2a	-	-	-	-	-	-
5-HT4	-	-	-	-	-	-
5-HT6	-0.06	0.7641	-0.11	0.7756	-0.03	0. 9659
A4B2	-	-	-	-	-	-
CB1	-	-	-	-	-	-
D1	-	-	-0.16	0.6141	-0.07	0. 9659
D2	-	-	-0.03	0.9121	0.02	0. 9659
DAT	-	-	-0.01	0.9121	-0.02	0. 9659
GABAa	-0.16	0. 3969	**-0.38**	**0.0317**	-0.11	0. 9659
H3	-	-	-0.02	0.9121	0.01	0. 9659
M1	-0.22	0. 3969	-	-	-0.21	0. 9659
Mu	-	-	-	-	-	-
NET	-	-	0.13	0.7508	0.02	0. 9659
NMDA	-	-	-0.02	0.9121	-0.06	0. 9659
SERT	-	-	-	-	0.07	0. 9659
VAChT	-	-	0.18	0.6141	-	-
mGluR5	0.04	0. 7641	-0.09	0.8153	0.01	0. 9659

Bold numbers highlight significant correlations. Empty cells indicate pairs of functional measure and neurotransmitter system whose co-localization in PD was not significantly different from the norm.

Supplementary Table 22: Correlation between deviation scores and reported disease duration in subjects with manifest PD – *after atrophy correction*.

	fALFF		LCOR		GCOR	
Neurotransmitter system	Pearson r	P_{FDR}	Pearson r	P_{FDR}	Pearson r	P_{FDR}
5-HT1a	-	-	-	-	-	-
5-HT1b	-0.14	0.4986	-	-	-0.12	0.9744
5-HT2a	-	-	-	-	-	-
5-HT4	-	-	-	-	-	-
5-HT6	-0.05	0.7495	-0.09	0.9335	-0.03	0. 9744
A4B2	-	-	-	-	-	-
CB1	-	-	-	-	-	-
D1	-	-	-0.16	0. 9335	-0.07	0. 9744
D2	-	-	-0.02	0. 9335	0.03	0. 9744
DAT	-	-	-0.02	0. 9335	-0.02	0. 9744
GABAa	-0.16	0. 4986	**-0.38**	**0.0295**	-0.10	0. 9744
H3	-	-	-0.01	0. 9335	0.004	0. 9744
M1	-0.20	0. 4986	-	-	-0.20	0. 9744
Mu	-	-	-	-	-	-
NET	-	-	0.13	0. 9335	0.02	0. 9744
NMDA	-	-	-0.02	0. 9335	-0.06	0. 9744
SERT	-	-	-	-	0.07	0. 9744
VAChT	-	-	-	-	-	-
mGluR5	0.04	0. 7495	-0.08	0. 9335	0.01	0. 9744

Bold numbers highlight significant correlations. Empty cells indicate pairs of functional measure and neurotransmitter system whose co-localization in PD was not significantly different from the norm.

Supplementary Table 23: Correlation between deviation scores and cognitive scores in subjects with manifest PD – fALFF, *before atrophy correction*.

fALFF	Fluid intelligence (DF: 20016)		Numeric memory (DF: 4282)		Associated learning (DF: 20197)		Prospective memory (DF: 20018)		Reaction time (DF: 20023)		Symbol digit modality test (DF: 23324)		Trail making test, AN (DF: 6350)	
Neurotransmitter system	r	P_{FDR}	r	P_{FDR}	r	P_{FDR}	r	P_{FDR}	r	P_{FDR}	r	P_{FDR}	r	P_{FDR}
5-HT1b	-0.03	0.96	-0.11	0.84	0.03	0.96	0.35	0.54	0.07	0.92	-0.21	0.75	0.08	0.92
5-HT6	-0.02	0.96	-0.13	0.82	-0.05	0.96	-0.05	0.96	0.13	0.75	-0.19	0.75	0.21	0.75
GABAa	-0.18	0.75	-0.35	0.54	0.04	0.96	0	0.98	0.21	0.75	-0.05	0.96	0.26	0.75
MI	-0.16	0.75	-0.11	0.84	0.15	0.75	0.13	0.75	-0.01	0.96	-0.18	0.75	0.09	0.91
mGluR5	-0.13	0.75	-0.26	0.75	-0.02	0.96	-0.1	0.84	0.17	0.75	-0.25	0.75	0.25	0.75

DF: Datafield of cognitive score (instance 2: imaging visit) used for correlation analysis (cf.https://biobank.ndph.ox.ac.uk/showcase/).
AN: Trail making test, alphanumeric path.

Supplementary Table 24: Correlation between deviation scores and cognitive scores in subjects with manifest PD – fALFF, *after atrophy correction*.

fALFF	Fluid intelligence (DF: 20016)		Numeric memory (DF: 4282)		Associated learning (DF: 20197)		Prospective memory (DF: 20018)		Reaction time (DF: 20023)		Symbol digit modality test (DF: 23324)		Trail making test, AN (DF: 6350)	
Neurotransmitter system	r	P_{FDR}	r	P_{FDR}	r	P_{FDR}	r	P_{FDR}	r	P_{FDR}	r	P_{FDR}	r	P_{FDR}
5-HT1b	-0.02	0.98	-0.12	0.79	0.03	0.98	0.34	0.57	0.08	0.83	-0.21	0.7	0.07	0.9
5-HT6	-0.03	0.98	-0.15	0.74	-0.09	0.83	-0.01	0.98	0.16	0.7	-0.2	0.7	0.19	0.7
GABAa	-0.21	0.7	-0.32	0.7	0.01	0.98	0.04	0.98	0.23	0.7	-0.09	0.83	0.27	0.7
MI	-0.18	0.7	-0.11	0.81	0.14	0.74	0.12	0.74	0.02	0.98	-0.18	0.7	0.11	0.81
mGluR5	-0.13	0.74	-0.24	0.7	0	0.98	-0.11	0.79	0.14	0.74	-0.23	0.7	0.23	0.7

DF: Datafield of cognitive score (instance 2: imaging visit) used for correlation analysis (cf.https://biobank.ndph.ox.ac.uk/showcase/).
AN: Trail making test, alphanumeric path.

Supplementary Table 25: Correlation between deviation scores and cognitive scores in subjects with manifest PD - LCOR, *before atrophy correction*.

LCOR	Fluid intelligence (DF: 20016)		Numeric memory (DF: 4282)		Associated learning (DF: 20197)		Prospective memory (DF: 20018)		Reaction time (DF: 20023)		Symbol digit modality test (DF: 23324)		Trail making test, AN (DF: 6350)	
Neurotransmitter system	r	P_{FDR}	r	P_{FDR}	r	P_{FDR}	r	P_{FDR}	r	P_{FDR}	r	P_{FDR}	r	P_{FDR}
5-HT1b	-0.06	0.99	-0.01	0.99	0.19	0.99	0.02	0.99	-0.1	0.99	-0.15	0.99	0.14	0.99
5-HT6	0.04	0.99	0	0.99	0.05	0.99	0.03	0.99	0.02	0.99	-0.17	0.99	0.01	0.99
D1	0.13	0.99	-0.19	0.99	0.07	0.99	0.04	0.99	0.07	0.99	-0.13	0.99	0.06	0.99
D2	-0.03	0.99	-0.01	0.99	0.04	0.99	-0.04	0.99	0.18	0.99	-0.1	0.99	-0.03	0.99
DAT	0.14	0.99	-0.31	0.99	-0.22	0.99	-0.01	0.99	0.08	0.99	0	0.99	-0.09	0.99
GABAa	0.03	0.99	-0.16	0.99	0.07	0.99	0.19	0.99	0.13	0.99	-0.04	0.99	0.03	0.99
H3	0.05	0.99	-0.22	0.99	0.06	0.99	0.12	0.99	0.02	0.99	-0.17	0.99	0.07	0.99
NET	-0.2	0.99	-0.2	0.99	-0.22	0.99	-0.04	0.99	0.28	0.99	-0.24	0.99	-0.1	0.99
NMDA	0.16	0.99	-0.25	0.99	-0.23	0.99	0.06	0.99	0.13	0.99	-0.07	0.99	-0.13	0.99
VAChT	0.11	0.99	-0.36	0.99	-0.25	0.99	-0.03	0.99	0.01	0.99	-0.04	0.99	-0.02	0.99
mGluR5	-0.03	0.99	-0.17	0.99	0.03	0.99	0.09	0.99	0.1	0.99	-0.2	0.99	0.12	0.99

DF: Datafield of cognitive score (instance 2: imaging visit) used for correlation analysis (cf.https://biobank.ndph.ox.ac.uk/showcase/).
AN: Trail making test, alphanumeric path.

Supplementary Table 26: Correlation between deviation scores and cognitive scores in subjects with manifest PD - LCOR, *after atrophy correction*.

LCOR	Fluid intelligence (DF: 20016)		Numeric memory (DF: 4282)		Associated learning (DF: 20197)		Prospective memory (DF: 20018)		Reaction time (DF: 20023)		Symbol digit modality test (DF: 23324)		Trail making test, AN (DF: 6350)	
Neurotransmitter system	r	P_{FDR}	r	P_{FDR}	r	P_{FDR}	r	P_{FDR}	r	P_{FDR}	r	P_{FDR}	r	P_{FDR}
5-HT1b	-0.07	0.99	-0.01	0.99	0.19	0.99	0.01	0.99	-0.09	0.99	-0.15	0.99	0.13	0.99
5-HT6	0.02	0.99	0	0.99	0.06	0.99	0.03	0.99	0.04	0.99	-0.19	0.99	0.03	0.99
D1	0.13	0.99	-0.2	0.99	0.07	0.99	0.05	0.99	0.07	0.99	-0.11	0.99	0.05	0.99
D2	-0.03	0.99	-0.02	0.99	0.07	0.99	-0.02	0.99	0.21	0.99	-0.09	0.99	-0.05	0.99
DAT	0.15	0.99	-0.29	0.99	-0.21	0.99	-0.01	0.99	0.09	0.99	-0.01	0.99	-0.11	0.99
GABAa	0.03	0.99	-0.14	0.99	0.1	0.99	0.2	0.99	0.17	0.99	-0.05	0.99	0	0.99
H3	0.04	0.99	-0.21	0.99	0.08	0.99	0.12	0.99	0.04	0.99	-0.19	0.99	0.09	0.99
NET	-0.19	0.99	-0.21	0.99	-0.2	0.99	-0.04	0.99	0.27	0.99	-0.24	0.99	-0.11	0.99
NMDA	0.16	0.99	-0.24	0.99	-0.22	0.99	0.05	0.99	0.15	0.99	-0.08	0.99	-0.12	0.99
VAChT	0.11	0.99	-0.34	0.99	-0.24	0.99	-0.02	0.99	0.02	0.99	-0.04	0.99	-0.02	0.99
mGluR5	-0.03	0.99	-0.15	0.99	0.04	0.99	0.11	0.99	0.13	0.99	-0.21	0.99	0.13	0.99

DF: Datafield of cognitive score (instance 2: imaging visit) used for correlation analysis (cf.https://biobank.ndph.ox.ac.uk/showcase/).
AN: Trail making test, alphanumeric path.

Supplementary Table 27: Correlation between deviation scores and cognitive scores in subjects with manifest PD - GCOR, *before atrophy correction*.

GCOR	Fluid intelligence (DF: 20016)		Numeric memory (DF: 4282)		Associated learning (DF: 20197)		Prospective memory (DF: 20018)		Reaction time (DF: 20023)		Symbol digit modality test (DF: 23324)		Trail making test, AN (DF: 6350)	
Neurotransmitter system	r	P_{FDR}	r	P_{FDR}	r	P_{FDR}	r	P_{FDR}	r	P_{FDR}	r	P_{FDR}	r	P_{FDR}
5-HT1b	-0.38	0.44	-0.24	0.63	-0.04	0.95	-0.06	0.95	0.04	0.95	-0.14	0.95	0.35	0.55
5-HT6	-0.27	0.63	-0.27	0.63	-0.1	0.95	0.04	0.95	0.14	0.91	-0.31	0.63	0.37	0.47
D1	0.04	0.95	-0.26	0.63	0.16	0.91	0.04	0.95	-0.02	0.95	-0.02	0.96	0.15	0.95
D2	-0.06	0.95	0.12	0.95	0.26	0.63	0.08	0.95	0.02	0.95	-0.03	0.95	-0.09	0.95
DAT	0.11	0.95	-0.16	0.91	0.06	0.95	-0.03	0.95	0.06	0.95	0.02	0.95	0.01	0.96
GABAa	-0.17	0.8	-0.39	0.44	-0.26	0.63	-0.14	0.91	0.05	0.95	-0.05	0.95	0.11	0.95
H3	-0.09	0.95	-0.24	0.63	0.03	0.95	0.11	0.95	0	0.99	-0.2	0.76	0.26	0.63
MI	-0.09	0.95	0.01	0.96	0.19	0.8	-0.04	0.95	-0.05	0.95	0.08	0.95	-0.03	0.95
NET	-0.15	0.91	-0.23	0.69	-0.44	0.44	-0.02	0.95	0.26	0.63	-0.22	0.69	0.2	0.8
NMDA	0.12	0.95	-0.24	0.63	-0.28	0.63	-0.06	0.95	0.1	0.95	-0.03	0.95	0.11	0.95
SERT	0.12	0.95	-0.27	0.63	0.05	0.95	0.04	0.95	0.11	0.95	0.02	0.95	-0.09	0.95
mGluR5	-0.19	0.76	-0.27	0.63	-0.09	0.95	0.11	0.95	0.05	0.95	-0.21	0.75	0.26	0.63

DF: Datafield of cognitive score (instance 2: imaging visit) used for correlation analysis (cf.https://biobank.ndph.ox.ac.uk/showcase/).
AN: Trail making test, alphanumeric path.

Supplementary Table 28: Correlation between deviation scores and cognitive scores in subjects with manifest PD - GCOR, *after atrophy correction*.

GCOR	Fluid intelligence (DF: 20016)		Numeric memory (DF: 4282)		Associated learning (DF: 20197)		Prospective memory (DF: 20018)		Reaction time (DF: 20023)		Symbol digit modality test (DF: 23324)		Trail making test, AN (DF: 6350)	
Neurotransmitter system	r	P_{FDR}	r	P_{FDR}	r	P_{FDR}	r	P_{FDR}	r	P_{FDR}	r	P_{FDR}	r	P_{FDR}
5-HT1b	-0.37	0.32	-0.26	0.66	-0.05	0.99	-0.06	0.99	0.02	0.99	-0.15	0.83	0.36	0.52
5-HT6	-0.29	0.62	-0.25	0.66	-0.11	0.94	0.01	0.99	0.14	0.82	-0.34	0.56	0.41	0.32
D1	0.03	0.99	-0.25	0.66	0.19	0.77	0.04	0.99	0	0.99	-0.03	0.99	0.17	0.81
D2	-0.05	0.99	0.15	0.83	0.28	0.66	0.08	0.97	0.02	0.99	-0.03	0.99	-0.1	0.97
DAT	0.1	0.94	-0.14	0.83	0.05	0.99	-0.03	0.99	0.07	0.98	0	0.99	0.03	0.99
GABAa	-0.18	0.74	-0.37	0.47	-0.25	0.66	-0.16	0.77	0.06	0.99	-0.07	0.99	0.13	0.9
H3	-0.11	0.94	-0.24	0.66	0.02	0.99	0.11	0.91	0.01	0.99	-0.21	0.74	0.27	0.66
M1	-0.12	0.9	0	0.99	0.18	0.77	-0.05	0.99	-0.02	0.99	0.06	0.99	0.02	0.99
NET	-0.17	0.77	-0.23	0.67	-0.44	0.32	-0.01	0.99	0.25	0.66	-0.23	0.67	0.19	0.77
NMDA	0.08	0.97	-0.25	0.66	-0.25	0.66	-0.06	0.99	0.13	0.83	-0.06	0.99	0.17	0.81
SERT	0.11	0.91	-0.22	0.67	0.09	0.97	0.04	0.99	0.15	0.81	0.03	0.99	-0.09	0.97
mGluR5	-0.19	0.72	-0.26	0.66	-0.09	0.97	0.1	0.94	0.04	0.99	-0.22	0.67	0.27	0.66

DF: Datafield of cognitive score (instance 2: imaging visit) used for correlation analysis (cf.https://biobank.ndph.ox.ac.uk/showcase/).
AN: Trail making test, alphanumeric path.

Supplementary Table 29: Statistics on the correlation of effect sizes (Cohen's d) in fALFF, LCOR, and GCOR between PD and HCmatched and the regional contributions ($\Delta\rho^2$) – *before atrophy correction*. This analysis was performed only for the pairs of brain measure and neurotransmitter system in which PD deviated significantly from the norm.

	fALFF		LCOR		GCOR	
Neurotransmitter map	Pearson r	P_{FDR}	Pearson r	P_{FDR}	Pearson r	P_{FDR}
5-HT1b	0.02	0.80	|r|<0.01	0.98	-0.1	0.42
5-HT6	0.11	0.48	0.12	0.34	0.15	0.31
D1	-	-	0.05	0.72	|r|<0.01	0.97
D2	-	-	-0.06	0.68	-0.05	0.69
DAT	-	-	0.16	0.28	0.14	0.31
GABAa	0.07	0.57	0.14	0.28	0.06	0.69
H3	-	-	-0.09	0.55	-0.02	0.91
M1	0.19	0.21	-	-	-0.11	0.39
NET	-	-	0.14	0.28	0.11	0.39
NMDA	-	-	**0.37**	**0.0003**	**0.44**	**<0.0001**
SERT	-	-	-	-	0.20	0.11
VAChT	-	-	-0.04	0.72	-	-
mGluR5	-0.10	0.48	**-0.28**	**0.013**	**0.28**	**0.014**

Bold numbers highlight significant correlation between effect sizes and regional contribution.

Supplementary Table 30: Statistics on the correlation of effect sizes (Cohen's d) in fALFF, LCOR, and GCOR between PD and HCmatched and the regional contributions ($\Delta\rho^2$) – *after atrophy correction*. This analysis was performed only for the pairs of brain measure and neurotransmitter system in which PD deviated significantly from the norm.

	fALFF		LCOR		GCOR	
Neurotransmitter map	Pearson r	P_{FDR}	Pearson r	P_{FDR}	Pearson r	P_{FDR}
5-HT1b	0.02	0.80	-	-	-0.13	0.27
5-HT6	0.12	0.49	0.10	0.48	**0.25**	**0.04**
D1	-	-	0.06	0.52	0.01	0.98
D2	-	-	-0.07	0.52	-0.06	0.63
DAT	-	-	0.17	0.20	0.14	0.27
GABAa	0.04	0.79	0.06	0.52	0.12	0.31
H3	-	-	-0.08	0.52	|r|<0.01	0.98
M1	**0.25**	**0.03**	-	-	-0.08	0.50
NET	-	-	0.12	0.44	0.14	0.27
NMDA	-	-	**0.35**	**0.0009**	**0.42**	**<0.0001**
SERT	-	-	-	-	0.20	0.10
VAChT	-	-	-	-	-	-
mGluR5	-0.09	0.48	**-0.28**	**0.0092**	0.22	0.06

Bold numbers highlight significant correlation between effect sizes and regional contribution.

Supplementary Table 31: Statistics on regional differences in fALFF, LCOR, and GCOR between PD and HCmatched assessed using the Mann-Whitney-U test – *before atrophy correction*.

	fALFF				LCOR				GCOR			
	Left		Right		Left		Right		Left		Right	
Region	U statistic	P_{FDR}	U statistic	P_{FDR}	U statistic	P_{FDR}	U statistic	P_{FDR}	U statistic	P_{FDR}	U statistic	P_{FDR}
Accumbens	1.64	0.4662	1.11	0.6261	**4.1**	**0.0013**	1.85	0.1216	**3.47**	**0.0087**	**2.56**	**0.0199**
Caudate	2.18	0.3162	1.69	0.4662	**3.12**	**0.0119**	1.81	0.1302	**3.95**	**0.0084**	**3.22**	**0.0101**
Putamen	1.26	0.5564	0.55	0.8665	**3.97**	**0.0017**	**2.66**	**0.0322**	**3.81**	**0.0084**	**3.11**	**0.0101**
Pallidum	1.25	0.5564	0.09	0.996	**3.4**	**0.0047**	2.22	0.0622	**2.63**	**0.0186**	**2.91**	**0.011**
Amygdala	0.67	0.8421	-0.13	0.996	**2.46**	**0.0475**	0.89	0.4933	**2.6**	**0.019**	2.03	0.0509
Hippocampus	0.72	0.8345	-0.08	0.996	**2.66**	**0.0322**	0.93	0.4761	**3.52**	**0.0087**	**2.13**	**0.0418**
Ant Cing Gyrus	0.96	0.7272	0.76	0.8139	1.96	0.0981	2.04	0.084	**2.38**	**0.0289**	**2.75**	**0.0152**
Mid Cing Gyrus	0.7	0.8421	0.63	0.8421	1.23	0.3314	1.32	0.287	**2.96**	**0.0106**	**3.03**	**0.0101**
Post Cing Gyrus	-0.16	0.996	-0.03	0.996	0.85	0.5198	0.56	0.6829	**2.21**	**0.0372**	**2.55**	**0.0199**
Parahip. Gyrus	-0.07	0.996	0.87	0.7707	1.58	0.1947	1.52	0.2104	**2.42**	**0.0267**	**2.6**	**0.019**
Subcallosal Area	0.21	0.996	0.24	0.996	2.23	0.0622	-0.35	0.8179	**2.07**	**0.0467**	0.48	0.63
Thalamus	1.21	0.5573	0.66	0.8421	1.69	0.157	0.99	0.4458	**2.76**	**0.015**	**2.3**	**0.0326**
Basal Forebrain	0.15	0.996	1.26	0.5564	**2.4**	**0.0496**	2.38	0.0504	**2.1**	**0.0445**	**2.87**	**0.0121**
Frontal Pole	0.37	0.9503	-0.19	0.996	0.51	0.7019	0.3	0.8449	0.78	0.4404	0.94	0.3558
Gyrus Rectus	0.43	0.9185	-0.08	0.996	1.08	0.4018	-0.07	0.9763	1.38	0.1815	**2.58**	**0.0195**
Frontal Operculum	1.81	0.4662	1.51	0.4874	**3.03**	**0.0134**	2.21	0.0622	**3.12**	**0.0101**	**2.56**	**0.0199**
Ant Orbital	1.39	0.5339	0.8	0.7994	**2.62**	**0.0347**	2.2	0.0622	**2.93**	**0.0109**	**2.14**	**0.0409**
Lat Orbital	1.57	0.4662	1.45	0.5282	**3.04**	**0.0134**	**3.06**	**0.0133**	**3.06**	**0.0101**	**2.84**	**0.0123**
Med Orbital	0.79	0.7994	0.93	0.7346	2.24	0.0622	**2.39**	**0.0496**	1.75	0.0917	**2.91**	**0.011**
Post Orbital	1.41	0.5339	1.24	0.5564	**2.72**	**0.0297**	2.35	0.0532	**2.61**	**0.019**	2.34	0.03
Frontal (Inf Tri)	1.76	0.4662	2.49	0.217	**2.87**	**0.0202**	**2.52**	**0.043**	**2.66**	**0.0179**	**2.9**	**0.0112**
Frontal (Inf Oper)	1.76	0.4662	1.24	0.5564	**2.43**	**0.0493**	**2.98**	**0.0147**	**2.35**	**0.0299**	**2.46**	**0.0241**
Frontal (Inf Orbit)	1.67	0.4662	1.95	0.4647	**2.61**	**0.0347**	**2.4**	**0.0496**	**3.14**	**0.0101**	**2.6**	**0.019**
Frontal (Med)	1.33	0.5564	0.63	0.8421	**2.5**	**0.0443**	1.36	0.2773	**2.23**	**0.0365**	**2.38**	**0.0289**
Frontal (Mid)	0.99	0.7108	0.67	0.8421	1.51	0.2131	1.78	0.1351	**2.55**	**0.0199**	**2.21**	**0.0372**
Frontal (Sup med)	0.86	0.7707	1.17	0.5875	2.32	0.0554	2.25	0.0622	**2.23**	**0.0365**	**2.66**	**0.0179**
Frontal (Sup)	-0.01	0.996	-0.15	0.996	0.27	0.8477	0.14	0.9356	**2.15**	**0.0409**	1.65	0.1107
SMA	1.0	0.7108	0.52	0.8748	1.11	0.3891	0.82	0.5302	**2.61**	**0.019**	**2.38**	**0.0289**
Precentral (Med)	-0.16	0.996	0.29	0.9944	0.6	0.656	0.79	0.5442	1.33	0.1941	1.36	0.1859
Precentral	0.64	0.8421	0.49	0.894	1.34	0.2822	2.17	0.0654	**2.36**	**0.0293**	**2.51**	**0.0217**
Postcentral (Med)	0.39	0.9402	-0.18	0.996	1.18	0.3473	0.64	0.6366	2.03	0.0509	1.25	0.2195
Postcentral	0.57	0.8643	-0.14	0.996	1.23	0.3314	1.55	0.2033	**2.28**	**0.0334**	**2.24**	**0.0365**

Central Operculum	2.67	0.1977	2.22	0.3118	**3.62**	**0.003**	**3.81**	**0.0028**	**3.21**	**0.0101**	**3.08**	**0.0101**
Parietal Operculum	2.28	0.3092	3.07	0.1977	**3.68**	**0.003**	**4.43**	**0.001**	**2.97**	**0.0104**	**2.85**	**0.0123**
Angular Gyrus	-0.01	0.996	0.79	0.7994	**2.46**	**0.0475**	**3.45**	**0.0044**	**3.08**	**0.0101**	3.44	**0.0087**
Supramarginal	0.73	0.8345	0.99	0.7108	**2.67**	**0.0322**	**4.23**	**0.001**	**3.49**	**0.0087**	**3.29**	**0.0101**
Parietal (Sup)	-0.91	0.7457	-0.59	0.8598	1.87	0.1192	2.06	0.0824	**3.11**	**0.0101**	**2.82**	**0.0129**
Precuneus	0.14	0.996	0.32	0.9797	**2.26**	**0.0622**	2.34	0.0532	**3.03**	**0.0101**	3.17	**0.0101**
Insula (Ant)	1.43	0.5339	1.34	0.5564	**2.76**	**0.0273**	**2.42**	**0.0493**	**3.48**	**0.0087**	**2.97**	**0.0104**
Insula (Post)	2.49	0.217	1.76	0.4662	**3.72**	**0.003**	**3.08**	**0.013**	**3.26**	**0.0101**	**2.98**	**0.0104**
Entorhinal	0.46	0.9028	0.01	0.996	1.71	0.1513	0.45	0.7488	**1.77**	**0.088**	**2.34**	**0.0302**
Fusiform Gyrus	-0.06	0.996	0.01	0.996	2.0	0.0927	1.2	0.3402	**3.02**	**0.0101**	**3.16**	**0.0101**
Temporal (Inf)	0.08	0.996	-0.2	0.996	2.21	0.0622	0.34	0.8185	**2.23**	**0.0365**	1.51	0.1456
Temporal (Mid)	0.53	0.8748	0.59	0.8598	2.08	0.0789	2.22	0.0622	**2.55**	**0.0199**	**3.03**	**0.0101**
Temporal (Sup)	1.28	0.5564	1.92	0.4647	2.19	0.0634	**3.44**	**0.0044**	**3.06**	**0.0101**	**3.1**	**0.0101**
Temporal Pole	0.55	0.8665	-0.16	0.996	1.85	0.1216	1.38	0.2682	**2.73**	**0.0154**	**2.16**	**0.0402**
Transverse temporal	2.27	0.3092	1.74	0.4662	**3.66**	**0.003**	**3.61**	**0.003**	**3.18**	**0.0101**	**2.93**	**0.0109**
Planum Polare	2.64	0.1977	2.07	0.3776	**3.71**	**0.003**	**3.46**	**0.0044**	**3.24**	**0.0101**	**3.47**	**0.0087**
Planum Temporale	2.89	0.1977	2.77	0.1977	**3.48**	**0.0044**	**4.22**	**0.001**	**2.7**	**0.0163**	**2.54**	**0.0199**
Calcarine Fissure	-1.57	0.4662	-1.22	0.5573	-0.21	0.8828	0.06	0.9763	**2.18**	**0.0387**	**2.31**	**0.0321**
Cuneus	-1.63	0.4662	-1.6	0.4662	0.03	0.9763	0.26	0.8556	**2.83**	**0.0126**	**2.65**	**0.0179**
Lingual Gyrus	-0.93	0.7346	-0.42	0.9204	0.04	0.9763	0.44	0.7493	1.91	0.0651	**2.23**	**0.0365**
Occipital fusiform	-1.12	0.6261	-0.81	0.7994	-0.1	0.9582	0.79	0.5442	2.01	0.0519	**2.37**	**0.0293**
Occipital (Inf)	-1.39	0.5339	-1.28	0.5564	0.04	0.9763	0.71	0.5947	2.03	0.0509	**3.0**	**0.0104**
Occipital (Mid)	-1.54	0.4786	-0.65	0.8421	1.0	0.4458	0.9	0.4927	**3.06**	**0.0101**	**2.73**	**0.0154**
Occipital (Sup)	-1.71	0.4662	-1.71	0.4662	0.54	0.6917	0.28	0.8477	**2.2**	**0.0372**	1.98	0.056
Occipital Pole	-1.73	0.4662	-1.59	0.4662	-0.7	0.6021	-0.93	0.4761	1.28	0.2103	1.4	0.1777
Cerebellum Exterior	-0.05	0.996	0.46	0.9028	1.8	0.1302	1.77	0.1372	**2.15**	**0.0409**	**2.14**	**0.041**
Vermis I-V	-0.35	0.9567	-	-	0.52	0.7002	-	-	1.39	0.1791	-	-
Vermis VI-VII	-0.04	0.996	-	-	0.68	0.6113	-	-	1.04	0.31	-	-
Vermis VIII-X	-0.01	0.996	-	-	1.02	0.4354	-	-	0.75	0.4562	-	-

Bold numbers highlight regions with significant differences in a specific measure (fALFF, LCOR, or GCOR) between PD and the matched subgroup of HC.

Supplementary Table 32: Statistics on regional differences in fALFF, LCOR, and GCOR between PD and HCmatched assessed using the Mann-Whitney-U test – *after atrophy correction*.

	fALFF				LCOR				GCOR			
	Left		Right		Left		Right		Left		Right	
Region	U statistic	P_{FDR}	U statistic	P_{FDR}	U statistic	P_{FDR}	U statistic	P_{FDR}	U statistic	P_{FDR}	U statistic	P_{FDR}
Accumbens	1.64	0.4111	1.09	0.6462	**4.08**	**0.0013**	1.81	0.1329	**3.47**	**0.0103**	**2.54**	**0.0206**
Caudate	2.07	0.4111	1.63	0.4111	**2.86**	**0.021**	1.66	0.1709	**3.8**	**0.0087**	**3.19**	**0.0103**
Putamen	1.32	0.5456	0.56	0.8821	**3.98**	**0.0016**	**2.65**	**0.0347**	**3.8**	**0.0087**	**3.11**	**0.0103**
Pallidum	1.26	0.5714	0.1	0.9934	**3.42**	**0.0052**	2.23	0.0629	**2.66**	**0.0183**	**2.92**	**0.011**
Amygdala	0.64	0.8632	-0.14	0.9934	2.43	0.0515	0.87	0.5169	**2.58**	**0.02**	2.03	0.051
Hippocampus	0.55	0.8821	-0.2	0.9934	2.41	0.0515	0.83	0.5323	**3.31**	**0.0103**	2.02	0.0519
Ant Cing Gyrus	0.95	0.7393	0.79	0.8157	1.98	0.0971	2.07	0.08	**2.39**	**0.0291**	**2.77**	**0.0146**
Mid Cing Gyrus	0.76	0.8191	0.65	0.8632	1.26	0.3172	1.32	0.2931	**2.97**	**0.011**	**3.03**	**0.0103**
Post Cing Gyrus	-0.19	0.9934	-0.03	0.9934	0.86	0.5178	0.57	0.6759	**2.21**	**0.0385**	**2.55**	**0.0206**
Parahip. Gyrus	-0.15	0.9934	0.8	0.8112	1.51	0.2193	1.48	0.2264	**2.37**	**0.0299**	**2.53**	**0.0206**
Subcallosal Area	0.23	0.9934	0.26	0.9934	2.29	0.0593	-0.34	0.8207	**2.06**	**0.0481**	0.47	0.6365
Thalamus	1.16	0.6016	0.64	0.8632	1.63	0.1783	0.95	0.4721	**2.73**	**0.0156**	**2.29**	**0.0338**
Basal Forebrain	0.09	0.9934	1.2	0.5797	2.34	0.0577	2.29	0.0593	**2.06**	**0.0481**	**2.77**	**0.0146**
Frontal Pole	0.38	0.9431	-0.16	0.9934	0.48	0.723	0.29	0.8306	0.76	0.4553	0.94	0.3567
Gyrus Rectus	0.41	0.943	-0.09	0.9934	1.04	0.4274	-0.07	0.9743	1.35	0.193	**2.58**	**0.02**
Frontal Operculum	1.77	0.4111	1.49	0.5098	**3.0**	**0.0153**	2.21	0.0633	**3.1**	**0.0103**	**2.54**	**0.0206**
Ant Orbital	1.38	0.5419	0.8	0.8112	**2.63**	**0.0349**	2.27	0.0606	**2.94**	**0.011**	**2.19**	**0.0388**
Lat Orbital	1.63	0.4111	1.44	0.5406	**3.07**	**0.0142**	**3.04**	**0.0142**	**3.05**	**0.0103**	**2.85**	**0.0127**
Med Orbital	0.76	0.8191	0.93	0.7401	2.25	0.062	2.4	0.0515	1.71	0.0987	**2.93**	**0.011**
Post Orbital	1.41	0.5419	1.21	0.5797	**2.7**	**0.0321**	2.32	0.0583	**2.6**	**0.0196**	**2.33**	**0.0312**
Frontal (Inf Tri)	1.73	0.4111	2.4	0.2822	**2.87**	**0.021**	**2.49**	**0.0471**	**2.66**	**0.0183**	**2.91**	**0.011**
Frontal (Inf Oper)	1.76	0.4111	1.25	0.5714	2.4	0.0515	**2.99**	**0.0153**	**2.33**	**0.0312**	**2.45**	**0.0247**
Frontal (Inf Orbit)	1.71	0.4111	1.91	0.4111	**2.62**	**0.0351**	2.38	0.0524	**3.14**	**0.0103**	**2.6**	**0.0196**
Frontal (Med)	1.36	0.5419	0.58	0.8821	**2.52**	**0.0444**	1.32	0.2931	**2.23**	**0.038**	**2.34**	**0.0312**
Frontal (Mid)	0.93	0.7401	0.59	0.8821	1.5	0.2193	1.74	0.1467	**2.55**	**0.0206**	**2.2**	**0.0388**
Frontal (Sup med)	0.84	0.7973	1.16	0.6016	2.31	0.0593	2.23	0.0629	**2.22**	**0.038**	**2.64**	**0.0185**
Frontal (Sup)	0.01	0.9934	-0.14	0.9934	0.29	0.8306	0.17	0.9147	**2.15**	**0.0411**	1.69	0.1023
SMA	1.02	0.7021	0.5	0.887	1.12	0.3805	0.81	0.5409	**2.62**	**0.0192**	**2.38**	**0.0294**
Precentral (Med)	-0.19	0.9934	0.21	0.9934	0.58	0.6715	0.74	0.5916	1.32	0.1981	1.33	0.1959
Precentral	0.54	0.8821	0.39	0.9431	1.29	0.3065	2.12	0.0757	**2.32**	**0.0313**	**2.46**	**0.0247**
Postcentral (Med)	0.35	0.9582	-0.17	0.9934	1.17	0.3627	0.66	0.6204	2.03	0.0512	1.29	0.2048
Postcentral	0.53	0.8821	-0.19	0.9934	1.21	0.343	1.51	0.2193	**2.24**	**0.0373**	**2.2**	**0.0388**

Central Operculum	2.61	0.2126	2.22	0.3521	**3.57**	**0.0035**	**3.81**	**0.0027**	**3.19**	**0.0103**	**3.09**	**0.0103**
Parietal Operculum	2.25	0.3521	3.03	0.2126	**3.63**	**0.0035**	**4.4**	**0.0013**	**2.92**	**0.011**	**2.81**	**0.0137**
Angular Gyrus	-0.17	0.9934	0.53	0.8821	2.4	0.0515	**3.35**	**0.0056**	**3.07**	**0.0103**	3.41	**0.0103**
Supramarginal	0.64	0.8632	0.84	0.7973	**2.65**	**0.0347**	**4.17**	**0.0013**	**3.49**	**0.0103**	**3.26**	**0.0103**
Parietal (Sup)	-0.98	0.7201	-0.72	0.8502	1.83	0.1284	1.99	0.095	**3.06**	**0.0103**	**2.79**	**0.0143**
Precuneus	0.03	0.9934	0.23	0.9934	2.2	0.0633	2.28	0.0593	**3.02**	**0.0103**	**3.17**	**0.0103**
Insula (Ant)	1.38	0.5419	1.32	0.5456	**2.72**	**0.0307**	2.43	0.0515	**3.44**	**0.0103**	**2.97**	**0.011**
Insula (Post)	2.41	0.2822	1.65	0.4111	**3.67**	**0.0035**	**3.05**	**0.0142**	**3.22**	**0.0103**	**2.94**	**0.011**
Entorhinal	0.47	0.9075	0.05	0.9934	1.71	0.1537	0.48	0.723	1.75	0.0924	**2.33**	**0.0312**
Fusiform Gyrus	-0.2	0.9934	-0.08	0.9934	1.87	0.1227	1.13	0.3781	**2.91**	**0.011**	**3.1**	**0.0103**
Temporal (Inf)	0.02	0.9934	-0.23	0.9934	2.08	0.08	0.29	0.8306	**2.18**	**0.0392**	1.5	0.1492
Temporal (Mid)	0.5	0.887	0.52	0.887	2.08	0.08	2.2	0.0633	**2.56**	**0.0206**	**3.02**	**0.0103**
Temporal (Sup)	1.22	0.5797	1.82	0.4111	2.14	0.0718	**3.39**	**0.0056**	**3.03**	**0.0103**	**3.05**	**0.0103**
Temporal Pole	0.67	0.8632	-0.08	0.9934	1.85	0.1242	1.37	0.2739	**2.72**	**0.0156**	**2.17**	**0.0395**
Transverse temporal	2.17	0.3536	1.65	0.4111	**3.59**	**0.0035**	**3.57**	**0.0035**	**3.1**	**0.0103**	**2.89**	**0.0114**
Planum Polare	2.62	0.2126	2.04	0.4111	**3.67**	**0.0035**	**3.48**	**0.0046**	**3.23**	**0.0103**	**3.47**	**0.0103**
Planum Temporale	2.77	0.2126	2.63	0.2126	**3.37**	**0.0056**	**4.12**	**0.0013**	**2.62**	**0.0192**	**2.49**	**0.0232**
Calcarine Fissure	-1.71	0.4111	-1.32	0.5456	-0.29	0.8306	-0.01	0.9917	**2.11**	**0.0445**	**2.25**	**0.037**
Cuneus	-1.67	0.4111	-1.68	0.4111	0.02	0.9917	0.24	0.8628	**2.83**	**0.0131**	**2.65**	**0.0185**
Lingual Gyrus	-1.01	0.7059	-0.54	0.8821	-0.01	0.9917	0.37	0.809	1.86	0.0722	**2.18**	**0.0392**
Occipital fusiform	-1.14	0.6093	-0.9	0.7516	-0.14	0.9293	0.72	0.596	2.01	0.0528	**2.35**	**0.0307**
Occipital (Inf)	-1.36	0.5419	-1.29	0.5565	0.02	0.9917	0.7	0.5995	**2.06**	**0.0481**	**3.01**	**0.0104**
Occipital (Mid)	-1.67	0.4111	-0.71	0.8506	0.97	0.4633	0.89	0.5055	**3.06**	**0.0103**	**2.73**	**0.0156**
Occipital (Sup)	-1.74	0.4111	-1.77	0.4111	0.54	0.6931	0.29	0.8306	**2.19**	**0.0388**	1.98	0.0556
Occipital Pole	-1.74	0.4111	-1.57	0.4442	-0.7	0.5995	-0.92	0.4885	1.29	0.2048	1.42	0.17
Cerebellum Exterior	-0.05	0.9934	0.46	0.9075	1.78	0.1385	1.77	0.1407	**2.11**	**0.0445**	**2.12**	**0.0441**
Vermis I-V	-0.38	0.9431	-	-	0.48	0.723	-	-	1.35	0.1916	-	-
Vermis VI-VII	-0.05	0.9934	-	-	0.66	0.6204	-	-	1.01	0.3212	-	-
Vermis VIII-X	0.01	0.9934	-	-	1.03	0.4299	-	-	0.75	0.4557	-	-

Bold numbers highlight regions with significant differences in a specific measure (fALFF, LCOR, or GCOR) between PD and the matched subgroup of HC.

Supplementary Figures

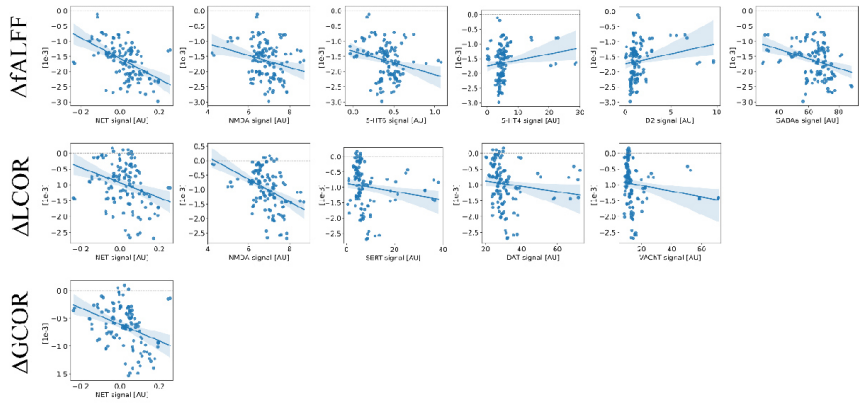

Supplementary Figure 1: Significant linear correlations between unthresholded age-effect (slope) maps in fALFF, LCOR, and GCOR, and neurotransmitter systems – *before atrophy correction*. Corresponding correlation coefficients are visualized in Figure 2B. ΔMeasure corresponds to the annual rate of in- or decrease in the respective measure of brain function (fALFF, LCOR, or GCOR) within one region.

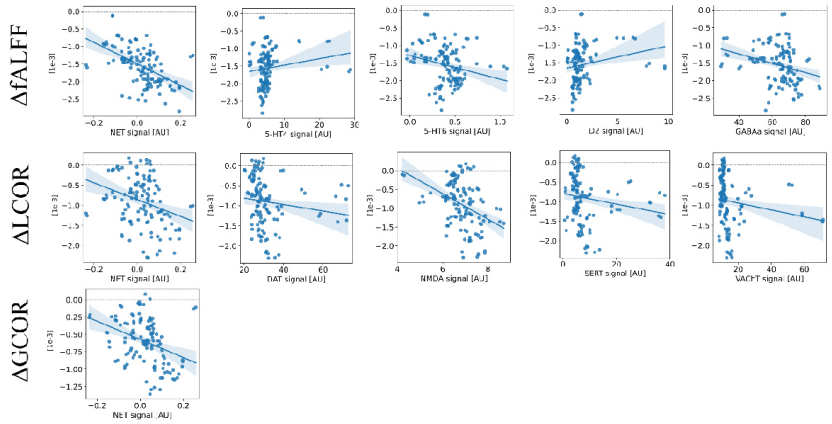

Supplementary Figure 2: Significant linear correlations between of unthresholded age-effects (slope maps) in fALFF, LCOR, and GCOR, and multiple neurotransmitter systems – *after atrophy correction*. ΔMeasure corresponds to the annual rate of in- or decrease in the respective measure of brain function (fALFF, LCOR, or GCOR) within one region.

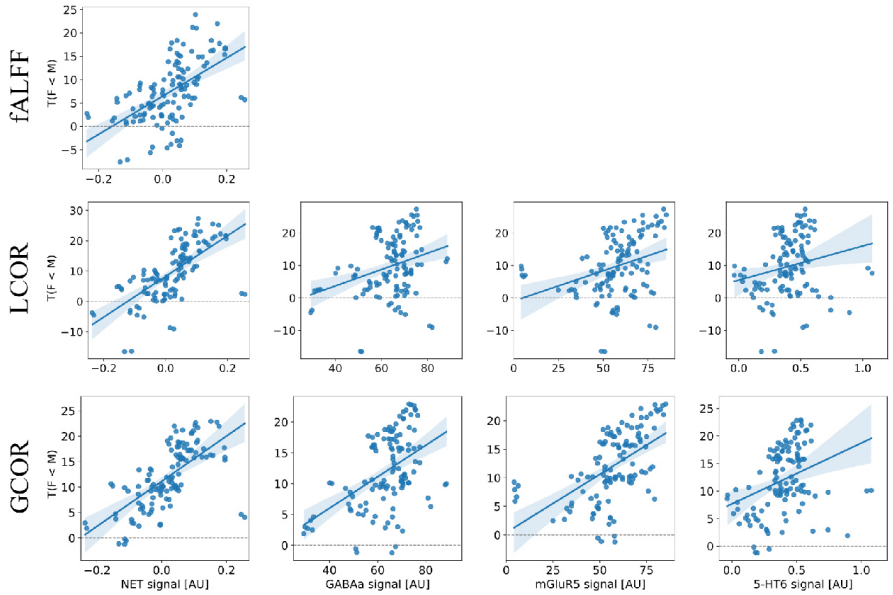

Supplementary Figure 3: Significant linear correlations of unthresholded sex effects (T-values) in fALFF, LCOR, and GCOR and NET, GABAa, mGluR5, and 5-HT6 availability – *before atrophy correction*.

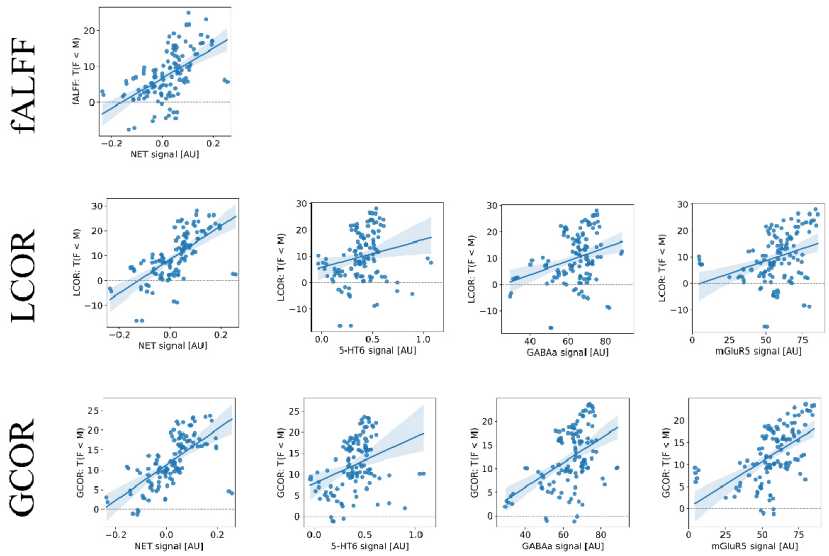

Supplementary Figure 4: Significant linear correlations of unthresholded sex effects (T-values) in fALFF, LCOR, and GCOR and NET, GABAa, mGluR5, and 5-HT6 availability – *after atrophy correction*.

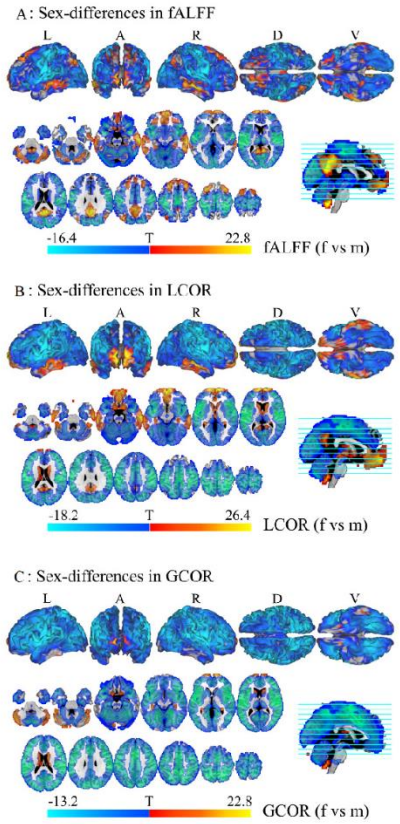

Supplementary Figure 5: Sex differences (T-values) in brain functional measures, thresholded. Red voxels indicate higher values in women compared to men and blue voxels indicate the inverse.

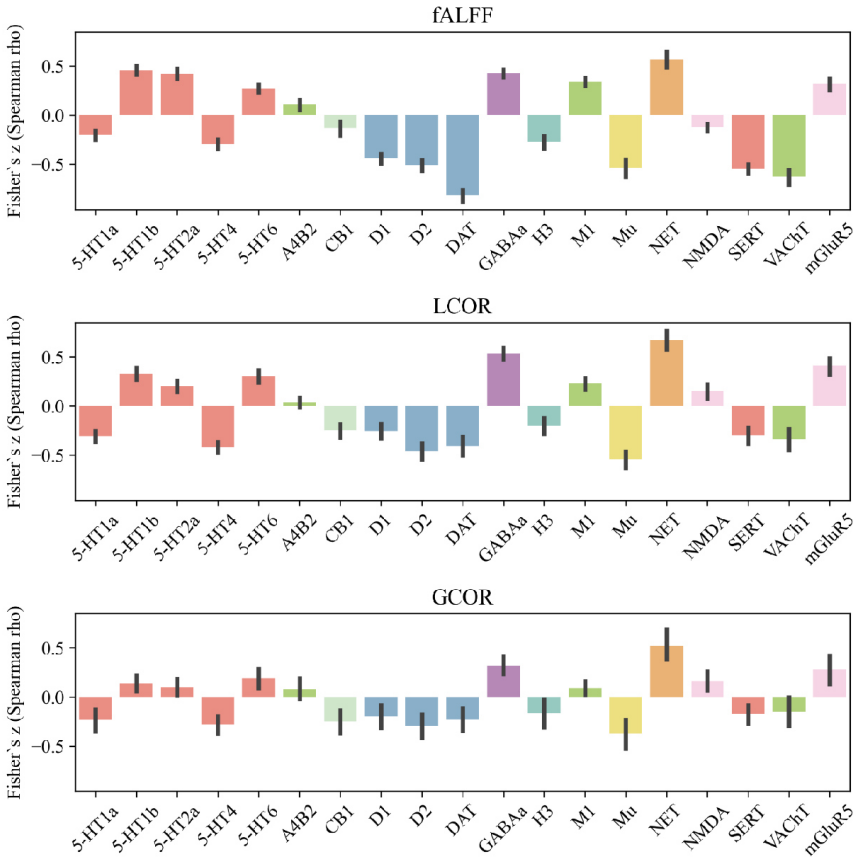

Supplementary Figure 6. Bar plots show the healthy control cohort's mean Fisher's z-transformed Spearman correlation coefficients. These coefficients were derived from the spatial correlation analyses of individual fALFF (top), LCOR (middle), and GCOR (bottom) maps and 19 PET maps of neurotransmitter systems. Vertical bars indicate the 50% quantile. Colors group receptors and transporters of the same neurotransmitter system, i.e., serotonin (red), dopamine (blue), acetylcholine (green), glutamate (pink) and GABA (purple), cannabinoid (mint), opioid (yellow), norepinephrine (orange), and histamine (turquoise).

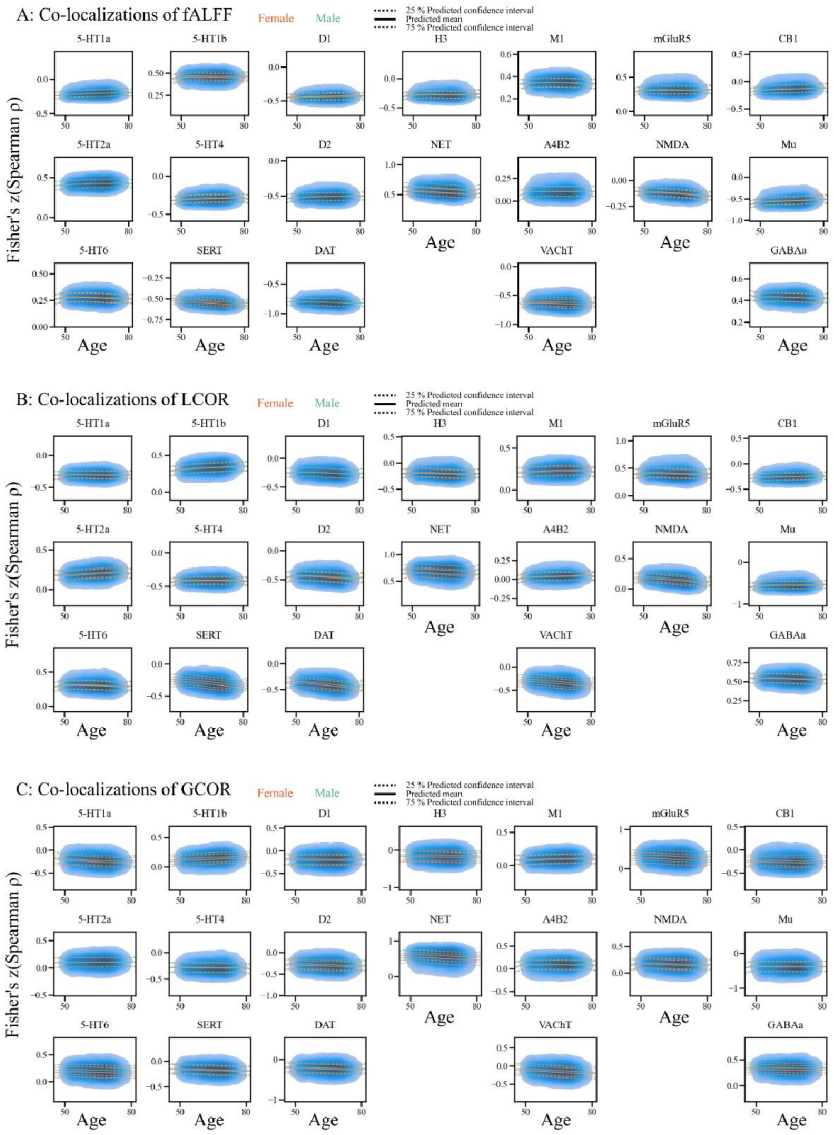

Supplementary Figure 7: Normative models of co-localizations between brain function (A: fALFF, B: LCOR, C: GCOR) and 19 PET maps – *before atrophy correction*. Within each subplot, the blue cloud (kernel density estimation) visualized the distribution of Fisher's z-transformed Spearman correlation coefficients of all healthy controls. Solid and dashed lines indicate the predicted median and 25 and 75% confidence interval of men (turquoise) and women (orange).

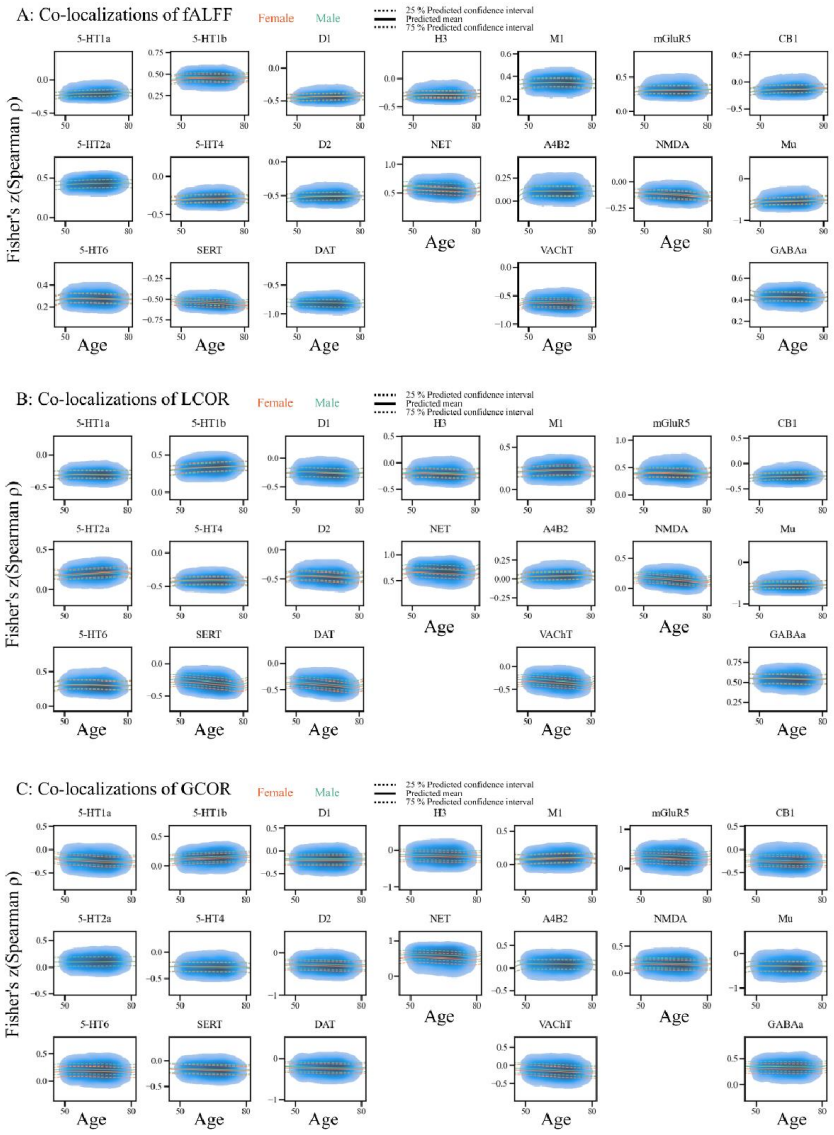

Supplementary Figure 8: Normative models of co-localizations between brain function (A: fALFF, B: LCOR, C: GCOR) and 19 PET maps – *after atrophy correction*. Within each subplot, the blue cloud (kernel density estimation) visualized the distribution of Fisher's z-transformed Spearman correlation coefficients of all healthy controls. Solid and dashed lines indicate the predicted median and 25 and 75% confidence interval of men (turquoise) and women (orange).

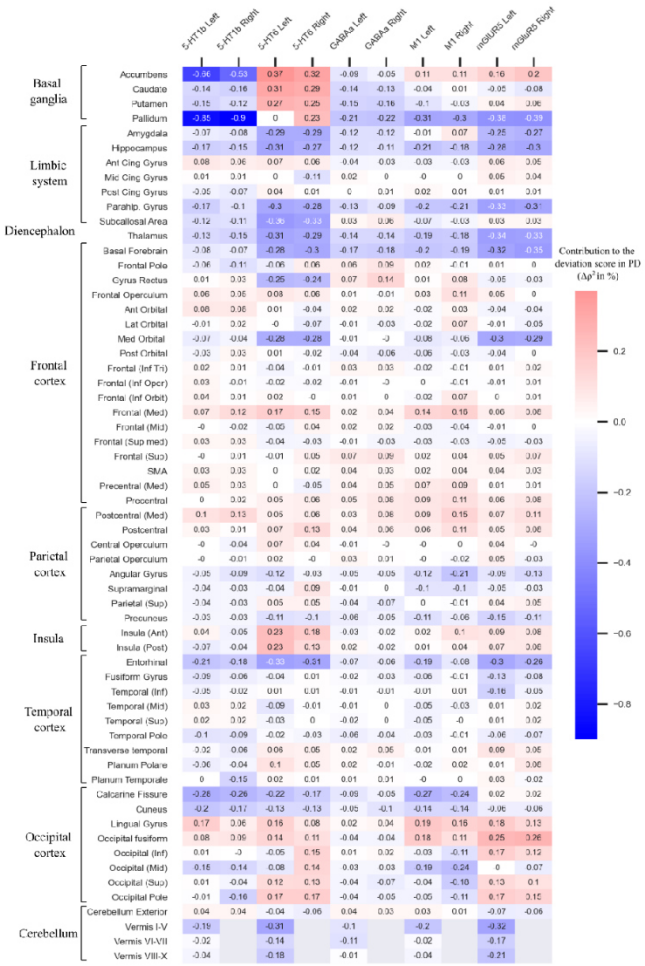

Supplementary Figure 9: Contribution of each region to the deviation in **fALFF** co-localizations in subjects with manifest Parkinson's disease – *before atrophy correction*. The contribution is quantified by the mean change in squared spatial correlation coefficient (mean $\Delta\rho^2$) after leaving the specific region out from the spatial correlation analysis. Values of regions of the left or right hemisphere are arranged next to each other (column-wise) for each neurotransmitter system. The rows are sorted from top to the bottom: Basal ganglia, limbic system, diencephalon, frontal cortex, motor area, parietal cortex, temporal cortex, occipital cortex, cerebellum. Red cells, i.e. positive values, indicate that leaving this specific region out in the individual co-localization analysis led to a correlation coefficient that was closer to the norm.

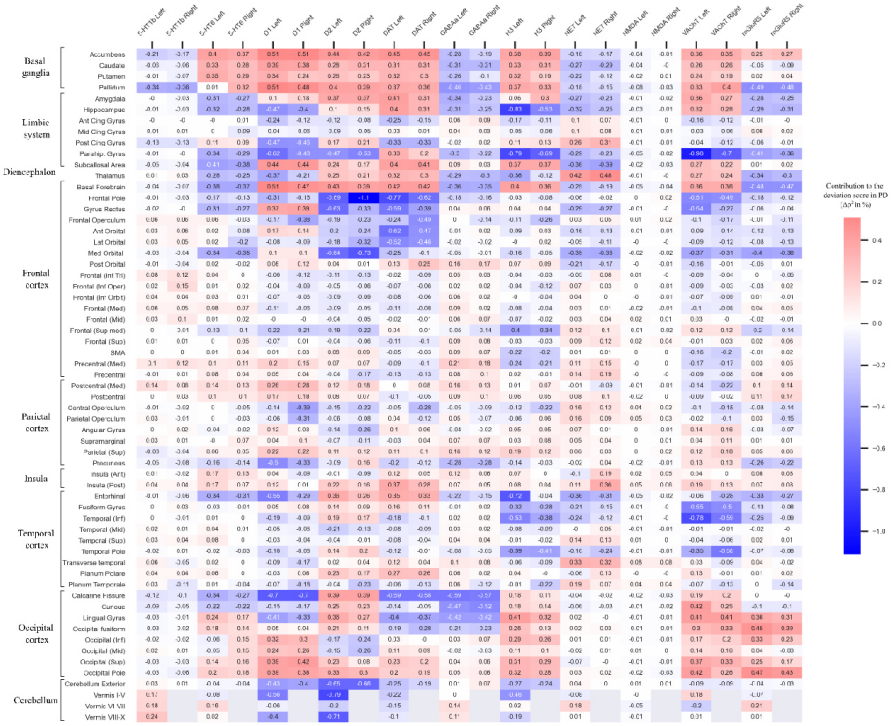

Supplementary Figure 10: Contribution of each region to the deviation in **LCOR** co-localizations in subjects with manifest Parkinson's disease – *before atrophy correction*. The contribution is quantified by the mean change in squared spatial correlation coefficient (mean $\Delta\rho^2$) after leaving the specific region out from the spatial correlation analysis. Values of regions of the left or right hemisphere are arranged next to each other (column-wise) for each neurotransmitter system. The rows are sorted from top to the bottom: Basal ganglia, limbic system, diencephalon, frontal cortex, parietal cortex, temporal cortex, occipital cortex, cerebellum. Red cells, i.e. positive values, indicate that leaving this specific region out in the individual co-localization analysis led to a correlation coefficient that was closer to the norm.

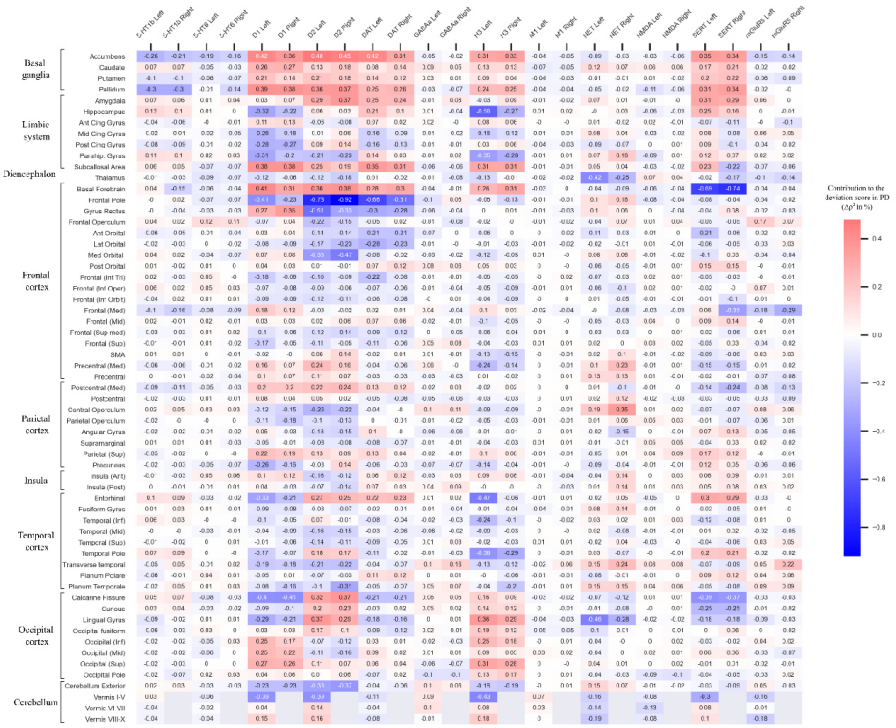

Supplementary Figure 11: Contribution of each region to the deviation in **GCOR** co-localizations in subjects with manifest Parkinson's disease – *before atrophy correction*. The contribution is quantified by the mean change in squared spatial correlation coefficient (mean Δp^2) after leaving the specific region out from the spatial correlation analysis. Values of regions of the left or right hemisphere are arranged next to each other (column-wise) for each neurotransmitter system. The rows are sorted from top to the bottom: Basal ganglia, limbic system, diencephalon, frontal cortex, parietal cortex, temporal cortex, occipital cortex, cerebellum. Red cells, i.e. positive values, indicate that leaving this specific region out in the individual co-localization analysis led to a correlation coefficient that was closer to the norm.

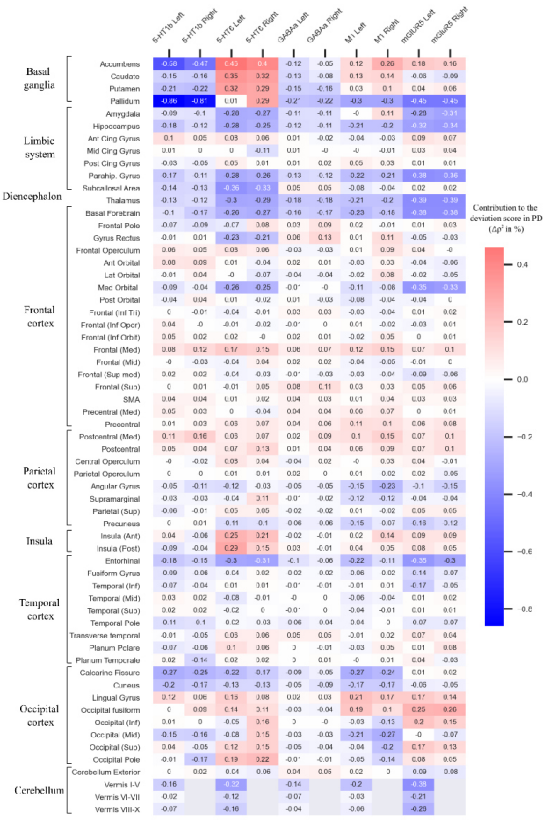

Supplementary Figure 12: Contribution of each region to the deviation in **fALFF** co-localizations in subjects with manifest Parkinson's disease – *after atrophy correction*. The contribution is quantified by the mean change in squared spatial correlation coefficient (mean $\Delta\rho^2$) after leaving the specific region out from the spatial correlation analysis. Values of regions of the left or right hemisphere are arranged next to each other (column-wise) for each neurotransmitter system. The rows are sorted from top to the bottom: Basal ganglia, limbic system, diencephalon, frontal cortex, parietal cortex, temporal cortex, occipital cortex, cerebellum. Red cells, i.e. positive values, indicate that leaving this specific region out in the individual co-localization analysis led to a correlation coefficient that was closer to the norm.

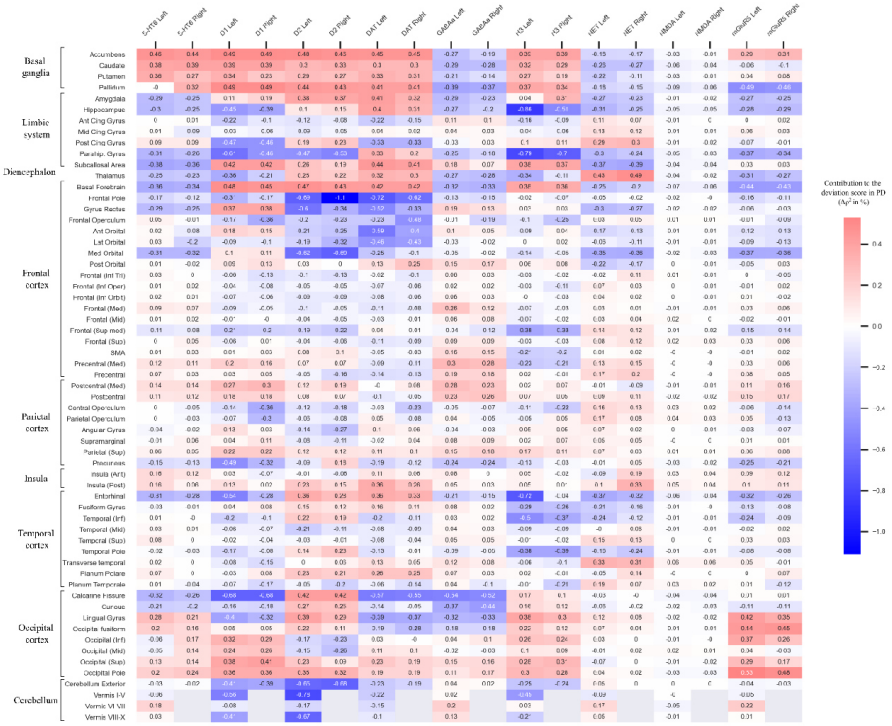

Supplementary Figure 13: Contribution of each region to the deviation in **LCOR** co-localizations in subjects with manifest Parkinson's disease – *after atrophy correction*. The contribution is quantified by the mean change in squared spatial correlation coefficient (mean $\Delta\rho^2$) after leaving the specific region out from the spatial correlation analysis. Values of regions of the left or right hemisphere are arranged next to each other (column-wise) for each neurotransmitter system. The rows are sorted from top to the bottom: Basal ganglia, limbic system, diencephalon, frontal cortex, parietal cortex, temporal cortex, occipital cortex, cerebellum. Red cells, i.e. positive values, indicate that leaving this specific region out in the individual co-localization analysis led to a correlation coefficient that was closer to the norm.

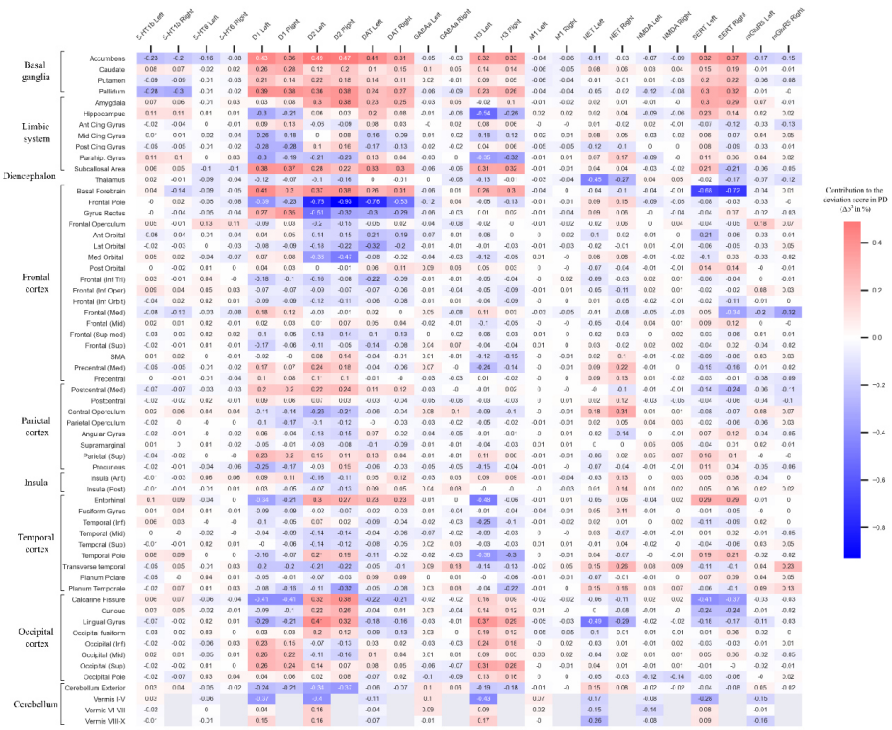

Supplementary Figure 14: Contribution of each region to the deviation in **GCOR** co-localizations in subjects with manifest Parkinson's disease – *after atrophy correction*. The contribution is quantified by the mean change in squared spatial correlation coefficient (mean $\Delta\rho^2$) after leaving the specific region out from the spatial correlation analysis. Values of regions of the left or right hemisphere are arranged next to each other (column-wise) for each neurotransmitter system. The rows are sorted from top to the bottom: Basal ganglia, limbic system, diencephalon, frontal cortex, parietal cortex, temporal cortex, occipital cortex, cerebellum. Red cells, i.e. positive values, indicate that leaving this specific region out in the individual co-localization analysis led to a correlation coefficient that was closer to the norm.

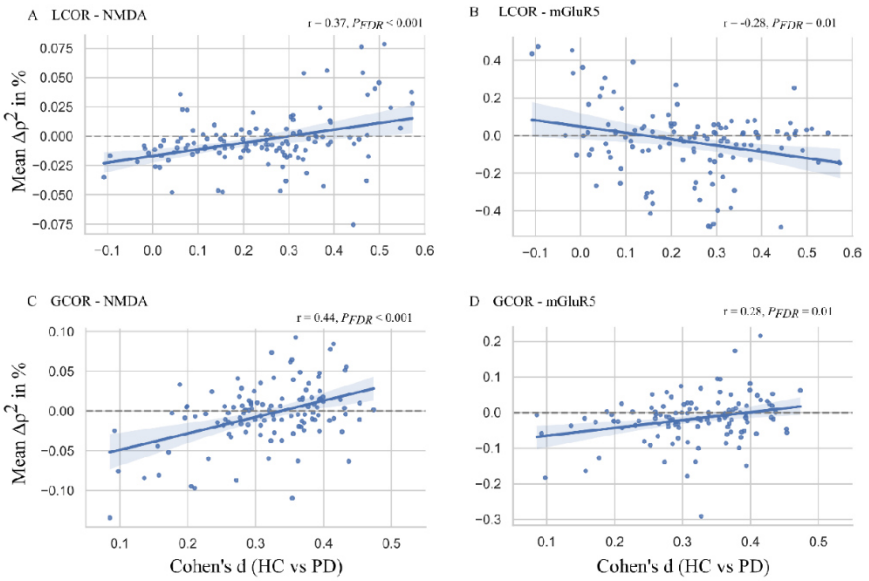

Supplementary Figure 15: Linear correlation of regional contribution (mean $\Delta\rho^2$) to the deviation score and functional differences (Cohen's d) between PD and the matched subcohort of healthy controls – *before atrophy correction*.

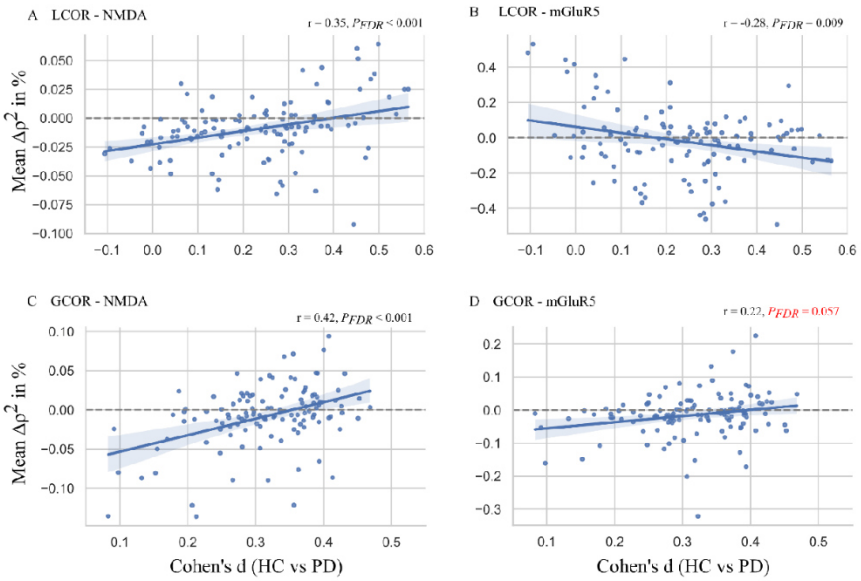

Supplementary Figure 16: Linear correlation of regional contribution (Mean $\Delta\rho^2$) to deviation score and functional differences (Cohen's d) between PD and the matched subcohort of healthy controls – *after atrophy correction*.

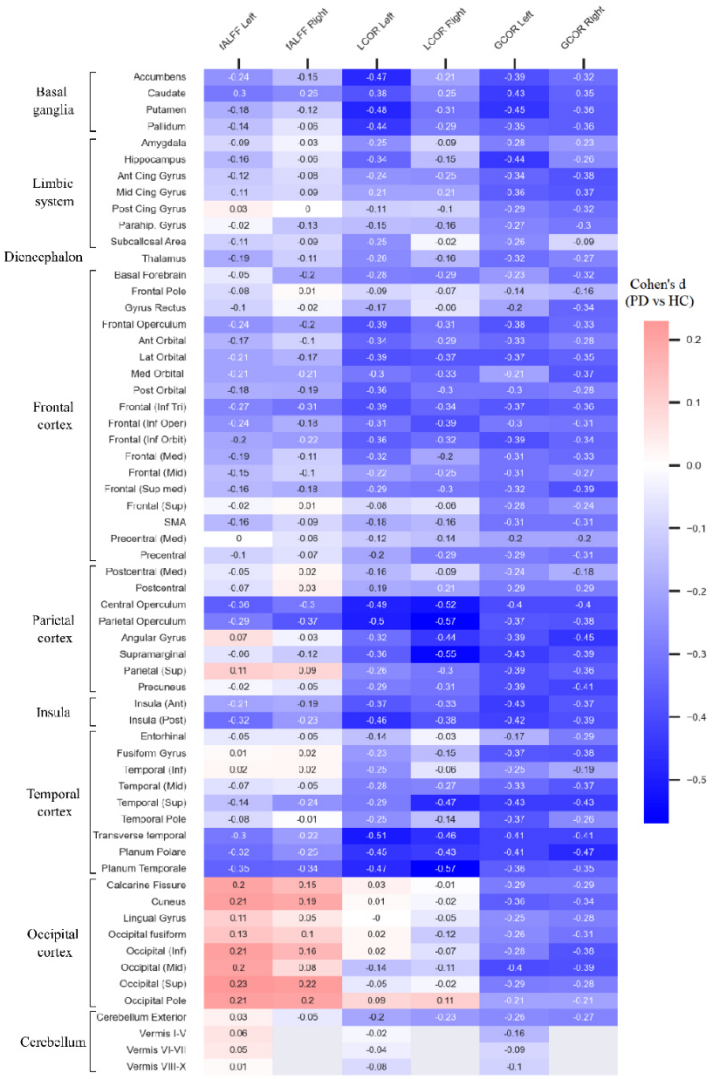

Supplementary Figure 17: Regional differences (effect sizes, Cohen's d) in fALFF, LCOR, and GCOR between manifest PD and the age- and sex-matched control group – *before atrophy correction*. Positive values (red cells) indicate higher values of brain functional measures in PD and negative values (blue cells) indicate the inverse. Values of regions of the left or right hemisphere are arranged next to each other (column-wise). The list is sorted from top to the bottom: Basal ganglia, limbic system, diencephalon, frontal cortex, parietal cortex, temporal cortex, occipital cortex, cerebellum. Regional values are visualized in Supplementary Figure 19A.

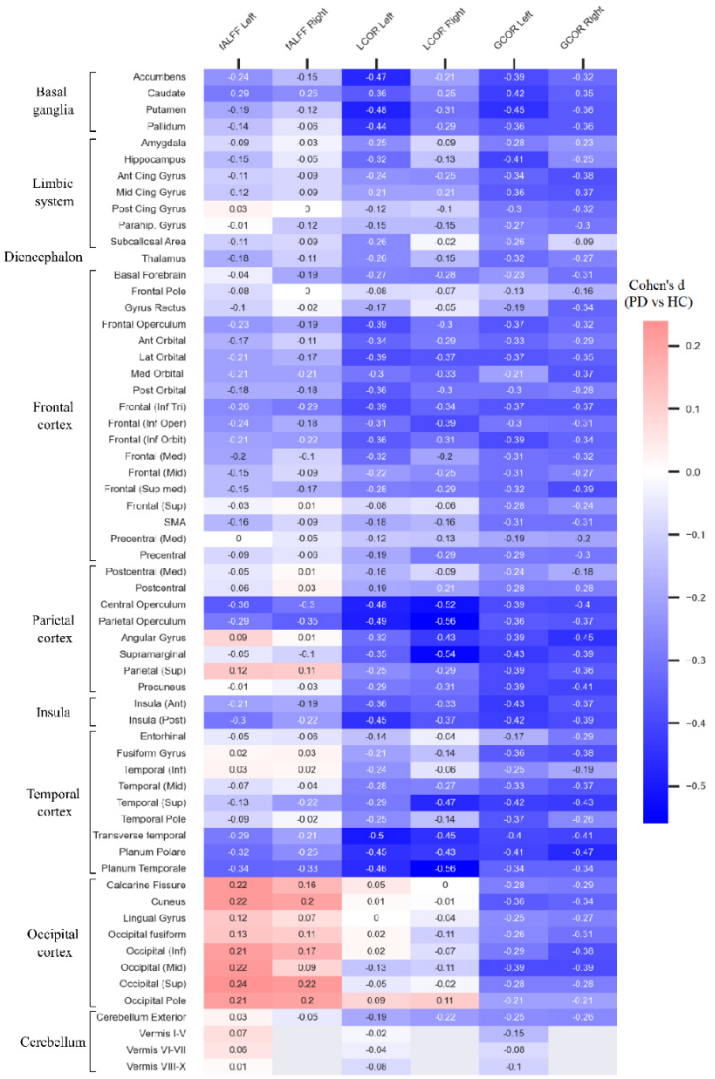

Supplementary Figure 18: Regional differences (effect sizes, Cohen's d) in fALFF, LCOR, and GCOR between the age- and sex-matched control group and PD – *after atrophy correction*. Positive values (red cells) indicate higher values of brain functional measures in PD and negative values (blue cells) indicate the inverse. Values of regions of the left or right hemisphere are arranged next to each other (column-wise). The list is sorted from top to the bottom: Basal ganglia, limbic system, diencephalon, frontal cortex, motor area, parietal cortex, temporal cortex, occipital cortex, cerebellum. Regional values are visualized in Supplementary Figure 19B.

A: Effect size (PD vs HCmatched) in functional measures

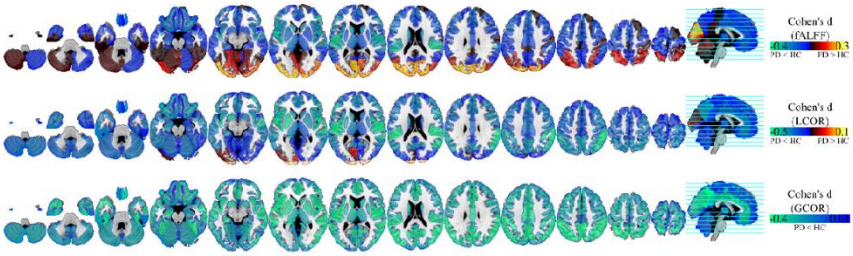

B: Effect size (PD vs HCmatched) in functional measures after atrophy correction

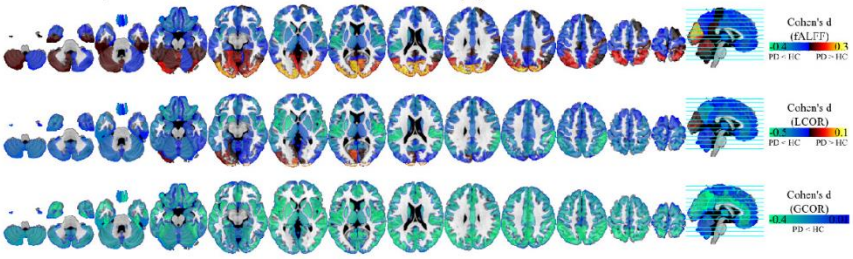

Supplementary Figure 19: Maps of regional differences in fALFF, LCOR, and GCOR between the age- and sex-matched control group and PD. Values of regions correspond to those of Supplementary Figure 17 and 18 (atrophy corrected).

Supplementary References

1. Friston, K. J. *et al.* Statistical parametric maps in functional imaging: A general linear approach. *Hum. Brain Mapp.* **2**, 189–210 (1994).
2. Jenkinson, M., Beckmann, C. F., Behrens, T. E. J., Woolrich, M. W. & Smith, S. M. FSL. *NeuroImage* **62**, 782–790 (2012).
3. Whitfield-Gabrieli, S. & Nieto-Castanon, A. Conn: A Functional Connectivity Toolbox for Correlated and Anticorrelated Brain Networks. *Brain Connectivity* **2**, 125–141 (2012).
4. Friston, K. J., Williams, S., Howard, R., Frackowiak, R. S. J. & Turner, R. Movement-Related effects in fMRI time-series: Movement Artifacts in fMRI. *Magn. Reson. Med.* **35**, 346–355 (1996).
5. Zou, Q.-H. *et al.* An improved approach to detection of amplitude of low-frequency fluctuation (ALFF) for resting-state fMRI: Fractional ALFF. *Journal of Neuroscience Methods* **172**, 137–141 (2008).
6. Deshpande, G., LaConte, S., Peltier, S. & Hu, X. Integrated local correlation: A new measure of local coherence in fMRI data. *Hum. Brain Mapp.* **30**, 13–23 (2009).
7. Saad, Z. S. *et al.* Correcting Brain-Wide Correlation Differences in Resting-State FMRI. *Brain Connectivity* **3**, 339–352 (2013).
8. Rutherford, S. *et al.* The normative modeling framework for computational psychiatry. *Nat Protoc* **17**, 1711–1734 (2022).
9. Marquand, A. PCNtoolkit; https://pcntoolkit.readthedocs.io/en/latest/,

4 Studie 3: Lifetime Exposure to Depression and Neuroimaging Measures of Brain Structure and Function

Xinyi Wang, BS[1,3]; Felix Hoffstaedter, PhD[2,3]; Jan Kasper, MS[2,3]; Simon B. Eickhoff, MD[2,3]; Kaustubh R. Patil, PhD[2,3]; Juergen Dukart, PhD[2,3]

[1]School of Biological Sciences and Medical Engineering, Child Development, and Learning Science, Key Laboratory of Ministry of Education, Southeast University, Nanjing, China

[2]Institute of Systems Neuroscience, Medical Faculty, Heinrich Heine University Düsseldorf, Düsseldorf, Germany

[3]Institute of Neuroscience and Medicine, INM-7: Brain and Behaviour, Research Centre Jülich, Jülich, Germany

Publiziert in: *JAMA Netw Open.* February 19, 2024;7(2):e2356787. https://doi.org/10.1001/jamanetworkopen.2023.56787; (163)

Korrespondierende Autoren:

Xinyi Wang, BS
School of Biological Sciences and Medical Engineering, Child Development, and Learning Science,
Key Laboratory of Ministry of Education, Southeast University,
Nanjing, 210096, China
E-Mail: xin.wang@fz-juelich.de

und

Juergen Dukart, PhD
Institute of Systems Neuroscience, Medical Faculty, Heinrich Heine University Düsseldorf
Institute of Neuroscience and Medicine - INM-7: Brain and Behaviour, Research Center Jülich
Wilhelm-Johnen-Straße,
52425 Jülich, Germany
E-Mail: j.dukart@fz-juelich.de

Eigenanteil:

Datenverarbeitung, Interpretation der Daten, kritisches Korrigieren des Manuskripts

JAMA Network Open

Original Investigation | Psychiatry

Lifetime Exposure to Depression and Neuroimaging Measures of Brain Structure and Function

Xinyi Wang, BS; Felix Hoffstaedter, PhD; Jan Kasper, MS; Simon B. Eickhoff, MD; Kaustubh R. Patil, PhD; Juergen Dukart, PhD

Abstract

IMPORTANCE Despite decades of neuroimaging studies reporting brain structural and functional alterations in depression, discrepancies in findings across studies and limited convergence across meta-analyses have raised questions about the consistency and robustness of the observed brain phenotypes.

OBJECTIVE To investigate the associations between 6 operational criteria of lifetime exposure to depression and functional and structural neuroimaging measures.

DESIGN, SETTING, AND PARTICIPANTS This cross-sectional study analyzed data from a UK Biobank cohort of individuals aged 45 to 80 years who were enrolled between January 1, 2014, and December 31, 2018. Participants included individuals with a lifetime exposure to depression and matched healthy controls without indications of psychosis, mental illness, behavior disorder, and disease of the nervous system. Six operational criteria of lifetime exposure to depression were evaluated: help seeking for depression; self-reported depression; antidepressant use; depression definition by Smith et al; hospital *International Statistical Classification of Diseases and Related Health Problems, Tenth Revision* (*ICD-10*) diagnosis codes F32 and F33; and Composite International Diagnostic Interview Short Form score. Six increasingly restrictive depression definitions and groups were defined based on the 6 depression criteria, ranging from meeting only 1 criterion to meeting all 6 criteria. Data were analyzed between January and October 2022.

MAIN OUTCOMES AND MEASURES Functional measures were calculated using voxel-wise fractional amplitude of low-frequency fluctuation (fALFF), global correlation (GCOR), and local correlation (LCOR). Structural measures were calculated using gray matter volume (GMV).

RESULTS The study included 20 484 individuals with lifetime depression (12 645 females [61.7%]; mean [SD] age, 63.91 [7.60] years) and 25 462 healthy controls (14 078 males [55.3%]; mean [SD] age, 65.05 [7.8] years). Across all depression criteria, individuals with lifetime depression displayed regionally consistent decreases in fALFF, LCOR, and GCOR (Cohen *d* range, −0.53 [95% CI, −0.88 to −0.15] to −0.04 [95% CI, −0.07 to −0.01]) but not in GMV (Cohen *d* range, −0.47 [95 % CI, −0.75 to −0.12] to 0.26 [95% CI, 0.15-0.37]). Hospital *ICD-10* diagnosis codes F32 and F33 (median [IQR] difference in effect sizes, −0.14 [−0.17 to −0.11]) and antidepressant use (median [IQR] difference in effect sizes, −0.12 [−0.16 to −0.10]) were criteria associated with the most pronounced alterations.

CONCLUSIONS AND RELEVANCE Results of this cross-sectional study indicate that lifetime exposure to depression was associated with robust functional changes, with a more restrictive depression definition revealing more pronounced alterations. Different inclusion criteria for depression may be associated with the substantial variation in imaging findings reported in the literature.

JAMA Network Open. 2024;7(2):e2356787. doi:10.1001/jamanetworkopen.2023.56787

Key Points

Question How are the 6 operational criteria of lifetime exposure to depression associated with functional and structural neuroimaging measures?

Findings In this cross-sectional study of 20 484 individuals with a lifetime exposure to depression and 25 462 healthy controls in the UK Biobank, robust functional alterations but not structural alterations were observed with more restrictive criteria of depression.

Meaning Findings of this study suggest that different inclusion criteria for depression may be associated with the substantial variation in imaging findings described in the literature.

+ Supplemental content

Author affiliations and article information are listed at the end of this article.

Introduction

Depression is a common health condition characterized by low mood, loss of interest, and feelings of excessive guilt.[1] The lifetime prevalence of depression is approximately 11%, with a higher prevalence in women.[2] Exposure to major depressive disorder (MDD) is associated with reduced quality of life and increased risk of suicide and self-wounding.[3,4] Understanding the neurobiological mechanisms underlying depression is a crucial aspect of developing improved therapeutic options and minimizing adverse outcomes.

Numerous functional and structural magnetic resonance imaging (MRI) studies have tested for neurobiological mechanisms of MDD, reporting a variety of MDD-related alterations, such as hippocampal volume reductions and increased amygdala activity during emotional tasks.[5] In contrast, neuroimaging meta-analyses and large-scale projects revealed less convergent findings or small effect sizes for most of the evaluated neuroimaging modalities.[6-9] When present, the identified brain alterations did not allow for reliable differentiation between patients with MDD and healthy controls, with accuracies being only marginally above chance level.[10] The small effect sizes and lack of differentiation point to currently limited diagnostic value of respective MRI modalities.[10,11] A confounding factor in this regard, which has been largely ignored to date, is the difference in definition of depression applied across various cross-sectional and longitudinal studies. Despite this limitation, these studies point to the existence of some MDD-related brain alterations that are either predisposing factors or a consequence of MDD diagnosis or treatment. However, it remains largely unknown whether and how far these alterations persist and whether prior exposure to depression affects brain function and structure later in life.

We used data from the UK Biobank[12,13] to systematically quantify the magnitude of structural and functional alterations associated with lifetime exposure to depression. Making use of the available in-depth phenotyping, we aimed to investigate the associations between 6 operational criteria of lifetime exposure to depression, ranging from self-reported to clinically defined depression, and functional and structural neuroimaging measures. We then evaluated the magnitude of case-control differences as manifested in brain structure and function for the different constellations of these criteria.

Methods

Data were obtained from the UK Biobank for individuals aged 45 to 80 years and who were enrolled from January 1, 2014, to December 31, 2018. The North-West Multicenter Research Ethics Committee approved the UK Biobank cohort study, which was conducted in accordance with the Declaration of Helsinki.[14] All participants provided written informed consent. The Heinrich Heine University Institutional Review Board approved this cross-sectional study, and the initial informed consent from the UK Biobank participants applies to this study. We followed the Strengthening the Reporting of Observational Studies in Epidemiology (STROBE) reporting guideline.

Participants

Six operational criteria of lifetime exposure to depression are commonly used in UK Biobank depression studies: help seeking for depression; self-reported depression; antidepressant use; depression definition by Smith et al[15]; hospital *International Statistical Classification of Diseases and Related Health Problems, Tenth Revision* (*ICD-10*) diagnosis codes F32 and F33; and Composite International Diagnostic Interview Short Form score.[16] The patients included in the study met at least 1 of these 6 criteria. Detailed descriptions of the 6 operational criteria and exclusion criteria are provided in the eMethods in Supplement 1.

To determine how exposure to lifetime depression differed in brain structural and resting-state functional measures across cumulative criteria, we first stratified all patients into 6 groups according to the number of criteria met. These 6 graded groups were classified from meeting only 1 criterion

to meeting all 6 criteria. Therefore, meeting *k* criteria indicated that participants met exactly rather than at least a specific number of criteria, ensuring that the 6 groups included no overlapping participants.

Healthy controls were defined as individuals without indications of psychosis, mental illness, behavior disorder, and disease of the nervous system. The exclusion criteria for healthy controls are detailed in the eMethods in Supplement 1. Healthy control groups were defined using 2 strategies. In strategy 1, we identified a single healthy control group that included all individuals who did not meet any of the exclusion criteria. Strategy 1 ensured that all patient subgroups were compared with the same, more representative healthy control group. To control for potential differences in demographics between the healthy control population and respective depression subgroups, we treated the demographic variables as covariates.

In strategy 2, we matched the 6 healthy control groups to the 6 depression groups by age, sex, and years of education using an automated 1:1 matching process whenever possible. Strategy 2 was a traditional control group approach to better control for potential demographic confounders. We considered the results from strategy 1 (all available healthy individuals) as the primary outcome and the results from strategy 2 as the control analysis.

Imaging Data Acquisition and Preprocessing

Resting-state functional MRI and T1-weight structural images were acquired using a 3T scanner (MAGNETOM Skyra; Siemens Healthcare) with a standard 32-channel head coil, according to available protocol. Structural images were preprocessed using SPM12, version r7770 (Functional Imaging Laboratory) and CAT12, version r1720 (Christian Gaser and Robert Dahnke),[17] with the default settings compiled under MATLAB 2019b, massively parallelized on the JURECA high-performance computing system (Jülich Supercomputing Centre). Functional images were preprocessed using SPM12, FSL5.0,[18] and the CONN toolbox.[19] The scans parameters and preprocessing are provided in the eMethods in Supplement 1.

Relative gray matter volume (GMV) was computed by dividing the total GMV by the total intracranial volume. The gray matter images were smoothed using an 8-mm full-width at half-maximum Gaussian kernel. We then computed functional measures using the default settings in the CONN toolbox, including the fractional amplitude of low-frequency fluctuation (fALFF), global correlation (GCOR), and local correlation (LCOR). The fALFF reflects the local amplitude of low-frequency fluctuation (0.008 Hz to 0.09 Hz) vs the overall frequency spectrum.[20] The LCOR is the local coherence between a voxel and its neighboring voxels.[21] The GCOR is the mean correlation coefficient between BOLD (blood oxygen level–dependent) signals of a voxel and all other voxels in the brain.

Statistical Analysis

We performed a 2-stage analysis to determine brain alterations using increasingly restrictive levels of definitions, ranging from meeting only 1 criterion to meeting all 6 criteria. Two-sample, 2-tailed *t* tests were used to compare each lifetime depression group with healthy controls at $P < .05$ (family-wise error–corrected for multiple comparisons at the cluster level), followed by computation of effect sizes between all constellations of lifetime depression and the single healthy control group. Data were analyzed between January and October 2022.

In stage 1 analysis, we identified clusters of voxels that differed substantially between healthy control and each depression group, from those meeting only 1 criterion to those meeting all 6 criteria. Voxel-wise 2-sample *t* tests (assuming unequal variance) were conducted using SPM12 implemented in MATLAB (The MathWorks Inc). First, a 2-sample *t* test was used to investigate group differences in voxel-wise fALFF, GCOR, LCOR, and GMV, adjusting for age, age^2, sex, and total intracranial volume. The 6 depression groups were compared separately with 2 types of healthy control groups (strategy 1 and strategy 2). The resulting statistical maps were at a threshold of $P < .001$ uncorrected at the voxel level combined with a whole-brain voxel-wise family-wise error correction at the cluster

level at a $P < .05$ threshold. Clusters that survived this correction were considered to be statistically significant. This procedure yielded 2 directional (increases and decreases) tests per imaging modality times 6 depression strata times 4 modalities, resulting in 48 tests per strategy overall.

In stage 2 analysis, to minimize the role of group sizes in the observed differences, we quantified the observed alterations using effect size measures (Cohen *d*). Cohen *d* was used to compute the mean difference between depression and healthy control groups divided by the pooled SD. For this calculation, we defined binary voxel-wise maps of significant cluster findings from the *t*-contrasts described (separate for increases and decreases). These masks, which represented regions with significant differences for the respective contrast, were referred to as mask 1 (meeting only 1 criterion) to mask 6 (meeting all 6 criteria). Theoretically, there can be 12 masks (6 groups ×2 directional *t*-contrasts) for each structural or functional measure. For each participant, we calculated the mean values in each mask for the respective structural or functional measures. We then calculated the Cohen *d* value for each mask between the 6 graded depression groups and the single healthy control group (strategy 1).

To further explore how the different lifetime depression groups and their combinations were associated with the observed differences, we computed the effect sizes (Cohen *d*) of group differences for each available combination of depression criteria and each mask. To ensure a more robust estimate of the effect size, we excluded criteria constellations with fewer than 10 available participants. To identify the criteria associated with increases or decreases of the observed effect sizes, we quantified the association of each criterion by computing the difference in effect size. Specifically, we categorized all criteria constellations into 2 groups: with the specific criterion and without the criterion. The difference in effect size was defined as the mean effect size of combinations with the specific criterion minus the mean effect sizes of combinations without the criterion. For each identified mask per modality, this resulted in 6 differences in effect size values representing the associations of the 6 criteria.

Results

Sample

Among the individuals with imaging data in the UK Biobank, 20 484 met at least 1 of the criteria of lifetime exposure to depression and 25 462 met the criteria for healthy controls. Of the participants with lifetime exposure to depression, 12 645 (61.7%) self-reported as female and 7839 (38.3%) as male, with a mean (SD) age of 63.91 (7.60) years and mean (SD) years of education of 16.65 (3.82). Demographic characteristics of participants for 6 operational criteria and 6 graded depression groups are shown in the **Table**. Group sizes differed slightly for functional and structural analyses due to different dropouts for quality control reasons (eTable 1 in Supplement 1).

The healthy controls comprised 11 384 participants who self-reported as female (44.7%) and 14 078 as male (55.3%), with a mean (SD) age of 65.05 (7.80) years and mean (SD) years of education of 16.69 (3.77). The demographics of all healthy controls (strategy 1) are provided in eTable 2 in Supplement 1, and eTable 3 in Supplement 1 shows the characteristics for matched healthy controls (strategy 2). There were 63 unique constellations of the 6 criteria, ranging from meeting at least 1 criterion to meeting all 6 criteria. For example, participants meeting all 6 criteria would also be represented in any other constellation. The number of participants for 63 constellations are shown in eFigure 1 in Supplement 1.

Structural and Functional Alterations

We found significant alterations in all functional and structural measures for most lifetime depression groups, except in patients who met all 6 criteria or met only 1 criterion when using GMV and GCOR (eFigures 2 and 3 in Supplement 1) compared with the single healthy control group. Group comparisons in functional measures revealed consistently decreased fALFF, GCOR, and LCOR in the lifetime depression groups but not GMV compared with healthy controls. Clusters of significant

functional alterations covered multiple regions encompassing the prefrontal cortex, parietal cortex, middle temporal cortex, fusiform gyrus, occipital cortex, and cerebellum (t_{15095} = 9.59; P < .001) (eTables 4-6 in Supplement 1). Specifically, fALFF and LCOR alterations displayed similar spatial patterns of decreases in the bilateral precentral and postcentral gyrus. Decreased GCOR was primarily observed in the middle inferior temporal cortex, superior temporal cortex, precuneus, insula, and lingual cortex (t_{15095} = 7.68; P < .001). We found a bidirectional pattern of GMV alterations with increases in the right superior medial frontal cortex and precentral gyrus and decreases in the right hippocampus and superior temporal cortex (t_{22389} = 6.86; P < .001) (eTable 7 in Supplement 1). The outcomes of comparisons of all depression groups to matched healthy controls were largely consistent with the primary analysis (eTables 8-11 in Supplement 1).

Differences Between Depression Groups and Healthy Controls by Observed Alterations

Given that some of the observed imaging differences across the increasingly restrictive depression definitions may simply reflect differences in sample size, effect sizes for each criteria constellation and each significance mask derived from the group comparisons are presented in **Figure 1**. Effect sizes were consistently reduced in depression group for all functional measures (Cohen *d* range, −0.53 [95% CI, −0.88 to −0.15] to −0.04 [95% CI, −0.07 to −0.01]) but not for GMV (Cohen *d* range, −0.47 [95% CI, −0.75 to −0.12] to 0.26 [95% CI, 0.15-0.37]). Additionally, effect sizes increased with a higher number of criteria met for functional measures. The group that met all 6 criteria consistently showed the largest effect sizes in fALFF, LCOR, and GCOR. Effect sizes were generally lower for GMV, and only mask 3 and mask 4 from the decreased GMV displayed consistently reduced depression but overall negligible effect sizes. Results for mask 2 and mask 5 derived from the increased GMV clusters were not consistent.

Association of 6 Criteria With Observed Alterations

A higher absolute value in the difference in effect sizes indicates a higher association with the respective criterion. Constellations involving hospital *ICD-10* diagnosis codes F32 and F33 followed by antidepressant use displayed higher associations with the observed effect sizes for all functional measures (median [IQR] difference in effect sizes: hospital *ICD-10* diagnosis codes, −0.14 [−0.17 to −0.11]); antidepressant use, −0.12 [−0.16 to −0.10]) and for the GMV-decreased masks (median [IQR] difference in effect sizes: hospital *ICD-10* diagnosis codes, −0.09 [−0.12 to −0.05]; antidepressant

Table. Demographic Characteristics of Participants With Lifetime Exposure to Depression

Characteristic	Total No.	Female sex, No. (%)	Male sex, No. (%)	Age, mean (SD), y	Years of education, mean (SD)
Criteria of lifetime exposure to depression					
Help seeking for depression	19 182	11 828 (61.7)	7354 (38.3)	63.91 (7.60)	16.65 (3.82)
Self-reported depression	4691	2879 (61.4)	1812 (38.6)	63.98 (7.62)	16.64 (3.82)
Antidepressant use	4222	2602 (61.6)	1620 (38.4)	63.98 (7.64)	16.65 (3.81)
Depression definition by Smith et al[15]	3166	1963 (62.0)	1203 (38.0)	63.99 (7.67)	16.65 (3.83)
Hospital *ICD-10* diagnosis codes F32 and F33	1605	990 (61.7)	615 (38.3)	64.04 (7.67)	16.67 (3.83)
CIDI-SF score	3571	2200 (61.6)	1371 (38.4)	63.99 (7.66)	16.66 (3.82)
No. of criteria met					
1	10 977	6487 (59.1)	4490 (40.9)	64.54 (7.57)	16.52 (3.90)
2	5233	3307 (63.2)	1926 (36.8)	63.62 (7.53)	16.77 (3.76)
3	2574	1691 (65.7)	883 (34.3)	63.02 (7.58)	16.77 (3.74)
4	1275	859 (67.4)	416 (32.6)	62.40 (7.55)	16.80 (3.76)
5	378	270 (71.4)	108 (28.6)	61.79 (7.70)	17.39 (3.27)
6	47	31 (66.0)	16 (34.0)	59.22 (6.76)	17.81 (2.35)

Abbreviations: CIDI-SF, Composite International Diagnostic Interview Short Form; *ICD-10*, *International Statistical Classification of Diseases and Related Health Problems, Tenth Revision*.

use, −0.06 [−0.09 to −0.03]) (**Figure 2**). Higher (negative and positive) difference in effect sizes indicated associations with the respective criterion. None of the criteria displayed a consistent association for the GMV-increased mask.

Discussion

In this cross-sectional study, we systematically tested for associations between lifetime exposure to depression and brain structural and functional measures. We found that both functional and structural alterations varied according to the different definitions of depression available in the UK Biobank, with more restrictive definitions associated with functional but not necessarily structural

Figure 1. Effect Sizes for Different Lifetime Depression on the Observed Imaging Alterations

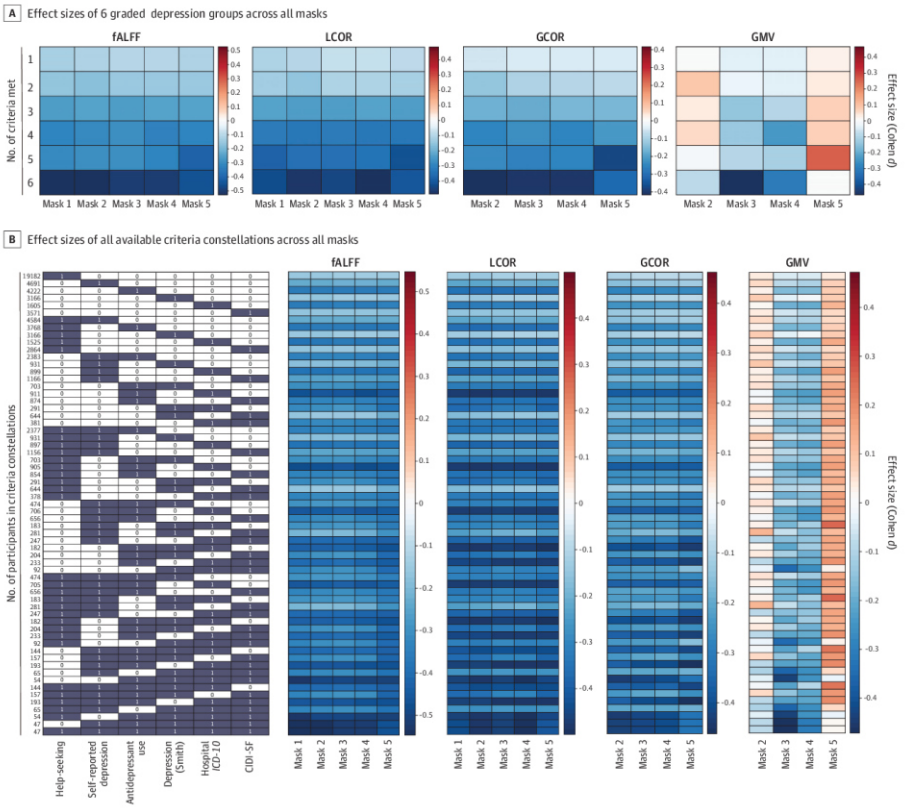

A, Masks indicate the number of criteria met (eg, mask 1 indicates meeting 1 criterion; mask 5, meeting 5 criteria). Effect sizes were calculated in all depression stratum–mask pairs. B, The dark element indicates that the column contains corresponding criteria. Other blocks show the effect size values (Cohen *d*). Red indicates increased imaging measures in depression group, and blue indicates reduced imaging measures in depression group. CIDI-SF indicates Composite International Diagnostic Interview Short Form; fALFF, fractional amplitude of low-frequency fluctuations; GCOR, global correlation; GMV, gray matter volume; *ICD-10, International Statistical Classification of Diseases and Related Health Problems, Tenth Revision;* LCOR, local correlation.

alterations. Specifically, decreases in local functional activity were consistent across all criteria, with hospital *ICD-10* diagnosis codes F32 and F33 and antidepressant use being associated with the observed alterations.

Increases and decreases in brain functional measures have been associated with depression in previous studies.[22-25] In contrast to some of these findings, we observed only decreases in local activity and in local and global connectivity measures across all constellations of lifetime depression. These findings are in line with recent larger studies and meta-analyses reporting reduced functional connectivity in the default mode networks and convergent regions only for decreased functional findings in MDD.[7,26] Despite the matching direction of change, we found only limited convergence in sensorimotor regions in terms of location of the observed alteration patterns. While differences in the samples and applied methods likely accounted for some of the discrepancies, a main difference is that this study characterized lifetime depression criteria as opposed to the more acute effects of depression as reported in the literature. The findings from this study suggest the existence of a persistent depression-related brain functional phenotype with small to moderate effect sizes.

We found that the hospital *ICD-10* diagnosis codes F32 and F33 and antidepressant use criteria were associated with the observed functional alterations in depression groups compared with healthy controls. Only limited association was observed for all other applied criteria. This observation

Figure 2. Violin Plots of Associations of 6 Criteria With Observed Alterations

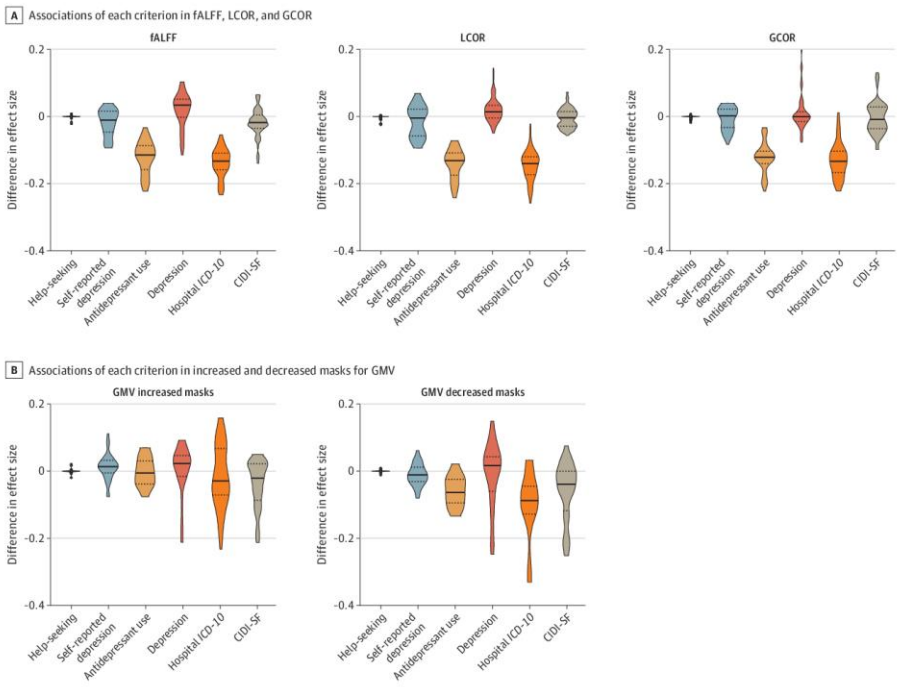

The extent of the violin plot is the range of difference in effect size. Solid lines indicate the median, and dotted lines indicate the quartiles of difference in effect size. Each side of the violin plot represents the kernel density estimation of the distribution shape of the difference in effect size. CIDI-SF indicates Composite International Diagnostic Interview Short Form; fALFF, fractional amplitude of low-frequency fluctuations; GCOR, global correlation; GMV, gray matter volume; *ICD-10, International Statistical Classification of Diseases and Related Health Problems, Tenth Revision;* LCOR, local correlation.

may indicate some conceptual advantages of these 2 criteria over the other definitions of depression in the UK Biobank. We did not find similarly high effect sizes for participants meeting the Composite International Diagnostic Interview Short Form score criterion, although the screening was designed to provide lifetime information about depression and additional factors that may be associated with the observed imaging alterations. As the antidepressant use criterion is typically directly associated with a depression diagnosis, any causal interpretation of the observed alterations or conclusion about the cause or consequence of requiring medication should be limited. Despite this limitation, given that numerous treatment interventions for depression are not medication-based but psychological (eg, cognitive behavioral therapy and stimulation therapies) and that patients often refuse antidepressant treatment, these 2 criteria are not necessarily identical. The separate roles of hospital *ICD-10* diagnosis codes F32 and F33 and antidepressant use observed in the study may point to such a differential association of both variables with the observed decreases in brain functional measures. Additionally, causal interpretation is precluded in this case because the observed associations can still be attributed to either the necessity of prescribing antidepressants or the consequence of exposure to antidepressants.

We found that decreased local functional activity and synchronicity in precentral and postcentral gyrus and decreased global functional connectivity in parts of the limbic system were consistently associated with lifetime depression. The reduced local activity in sensorimotor regions may be attributed to the consequence of exposure to treatments and depression-associated vulnerability. For treatment effects, a meta-analysis found that stimulation therapy for depression altered the activity in the right precentral gyrus, right posterior cingulate, left inferior frontal gyrus, and left middle frontal gyrus.[27] After electroconvulsive therapy, fALFF was reported to decrease in the right precentral gyrus.[28] Additionally, antidepressant use was associated with reduced hyperconnectivity within the limbic system.[29] Contrary to the functional measures, the findings for GMV were only partially consistent with previous studies. The observed reduced hippocampal volume is commonly reported in meta-analyses and case-control studies.[30] The effect size of GVM alterations was substantially smaller compared with functional measures.

Overall, the findings of the present study provide evidence of the implications of different depression definitions for the observed imaging outcomes. The UK Biobank contains extensive data items associated with depression. However, the availability of multiple sources of information presents challenges in achieving consistent definitions of depression across different studies. Stricter definitions often conflict with the available sample size, but researchers might be tempted to apply fewer restrictions to putatively increase statistical power. This study showed that such an approach may become futile in neuroimaging because less restrictive definitions may lead to dilution of potential imaging alterations. Recent studies have explored the association of different depression phenotypes in the UK Biobank with genetic and cortical thickness measures.[31] Although 1 of these studies suggested that a broader definition of depression may provide more tractable phenotypes,[32] others recommended more restrictive definitions, suggesting that minimal phenotyping may play a role in biased potential findings by introducing conceptual differences in the selected cohorts.[33,34] Expanding on these earlier findings, we believe that while restrictiveness is generally rather beneficial, the specific criteria should be carefully weighted and evaluated. Only 2 of the 6 applied depression criteria were consistently associated with the magnitude of the functional imaging alterations observed in the present study. These findings suggest that mere restrictiveness may become counterproductive and that the implications of each criterion need to be carefully evaluated in future research.

Limitations

Several limitations apply with respect to the interpretation of the findings. To our knowledge, the UK Biobank is the largest available cohort to date and is biased in terms of cultural and educational background, primarily representing participants of White ethnicity.[35] This bias may limit the generalizability of the results to other populations. Furthermore, the observed associations do not

allow a causal interpretation of the findings regarding whether the observed imaging alterations are the cause or consequence of exposure to depression.

Conclusions

This study found an association of lifetime depression with functional and structural imaging alterations. More restrictive depression definition revealed more pronounced changes. Different inclusion criteria for depression may be associated with the substantial variation in imaging findings in the literature. Each criterion warrants further study.

ARTICLE INFORMATION

Accepted for Publication: December 28, 2023.

Published: February 19, 2024. doi:10.1001/jamanetworkopen.2023.56787

Corresponding Author: Xinyi Wang, BS, School of Biological Sciences and Medical Engineering, Child Development, and Learning Science, Key Laboratory of Ministry of Education, Southeast University, Nanjing, 210096, China (xin.wang@fz-juelich.de); Juergen Dukart, PhD, Institute of Neuroscience and Medicine, INM-7: Brain and Behaviour, Research Centre Jülich, Jülich, 52428, Germany (j.dukart@fz-juelich.de).

Author Affiliations: School of Biological Sciences and Medical Engineering, Child Development, and Learning Science, Key Laboratory of Ministry of Education, Southeast University, Nanjing, China (Wang); Institute of Systems Neuroscience, Medical Faculty, Heinrich Heine University Düsseldorf, Düsseldorf, Germany (Hoffstaedter, Kasper, Eickhoff, Patil, Dukart); Institute of Neuroscience and Medicine, INM-7: Brain and Behaviour, Research Centre Jülich, Jülich, Germany (Wang, Hoffstaedter, Kasper, Eickhoff, Patil, Dukart).

Author Contributions: Ms Wang had full access to all of the data in the study and takes responsibility for the integrity of the data and the accuracy of the data analysis. Drs Patil and Dukart contributed equally to this work.

Concept and design: Wang, Eickhoff, Patil, Dukart.

Acquisition, analysis, or interpretation of data: Wang, Hoffstaedter, Kasper, Patil, Dukart.

Drafting of the manuscript: Wang, Patil.

Critical review of the manuscript for important intellectual content: All authors.

Statistical analysis: Wang, Hoffstaedter, Patil, Dukart.

Obtained funding: Wang, Patil, Dukart.

Administrative, technical, or material support: Eickhoff, Dukart.

Supervision: Eickhoff, Patil, Dukart.

Conflict of Interest Disclosures: Ms Wang reported receiving a grant from Chinese Scholarship Council during the conduct of the study. Dr Patil reported receiving a grant from Helmholtz Portfolio Theme Supercomputing and Modeling for the Human Brain (SMHB) during the conduct of the study. Dr Dukart reported receiving a grant from European Union's Horizon 2020 research and innovation program The Virtual Brain-Cloud during the conduct of the study. No other disclosures were reported.

Funding/Support: This study was supported by grant CSC202006090244 from the Chinese Scholarship Council (Ms Wang), by the SMHB (Dr Patil), and by grant 826421 from the European Union's Horizon 2020 research and innovation program The Virtual Brain-Cloud (Dr Dukart).

Role of the Funder/Sponsor: The funders had no role in the design and conduct of the study; collection, management, analysis, and interpretation of the data; preparation, review, or approval of the manuscript; and decision to submit the manuscript for publication.

Data Sharing Statement: See Supplement 2.

Additional Contributions: The Jülich Aachen Research Alliance (JARA) Vergabegremium granted computing time on the JARA Partition, part of the supercomputer JURECA at Research Centre Jülich.

REFERENCES

1. World Health Organization. Depression. Accessed December 16, 2022. https://www.who.int/news-room/fact-sheets/detail/depression

2. Lim GY, Tam WW, Lu Y, Ho CS, Zhang MW, Ho RC. Prevalence of depression in the community from 30 countries between 1994 and 2014. *Sci Rep*. 2018;8(1):2861. doi:10.1038/s41598-018-21243-x

3. Cai H, Xie XM, Zhang Q, et al. Prevalence of suicidality in major depressive disorder: a systematic review and meta-analysis of comparative studies. *Front Psychiatry*. 2021;12:690130. doi:10.3389/fpsyt.2021.690130

4. Herrman H, Patel V, Kieling C, et al. Time for united action on depression: a Lancet-World Psychiatric Association Commission. *Lancet*. 2022;399(10328):957-1022. doi:10.1016/S0140-6736(21)02141-3

5. Li X, Wang J. Abnormal neural activities in adults and youths with major depressive disorder during emotional processing: a meta-analysis. *Brain Imaging Behav*. 2021;15(2):1134-1154. doi:10.1007/s11682-020-00299-2

6. Müller VI, Cieslik EC, Serbanescu I, Laird AR, Fox PT, Eickhoff SB. Altered brain activity in unipolar depression revisited: meta-analyses of neuroimaging studies. *JAMA Psychiatry*. 2017;74(1):47-55. doi:10.1001/jamapsychiatry.2016.2783

7. Gray JP, Müller VI, Eickhoff SB, Fox PT. Multimodal abnormalities of brain structure and function in major depressive disorder: a meta-analysis of neuroimaging studies. *Am J Psychiatry*. 2020;177(5):422-434. doi:10.1176/appi.ajp.2019.19050560

8. Schmaal L, Veltman DJ, van Erp TG, et al. Subcortical brain alterations in major depressive disorder: findings from the ENIGMA major depressive disorder working group. *Mol Psychiatry*. 2016;21(6):806-812. doi:10.1038/mp.2015.69

9. Winter NR, Leenings R, Ernsting J, et al. Quantifying deviations of brain structure and function in major depressive disorder across neuroimaging modalities. *JAMA Psychiatry*. 2022;79(9):879-888. doi:10.1001/jamapsychiatry.2022.1780

10. Fried EI, Kievit RA. The volumes of subcortical regions in depressed and healthy individuals are strikingly similar: a reinterpretation of the results by Schmaal et al. *Mol Psychiatry*. 2016;21(6):724-725. doi:10.1038/mp.2015.199

11. Schmaal L, Veltman DJ, van Erp TG, et al. Response to Dr Fried & Dr Kievit, and Dr Malhi et al. *Mol Psychiatry*. 2016;21(6):726-728. doi:10.1038/mp.2016.9

12. Bycroft C, Freeman C, Petkova D, et al. The UK Biobank resource with deep phenotyping and genomic data. *Nature*. 2018;562(7726):203-209. doi:10.1038/s41586-018-0579-z

13. Miller KL, Alfaro-Almagro F, Bangerter NK, et al. Multimodal population brain imaging in the UK Biobank prospective epidemiological study. *Nat Neurosci*. 2016;19(11):1523-1536. doi:10.1038/nn.4393

14. World Medical Association. World Medical Association Declaration of Helsinki: ethical principles for medical research involving human subjects. *JAMA*. 2013;310(20):2191-2194. doi:10.1001/jama.2013.281053

15. Smith DJ, Nicholl BI, Cullen B, et al. Prevalence and characteristics of probable major depression and bipolar disorder within UK biobank: cross-sectional study of 172,751 participants. *PLoS One*. 2013;8(11):e75362. doi:10.1371/journal.pone.0075362

16. Kessler RC, Andrews G, Mroczek D, Ustun B, Wittchen HU. The World Health Organization Composite International Diagnostic Interview Short-Form (CIDI-SF). *Int J Methods Psychiatr Res*. 1998;7(4):171-185. doi:10.1002/mpr.47

17. Gaser C, Dahnke R, Thompson PM, Kurth F, Luders E; Alzheimer's Disease Neuroimaging Initiative. CAT – A computational anatomy toolbox for the analysis of structural MRI data. *bioRxiv*. Preprint posted online June 13, 2022. doi:10.1101/2022.06.11.495736

18. Jenkinson M, Beckmann CF, Behrens TEJ, Woolrich MW, Smith SM. FSL. *Neuroimage*. 2012;62(2):782-790. doi:10.1016/j.neuroimage.2011.09.015

19. Whitfield-Gabrieli S, Nieto-Castanon A. Conn: a functional connectivity toolbox for correlated and anticorrelated brain networks. *Brain Connect*. 2012;2(3):125-141. doi:10.1089/brain.2012.0073

20. Zou QH, Zhu CZ, Yang Y, et al. An improved approach to detection of Amplitude of Low-Frequency Fluctuation (ALFF) for resting-state fMRI: fractional ALFF. *J Neurosci Methods*. 2008;172(1):137-141. doi:10.1016/j.jneumeth.2008.04.012

21. Deshpande G, LaConte S, Peltier S, Hu X. Integrated local correlation: a new measure of local coherence in fMRI data. *Hum Brain Mapp*. 2009;30(1):13-23. doi:10.1002/hbm.20482

22. Hao H, Chen C, Mao W, Zhong J, Dai Z. Aberrant brain regional homogeneity in first-episode drug-naïve patients with major depressive disorder: a voxel-wise meta-analysis. *J Affect Disord*. 2019;245:63-71. doi:10.1016/j.jad.2018.10.113

23. Gong J, Wang J, Qiu S, et al. Common and distinct patterns of intrinsic brain activity alterations in major depression and bipolar disorder: voxel-based meta-analysis. *Transl Psychiatry*. 2020;10(1):353. doi:10.1038/s41398-020-01036-5

24. Wang W, Zhao Y, Hu X, et al. Conjoint and dissociated structural and functional abnormalities in first-episode drug-naive patients with major depressive disorder: a multimodal meta-analysis. *Sci Rep*. 2017;7(1):10401. doi:10.1038/s41598-017-08944-5

25. Fang J, Mao N, Jiang X, Li X, Wang B, Wang Q. Functional and anatomical brain abnormalities and effects of antidepressant in major depressive disorder: combined application of voxel-based morphometry and amplitude of frequency fluctuation in resting state. *J Comput Assist Tomogr*. 2015;39(5):766-773. doi:10.1097/RCT.0000000000000264

26. Yan CG, Chen X, Li L, et al. Reduced default mode network functional connectivity in patients with recurrent major depressive disorder. *Proc Natl Acad Sci U S A*. 2019;116(18):9078-9083. doi:10.1073/pnas.1900390116

27. Deng Y, Li W, Zhang B. Functional activity in the effect of transcranial magnetic stimulation therapy for patients with depression: a meta-analysis. *J Pers Med*. 2023;13(3):405. doi:10.3390/jpm13030405

28. Li X, Yu R, Huang Q, et al. Alteration of whole brain ALFF/fALFF and degree centrality in adolescents with depression and suicidal ideation after electroconvulsive therapy: a resting-state fMRI study. *Front Hum Neurosci*. 2021;15:762343. doi:10.3389/fnhum.2021.762343

29. Siegel JS, Palanca BJA, Ances BM, et al. Prolonged ketamine infusion modulates limbic connectivity and induces sustained remission of treatment-resistant depression. *Psychopharmacology (Berl)*. 2021;238(4):1157-1169. doi:10.1007/s00213-021-05762-6

30. Schmaal L, Pozzi E, C Ho T, et al. ENIGMA MDD: seven years of global neuroimaging studies of major depression through worldwide data sharing. *Transl Psychiatry*. 2020;10(1):172. doi:10.1038/s41398-020-0842-6

31. Harris MA, Cox SR, de Nooij L, et al. Structural neuroimaging measures and lifetime depression across levels of phenotyping in UK biobank. *Transl Psychiatry*. 2022;12(1):157. doi:10.1038/s41398-022-01926-w

32. Howard DM, Adams MJ, Shirali M, et al; 23andMe Research Team. Genome-wide association study of depression phenotypes in UK Biobank identifies variants in excitatory synaptic pathways. *Nat Commun*. 2018;9(1):1470. doi:10.1038/s41467-018-03819-3

33. Glanville KP, Coleman JRI, Howard DM, et al. Multiple measures of depression to enhance validity of major depressive disorder in the UK Biobank. *BJPsych Open*. 2021;7(2):e44. doi:10.1192/bjo.2020.145

34. Cai N, Revez JA, Adams MJ, et al; MDD Working Group of the Psychiatric Genomics Consortium. Minimal phenotyping yields genome-wide association signals of low specificity for major depression. *Nat Genet*. 2020;52(4):437-447. doi:10.1038/s41588-020-0594-5

35. Fry A, Littlejohns TJ, Sudlow C, et al. Comparison of sociodemographic and health-related characteristics of UK Biobank participants with those of the general population. *Am J Epidemiol*. 2017;186(9):1026-1034. doi:10.1093/aje/kwx246

SUPPLEMENT 1.

eMethods.

eFigure 1. The Number of Participants in Criteria Constellations

eFigure 2. The Cerebral Parts of the Clusters Showing Significant Functional or Structural Differences Between Different Depression Stratums and HC

eFigure 3. The Cerebellum Parts of the Clusters Showing Significant Functional or Structural Differences Between Different Depression Stratums and HC

eTable 1. Demographic of Six Depression Groups Involving Analyses

eTable 2. Demographic of the Single Healthy Groups (Strategy 1)

eTable 3. Demographic of Six Matched Healthy Groups (Strategy 2)

eTable 4. Regions Showing Significant Differences in fALFF Between Individuals With Lifetime Depression and the Single HC Group (Strategy 1)

eTable 5. Regions Showing Significant Differences in LCOR Between Individuals With Lifetime Depression and the Single HC Group (Strategy 1)

eTable 6. Regions Showing Significant Differences in GCOR Between Individuals With Lifetime Depression and the Single HC Group (Strategy 1)

Supplemental Online Content

Wang X, Hoffstaedter F, Kasper J, Eickhoff S, Patil KR, Dukart J. Lifetime exposure to depression and neuroimaging measures of brain structure and function. *JAMA Netw Open*. 2024;7(2):e2356787. doi:10.1001/jamanetworkopen.2023.56787

This supplemental material has been provided by the authors to give readers additional information about their work.

eMethods.

Six operational criteria for exposure to lifetime depression

(1) Help-seeking was responding “Yes” to the following questions: "Have you ever seen a general practitioner for nerves, anxiety, tension, or depression?" [Data-Field: 2090] or "Have you ever seen a psychiatrist for nerves, anxiety, tension, or depression?" [Data-Field: 2100].

(2) Self-reported Depression was having experienced depression at present or past [Data-Field ID: 20002] before the neuroimaging scan.

(3) The Antidepressant usage was taking antidepressant medication at baseline or follow-up assessment [Data-Field ID: 20003]. The antidepressant codes are listed in eMethod (Medications codes).

(4) Depression (Smith) is an approximate measure of lifetime depression by Smith.[1] Smith et.al defined three types of depression through relevant questions in the mental health questionnaire, including “probable single episode”, “probable mild recurrent”, and “probable severe recurrent”. Participants met one of three lifetime depression were defined as Depression (Smith).

(5) Hospital ICD-10 is the hospital recorder for patients’ primary and secondary diagnoses [Data-field ID: 41202 and 41204]. Patients with the diagnosis of the depressive episode (F32-F32.9) or recurrent depressive disorder (F33-F33.8) were included in this criteria.

(6) CIDI-SF is derived from the mental health questionnaire.[2] The CIDI-SF is a brief survey instrument design to identify mental disorders including MDD based on the Diagnostic and Statistical Manual of Mental Disorders (DSM) criteria.[3]

The exclusion criteria for lifetime depression

The exclusion criteria of individuals in the lifetime depression group were:

(1) Having self-reported psychosis. The self-reported psychosis was defined as having experienced schizophrenia or mania/bipolar disorder/manic depression at present or past [Data-Field ID: 20002].
(2) Having taken antipsychotic medications. The antipsychotic codes were listed in supplementary materials.
(3) The hospital records [Data-Field ID: 41202 or 41204] included Schizophrenia, schizotypal and delusional disorders (F20-F29), and other mood disorders (F30-F39, excluding depression code: F32-F33).
(4) Having been defined as psychosis in mental health questionnaire (MHQ) screen. The answer to the question “Have you been diagnosed with one or more of the following mental health problems by a professional, even if you don’t have it currently” [Data-field ID: 20544] is “Schizophrenia” or “Any other type of psychosis or psychotic illness”, or “Mania, hypomania, bipolar or manic-depression”.

The exclusion criterion for healthy controls

The healthy individuals were enrolled with the following exclusive criterion:

(1) Did not meet the criteria for any indications of depression as described in the above depression phenotypes.
(2) Did not meet the criteria for any indications of psychosis which was described in the depression exclusive criterion, including self-reported psychosis, antipsychotic medications usage, MHQ psychosis.
(3) Did not endorse disorder in any mental illness and behavior disorder (Hospital ICD10 Chapter V, F00-F99) and diseases of the nervous system (Hospital ICD10 Chapter VI G00-G99）.

Medications codes

The antidepressants are coded as follows [UKB Data-Coding 4]:
1140879616, 1140921600, 1140879540, 1140867878, 1140916282, 1140909806, 1140867888, 1141152732, 1141180212, 1140879634, 1140867876, 1140882236, 1141190158, 1141200564, 1140867726, 1140879620, 1140867818, 1140879630, 1140879628, 1141151946, 1140867948, 1140867624, 1140867756, 1140867884, 1141151978, 1141152736, 1141201834, 1140867690, 1140867640, 1140867920, 1140867850, 1140879544, 1141200570, 1140867934, 1140867758, 1140867914, 1140867820, 1141151982, 1140882244, 1140879556, 1140867852, 1140867860, 1140917460, 1140867938, 1140867856, 1140867922, 1140910820, 1140882312, 1140867944, 1140867784, 1140867812, 1140867668.

The antipsychotics in UK biobank are coded as follows:
1140868170, 1140928916, 1141152848, 1140867444, 1140879658, 1140868120, 1141153490, 1140867304, 1141152860, 1140867168, 1141195974, 1140867244, 1140867152, 1140909800, 1140867420, 1140879746, 1141177762, 1140867456, 1140867952, 1140867150, 1141167976, 1140882100, 1140867342, 1140863416, 1141202024, 1140882098, 1140867184, 1140867092, 1140882320, 1140910358, 1140867208, 1140909802, 1140867134, 1140867306, 1140867210, 1140867398, 1140867078, 1140867218, 1141201792, 1141200458, 1140867136, 1140879750, 1140867180, 1140867546, 1140928260, 1140927956.

Imaging data acquisition and pre-processing

The present study focused on resting-sate functional MRI and T1-weight structural images in initial neuroimaging scans of these patients in the UK biobank. MRI data were acquired using a Siemens Skyra 3T scanner (Siemens Healthcare, Erlangen, Germany) using a standard 32-channel head coil, according to a freely available protocol (http://www.fmrib.ox.ac.uk/ukbiobank/protocol/V4_23092014.pdf). As part of the scanning protocol, high-resolution T1-weighted images and resting-state fMRI were obtained. High-resolution T1-weighted images were obtained using an MPRAGE sequence with the following parameters: repetition time (TR) =2000ms, echo time (TE) =2.01ms, 208 slices, flip angle=8°, field of view (FOV) =256mm, matrix=256×256, slice thickness=1.0mm, voxel size 1×1×1mm. The resting-state functional MRI were obtained with with a multi-band gradient echo EPI sequence: TR=735ms;

TE=39ms; 64 slices; flip angle=52°; FOV=210mm; matrix=88×88; slice thickness=2.4mm, voxel size=2.4×2.4×2.4mm^3. Images that did not pass the existing UKB preprocessing and quality control pipeline[4] were excluded.

For T1-weight images, raw T1 images were registered to functional images, bias and noise corrected, global intensity normalized, and then segmented into gray matter (GM), white matter, and cerebrospinal fluid. Next, the images were spatially normalized to the standard Montreal Neurological Institute (MNI) templates using Geodesic Shooting.[5] A whole-brain gray matter mask with a probability of gray matter above 0.3 was applied prior to the analyses.

For functional images, we used the resting-state fMRI processed by the UK Biobank as "filtered_func_data_clean.nii" (https://biobank.ctsu.ox.ac.uk/crystal/crystal/docs/brain_mri.pdf). Functional images were processed by motion correction, grand-mean intensity normalization, high-pass temproal filtering, echo planar imaging unwarping, gradient distortion correction unwarping, and the removal of structural artefacts. Images were then co-registered to the corresponding high-resolution T1 anatomical images which were transformed into the MNI space. The resulting images were resampled to 3×3×3 mm^3 voxels, smoothed with a 4-mm-full-width, half-maximum Gaussian kernel. We discarded the first five functional time points to ensure signal equilibrium. Subsequently, temporal band-pass filtering (0.008-0.09 Hz) was performed (not for caculating the fractional amplitude of low-frequency fluctuations). Motion parameters (Friston 24 motor parameters)[6], average white matter and average cerebrospinal fluid signals were regressed out. We exclued the subjects with excessive head movement (frame-wise displacement > 3 mm and rotation > 2 °).

eFigure 1. The Number of Participants in Criteria Constellations

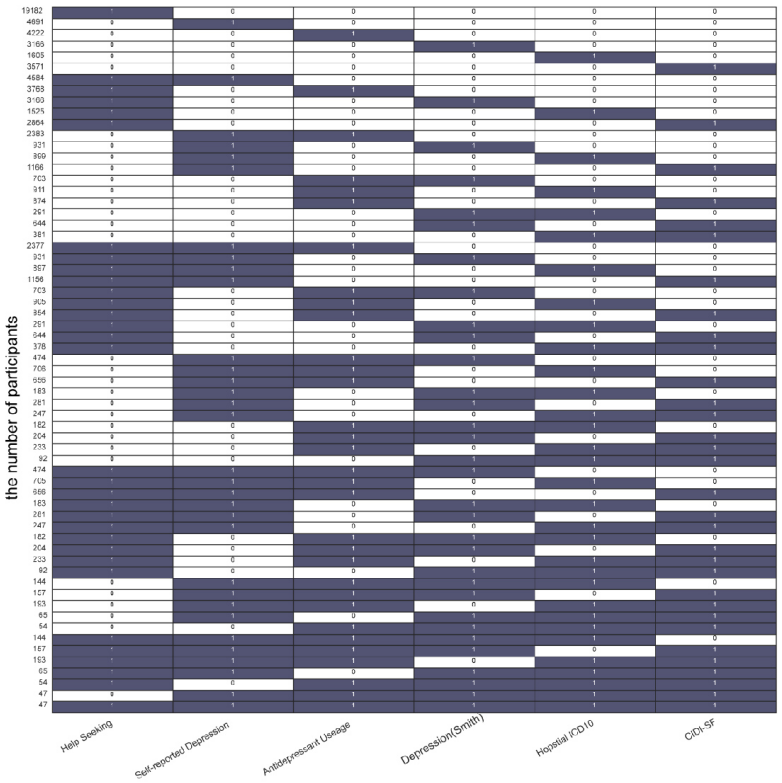

The first column indicates the number of participants in each cumulative constellation from meeting at least one criterion to meeting all six criteria. The tabular part indicates which criteria are involved. The dark element means that the current column contains corresponding criteria.

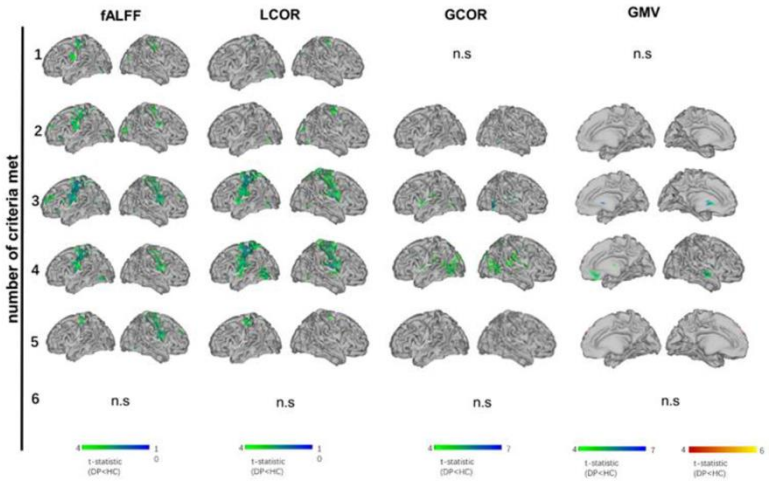

eFigure 2. The Cerebral Parts of the Clusters Showing Significant Functional or Structural Differences Between Different Depression Stratums and HC.

The n.s indicates no significant clusters. Abbreviations: fALFF: fractional amplitude of low-frequency fluctuations. GCOR: global correlation, LCOR: local correlation, GMV: gray matter volumes.

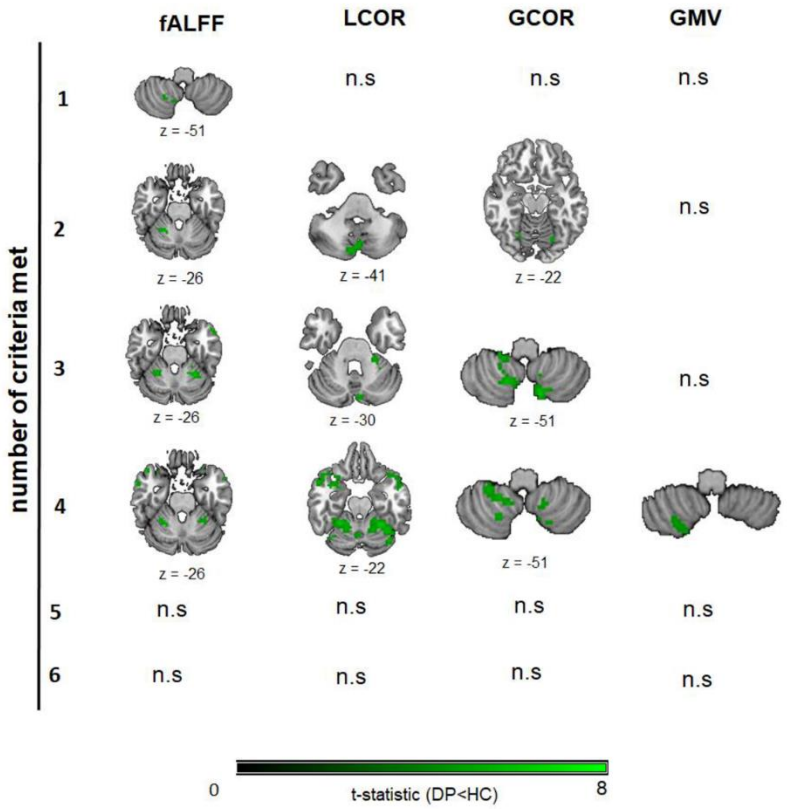

eFigure 3. The Cerebellum Parts of the Clusters Showing Significant Functional or Structural Differences Between Different Depression Stratums and HC

The n.s indicates the no significant difference in the cerebellum. Abbreviations: fALFF: fractional amplitude of low-frequency fluctuations. GCOR: global correlation, LCOR: local correlation, GMV: gray matter volumes.

eTable 1. Demographic of Six Depression Groups Involving Analyses

Modality	N criteria met	Gender (female/male)	Age (years)	Education (years)
Function	1	3936/2572	64.01±7.4	16.59±3.84
	2	1971/1121	63.07±7.36	16.83±3.7
	3	1054/530	62.74±7.46	16.78±3.7
	4	530/238	61.94±7.43	16.73±3.8
	5	174/70	61.31±7.76	17.44±3.23
	6	19/10	59.82±7.16	17.48±2.71
Structure	1	5183/3419	63.99±7.38	16.58±3.85
	2	2628/1482	63.09±7.34	16.78±3.73
	3	1377/681	62.64±7.38	16.82±3.69
	4	706/335	62.03±7.41	16.85±3.71
	5	219/88	61.49±7.69	17.33±3.32
	6	27/12	59.09±7.06	17.77±2.45

eTable 2. Demographic of the Single Healthy Groups (Strategy 1)

	Gender (female/male)	Age (years)	Education (years)
Initial HC group	11384/14078	65.05±7.8	16.69±3.77
Function	6606/7723	64.46±7.58	16.77±3.7
Structure	9263/11070	64.48±7.61	16.75±3.72

eTable 3. Demographic of Six Matched Healthy Groups (Strategy 2)

Modalities	Healthy controls			
	N criteria met	Gender (female/male)	Age (mean±std)	Years of Education (mean±std)
Function	1	3945/2573	63.76±7.39	16.8±3.69
	2	1976/1120	63.05±7.31	16.87±3.68
	3	1053/534	62.66±7.44	16.86±3.61
	4	529/236	61.93±7.44	16.98±3.56
	5	172/71	61.39±7.4	17.59±2.97
	6	19/10	59.85±7.2	17.52±2.43
Structure	1	5184/3418	63.89±7.41	16.68±3.79
	2	2630/1480	63.13±7.32	16.91±3.63
	3	1375/683	62.63±7.36	16.9±3.59
	4	707/334	62.06±7.38	16.9±3.64
	5	220/87	61.6±7.62	17.36±3.23
	6	28/11	59.49±6.81	17.9±2.19

eTable 4. Regions Showing Significant Differences in fALFF Between Individuals With Lifetime Depression and the Single HC Group (Strategy 1)

N criteria me	Contrast	Cluster size	Cluster p-value	Peak T statistic	Peak effect size	MNI coordinates	Anatomical region
1	DP<HC	43	p<.001	6.440	-0.109	[-51;27;-12]	left posterior orbital gyrus
		34	p<.001	6.407	-0.097	[-21;-84;45]	left superior temporal cortex
		31	p<.001	6.373	-0.097	[-63;-51;24]	left supraMarginal gyrus and middle temproal cortex
		49	p<.001	6.142	-0.103	[24;-48;-27]	right Lobule IV, V, VI of cerebellar hemisphere
2	DP<HC	55	p<.001	6.208	-0.134	[48;-69;-12]	right inferior temporal and occipital cortex
		156	p<.001	6.181	-0.139	[-33;48;33]	left middle and superior frontal cortex
		49	p<.001	6.027	-0.133	[21;-51;-27]	righ Lobule IV, V, VI of cerebellar hemisphere
		69	p<.001	5.969	-0.150	[-21;-57;-48]	left Lobule VIIB, VIII of cerebellar hemisphere
3	DP<HC	5545	p<.001	9.552	-0.250	[-42;-33;54]	bilateral medial and lateral pre- and postercentral gyrus
		271	p<.001	7.546	-0.220	[15;-60;-51]	bilateral loublue VIII and IX of cerebellar
		712	p<.001	7.494	-0.220	[-36;48;30]	left superiror medial frontal cortex
		318	p<.001	6.671	-0.205	[27;42;27]	right superior and medial frontal cortex
		156	p<.001	6.580	-0.222	[36;30;-12]	right inferior frontal gyrus
		63	p<.001	6.463	-0.198	[-21;-39;-24]	Left Lobule IV, V,VI of cerebellar hemisphere
		161	p<.001	6.362	-0.167	[-18;-102;15]	left middle and superiror occipital cortex
		90	p<.001	6.303	-0.191	[21;-51;-24]	right Lobule IV, V,VI of cerebellar hemisphere
		56	p<.001	6.168	-0.171	[48;-66;-12]	right inferior temporal gyrus
		92	p<.001	6.135	-0.191	[-57;-63;12]	left middle temporal gyrus
		47	p<.001	6.069	-0.174	[3;54;0]	right superior and medial frontal cortex

		29	p<.001	5.817	-0.149	[21;-96;24]	right occipital cortex
		25	p<.001	5.615	-0.162	[-21;-66;57]	left superior parietal cortex
4	DP<HC	4012	p<.001	9.061	-0.317	[-3;-9;51]	bilateral pre- and postcentral gyrus
		79	p<.001	7.045	-0.238	[-12;-99;24]	left superior and middle occipital cortex
		198	p<.001	6.419	-0.279	[-45;-66;-9]	left middle and inferior occipital cortex
		74	p<.001	6.411	-0.265	[24;-51;-21]	right Lobule IV, V,VI of cerebellar hemisphere
		60	p<.001	6.357	-0.239	[-9;66;24]	left superior frontal cortex
		57	p<.001	6.331	-0.276	[-6;-75;-45]	left Lobule VII, VIII of cerebellar hemisphere
		30	p<.001	6.327	-0.215	[12;-99;21]	right superior occipital cortex
		55	p<.001	6.216	-0.237	[39;57;15]	right superior and middle frontal cortex
		48	p<.001	6.162	-0.285	[-24;0;-12]	left amygdala and putamen and putamen
		36	p<.001	6.058	-0.250	[12;-69;-48]	right Lobule VIII of cerebellar hemisphere
		33	p<.001	6.006	-0.265	[24;3;-12]	right amygdala
		44	p<.001	5.821	-0.271	[36;21;-33]	right superior and middle temporal cortex
		38	p<.001	5.738	-0.245	[-18;-54;-18]	left Lobule IV, V of cerebellar hemisphere
		27	p<.001	5.568	-0.240	[-48;21;-15]	left posterior orbital gyrus and superior tempral pole cortex
		39	p<.001	5.511	-0.226	[45;-69;-9]	right fusiform
		28	p<.001	5.465	-0.243	[-57;9;-24]	left middle temporal cortex
5	DP<HC	312	p<.001	6.700	-0.410	[-42;-36;63]	left pre-and postcentral gyrus

eTable 5. Regions Showing Significant Differences in LCOR Between Individuals With Lifetime Depression and the Single HC Group (Strategy 1)

N criteria met	Contrast	Cluster size	Cluster p-value	Peak T statistic	Peak effect size	MNI coordinates	Anatomical region
1	DP<HC	230	p<.001	6.686	-0.088	[0,-18,72]	left paracentral loubel and support motor area
		299	p<.001	6.329	-0.086	[39,-18,66]	right pre- and postcentral gyrus
		258	p<.001	6.216	-0.087	[-48,-27,60]	left pre-and postcentral gyrus
		34	p<.001	6.032	-0.084	[-9,-102,18]	left superior occipital cortex
		112	p<.001	5.487	-0.085	[36,-84,27]	right middle occipital cortex
		41	p<.001	5.281	-0.083	[-51,-72,-9]	left inferior temporal cortex
2	DP<HC	1155	p<.001	6.990	-0.129	[30,-15,63]	right pre- and postcentral gyrus
		82	p<.001	6.232	-0.130	[3,-75,-42]	left Crus II, Lobule VIII of cerebellar hemisphere
		87	p<.001	6.036	-0.124	[48,-66,-15]	right inferior occipital and temporal cortex
		122	p<.001	5.996	-0.131	[12,-57,-51]	right Lobule VIII, IX, X of cerebellar hemisphere
		356	p<.001	5.991	-0.123	[-33,-21,63]	left pre-and postcentral gyrus
		154	p<.001	5.830	-0.121	[6,-96,18]	left middle and superior occipital cortex
		175	p<.001	5.826	-0.110	[30,-87,33]	right superior and middle occipital cortex
		86	p<.001	5.629	-0.119	[-54,-75,3]	left inferior occipital and temporal cortex
		27	p<.001	5.605	-0.110	[-48,33,30]	left triangular part of inferior frontal cortex
		30	p<.001	5.309	-0.102	[57,-12,36]	right pre-and postcentral gyrus
3	DP<HC	6979	p<.001	9.066	-0.228	[-45,-33,63]	bilateral pre- and postcentral gyrus
		594	p<.001	6.922	-0.203	[3,-72,-42]	bilateral Lobule VIII and IX of cerebellar heimsphere
		124	p<.001	6.619	-0.174	[-21,-48,-15]	left fusiform gyrus
		105	p<.001	5.984	-0.159	[48,-63,-12]	right inferior temporal and occipital cortex

		60	p<.001	5.507	-0.155	[63;-57;9]	right middle temporal cortex
		105	p<.001	5.479	-0.160	[-33;30;0]	left triangular part of inferior frontal gyrus
		87	p<.001	5.463	-0.156	[-48;-66;-6]	left inferior temporal and occipital cortex
		41	p<.001	5.230	-0.144	[-54;-60;12]	left middle temporal gyrus
		52	p<.001	5.163	-0.161	[15;-36;-3]	right fusiform gyrus and lingual cortex
4	DP<HC	7633	p<.001	9.593	-0.313	[-48;-27;60]	bilateral pre-and postcentral gyrus
		1212	p<.001	7.797	-0.300	[-48;-69;-6]	left middle and inferior temproal cortex and bilateral fusiform gyrus
		423	p<.001	6.627	-0.264	[-3;-75;-42]	bilateral Lobule VIIB, and VIII of cerebellar hemisphere
		37	p<.001	5.891	-0.217	[-42;33;39]	left middle frontal cortex
		61	p<.001	5.707	-0.205	[-18;-99;21]	left superior occipital cortex
		29	p<.001	5.656	-0.216	[-24;0;-9]	left putamen and amygdala
		36	p<.001	5.618	-0.211	[42;27;36]	right middle frontal cortex
		38	p<.001	5.591	-0.205	[-6;39;24]	left superior medial frontal cortex and anterior cingulate cortex
		47	p<.001	5.444	-0.208	[39;-69;-48]	right Crus II, Lobule VIIB, and VIII of cerebellar hemisphere
5	DP<HC	464	p<.001	6.892	-0.394	[-45;-27;63]	left pre-and postcentral gyrus
		48	p<.001	6.043	-0.392	[-48;-21;21]	left ralandic operculum and supramarginal cortex
		193	p<.001	5.770	-0.384	[-3;-18;51]	bilateral support motor area
		46	p<.001	5.691	-0.360	[-63;-6;12]	left postcentral gyrus and superior temporal cortex
		255	p<.001	5.664	-0.361	[39;-30;48]	right pre- and postcentral gyrus
		106	p<.001	5.655	-0.363	[-12;-33;78]	bilateral paracentral lobule; bilateral pre- and postcentral cortex
		59	p<.001	5.357	-0.361	[66;-12;27]	Right postcentral gyrus

eTable 6. Regions Showing Significant Differences in GCOR Between Individuals With Lifetime Depression and the Single HC Group (Strategy 1)

N criteria met	Contrast	Cluster size	Cluster p-value	Peak T statistic	Peak effect size	MNI coordinates	Anatomical region
2	DP<HC	28	p<.001	6.051	-0.113	[-54,-75,3]	left middle and inferior temporal cortex
		41	p<.001	5.850	-0.114	[57,-63,-3]	right middle and inferior temporal cortex
		33	p<.001	5.771	-0.111	[18,-54,-9]	right lingual and fusiform gyrus
		26	p<.001	5.457	-0.109	[-39,21,30]	left inferior frontal cortex
3	DP<HC	826	p<.001	7.483	-0.170	[-39,0,12]	left insula and superior temporal cortex
		2852	p<.001	7.071	-0.175	[-21,-45,-15]	left middle cingulate cortex, precuneus and lingual cortex
		669	p<.001	6.245	-0.162	[39,-3,15]	right insular and rolandic operculum
		192	p<.001	6.225	-0.182	[9,-69,-45]	bilateral Lobule VIII of cerebellar hemisphere
		43	p<.001	5.675	-0.150	[48,3,39]	right precentral cortex
		90	p<.001	5.408	-0.149	[-60,-18,42]	left inferior parietal superior cortex
		36	p<.001	5.283	-0.160	[39,6,-15]	right superior temporal cortex
		31	p<.001	5.225	-0.140	[-48,3,39]	left precentral cortex
4	DP<HC	7471	p<.001	7.684	-0.250	[9,-60,69]	bilateral precuneus, lingual cortex, fusiform, middle and superior temporal cortex
		148	p<.001	6.912	-0.231	[-36,3,33]	left precentral cortex
		191	p<.001	6.772	-0.249	[15,-66,-45]	bilateral Lobule VIII and left Lobule VIIB of cerebellar hemisphere

		32	p<.001	6.419	-0.236	[-24;0;-12]	left amygdala and putamen
		52	p<.001	6.238	-0.241	[27;-42;-48]	right Lobule VIII of cerebellar hemisphere
		165	p<.001	5.824	-0.224	[39;9;33]	right precentral cortex and inferior frontal cortex
		28	p<.001	5.355	-0.199	[-33;-42;42]	left inferior parietal cortex
		25	p<.001	5.121	-0.198	[-36;-3;54]	left precentral cortex
5	DP<HC	59	p<.001	5.825	-0.361	[-48;-33;24]	left supramarginal gyrus and superior temproal cortex

eTable 7. Regions Showing Significant Differences in GMV Between Individuals With Lifetime Depression and the Single HC Group (Strategy 1)

N criteria met	Contrast	Cluster size	Cluster p-value	Peak T statistic	Peak effect size	MNI coordinates	Anatomical region
2	DP>HC	56	p<.001	5.286	0.086	[12;-30;75]	right pre- and post-central gyrus
3	DP<HC	396	p<.001	6.855	-0.142	[3;4.5;3]	bilateral Olfactory cortex
	DP<HC	60	p<.001	5.038	-0.110	[18;-13.5;-10.5]	right hippocampus
4	DP<HC	1608	p<.001	6.285	-0.183	[0;33;-15]	bilateral medial frontal cortex
		218	p<.001	6.058	-0.185	[28.5;30;36]	right superior and medial frontal cortex
		1051	p<.001	5.761	-0.179	[58.5;-10.5;-9]	right superior and middle temporal cortex
		434	p<.001	5.568	-0.182	[-3;-16.5;49.5]	bilateral middle cingulate cortex
		147	p<.001	5.317	-0.162	[18;-16.5;-12]	right hippocampus
		70	p<.001	5.192	-0.160	[21;-45;-4.]	right lingual cortex and parahippocampus
		161	p<.001	5.129	-0.162	[-49.5;3;-3]	left superior temporal cortex
		391	p<.001	5.074	-0.176	[-49.5;3;-28.5]	left inferior and middle temporal cortex
		208	p<.001	5.036	-0.157	[0;-9;9]	bilateral media dorsal medial magnocellular
		113	p<.001	4.981	-0.163	[-45;-28.5;48]	left postcentral gyrus
		171	p<.001	4.921	-0.163	[1.5;37.5;25.5]	left anterior cingulate cortex
		84	p<.001	4.920	-0.158	[-58.5;-33;16.5]	left superior temporal
		112	p<.001	4.885	-0.160	[52.5; 3;0]	right insula and righ rolandic operculum
		215	p<.001	4.870	-0.153	[25.5;-63;-58.5]	right Lobule VIII of cerebellar hemisphere
		177	p<.001	4.856	-0.157	[43.5;-15;9]	right insula
		51	p<.001	4.714	-0.150	[30;12;-25.5]	right temporal pole: superior temporal gyrus
5	DP>HC	62	p<.001	4.670	0.259	[12;64.5;33]	right superior medial frontal cortex

eTable 8. Regions Showing Significant Differences in fALFF Between Individuals With Lifetime Depression and Matched HC Group (Strategy 2)

N criteria met	Contrast	Cluster size	Cluster p-value	Peak T statistic	MNI coordinates	Anatomical region
2	DP<HC	537	p<.001	6.61	[27,-78,-6]	right Fusiform gyrus, lingual gyrus, occipital pole
		196	p<.001	5.91	[-39,-81,-9]	left middle occipital cortex
		75	p<.001	5.72	[-6,-21,66]	left thalamus
		46	p<.001	5.65	[-30,-9,60]	left precentral gyrus
3	DP<HC	2759	p<.001	8.05	[0,-30,63]	bilateral medial and lateral primary sensorimotor regions
		90	p<.001	6.46	[18,-60,-51]	right Lobule VIII of cerebellar hemisphere
		121	p<.001	6.17	[-39,-24,21]	left parietal operculum cortex
		70	p<.001	6.04	[0,60,27]	superior medial frontal
		115	p<.001	5.96	[-27,60,21]	left superior frontal cortex
		32	p<.001	5.93	[-30,-51,-48]	left Lobule VIII of cerebellar hemisphere
		28	p<.001	5.79	[0,54,-9]	left medial frontal cortex
		34	p<.001	5.72	[-9,-72,-48]	left Lobule VIII of cerebellar hemisphere
		30	p<.001	5.57	[42,-69,-12]	right lateral occipital cortex
		30	p<.001	5.55	[-27,-87, 0]	left middle occipital cortex
4	DP<HC	137	p<.001	7.63	[0,-9,51]	bilateral support motor regions
		683	p<.001	7.19	[-54,-12,33]	left postcentral gyrus
		280	p<.001	6.74	[60,-9,33]	right postcentral gyrus

68	p<.001	6.13	[-3;-36;60]	left postcentral gyrus
32	p<.001	6.06	[12;54;39]	right superior medial frontal cortex
119	p<.001	5.92	[3;57;30]	right superior medial frontal cortex
46	p<.001	5.48	[-45;-69;-9]	left inferior occipital cortex

eTable 9. Regions Showing Significant Differences in LCOR Between Individuals With Lifetime Depression and Matched HC (Strategy 2)

N criteria met	Contrast	Cluster size	Cluster p-value	Peak T statistic	MNI coordinates	Anatomical region
2	DP<HC	79	p<.001	6.22	[27,-48,-51]	right inferior cerebellum
		38	p<.001	5.77	[15,-45,-51]	right Lobule IX of cerebellar hemisphere
		259	p<.001	5.65	[33,-84,-12]	right inferior occipital
		31	p<.001	5.24	[0,-93,12]	calcarine
		31	p<.001	5.16	[-42,-75,-9]	left inferior occipital
3	DP<HC	2734	p<.001	6.94	[-3,-30,60]	bilateral medial and superior sensorimotor regions
		190	p<.001	6.61	[-12,-72,-51]	left Lobule VIII of cerebellar hemisphere
		168	p<.001	6.12	[15,-60,-51]	right Lobule VIII of cerebellar hemisphere
		45	p<.001	6.12	[-42,-6,3]	left insula
		50	p<.001	5.90	[-12,-57,-48]	left Lobule IX of cerebellar hemisphere
		27	p<.001	5.76	[-42,-51,-21]	left fusiform
		99	p<.001	5.54	[-15,-48,-3]	left lingual and fusiform, parahippocampus
		27	p<.001	5.35	[-39,-75,-12]	left fusiform
4	DP<HC	623	p<.001	6.77	[-42,-24,63]	bilateral medial and lateral sensorimotor regions
		172	p<.001	6.09	[63,-15,30]	postcentral gyrus
		66	p<.001	5.58	[0,-6,48]	left middle cingulate cortex
		64	p<.001	5.57	[-15,-45,75]	left precuneus
		55	p<.001	5.56	[51,-24,60]	right precentral gyrus

		38	p<.001	5.53	[63,-9,-27]	right anterior middle temporal gyrus
		70	p<.001	5.52	[-51,-66,-6]	left inferior temporal cortex
5	DP<HC	92	p<.001	5.44	[-45,-21,63]	left postcentral gyrus

eTable 10. Regions Showing Significant Differences in GCOR Between Individuals With Lifetime Depression and Matched HC (Strategy 2)

N criteria met	Contrast	Cluster size	Cluster p-value	Peak T statistic	MNI coordinates	Anatomical region
3	DP<HC	42	p<.001	5.43	[-24,-42,-3]	left lingual cortex and parahippocampus

eTable 11. Regions Showing Significant Differences in GMV Between Individuals With Lifetime Depression and Matched HC (Strategy 2)

N criteria met	Contrast	Cluster size	Cluster *p*-value	Peak T statistic	MNI coordinates	Anatomical region
2	DP>HC	56	0.002	5.14	[14,-33,75]	Right postcentral gyrus
3	DP<HC	152	0.004	5.64	[3,4,3]	Subcallosal cortex
4	DP<HC	218	0.003	5.06	[-44,-15,44]	left precentral gyrus
		64	0.015	4.87	[0,-17,50]	left precentral gyrus
		62	0.015	4.69	[0,32,-17]	Medial frontal cortex
5	DP<HC	129	0.094	5.52	[41,-24,48]	right postcentral cortex

eReferences

1. Smith DJ, Nicholl BI, Cullen B, et al. Prevalence and characteristics of probable major depression and bipolar disorder within UK biobank: cross-sectional study of 172,751 participants. *PLoS One*. 2013;8(11):e75362. doi:10.1371/journal.pone.0075362
2. Davis KAS, Coleman JRI, Adams M, et al. Mental health in UK Biobank - development, implementation and results from an online questionnaire completed by 157 366 participants: a reanalysis. *BJPsych Open*. Feb 6 2020;6(2):e18. doi:10.1192/bjo.2019.100
3. American Psychiatric Association D, Association AP. *Diagnostic and statistical manual of mental disorders: DSM-5*. vol 5. American psychiatric association Washington, DC; 2013.
4. Alfaro-Almagro F, Jenkinson M, Bangerter NK, et al. Image processing and Quality Control for the first 10,000 brain imaging datasets from UK Biobank. *Neuroimage*. Feb 1 2018;166:400-424. doi:10.1016/j.neuroimage.2017.10.034
5. Ashburner J, Friston KJ. Diffeomorphic registration using geodesic shooting and Gauss-Newton optimisation. *Neuroimage*. Apr 1 2011;55(3):954-67. doi:10.1016/j.neuroimage.2010.12.049
6. Friston KJ, Williams S, Howard R, Frackowiak RS, Turner R. Movement-related effects in fMRI time-series. *Magn Reson Med*. Mar 1996;35(3):346-55. doi:10.1002/mrm.1910350312

5 Diskussion

In den vorliegenden Studien wurde die Funktionsweise des typischen und pathologischen erwachsenen menschlichen Gehirns untersucht, wobei der Schwerpunkt auf den Effekten des typischen Alterungsprozesses, von Morbus Huntington, Morbus Parkinson und Depressionserfahrungen lag. Metriken lokaler spontaner neuronaler Aktivität und Synchronizität wurden aus rs-fMRI-Daten abgeleitet und mit klinischen sowie verhaltensbezogenen Daten kombiniert. Dies ermöglichte eine detaillierte Abbildung der Topographie funktioneller Veränderungen und lieferte Hinweise auf zugrundeliegende biologische Mechanismen und potentielle Biomarker.

In den ersten beiden Studien wurde Evidenz für die Vulnerabilität von Zellen mit spezifischen neurochemischen, insbesondere monoaminergen, Eigenschaften gegenüber typischen altersbedingten Veränderungen sowie den Auswirkungen von Morbus Huntington und Morbus Parkinson auf das Gehirn gefunden. In Morbus Huntington waren lokale funktionelle Veränderungen am stärksten mit der Verfügbarkeit der dopaminergen Rezeptoren D_1 und D_2, sowie den Transportern von Dopamin und Serotonin assoziiert. Die Assoziationsstärke der funktionellen Veränderung in HD und D_1 sowie dem Serotonintransporter korrelierte zudem mit der Krankheitsschwere und die Ausprägung der Synchronizität im dopaminreichen Nucleus caudatus hing mit der Schwere der motorischen Symptomatik zusammen. Altersbedingte funktionelle Hirnveränderungen waren mit der Verfügbarkeit von dopaminergen und serotonergen Rezeptoren, aber auch mit GABAergen, glutamatergen Rezeptoren und dem Noradrenalintransporter assoziiert. Bei Morbus Parkinson wurden Abweichungen von der Norm in den Assoziationsstärken einer Reihe unterschiedlicher Neurotransmittersysteme identifiziert, darunter monoaminerge, cholinerge, glutamaterge und GABAerge Systeme. Das Abweichungslevel in PD bezüglich des $GABA_A$-Rezeptors korrelierte mit der Krankheitsdauer. Die Stärke dieser Assoziationen oder Abweichungen von der Norm in den verschiedenen Neurotransmittersystemen könnte darüber hinaus auf die unterschiedliche Relevanz dieser Systeme in den untersuchten Erkrankungs- und Alterungsprozessen hinweisen. Die Korrelationen dieser Assoziationsstärken bzw. Abweichungen von der Norm mit der Krankheitsschwere und -dauer deuten auf potentielle Biomarker der Krankheitsschwere hin. Die Ergebnisse können Impulse für die Entwicklung effektivere Medikamentenzusammensetzungen geben und bestätigen die Wirksamkeit bestehender Pharmazeutika, wie beispielsweise L-Dopa gegen Bewegungssymptomatiken oder selektive Serotonin-Wiederaufnahmehemmer gegen depressive Verstimmungen. Zur weiteren Bestätigung der Wirksamkeit dieser und zukünftiger Medikamente auf Ebene der Hirnfunktion sind jedoch zusätzliche Studien mit direktem Kohortenvergleich notwendig, wie beispielsweise bei Dukart et al. (23) und Zhang et al. (164) durchgeführt.

Die dritte Studie nutzte individuelle funktionelle und strukturelle Hirnkarten, die teilweise im Rahmen der zweiten Studie entstanden. Ziel war es, Abweichungen in Gruppen mit unterschiedlichen Depressionskriterien zu Probanden ohne Depressionserfahrungen abzubilden und die Relevanz dieser Kriterien für depressionsbezogene Hirnveränderungen zu bewerten. Es konnte gezeigt werden, dass die gegenwärtige oder frühere Einnahme von Antidepressiva und die Diagnose von depressiven Episoden im Lebenslauf der Probanden (unter den untersuchten Kriterien) am stärksten zu Hirnfunktionsveränderungen beitrugen, was auf einen potentiell persistierenden Effekt von Depressionserfahrungen im Alltag auf die Hirnfunktion hindeutet. Aus den Unterschieden in den Effekten von Definitionskriterien auf funktionelle und strukturelle Abweichungen ergeben sich wichtige Implikationen für Forschung und Klinik: Alle relevanten Kriterien zur Definition einer Depressionskohorte sollten sorgfältig während des Studiendesigns ausgewählt werden. Unterschiedliche Effekte verschiedener Symptome auf Hirnfunktion und -struktur können auch Hinweise auf differenzierte Subtypen, Differentialdiagnosen (wie nicht diagnostizierte bipolare Tendenzen) oder (latente) Komorbiditäten liefern, die in der großen Kohorte von Probanden mit Depressionserfahrungen subsumiert wurden.

Die im Rahmen dieses Dissertationsvorhabens durchgeführten Studien haben ihre Ziele erreicht und unser Verständnis darüber erweitert, wie sich das erwachsene menschliche Gehirn im typischen und pathologischen Alterungsprozess sowie bei Depression verändern kann. Multimodale Assoziationen lieferten zudem Hinweise auf die neurochemischen Ausprägungen der in den Gehirnveränderungen involvierten Neurone. Damit konnte ein wichtiger Betrag zum übergeordneten Ziel geleistet werden, Erkenntnisse über die Ursachen und Mechanismen der physiologischen Vorgänge zu gewinnen, um letztlich präzisere Diagnostik und Prognostik im klinischen Alltag zu ermöglichen und potentiell den Weg zu krankheitsmodifizierenden Therapien zu ebnen. In den folgenden Abschnitten wird die Bedeutung der verwendeten Methodik in der heutigen wissenschaftlichen Praxis diskutiert. Außerdem werden die fachlichen und datenbezogene Limitationen der durchgeführten Studien sowie mögliche Ansätze zur Bewältigung dieser Herausforderungen zur weiteren Annäherung an das übergeordnete Ziel dargestellt.

5.1 Bedeutung der Metriken und Methodik in der Forschung

Auch wenn die Interpretation der hier verwendeten lokalen Metriken der Hirnfunktion in Bezug auf die zugrunde liegenden biologischen Entitäten noch nicht vollständig geklärt ist (38), ermöglichen sie dennoch wertvolle Einblicke in die funktionelle Organisation des menschlichen Gehirns mittels nicht-invasiver Methodik. Mit ihrer Hilfe konnten in früheren Studien Netzwerke und topologische Muster diverser kognitiver Funktionen (wie z. B. Konzentration oder Gedächtnis) untersucht werden (165). Abweichungen von typischen Mustern lieferten Erklärungsansätze für Pathomechanismen und

potentielle diagnostische oder prognostische Biomarker für neurologische (166–168) und psychiatrische (169–171) Erkrankungen. Damit trugen funktionelle Maße, wie solche abgeleitet aus rs-fMRI-Daten, enorm zum Verständnis der biologischen Mechanismen des typischen und erkrankten menschlichen Gehirns bei.

Die multimodalen Assoziationen von funktionellen oder strukturellen und neurochemischen Bildgebungsdaten des Gehirns stellen eine vielversprechende Methode dar, die Rolle von Neurotransmitterausprägungen auf die Zellvulnerabilität bei Krankheiten und im Alterungsprozess zu untersuchen. Zuletzt wurde mithilfe dieses Ansatzes im Umfeld der bildgebenden Neurowissenschaften ein wesentlicher Beitrag zur neurophysiologischen Grundlagenforschung geleistet. So wurden beispielsweise der Zusammenhang von Progesteron auf die funktionelle Reorganisation des mütterlichen Gehirns postpartum (172), die Relevanz von Neurotransmittersystemen auf strukturelle und funktionelle Organisation des Neokortex (24), Alterseffekte im Zusammenhang von Neurotransmission auf die Kortexdicke (173), oder der Einfluss von Neurotransmitterausprägung auf die Hirnfunktionsveränderungen in neurodegenerativen Erkrankungen untersucht (23, 174). Durch die Analyse der räumlichen Korrelation zwischen rs-fMRI-Metriken und Verteilungskarten verschiedener Neurotransmittersysteme konnten wir nachweisen, dass lokale Hirnfunktionsmetriken Informationen über die zu Grunde liegende Neurotransmission enthalten. Weiterhin konnten wir zeigen, dass diese Metriken auch neurophysiologische Informationen zu den untersuchten NDs liefern und potentielle Biomarker für den Krankheitsverlauf darstellen.

5.2 Open Science

Die Ziele der hier dargestellten Studien konnten mit Hilfe von in der wissenschaftlichen Gemeinschaft geteilten Neurobildgebungsdaten erreicht werden. Unsere Studien zeigen, dass die Verbreitung von Datensätzen, deren Generierung kostspielig (finanziell und zeitlich) und mitunter auch invasiv ist, den wissenschaftlichen Fortschritt enorm beschleunigen und die Anzahl individueller Belastungen von Erkrankten und Personen höheren Alters minimieren können. Außergewöhnliche Institutionen wie Biobanken, welche Daten mehrerer Tausend Probanden enthalten, sowie die methodische Weiterentwicklung von Modellierungstechniken, ermöglichen erst die Generierung komplexer normativer Modelle von Hirnfunktion oder abgeleiteter Metriken. Der Wert dieser normativen Modelle zeigte sich hier insbesondere durch die Erweiterung der Spanne an potentiell besonders für funktionelle Veränderungen vulnerablen Neurotransmittersystemen im Alterungsprozess und PD: Diese Spanne schränkt die Wahl der direkt zu untersuchenden Neurotransmittersysteme in zukünftigen Fall-Kontroll-Studien unter der Vielzahl an Möglichkeiten stark ein. Wie zuvor erwähnt existieren neben den hier untersuchten Systemen hunderte weitere

Neurotransmittersysteme. Durch die zukünftige Entwicklung und Bereitstellung weiterer Verteilungskarten könnte aus den verschiedenen Assoziationsstärken ein Kanon der für eine gewisse Kondition relevanten Neurotransmittersysteme erstellt werden. Dieser Kanon könnte die Rolle der darin enthaltenen Rezeptoren und Transporter für die typische oder atypische funktionelle Organisation des menschlichen Gehirns abbilden (im Rahmen der im Abschnitt 5.3.2 diskutierten Limitationen) und einen fundamentalen Beitrag zur Grundlagenforschung leisten. Mithilfe der nicht-invasiven MRT könnten individuelle Abweichungen in den Assoziationsstärken erfasst werden, die Hinweise auf Erkrankungen liefern, womit letztlich ein Einzug dieses Ansatzes in den klinischen Alltag denkbar wäre.

5.3 Fachliche Limitationen

Diese Kategorie umfasst Limitationen, die sich auf die inhaltliche und fachliche Ebene der Untersuchungen beziehen.

5.3.1 Interpretation von räumlichen Korrelationen

Hinweise auf eine besondere Vulnerabilität von Zellen mit gewisser Neurotransmitterausprägung auf funktionelle Veränderungen im Alter und in Krankheit wurden in unseren Studien auf Grundlage von räumlichen Korrelationen (oder deren Veränderungen) gefunden. Wie gezeigt sind solche Korrelationsanalysen im weiten Umfeld der Neurobildgebung etabliert, die Korrelationsstärke und ihre Veränderung allein lassen jedoch keine Schlussfolgerungen auf die Art funktioneller Veränderung (erhöht oder verringert) in Regionen mit hoher oder geringer Neurotransmitterausprägung zu, da sie nur die Güte eines (linearen) Zusammenhang darstellen. Erkenntnisse darüber hinaus bedürfen detaillierterer Folgeanalysen, die die Ursache für die gefundenen räumlichen Zusammenhänge beschreiben. Dazu könnte zusätzlich zur Korrelationsrichtung (positiv oder negativ) auch die regionale Verteilung der Funktionsveränderung betrachtet werden, d. h. ob es sowohl Regionen mit erhöhter und verringerter Funktion im Vergleich zur Norm gab, oder die Funktion in allen Regionen nur verringert oder nur erhöht war.

Hinweise auf vulnerable Zelltypen können die Erprobung neuerer diagnostischer Verfahren oder Therapieansätze motivieren, da sie potentielle Ziele vorschlagen. Für die Gewissheit, dass Zellen gewisser Neurotransmitterausprägung jedoch tatsächlich ursächlich sind für die gefundenen funktionellen Veränderungen, müssen weiterführende Studien Hinweise für einen potentiellen kausalen Zusammenhang finden. Dazu eignen sich verschiedene Methoden der kausalen Inferenz, darunter beispielsweise die von Bradford Hill postulierten und in der Neurowissenschaft und Medizin etablierten (175, 176) Kriterien zur Stärkung einer vermuteten Ursache-Wirkungs-Beziehung (177). Für einen kausalen Zusammenhang spricht dabei (wie teilweise in den hier dargestellten Studien gefunden), dass die gefundenen Assoziationen stark sind, unter verschiedenen

Bedingungen reproduziert wurden und analoge Ansätze zu gleichen Schlüssen führen (z. B. die Wirksamkeit von Levodopa gegen motorische Störungen in PD und die in PD gefundenen Hinweise auf eine funktionelle Beeinträchtigung des dopaminergen Systems). Wesentliche, jedoch noch fehlende Hinweise auf einen kausalen Zusammenhang sind die zeitliche Abfolge der Ursache-Wirkungs-Beziehung, die Spezifizität und die Skalierbarkeit („biologischer Gradient“). Evidenz für die zeitliche Abfolge, Skalierbarkeit und Spezifität könnten beispielsweise in pharmakologischen Studien mit Bildgebung gefunden werden, die den Effekt zweier unterschiedlich dosierter, spezifische NT-Systeme beeinflussender Pharmazeutika auf die Hirnfunktion untersuchen (178, 179).

5.3.2 Messung neurochemischer Eigenschaften mittels PET/SPECT

Als Information für die typische Verteilung von Rezeptoren und Transportern im menschlichen Gehirn wurden Karten verwendet, die in PET- und SPECT-Studien an unterschiedlich großen Stichproben mit verschiedenen Geschlechter- und Altersverteilungen abgeleitet wurden. Da die Rezeptorverteilung (neben inter-individuellen Unterschieden) mit dem Alter (180) und zwischen den biologischen Geschlechtern (181) variiert, sind die verwendeten Neurotransmitterkarten nur als Näherung für die tatsächliche individuelle Verteilung zu verstehen.

Kombinierte PET/fMRT-Scanner könnten in zukünftigen Studien diese Näherung überwinden, indem sie die individuelle Beteiligung eines Neurotransmittersystems an der zeitgleich gemessenen Hirnfunktion bestimmen (182, 183). Neben Invasivität durch Strahlenexposition wäre es hiermit jedoch nur möglich, pro Messdurchlauf die Rolle eines einzelnen Rezeptors/Transporters an der individuellen Hirnfunktion zu messen. Untersuchungen an großen Stichproben und verschiedenen Neurotransmittersystemen wären zudem mit hohen Kosten verbunden. Der hier verwendete Ansatz umgeht diese Exposition zu Kosten der interindividuellen Variabilität.

5.4 Datenspezifische Limitationen

Diese Kategorie umfasst Limitationen, die sich auf die Datenherkunft und -eigenschaften beziehen.

5.4.1 Limitierte Generalisierbarkeit der Studienergebnisse

Die Daten der ersten Studie wurden in zwei unabhängigen Bildgebungszentren in Deutschland erhoben. Für die Robustheit der Ergebnisse spricht, dass die räumlichen Korrelationen von Neurotransmitterkarten mit Hirnfunktionsmaßen in der ersten und zweiten Kohorte trotz unterschiedlicher Hardware, Parameter der Bildgebung und durchführenden Personen stark übereinstimmen. Die im Vergleich zu den beiden anderen durchgeführten Studien geringe Stichprobengröße unterband jedoch eine Unterteilung der an HD erkrankten Personen in

Untergruppen verschiedener Krankheitsausprägung. Dadurch war es uns nur möglich, den Effekt des Krankheitsverlaufs auf die Hirnfunktion und auf die räumliche Korrelation zwischen veränderter Hirnfunktion und Neurotransmitterkarten anhand zweier HD-Kohorten, deren Krankheitsstadien sich statistisch leicht voneinander unterschieden, grob zu quantifizieren.

Der verwendete funktionelle Datensatz der 2. und 3. Studie wurde in 4 Bildgebungszentren in England (Newcastle upon Tyne, Stockport, Reading und Bristol) erhoben. Dies brachte den Vorteil der enormen Stichprobengröße und die Möglichkeit, Teilstichproben mit spezifischen Eigenschaften zu analysieren. Dennoch ist die Interpretation der Ergebnisse nicht auf eine größere Population (z. B. jenseits von England) generalisierbar. Unter Zuhilfenahme weiterer nationaler Biobanken (beispielsweise der NAKO in Deutschland, www.nako.de) können zukünftige Studien regionale Unterschiede und regional unabhängige (generelle) Eigenschaften der Krankheits- oder Alterungseffekte identifizieren und quantifizieren, die bei der Entwicklung präziserer Therapien unterstützen könnten.

Zwar ist die UK-Biobank eine groß angelegte biomedizinische Datenbank, dennoch ist die Anzahl an Probanden mit diagnostizierten neurodegenerativen Erkrankungen gering und es fehlt an klinisch relevanten Messwerten, die über Selbstberichte und kognitive Bewertungen hinausgehen (184). Nichtsdestotrotz ist der bisherige Datenstand bereits von hohem Wert für jetzige und zukünftige Grundlagenforschung zu neurodegenerativen Erkrankungen. Hinsichtlich der Prävalenz von ND sollten sich innerhalb der untersuchten Kontrollkohorte (25000 Probanden im Alter zwischen 40 und 80 Jahren) im Nachhinein Teilgruppen definieren lassen, deren Mitglieder sich momentan im Vorstadium einer ND befinden und potentiell erste Anzeichen einer prodromalen Krankheitsphase aufweisen (185).

5.4.2 Krankheitsbilder und Abstufungen

Eine weitere Limitation ergibt sich aus den Kriterien, die die Probanden der untersuchten Kohorten definierten. Aufgrund der begrenzten Stichprobengröße der ND-Kohorten der ersten beiden Studien konnten keine Sub-Kohorten hinsichtlich der Geschlechter oder des Alters separat untersucht werden. Um eine geschlechtergetrennte und altersaufgelöste Betrachtung der untersuchten ND vorzunehmen, bedarf es entweder teurer Fall-Kontroll-Studien mit sehr großen Stichproben, oder der Kombination von Bildgebungsdaten, die in verschiedenen Studien gesammelt wurden. Aufgrund der Differenzen in Neurobildgebungsdaten, die auf unterschiedliche Akquisitionsorte zurückzuführen sind, müssten bei MRT-Studien die Daten zunächst um diese Effekte bereinigt werden, um größere Stichproben von Probanden einer spezifischen Krankheitsausprägung zu definieren. Die Quellen dieser Effekte sind vielseitig und gibt es heute noch keinen etablierten Standard zur Korrektur des

Akquisitionsorteffekts, jedoch existieren internationale Kollaborationsbemühungen zur Entwicklung von statistischen Methoden unter Verwendung von maschinellem Lernen (186).

5.4.3 Small & Big Data

Während in der ersten dargestellten Studie Krankheitseffekte in HD auf Grundlage eines Fall-Kontroll-Ansatzes mit Daten von unter 100 Probanden untersucht wurden, nutzten wir in der zweiten und dritten Studie einen großen Datensatz der UK-Biobank mit Daten von über 20000 Probanden. Vorteile des Fall-Kontroll-Ansatzes in kleineren Stichproben liegen im effizienteren Ressourceneinsatz der Datengenerierung sowie in der genaueren klinischen Charakterisierung und Diagnostik. Dieser Ansatz bietet sich in der Regel an, um neue Fragestellungen zu untersuchen, indem die gewünschten Variablen bei der Messung miterhoben werden. Zudem können Replikationsdatensätze, die anderswo und mit anderen Probanden erhoben wurden, anschließend dazu verwendet werden, die initial gefundenen Ergebnisse auf Robustheit und Verallgemeinerungspotential zu untersuchen. Dank der uns zur Verfügung gestellten Daten aus zwei verschiedenen Akquisitionsorten war es uns einerseits möglich, die in der Observationskohorte gefundenen Ergebnisse in der Replikationskohorte zu validieren und andererseits, dank der erhobenen klinischen Parameter, potentielle Biomarker des Krankheitsstadiums zu identifizieren.

Große Datenmengen dienen eher holistischeren Untersuchungen, deren Ergebnisse zu spezifischeren Fragestellungen führen können, die anschließend in Fall-Kontroll-Studien analysiert werden. Der auf der Hand liegende Vorteil großer Stichproben liegt darin, auch Effekte geringerer Stärke oder hoher Varianz identifiziert zu können, welche in Studien kleinerer Stichprobengröße potentiell unentdeckt geblieben wären. Groß angelegte Studien bergen weiterhin das Potential, die den Daten zu Grunde liegende Population am ehesten abzubilden und so repräsentativere normative Modelle zu ermöglichen. Dieser Vorteil steht der Nachteil des Einflusses niederqualitativer Daten gegenüber, welche nicht durch Vorkehrungen zur Sicherung der Datenqualität zur Gänze berücksichtigt werden könnten und letztlich latenten Faktoren zu Grunde liegen.

Sowohl in klinischen Fall-Kontroll-Studien mit kleiner Stichprobengröße als auch in explorativen Studien mit großer Stichprobe existiert die Gefahr einer Verzerrung der Ergebnisse aufgrund von Selektionseffekten, die das Verallgemeinerungspotential der gefundenen Ergebnisse einschränken. Kleinere Stichproben sind anfällig für das Risiko, dass tatsächlich vorhandene, jedoch schwache Effekte im Kohortenvergleich als nicht signifikant erscheinen und somit möglicherweise nicht detektiert werden. Dies steht im Zusammenhang mit Rekrutierungs- und Selektionseffekten in klinischen Fall-Kontroll-Studien (187). Es besteht die Möglichkeit des Beobachter-Erwartungseffekts, bei dem eher Probanden in die Studie eingeschlossen werden, die bereits die erwarteten Merkmale aufweisen, um die Effektstärke zu maximieren (188). Weiterhin neigen

weibliche Personen, Personen mit höherem sozioökonomischen Status, höherem Bildungsniveau und einer derzeitigen Beschäftigung eher zu Studienteilnahmen (189) und Personen mit höherem sozioökonomischen Status und geringerem Alkohol- und Tabakkonsum sind im UK-Biobank-Datensatz höher repräsentiert als in der tatsächlichen Population (184). Um Effekte dieser Abweichungen zur Population zu minimieren, könnten die Effekte dieser Charakteristika aus den gemessenen Daten ermittelt und mittels Regressionsanalyse aus diesen näherungsweise entfernt werden. Alternativ könnte, im Falle einer genügend großen Kontrollkohorte, eine Subkohorte definiert werden, deren Charakteristika mit denen der Population übereinstimmen, die sie repräsentieren soll.

5.5 Fazit

Die Ergebnisse der im Rahmen dieses Promotionsvorhabens durchgeführten Studien erweiterten unser Gesamtbild von alters- und krankheitsbedingten Veränderungen des menschlichen Gehirns. Unter Verwendung neuester statistischer Methoden und großen, öffentlichen Datensätzen konnten wir sowohl die Veränderungen der Hirnfunktion selbst, als auch Hinweise für den Einfluss diverser neurochemischer Eigenschaften auf die Veränderung der Hirnfunktion in einer bisher noch nicht vorhandenen Detailtiefe abbilden. Dieses erweiterte Gesamtbild kann eine Hilfestellung für zukünftige Studien sein, um ein tieferes Verständnis der (Patho-)Mechanismen von Erkrankung und typischem Altern zu erhalten, diagnostische oder prognostische Biomarker zu entwickeln und neue Therapieansätze zu etablieren.

6 Literatur- und Quellenverzeichnis

1. Chang CK, Hayes RD, Perera G, Broadbent MTM, Fernandes AC, Lee WE, u. a. Life Expectancy at Birth for People with Serious Mental Illness and Other Major Disorders from a Secondary Mental Health Care Case Register in London. Scott JG, Herausgeber. PLoS ONE. 18. Mai 2011;6(5):e19590.

2. Berghöfer A, Martin L, Hense S, Weinmann S, Roll S. Quality of life in patients with severe mental illness: a cross-sectional survey in an integrated outpatient health care model. Qual Life Res. August 2020;29(8):2073–87.

3. Liang CS, Li DJ, Yang FC, Tseng PT, Carvalho AF, Stubbs B, u. a. Mortality rates in Alzheimer's disease and non-Alzheimer's dementias: a systematic review and meta-analysis. The Lancet Healthy Longevity. August 2021;2(8):e479–88.

4. Batista P, Pereira A. Quality of Life in Patients with Neurodegenerative Diseases. J Neurol Neurosci [Internet]. 2016 [zitiert 2. Juni 2024];7(1). Verfügbar unter: http://www.jneuro.com/neurology-neuroscience/quality-of-life-in-patients-with-neurodegenerative-diseases.php?aid=8682

5. Kern RZ, Brown AD. Disease adaptation may have decreased quality-of-life responsiveness in patients with chronic progressive neurological disorders. Journal of Clinical Epidemiology. Oktober 2004;57(10):1033–9.

6. Lucas-Carrasco R, Pascual-Sedano B, Galán I, Kulisevsky J, Sastre-Garriga J, Gómez-Benito J. Using the WHOQOL-DIS to Measure Quality of Life in Persons with Physical Disabilities Caused by Neurodegenerative Disorders. Neurodegener Dis. 2011;8(4):178–86.

7. Hou Y, Dan X, Babbar M, Wei Y, Hasselbalch SG, Croteau DL, u. a. Ageing as a risk factor for neurodegenerative disease. Nat Rev Neurol. Oktober 2019;15(10):565–81.

8. Van Schependom J, D'haeseleer M. Advances in Neurodegenerative Diseases. JCM. 21. Februar 2023;12(5):1709.

9. Gustavsson A, Norton N, Fast T, Frölich L, Georges J, Holzapfel D, u. a. Global estimates on the number of persons across the Alzheimer's disease continuum. Alzheimer's & Dementia. Februar 2023;19(2):658–70.

10. Maserejian N, Vinikoor-Imler L, Dilley A. Estimation of the 2020 Global Population of Parkinson's Disease (PD) [Internet]. Meeting: MDS Virtual Congress 2020: Movement Disorder Society; 2020 [zitiert 13. Dezember 2023] S. 35 (suppl 1). Verfügbar unter: https://www.mdsabstracts.org/abstract/estimation-of-the-2020-global-population-of-parkinsons-disease-pd/

11. Roth GA, Abate D, Abate KH, Abay SM, Abbafati C, Abbasi N, u. a. Global, regional, and national age-sex-specific mortality for 282 causes of death in 195 countries and territories, 1980–2017: a systematic analysis for the Global Burden of Disease Study 2017. The Lancet. November 2018;392(10159):1736–88.

12. Gouda NA, Elkamhawy A, Cho J. Emerging Therapeutic Strategies for Parkinson's Disease and Future Prospects: A 2021 Update. Biomedicines. 3. Februar 2022;10(2):371.

13. Wilson DM, Cookson MR, Van Den Bosch L, Zetterberg H, Holtzman DM, Dewachter I. Hallmarks of neurodegenerative diseases. Cell. Februar 2023;186(4):693–714.

14. Gan L, Cookson MR, Petrucelli L, La Spada AR. Converging pathways in neurodegeneration, from genetics to mechanisms. Nat Neurosci. Oktober 2018;21(10):1300–9.

15. Brettschneider J, Tredici KD, Lee VMY, Trojanowski JQ. Spreading of pathology in neurodegenerative diseases: a focus on human studies. Nat Rev Neurosci. Februar 2015;16(2):109–20.

16. Müller HP, Kassubek J. Diffusion Tensor Magnetic Resonance Imaging in the Analysis of Neurodegenerative Diseases. JoVE. 28. Juli 2013;(77):50427.

17. Nasseroleslami B, Dukic S, Broderick M, Mohr K, Schuster C, Gavin B, u. a. Characteristic Increases in EEG Connectivity Correlate With Changes of Structural MRI in Amyotrophic Lateral Sclerosis. Cerebral Cortex. 1. Januar 2019;29(1):27–41.

18. Roisin McMackin, Muthuraman Muthuraman, Sergiu Groppa, Claudio Babiloni, John-Paul Taylor, Matthew C Kiernan, u. a. Measuring network disruption in neurodegenerative diseases: New approaches using signal analysis. J Neurol Neurosurg Psychiatry. 1. September 2019;90(9):1011.

19. Montalà-Flaquer M, Cañete-Massé C, Vaqué-Alcázar L, Bartrés-Faz D, Peró-Cebollero M, Guàrdia-Olmos J. Spontaneous brain activity in healthy aging: An overview through fluctuations and regional homogeneity. Front Aging Neurosci. 12. Januar 2023;14:1002811.

20. Kubska ZR, Kamiński J. How Human Single-Neuron Recordings Can Help Us Understand Cognition: Insights from Memory Studies. Brain Sciences. 30. März 2021;11(4):443.

21. Sudlow C, Gallacher J, Allen N, Beral V, Burton P, Danesh J, u. a. UK Biobank: An Open Access Resource for Identifying the Causes of a Wide Range of Complex Diseases of Middle and Old Age. PLoS Med. 31. März 2015;12(3):e1001779.

22. Bamberg F, Kauczor HU, Weckbach S, Schlett CL, Forsting M, Ladd SC, u. a. Whole-Body MR Imaging in the German National Cohort: Rationale, Design, and Technical Background. Radiology. Oktober 2015;277(1):206–20.

23. Dukart J, Holiga S, Rullmann M, Lanzenberger R, Hawkins PCT, Mehta MA, u. a. JuSpace: A tool for spatial correlation analyses of magnetic resonance imaging data with nuclear imaging derived neurotransmitter maps. Hum Brain Mapp. 15. Februar 2021;42(3):555–66.

24. Hansen JY, Shafiei G, Markello RD, Smart K, Cox SML, Nørgaard M, u. a. Mapping neurotransmitter systems to the structural and functional organization of the human neocortex. Nat Neurosci. November 2022;25(11):1569–81.

25. Matsumoto J, Fukunaga M, Miura K, Nemoto K, Okada N, Hashimoto N, u. a. Cerebral cortical structural alteration patterns across four major psychiatric disorders in 5549 individuals. Mol Psychiatry [Internet]. 18. August 2023 [zitiert 13. Juli 2024]; Verfügbar unter: https://www.nature.com/articles/s41380-023-02224-7

26. Zhan X, Yu R. A Window into the Brain: Advances in Psychiatric fMRI. BioMed Research International. 2015;2015:1–12.

27. Miranda L, Paul R, Pütz B, Koutsouleris N, Müller-Myhsok B. Systematic Review of Functional MRI Applications for Psychiatric Disease Subtyping. Front Psychiatry. 22. Oktober 2021;12:665536.

28. Malhi GS, Mann JJ. Depression. The Lancet. November 2018;392(10161):2299–312.

29. Müller VI, Cieslik EC, Serbanescu I, Laird AR, Fox PT, Eickhoff SB. Altered Brain Activity in Unipolar Depression Revisited: Meta-analyses of Neuroimaging Studies. JAMA Psychiatry. 1. Januar 2017;74(1):47.

30. Biswal B, Zerrin Yetkin F, Haughton VM, Hyde JS. Functional connectivity in the motor cortex of resting human brain using echo-planar mri. Magnetic Resonance in Med. Oktober 1995;34(4):537–41.

31. Damoiseaux JS, Rombouts SARB, Barkhof F, Scheltens P, Stam CJ, Smith SM, u. a. Consistent resting-state networks across healthy subjects. Proc Natl Acad Sci USA. 12. September 2006;103(37):13848–53.

32. Moussa MN, Steen MR, Laurienti PJ, Hayasaka S. Consistency of Network Modules in Resting-State fMRI Connectome Data. Zang YF, Herausgeber. PLoS ONE. 31. August 2012;7(8):e44428.

33. Martuzzi R, Ramani R, Qiu M, Shen X, Papademetris X, Constable RT. A whole-brain voxel based measure of intrinsic connectivity contrast reveals local changes in tissue connectivity with anesthetic without a priori assumptions on thresholds or regions of interest. NeuroImage. Oktober 2011;58(4):1044–50.

34. Saad ZS, Reynolds RC, Jo HJ, Gotts SJ, Chen G, Martin A, u. a. Correcting Brain-Wide Correlation Differences in Resting-State FMRI. Brain Connectivity. August 2013;3(4):339–52.

35. Deshpande G, LaConte S, Peltier S, Hu X. Integrated local correlation: A new measure of local coherence in fMRI data. Hum Brain Mapp. Januar 2009;30(1):13–23.

36. Yang H, Long XY, Yang Y, Yan H, Zhu CZ, Zhou XP, u. a. Amplitude of low frequency fluctuation within visual areas revealed by resting-state functional MRI. NeuroImage. Mai 2007;36(1):144–52.

37. Lv H, Wang Z, Tong E, Williams LM, Zaharchuk G, Zeineh M, u. a. Resting-State Functional MRI: Everything That Nonexperts Have Always Wanted to Know. AJNR Am J Neuroradiol. 18. Januar 2018;ajnr;ajnr.A5527v1.

38. Deng S, Franklin CG, O'Boyle M, Zhang W, Heyl BL, Jerabek PA, u. a. Hemodynamic and metabolic correspondence of resting-state voxel-based physiological metrics in healthy adults. NeuroImage. April 2022;250:118923.

39. Zou QH, Zhu CZ, Yang Y, Zuo XN, Long XY, Cao QJ, u. a. An improved approach to detection of amplitude of low-frequency fluctuation (ALFF) for resting-state fMRI: Fractional ALFF. Journal of Neuroscience Methods. Juli 2008;172(1):137–41.

40. Biswal BB, Mennes M, Zuo XN, Gohel S, Kelly C, Smith SM, u. a. Toward discovery science of human brain function. Proc Natl Acad Sci USA. 9. März 2010;107(10):4734–9.

41. Hu S, Chao HHA, Zhang S, Ide JS, Li CSR. Changes in cerebral morphometry and amplitude of low-frequency fluctuations of BOLD signals during healthy aging: correlation with inhibitory control. Brain Struct Funct. Mai 2014;219(3):983–94.

42. Vieira BH, Rondinoni C, Garrido Salmon CE. Evidence of regional associations between age-related inter-individual differences in resting-state functional connectivity and cortical thinning revealed through a multi-level analysis. NeuroImage. Mai 2020;211:116662.

43. Wu T, Zang Y, Wang L, Long X, Li K, Chan P. Normal aging decreases regional homogeneity of the motor areas in the resting state. Neuroscience Letters. August 2007;423(3):189–93.

44. Harrison TM, Maass A, Adams JN, Du R, Baker SL, Jagust WJ. Tau deposition is associated with functional isolation of the hippocampus in aging. Nat Commun. 25. Oktober 2019;10(1):4900.

45. Pagano G, Niccolini F, Politis M. Current status of PET imaging in Huntington's disease. Eur J Nucl Med Mol Imaging. Juni 2016;43(6):1171–82.

46. Sarappa C, Salvatore E, Filla A, Cocozza S, Russo CV, Saccà F, u. a. Functional MRI signal fluctuations highlight altered resting brain activity in Huntington's disease. Brain Imaging and Behavior. Oktober 2017;11(5):1459–69.

47. Liu W, Yang J, Chen K, Luo C, Burgunder J, Gong Q, u. a. Resting-state fMRI reveals potential neural correlates of impaired cognition in Huntington's disease. Parkinsonism & Related Disorders. Juni 2016;27:41–6.

48. Pini L, Jacquemot C, Cagnin A, Meneghello F, Semenza C, Mantini D, u. a. Aberrant brain network connectivity in presymptomatic and manifest Huntington's disease: A systematic review. Hum Brain Mapp. Januar 2020;41(1):256–69.

49. Zhu H, Zhu H, Liu X, Zhou Y, Wu S, Wei F, u. a. Alterations of Regional Homogeneity in Parkinson's Disease: A Resting-State Functional Magnetic Resonance Imaging (fMRI) Study. Cureus [Internet]. 12. Juli 2022 [zitiert 23. Februar 2023]; Verfügbar unter: https://www.cureus.com/articles/101503-alterations-of-regional-homogeneity-in-parkinsons-disease-a-resting-state-functional-magnetic-resonance-imaging-fmri-study

50. Gray JP, Müller VI, Eickhoff SB, Fox PT. Multimodal Abnormalities of Brain Structure and Function in Major Depressive Disorder: A Meta-Analysis of Neuroimaging Studies. AJP. 1. Mai 2020;177(5):422–34.

51. for the ENIGMA-Major Depressive Disorder Working Group, Schmaal L, Veltman DJ, Van Erp TGM, Sämann PG, Frodl T, u. a. Subcortical brain alterations in major depressive disorder: findings from the ENIGMA Major Depressive Disorder working group. Mol Psychiatry. Juni 2016;21(6):806–12.

52. Loewi O. An Autobiographic Sketch. Perspectives in Biology and Medicine. 1960;4(1):3–25.

53. Teleanu RI, Niculescu AG, Roza E, Vladâcenco O, Grumezescu AM, Teleanu DM. Neurotransmitters—Key Factors in Neurological and Neurodegenerative Disorders of the Central Nervous System. IJMS. 25. Mai 2022;23(11):5954.

54. Moroz LL, Romanova DY, Kohn AB. Neural versus alternative integrative systems: molecular insights into origins of neurotransmitters. Phil Trans R Soc B. 29. März 2021;376(1821):20190762.

55. Wang DD, Kriegstein AR. Defining the role of GABA in cortical development. The Journal of Physiology. Mai 2009;587(9):1873–9.

56. Pal MM. Glutamate: The Master Neurotransmitter and Its Implications in Chronic Stress and Mood Disorders. Front Hum Neurosci. 29. Oktober 2021;15:722323.

57. Bañuelos C, Beas BS, McQuail JA, Gilbert RJ, Frazier CJ, Setlow B, u. a. Prefrontal Cortical GABAergic Dysfunction Contributes to Age-Related Working Memory Impairment. J Neurosci. 5. März 2014;34(10):3457–66.

58. Porges EC, Woods AJ, Edden RAE, Puts NAJ, Harris AD, Chen H, u. a. Frontal Gamma-Aminobutyric Acid Concentrations Are Associated With Cognitive Performance in Older Adults. Biological Psychiatry: Cognitive Neuroscience and Neuroimaging. Januar 2017;2(1):38–44.

59. Schultz W. Multiple Dopamine Functions at Different Time Courses. Annu Rev Neurosci. 1. Juli 2007;30(1):259–88.

60. Berger M, Gray JA, Roth BL. The Expanded Biology of Serotonin. Annu Rev Med. 1. Februar 2009;60(1):355–66.

61. Sam C, Bordoni B. Physiology, Acetylcholine [Internet]. Treasure Island (FL): StatPearls Publishing; 2023; 2023 Apr [zitiert 13. Dezember 2023]. (Physiology, Acetylcholine). Verfügbar unter: https://www.ncbi.nlm.nih.gov/books/NBK557825/

62. Diehl DJ, Gershon S. The role of dopamine in mood disorders. Comprehensive Psychiatry. März 1992;33(2):115–20.

63. Jones LA, Sun EW, Martin AM, Keating DJ. The ever-changing roles of serotonin. The International Journal of Biochemistry & Cell Biology. August 2020;125:105776.

64. Picciotto MR, Higley MJ, Mineur YS. Acetylcholine as a Neuromodulator: Cholinergic Signaling Shapes Nervous System Function and Behavior. Neuron. Oktober 2012;76(1):116–29.

65. Mansvelder HD, Mertz M, Role LW. Nicotinic modulation of synaptic transmission and plasticity in cortico-limbic circuits. Seminars in Cell & Developmental Biology. Juni 2009;20(4):432–40.

66. Passani MB, Panula P, Lin JS. Histamine in the brain. Front Syst Neurosci [Internet]. 28. April 2014 [zitiert 13. Dezember 2023];8. Verfügbar unter: http://journal.frontiersin.org/article/10.3389/fnsys.2014.00064/abstract

67. Torrealba F, Riveros ME, Contreras M, Valdes JL. Histamine and motivation. Front Syst Neurosci [Internet]. 2012 [zitiert 13. Dezember 2023];6. Verfügbar unter: http://journal.frontiersin.org/article/10.3389/fnsys.2012.00051/abstract

68. Vohora D, Bhowmik M. Histamine H3 receptor antagonists/inverse agonists on cognitive and motor processes: relevance to Alzheimer's disease, ADHD, schizophrenia, and drug abuse. Front Syst Neurosci [Internet]. 2012 [zitiert 13. Dezember 2023];6. Verfügbar unter: http://journal.frontiersin.org/article/10.3389/fnsys.2012.00072/abstract

69. Brown RE, Basheer R, McKenna JT, Strecker RE, McCarley RW. Control of Sleep and Wakefulness. Physiological Reviews. Juli 2012;92(3):1087–187.

70. Aston-Jones G, Rajkowski J, Cohen J. Role of locus coeruleus in attention and behavioral flexibility. Biological Psychiatry. November 1999;46(9):1309–20.

71. Sara SJ. The locus coeruleus and noradrenergic modulation of cognition. Nat Rev Neurosci. März 2009;10(3):211–23.

72. Vijayraghavan S, Wang M, Birnbaum SG, Williams GV, Arnsten AFT. Inverted-U dopamine D1 receptor actions on prefrontal neurons engaged in working memory. Nat Neurosci. März 2007;10(3):376–84.

73. Stiedl O, Pappa E, Konradsson-Geuken Ã, Ã–gren SO. The role of the serotonin receptor subtypes 5-HT1A and 5-HT7 and its interaction in emotional learning and memory. Front Pharmacol [Internet]. 7. August 2015 [zitiert 13. Dezember 2023];6. Verfügbar unter: http://journal.frontiersin.org/Article/10.3389/fphar.2015.00162/abstract

74. Pithadia A. 5-Hydroxytryptamine Receptor Subtypes and their Modulators with Therapeutic Potentials. J Clin Med Res [Internet]. 2009 [zitiert 13. Dezember 2023]; Verfügbar unter: http://www.jocmr.org/index.php/JOCMR/article/view/61

75. Martel JC, Gatti McArthur S. Dopamine Receptor Subtypes, Physiology and Pharmacology: New Ligands and Concepts in Schizophrenia. Front Pharmacol. 14. Juli 2020;11:1003.

76. Sieghart W, Sperk G. Subunit Composition, Distribution and Function of GABA-A Receptor Subtypes. CTMC. 1. August 2002;2(8):795–816.

77. Karrer TM, McLaughlin CL, Guaglianone CP, Samanez-Larkin GR. Reduced serotonin receptors and transporters in normal aging adults: a meta-analysis of PET and SPECT imaging studies. Neurobiology of Aging. August 2019;80:1–10.

78. Sheline YI, Mintun MA, Moerlein SM, Snyder AZ. Greater Loss of 5-HT $_{2A}$ Receptors in Midlife Than in Late Life. AJP. März 2002;159(3):430–5.

79. Nord M, Cselenyi Z, Forsberg A, Rosenqvist G, Tiger M, Lundberg J, u. a. Distinct regional age effects on [11 C]AZ10419369 binding to 5-HT 1B receptors in the human brain. NeuroImage. Dezember 2014;103:303–8.

80. Radhakrishnan R, Nabulsi N, Gaiser E, Gallezot JD, Henry S, Planeta B, u. a. Age-Related Change in 5-HT $_{6}$ Receptor Availability in Healthy Male Volunteers Measured with ^{11} C-GSK215083 PET. J Nucl Med. September 2018;59(9):1445–50.

81. Antonini A, Leenders KL, Reist H, Thomann R, Beer HF, Locher J. Effect of Age on D2 Dopamine Receptors in Normal Human Brain Measured by Positron Emission Tomography and 11C-Raclopride. Archives of Neurology. 1. Mai 1993;50(5):474–80.

82. Seaman KL, Smith CT, Juarez EJ, Dang LC, Castrellon JJ, Burgess LL, u. a. Differential regional decline in dopamine receptor availability across adulthood: Linear and nonlinear effects of age. Hum Brain Mapp. April 2019;hbm.24585.

83. Wang Y, Chan GLY, Holden JE, Dobko T, Mak E, Schulzer M, u. a. Age-dependent decline of dopamine D1 receptors in human brain: A PET study. Synapse. September 1998;30(1):56–61.

84. Karrer TM, Josef AK, Mata R, Morris ED, Samanez-Larkin GR. Reduced dopamine receptors and transporters but not synthesis capacity in normal aging adults: a meta-analysis. Neurobiology of Aging. September 2017;57:36–46.

85. Magnusson. Selective vulnerabilities of N-methyl-D-aspartate (NMDA) receptors during brain aging. FrontiAgNeurosci [Internet]. 2010 [zitiert 3. Mai 2023]; Verfügbar unter: http://journal.frontiersin.org/article/10.3389/fnagi.2010.00011/abstract

86. Perry EK, Piggott MA, Court JA, Johnson M, Perry RH. Transmitters in the Developing and Senescent Human Brain. Annals of the New York Academy of Sciences. September 1993;695(1):69–72.

87. Piggott MA, Perry EK, Perry RH, Court JA. [3H]MK-801 binding to the NMDA receptor complex, and its modulation in human frontal cortex during development and aging. Brain Research. August 1992;588(2):277–86.

88. Zubieta JK, Koeppe RA, Frey KA, Kilbourn MR, Mangner TJ, Foster NL, u. a. Assessment of muscarinic receptor concentrations in aging and Alzheimer disease with [11C]NMPB and PET. Synapse. 15. März 2001;39(4):275–87.

89. Ding YS, Singhal T, Planeta-Wilson B, Gallezot JD, Nabulsi N, Labaree D, u. a. PET imaging of the effects of age and cocaine on the norepinephrine transporter in the human brain using (S,S)-[^{11} C]O-methylreboxetine and HRRT. Synapse. Januar 2010;64(1):30–8.

90. Cuypers K, Hehl M, Van Aalst J, Chalavi S, Mikkelsen M, Van Laere K, u. a. Age-related GABAergic differences in the primary sensorimotor cortex: A multimodal approach combining PET, MRS and TMS. NeuroImage. Februar 2021;226:117536.

91. Zubieta JK, Dannals RF, Frost JJ. Gender and Age Influences on Human Brain Mu-Opioid Receptor Binding Measured by PET. AJP. Juni 1999;156(6):842–8.

92. Cybulska K, Perk L, Booij J, Laverman P, Rijpkema M. Huntington's Disease: A Review of the Known PET Imaging Biomarkers and Targeting Radiotracers. Molecules. 23. Januar 2020;25(3):482.

93. Pavese N, Politis M, Tai YF, Barker RA, Tabrizi SJ, Mason SL, u. a. Cortical dopamine dysfunction in symptomatic and premanifest Huntington's disease gene carriers. Neurobiology of Disease. Februar 2010;37(2):356–61.

94. Ginovart N. PET study of the pre- and post-synaptic dopaminergic markers for the neurodegenerative process in Huntington's disease. Brain. 1. März 1997;120(3):503–14.

95. Kaasinen V, Vahlberg T, Stoessl AJ, Strafella AP, Antonini A. Dopamine Receptors in Parkinson's Disease: A Meta-Analysis of Imaging Studies. Mov Disord. August 2021;36(8):1781–91.

96. Takashima H, Terada T, Bunai T, Matsudaira T, Obi T, Ouchi Y. In vivo Illustration of Altered Dopaminergic and GABAergic Systems in Early Parkinson's Disease. Front Neurol. 17. Mai 2022;13:880407.

97. Yao NT, Zheng Q, Xu ZQ, Yin JH, Lu LG, Zuo Q, u. a. Positron emission computed tomography/single photon emission computed tomography in Parkinson disease. Chinese Medical Journal. 20. Juni 2020;133(12):1448–55.

98. Huot P, Fox SH, Brotchie JM. The serotonergic system in Parkinson's disease. Progress in Neurobiology. Oktober 2011;95(2):163–212.

99. Kang Y, Henchcliffe C, Verma A, Vallabhajosula S, He B, Kothari PJ, u. a. 18F-FPEB PET/CT Shows mGluR5 Upregulation in Parkinson's Disease: mGluR5 and DaT in PD. Journal of Neuroimaging. Januar 2019;29(1):97–103.

100. Zhang Z, Zhang S, Fu P, Zhang Z, Lin K, Ko JKS, u. a. Roles of Glutamate Receptors in Parkinson's Disease. IJMS. 6. September 2019;20(18):4391.

101. Sharma A, Muresanu DF, Patnaik R, Menon PK, Tian ZR, Sahib S, u. a. Histamine H3 and H4 receptors modulate Parkinson's disease induced brain pathology. Neuroprotective effects of nanowired BF-2649 and clobenpropit with anti-histamine-antibody therapy. In: Progress in Brain Research [Internet]. Elsevier; 2021 [zitiert 23. Februar 2023]. S. 1–73. Verfügbar unter: https://linkinghub.elsevier.com/retrieve/pii/S0079612321001497

102. Meyer PM, Tiepolt S, Barthel H, Hesse S, Sabri O. Radioligand imaging of α4β2* nicotinic acetylcholine receptors in Alzheimer's disease and Parkinson's disease. Q J Nucl Med Mol Imaging. Dezember 2014;58(4):376–86.

103. van der Zee S, Kanel P, Gerritsen MJJ, Boertien JM, Slomp AC, Müller MLTM, u. a. Altered Cholinergic Innervation in De Novo Parkinson's Disease with and Without Cognitive Impairment. Movement Disorders. April 2022;37(4):713–23.

104. Nahimi A, Kinnerup MB, Sommerauer M, Gjedde A, Borghammer P. Molecular Imaging of the Noradrenergic System in Idiopathic Parkinson's Disease. In: International Review of Neurobiology [Internet]. Elsevier; 2018 [zitiert 3. März 2023]. S. 251–74. Verfügbar unter: https://linkinghub.elsevier.com/retrieve/pii/S0074774218300576

105. Pascual-Torner M, Carrero D, Pérez-Silva JG, Álvarez-Puente D, Roiz-Valle D, Bretones G, u. a. Comparative genomics of mortal and immortal cnidarians unveils novel keys behind rejuvenation. Proc Natl Acad Sci USA. 6. September 2022;119(36):e2118763119.

106. Azam S, Haque MdE, Balakrishnan R, Kim IS, Choi DK. The Ageing Brain: Molecular and Cellular Basis of Neurodegeneration. Front Cell Dev Biol. 13. August 2021;9:683459.

107. López-Otín C, Blasco MA, Partridge L, Serrano M, Kroemer G. The Hallmarks of Aging. Cell. Juni 2013;153(6):1194–217.

108. Chou SM, Yen YH, Yuan F, Zhang SC, Chong CM. Neuronal Senescence in the Aged Brain. Aging and disease. 2023;14(5):1618.

109. Marquand AF, Kia SM, Zabihi M, Wolfers T, Buitelaar JK, Beckmann CF. Conceptualizing mental disorders as deviations from normative functioning. Mol Psychiatry. Oktober 2019;24(10):1415–24.

110. Fraza CJ, Dinga R, Beckmann CF, Marquand AF. Warped Bayesian linear regression for normative modelling of big data. NeuroImage. Dezember 2021;245:118715.

111. Bozek J, Griffanti L, Lau S, Jenkinson M. Normative models for neuroimaging markers: Impact of model selection, sample size and evaluation criteria [Internet]. 2022 [zitiert 20. Juli 2024]. Verfügbar unter: http://biorxiv.org/lookup/doi/10.1101/2022.09.22.509002

112. Rutherford S, Kia SM, Wolfers T, Fraza C, Zabihi M, Dinga R, u. a. The normative modeling framework for computational psychiatry. Nat Protoc. Juli 2022;17(7):1711–34.

113. Cole TJ. The development of growth references and growth charts. Annals of Human Biology. September 2012;39(5):382–94.

114. Deutsche Gesellschaft für Neurologie e.V. (DGN), Herausgeber. S2k Leitlinie Parkinson-Krankheit [Internet]. 2023 [zitiert 13. Dezember 2023]. Verfügbar unter: https://register.awmf.org/de/leitlinien/detail/030-010

115. Yi S, Wang L, Wang H, Ho MS, Zhang S. Pathogenesis of α-Synuclein in Parkinson's Disease: From a Neuron-Glia Crosstalk Perspective. Int J Mol Sci. 25. November 2022;23(23):14753.

116. Marsden CD. Parkinson's disease. The Lancet. April 1990;335(8695):948–9.

117. Ross CA, Aylward EH, Wild EJ, Langbehn DR, Long JD, Warner JH, u. a. Huntington disease: natural history, biomarkers and prospects for therapeutics. Nat Rev Neurol. April 2014;10(4):204–16.

118. Lang AE, Lozano AM. Parkinson's Disease. N Engl J Med. 8. Oktober 1998;339(15):1044–53.

119. Dauer W, Przedborski S. Parkinson's Disease. Neuron. September 2003;39(6):889–909.

120. Brown RC, Lockwood AH, Sonawane BR. Neurodegenerative Diseases: An Overview of Environmental Risk Factors. Environ Health Perspect. September 2005;113(9):1250–6.

121. Braak H, Tredici KD, Rüb U, de Vos RAI, Jansen Steur ENH, Braak E. Staging of brain pathology related to sporadic Parkinson's disease. Neurobiology of Aging. März 2003;24(2):197–211.

122. Jankovic J, Tan EK. Parkinson's disease: etiopathogenesis and treatment. J Neurol Neurosurg Psychiatry. August 2020;91(8):795–808.

123. Sanjari Moghaddam H, Zare-Shahabadi A, Rahmani F, Rezaei N. Neurotransmission systems in Parkinson's disease. Reviews in the Neurosciences. 26. Juli 2017;28(5):509–36.

124. Obeso JA, Rodriguez-Oroz MC, Goetz CG, Marin C, Kordower JH, Rodriguez M, u. a. Missing pieces in the Parkinson's disease puzzle. Nat Med. Juni 2010;16(6):653–61.

125. McFarthing K, Buff S, Rafaloff G, Fiske B, Mursaleen L, Fuest R, u. a. Parkinson's Disease Drug Therapies in the Clinical Trial Pipeline: 2023 Update. JPD. 13. Juni 2023;13(4):427–39.

126. Sharma N, Nehru B. Curcumin affords neuroprotection and inhibits α-synuclein aggregation in lipopolysaccharide-induced Parkinson's disease model. Inflammopharmacol. April 2018;26(2):349–60.

127. Wang MS, Boddapati S, Emadi S, Sierks MR. Curcumin reduces α-synuclein induced cytotoxicity in Parkinson's disease cell model. BMC Neurosci. Dezember 2010;11(1):57.

128. Ilijic E, Guzman JN, Surmeier DJ. The L-type channel antagonist isradipine is neuroprotective in a mouse model of Parkinson's disease. Neurobiology of Disease. August 2011;43(2):364–71.

129. Li Y, Hu X, Liu Y, Bao Y, An L. Nimodipine protects dopaminergic neurons against inflammation-mediated degeneration through inhibition of microglial activation. Neuropharmacology. März 2009;56(3):580–9.

130. Sahandi Far M, Eickhoff SB, Goni M, Dukart J. Exploring Test-Retest Reliability and Longitudinal Stability of Digital Biomarkers for Parkinson Disease in the m-Power Data Set: Cohort Study. J Med Internet Res. 13. September 2021;23(9):e26608.

131. Yamashita KY, Bhoopatiraju S, Silverglate BD, Grossberg GT. Biomarkers in Parkinson's disease: A state of the art review. Biomarkers in Neuropsychiatry. Dezember 2023;9:100074.

132. Ryman SG, Poston KL. MRI biomarkers of motor and non-motor symptoms in Parkinson's disease. Parkinsonism & Related Disorders. April 2020;73:85–93.

133. Martino D, Stamelou M, Bhatia KP. The differential diagnosis of Huntington's disease-like syndromes: „red flags" for the clinician. J Neurol Neurosurg Psychiatry. Juni 2013;84(6):650–6.

134. Andhale R, Shrivastava D. Huntington's Disease: A Clinical Review. Cureus [Internet]. 27. August 2022 [zitiert 13. Dezember 2023]; Verfügbar unter: https://www.cureus.com/articles/109169-huntingtons-disease-a-clinical-review

135. Macdonald M. A novel gene containing a trinucleotide repeat that is expanded and unstable on Huntington's disease chromosomes. Cell. März 1993;72(6):971–83.

136. Petracca M, Di Tella S, Solito M, Zinzi P, Lo Monaco MR, Di Lazzaro G, u. a. Clinical and genetic characteristics of late-onset Huntington's disease in a large European cohort. Euro J of Neurology. Juli 2022;29(7):1940–51.

137. Bakels HS, Roos RAC, Van Roon-Mom WMC, De Bot ST. Juvenile-Onset Huntington Disease Pathophysiology and Neurodevelopment: A Review. Movement Disorders. Januar 2022;37(1):16–24.

138. Kirkwood SC, Su JL, Conneally PM, Foroud T. Progression of Symptoms in the Early and Middle Stages of Huntington Disease. Arch Neurol. 1. Februar 2001;58(2):273.

139. Folstein SE. The psychopathology of Huntington's disease. Res Publ Assoc Res Nerv Ment Dis. 1991;69:181–91.

140. Foroud T, Gray J, Ivashina J, Conneally PM. Differences in duration of Huntington's disease based on age at onset. Journal of Neurology, Neurosurgery & Psychiatry. 1. Januar 1999;66(1):52–6.

141. Mouro Pinto R, Arning L, Giordano JV, Razghandi P, Andrew MA, Gillis T, u. a. Patterns of CAG repeat instability in the central nervous system and periphery in Huntington's disease and in spinocerebellar ataxia type 1. Human Molecular Genetics. 29. August 2020;29(15):2551–67.

142. Wolf RC, Thomann PA, Thomann AK, Vasic N, Wolf ND, Landwehrmeyer GB, u. a. Brain structure in preclinical Huntington's disease: a multi-method approach. Neurodegener Dis. 2013;12(1):13–22.

143. La Spada A, Weydt P, Pineda V. Huntington's Disease Pathogenesis: Mechanisms and Pathways. In: Neurobiology of Huntington's Disease: Applications to Drug Discovery [Internet]. CRC Press/Taylor & Francis; 2011 [zitiert 13. Dezember 2023]. Verfügbar unter: https://www.ncbi.nlm.nih.gov/books/NBK55992/

144. Tong H, Yang T, Xu S, Li X, Liu L, Zhou G, u. a. Huntington's Disease: Complex Pathogenesis and Therapeutic Strategies. IJMS. 29. März 2024;25(7):3845.

145. Ferguson MW, Kennedy CJ, Palpagama TH, Waldvogel HJ, Faull RLM, Kwakowsky A. Current and Possible Future Therapeutic Options for Huntington's Disease. J Cent Nerv Syst Dis. Januar 2022;14:117957352210925.

146. Khan A, Özçelik CE, Begli O, Oguz O, Kesici MS, Kasırga TS, u. a. Highly Potent Peptide Therapeutics To Prevent Protein Aggregation in Huntington's Disease. ACS Med Chem Lett. 14. Dezember 2023;14(12):1821–6.

147. Djajadikerta A, Keshri S, Pavel M, Prestil R, Ryan L, Rubinsztein DC. Autophagy Induction as a Therapeutic Strategy for Neurodegenerative Diseases. Journal of Molecular Biology. April 2020;432(8):2799–821.

148. Yoon Y, Kim HS, Jeon I, Noh JE, Park HJ, Lee S, u. a. Implantation of the clinical-grade human neural stem cell line, *CTX0E03* , rescues the behavioral and pathological deficits in the quinolinic acid-lesioned rodent model of Huntington's disease. Stem Cells. 1. August 2020;38(8):936–47.

149. DiFiglia M, Sena-Esteves M, Chase K, Sapp E, Pfister E, Sass M, u. a. Therapeutic silencing of mutant huntingtin with siRNA attenuates striatal and cortical neuropathology and behavioral deficits. Proc Natl Acad Sci USA. 23. Oktober 2007;104(43):17204–9.

150. Ekman FK, Ojala DS, Adil MM, Lopez PA, Schaffer DV, Gaj T. CRISPR-Cas9-Mediated Genome Editing Increases Lifespan and Improves Motor Deficits in a Huntington's Disease Mouse Model. Molecular Therapy - Nucleic Acids. September 2019;17:829–39.

151. Andrew SE, Paul Goldberg Y, Kremer B, Telenius H, Theilmann J, Adam S, u. a. The relationship between trinucleotide (CAG) repeat length and clinical features of Huntington's disease. Nat Genet. August 1993;4(4):398–403.

152. Schultz JL, Moser AD, Nopoulos PC. The Association between CAG Repeat Length and Age of Onset of Juvenile-Onset Huntington's Disease. Brain Sciences. 20. August 2020;10(9):575.

153. Keum JW, Shin A, Gillis T, Mysore JS, Abu Elneel K, Lucente D, u. a. The HTT CAG-Expansion Mutation Determines Age at Death but Not Disease Duration in Huntington Disease. The American Journal of Human Genetics. Februar 2016;98(2):287–98.

154. World Health Organization. Depressive disorder (depression) [Internet]. 2023 März [zitiert 13. Dezember 2023]. Verfügbar unter: https://www.who.int/news-room/fact-sheets/detail/depression

155. Chikatimalla R, Dasaradhan T, Koneti J, Cherukuri SP, Kalluru R, Gadde S. Depression in Parkinson's Disease: A Narrative Review. Cureus [Internet]. 7. August 2022 [zitiert 15. Dezember 2023]; Verfügbar unter: https://www.cureus.com/articles/104679-depression-in-parkinsons-disease-a-narrative-review

156. Hannan AJ. Chorea me a river: depression in Huntington's disease as an exemplar of precision medicine. Brain Communications. 2. November 2022;4(6):fcac294.

157. Baquero M. Depressive symptoms in neurodegenerative diseases. WJCC. 2015;3(8):682.

158. Diagnostic and statistical manual of mental disorders: DSM-5 (P. Xii). 5th ed. Washington: American psychiatric association; 2013.

159. World Health Organization. International Classification of Diseases, Eleventh Revision (ICD-11) [Internet]. 2019 2021. Verfügbar unter: https://icd.who.int/browse11

160. Miller KL, Alfaro-Almagro F, Bangerter NK, Thomas DL, Yacoub E, Xu J, u. a. Multimodal population brain imaging in the UK Biobank prospective epidemiological study. Nat Neurosci. November 2016;19(11):1523–36.

161. Kasper J, Eickhoff SB, Caspers S, Peter J, Dogan I, Wolf RC, u. a. Local synchronicity in dopamine-rich caudate nucleus influences Huntington's disease motor phenotype. Brain. 1. August 2023;146(8):3319–30.

162. Kasper J, Caspers S, Lotter LD, Hoffstaedter F, Eickhoff SB, Dukart J. Resting-State Changes in Aging and Parkinson's Disease Are Shaped by Underlying Neurotransmission: A Normative Modeling Study. Biological Psychiatry: Cognitive Neuroscience and Neuroimaging. April 2024;S2451902224001125.

163. Wang X, Hoffstaedter F, Kasper J, Eickhoff SB, Patil KR, Dukart J. Lifetime Exposure to Depression and Neuroimaging Measures of Brain Structure and Function. JAMA Netw Open. 19. Februar 2024;7(2):e2356787.

164. Zhang A, Wang X, Li J, Jing L, Hu X, Li H, u. a. Resting-State fMRI in Predicting Response to Treatment With SSRIs in First-Episode, Drug-Naive Patients With Major Depressive Disorder. Front Neurosci. 16. Februar 2022;16:831278.

165. Smitha K, Akhil Raja K, Arun K, Rajesh P, Thomas B, Kapilamoorthy T, u. a. Resting state fMRI: A review on methods in resting state connectivity analysis and resting state networks. Neuroradiol J. August 2017;30(4):305–17.

166. Damoiseaux JS. Resting-state fMRI as a biomarker for Alzheimer's disease? Alzheimers Res Ther. 2012;4(3):8.

167. Mousa D, Zayed N, Yassine IA. Alzheimer disease stages identification based on correlation transfer function system using resting-state functional magnetic resonance imaging. Ginsberg SD, Herausgeber. PLoS ONE. 12. April 2022;17(4):e0264710.

168. Hohenfeld C, Werner CJ, Reetz K. Resting-state connectivity in neurodegenerative disorders: Is there potential for an imaging biomarker? NeuroImage: Clinical. 2018;18:849–70.

169. Parkes L, Satterthwaite TD, Bassett DS. Towards precise resting-state fMRI biomarkers in psychiatry: synthesizing developments in transdiagnostic research, dimensional models of psychopathology, and normative neurodevelopment. Current Opinion in Neurobiology. Dezember 2020;65:120–8.

170. Greicius M. Resting-state functional connectivity in neuropsychiatric disorders. Current Opinion in Neurology. August 2008;21(4):424–30.

171. Davey CG, Cearns M, Jamieson A, Harrison BJ. Suppressed activity of the rostral anterior cingulate cortex as a biomarker for depression remission. Psychol Med. April 2023;53(6):2448–55.

172. Lotter LD, Nehls S, Losse E, Dukart J, Chechko N. Temporal dissociation between local and global functional adaptations of the maternal brain to childbirth: a longitudinal assessment. Neuropsychopharmacol [Internet]. 20. Mai 2024 [zitiert 1. Juni 2024]; Verfügbar unter: https://www.nature.com/articles/s41386-024-01880-9

173. Lotter LD, Saberi A, Hansen JY, Misic B, Barker GJ, Bokde ALW, u. a. Human cortex development is shaped by molecular and cellular brain systems [Internet]. Neuroscience; 2023 Mai [zitiert 29. September 2023]. Verfügbar unter: http://biorxiv.org/lookup/doi/10.1101/2023.05.05.539537

174. Premi E, Dukart J, Mattioli I, Libri I, Pengo M, Gadola Y, u. a. UNRAVELLING neurotransmitters impairment in primary progressive aphasias. Human Brain Mapping. 15. April 2023;44(6):2245–53.

175. Fedak KM, Bernal A, Capshaw ZA, Gross S. Applying the Bradford Hill criteria in the 21st century: how data integration has changed causal inference in molecular epidemiology. Emerg Themes Epidemiol. Dezember 2015;12(1):14.

176. Nowinski CJ, Bureau SC, Buckland ME, Curtis MA, Daneshvar DH, Faull RLM, u. a. Applying the Bradford Hill Criteria for Causation to Repetitive Head Impacts and Chronic Traumatic Encephalopathy. Front Neurol. 22. Juli 2022;13:938163.

177. Hill AB. The Environment and Disease: Association or Causation? Proceedings of the Royal Society of Medicine. Mai 1965;58(5):295–300.

178. Dukart J, Holiga Š, Chatham C, Hawkins P, Forsyth A, McMillan R, u. a. Cerebral blood flow predicts differential neurotransmitter activity. Sci Rep. Dezember 2018;8(1):4074.

179. Iturria-Medina Y, Carbonell FM, Evans AC. Multimodal imaging-based therapeutic fingerprints for optimizing personalized interventions: Application to neurodegeneration. NeuroImage. Oktober 2018;179:40–50.

180. Lee J, Kim HJ. Normal Aging Induces Changes in the Brain and Neurodegeneration Progress: Review of the Structural, Biochemical, Metabolic, Cellular, and Molecular Changes. Front Aging Neurosci. 30. Juni 2022;14:931536.

181. Cosgrove KP, Mazure CM, Staley JK. Evolving Knowledge of Sex Differences in Brain Structure, Function, and Chemistry. Biological Psychiatry. Oktober 2007;62(8):847–55.

182. Schlemmer HPW, Pichler BJ, Schmand M, Burbar Z, Michel C, Ladebeck R, u. a. Simultaneous MR/PET Imaging of the Human Brain: Feasibility Study. Radiology. September 2008;248(3):1028–35.

183. Sander CY, Hansen HD, Wey HY. Advances in simultaneous PET/MR for imaging neuroreceptor function. J Cereb Blood Flow Metab. Juni 2020;40(6):1148–66.

184. Fry A, Littlejohns TJ, Sudlow C, Doherty N, Adamska L, Sprosen T, u. a. Comparison of Sociodemographic and Health-Related Characteristics of UK Biobank Participants With Those of the General Population. American Journal of Epidemiology. 1. November 2017;186(9):1026–34.

185. Azevedo T, Bethlehem RAI, Whiteside DJ, Swaddiwudhipong N, Rowe JB, Lió P, u. a. Identifying healthy individuals with Alzheimer's disease neuroimaging phenotypes in the UK Biobank. Commun Med. 20. Juli 2023;3(1):100.

186. Bayer JMM, Thompson PM, Ching CRK, Liu M, Chen A, Panzenhagen AC, u. a. Site effects how-to and when: An overview of retrospective techniques to accommodate site effects in multi-site neuroimaging analyses. Front Neurol. 31. Oktober 2022;13:923988.

187. Savitz DA, Wellenius GA. Interpreting Epidemiologic Evidence: Connecting Research to Applications [Internet]. Oxford University Press; 2016 [zitiert 26. August 2024]. Verfügbar unter: http://www.oxfordscholarship.com/view/10.1093/acprof:oso/9780190243777.001.0001/acprof-9780190243777

188. Pandis N. Sources of bias in clinical trials. American Journal of Orthodontics and Dentofacial Orthopedics. Oktober 2011;140(4):595–6.

189. Aigner A, Grittner U, Becher H. Bias due to differential participation in case-control studies and review of available approaches for adjustment. Wiegand RE, Herausgeber. PLoS ONE. 24. Januar 2018;13(1):e0191327.

Danksagung

Während meiner Tätigkeit an der Heinrich-Heine-Universität, an dem Universitätsklinikum in Düsseldorf und am Forschungszentrum Jülich habe ich dank Anstrengungen vieler Kollegen lernen und verstehen dürfen, was es heißt, wissenschaftlich zu arbeiten. Vielen Dank an meinen Doktorvater Prof. Dr. Jürgen Dukart, der mir sowohl fachlich als auch persönlich mit Rat und Tat zur Seite stand. Danke an meine Kollegen, ohne die die Tätigkeit bei Weitem nicht so angenehm und spaßig verlaufen wäre: Dr. Claudia Eickhoff, Anja Spiewok und Dafina Sylaj für ihre enorme Hilfe im Universitätsklinikum Düsseldorf, meine Kollegen der Arbeitsgruppe Biomarkerentwicklung, sowie das gesamte Team des Instituts für Systemische Neurowissenschaften (INM-7) des Forschungszentrum Jülich unter der exzellenten Leitung von Prof. Dr. Simon Eickhoff. Ein besonderer Dank gilt meinen Eltern und Geschwistern, die mich bei allen von mir eingeschlagenen Wegen unterstützt und an mich geglaubt haben. Zu guter Letzt danke ich meiner Frau, die mich durch die Höhen und Tiefen meiner Promotion begleitet hat und ohne deren Unterstützung es diese Dissertationsschrift nicht gäbe.